

University of Strathclyde  
Department of Naval Architecture, Ocean and Marine Engineering

**Experimental and numerical investigation  
on wave-induced loads acting on intact and  
damaged naval combatant vessel**

Yue Gu

The thesis submitted in fulfilment of the requirements for the degree of

Doctor of Philosophy

July 2019

Learn extensively, inquire carefully, think deeply, differentiate clearly,  
and practice faithfully.

- The Doctrine of the Mean

博学之、审问之、慎思之、明辨之、笃行之。

——《礼记·中庸》

## **Statement of Originality**

This thesis is the result of the author's original research. It has been composed by the author and has not been previously submitted for examination which has led to the award of a degree. The copyright of this thesis belongs to the author under the terms of the United Kingdom Copyright Acts as qualified by University of Strathclyde Regulation 3.50. Due acknowledgement must always be made of the use of any material contained in, or derived from, this thesis

Signed:

Date:

# Acknowledgements

I would like to express my gratitude to all those who helped me during the whole seven years in Glasgow for my life and study.

My deepest gratitude goes first and foremost to my first supervisor, Professor Sandy Day, for his understanding, support, patience and constant encouragement. With his valuable guidance and suggestions, I suppose to spend even more time finishing my PhD.

Second, I would like to express my thanks to second supervisor, Dr. Evangelos Boulougouris, for his instructive advice and useful suggestions on my thesis.

I also want to express my heartfelt gratitude to Dr. Saishuai Dai, who led me into the world of CFD and physical hydrodynamic experiment. His constant guidance and suggestion was significantly contributed to my academic study.

High tribute shall be paid to Dr. Hanlin Wang, Dr. Ruoxin Li, Dr. Yuanchuan Liu, Mr. Enqian Liu, Dr. Zi Lin, Dr. Zhiming Yuan, Dr. Jianxin Hu, Dr. Zhiliang Gao, Dr. Mengshi Sun, Dr. Lei Ju, Dr. Haipeng Liu, Dr. Renyou Yang, Dr. Mei Liu, Mr. Zhenkai Zhao, Mr. Guangyu Shi, Dr. Liang Li, Dr. Yan Gao, Mr. Kai Zhao, Mr. Zheng Han, Miss. Luyao Gao, Ms. Hong Yue, Miss. Yunke Huang and all my classmates and colleagues in University of Strathclyde. I want to submit my thanks to those who helped me with my physical experiment in Kelvin Hydrodynamic Laboratory, Mr. Grant Dunning, Mr. Charles Keay, Mr. Edward Nixon, Mr. Bill Wright, Mr. Bill McGuffie. I am also greatly

indebted to the staffs that helped me with the five-year academic life in this department, including Mrs. Thelma Will, Ms. Susan Pawson, Ms. Carolyn McLellan, Mr. Roll Gilmour and Ms. Kay Cranston (University of Glasgow). Many thanks are given to Dr. Richard Martin and Dr. Karina Kubiak-Ossowska for their support to use high-performance computers.

I would also like to thank the University of Strathclyde Faculty of Engineering for provision of the ARCHIE-WeSt high-performance computing facilities. The CFD results were obtained using the EPSRC funded ARCHIE-WeSt High-Performance Computer ([www.archie-west.ac.uk](http://www.archie-west.ac.uk)), EPSRC grant no. EP/K000586/1.

I should owe a special debt of gratitude to my parents, for their love and support during last seven years either in spirit or in finance. Their selfless real love makes me realize how difficult to be parents, especially having a son like me.

Finally, I would like to express my deep gratitude to my best family-like friends, Mr. Xueliang Li, Mr. Yanjie Shao, Mr. Nan Zhao, Miss. Yunhan Sun, Ms. Xuwei Cong. Their friendship and care encourage me and firm my belief in my way forward and make me not feel lonely and hopeless. Meanwhile, I would like to thank some lecturers and friends in China, they are Mr. Ruiyu Wang, Ms. Jie Zhang, Ms. Peiyong Cong, Mr. Jingzheng Yao (Harbin Engineering University), Professor Niannian Jia (Harbin Engineering University), Miss. Liping Ji and Miss. Dansha Su.

# Abstract

In this study, wave-induced loads acting on an intact and damaged naval combatant vessel are investigated experimentally and numerically. Experimental tests are carried out with a double-bottom naval combatant vessel DTMB 5415, which has been widely used in benchmark studies for experimental investigation and the validation of numerical simulations. Free decay tests in roll with and without moorings are implemented in calm water, while the model is moored at the bow and stern during the tests in regular waves. In order to investigate the performance of the intact and damaged ship in beam waves the damaged opening is located at starboard midship so that floodwater may ingress and egress from the opening from which two compartments can be flooded.

It is shown that beam waves flooding in and out from the damaged opening and the interaction between ship behaviour and water surface effect in the damaged compartments have a significant impact on ship motions and wave-induced loads acting on the ship. And it can be observed that highly nonlinear wave-induced loads can be induced on the intact and damaged ship hull in regular beam waves.

Two cases under the regular beam wave condition are investigated by CFD-based RANS method. The method is proposed to calculate wave-induced loads acting on the intact and damaged ship model. For validation of the numerical method, comparison between numerical estimation and experimental measurement shows that solution by RANS method have a generally good qualitative agreement with physical tests.

# Contents

<b>1. Introduction.....</b>	<b>1</b>
1.1 Background .....	1
1.2 Motivation .....	2
1.3 Damaged ship stability .....	10
1.4 Physical model test in water tank .....	12
1.5 Numerical investigation .....	14
1.6 Research aim and objectives .....	14
1.7 Outline of the thesis .....	15
<b>2. Literature Review.....</b>	<b>17</b>
2.1 Inspiration for passenger ship safety investigation .....	17
2.2 Flooding procedure investigation .....	20
2.3 Experimental investigation .....	23
2.4 Sloshing and its coupling effect combined with behaviour of water tank ..	30
2.5 Numerical study on behaviour of a damaged ship and floodwater .....	34
2.6 Study on loads acting on intact and damaged ship.....	37
2.7 Chapter remarks .....	39
<b>3. Experimental Investigation .....</b>	<b>41</b>
3.1 Brief introduction .....	41
3.2 Facilities .....	42
3.3 Ship model.....	43
3.4 Experimental setup .....	47
3.4.1 Waves.....	47
3.4.2 Instrumentation .....	47
3.5 Test procedure .....	49
3.5.1 Force transducer (load cell) calibration and uncertainty analysis. ....	49
3.5.2 Cross coupling.....	54
3.5.3 Mass moment of inertia measurement .....	57
3.6 Decay tests in calm water .....	58

3.6.1	Free roll decay tests for the intact and damaged ship model .....	58
3.7	Tests in regular beam seas .....	60
3.7.1	Ship motions .....	61
3.7.2	Wave-induced loads .....	64
3.7.3	Comparison between two experiments .....	70
3.8	Chapter remarks .....	86
<b>4.</b>	<b>2D simulation by CFD-based approach .....</b>	<b>89</b>
4.1	Computational fluid dynamic (CFD) approach .....	89
4.1.1	Basic theory of adopted CFD-based method .....	89
4.1.2	Governing equations .....	90
4.1.3	Reynolds-Averaged Navier Stokes (RANS) equations.....	91
4.1.4	Shear Stress Transport (SST) $k-\omega$ turbulence model.....	92
4.1.5	Boundary conditions .....	92
4.1.6	SIMPLE .....	93
4.1.7	Volume of Fluid Method.....	94
4.1.8	$Y^+$ .....	94
4.2	Numerical wave tank .....	94
4.2.1	Calculation domain dimensions and boundaries.....	95
4.2.2	Physical modelling .....	96
4.2.3	Mesh sensitivity .....	96
4.2.4	Nonlinearity of generated waves.....	100
4.3	2-Dimensional investigation on free rolling decay .....	102
4.3.1	Rectangular structure roll-decay study in 2-dimensional.....	102
4.3.2	Ship-like body rolling decay study in 2-dimensions.....	104
4.4	2-Dimensional structure in regular beam seas.....	109
4.4.1	Geometry and boundary conditions of calculation domain .....	109
4.4.2	Wave setup .....	110
4.4.3	Mesh dependence study .....	110
4.4.4	Results .....	112
4.5	2-Dimensional liquid tank sloshing.....	114
4.5.1	One-DOF motion sloshing .....	115
4.5.2	3-DOF sloshing problem.....	123
4.6	Chapter remarks .....	127
<b>5.</b>	<b>RANS investigation on an intact and damaged naval combatant vessel... 130</b>	



5.1	Ship geometry.....	130
5.2	Free roll motion decay simulation.....	133
5.2.1	Calculation domain .....	133
5.2.2	Mesh distribution .....	134
5.2.3	Results presentation .....	135
5.3	Wave induced loads acting on ship hull in beam seas .....	137
5.3.1	Coordinate systems .....	137
5.3.2	Shear forces.....	137
5.3.3	Moments.....	140
5.4	CFD simulations for intact and damaged ship in regular beam waves .....	141
5.4.1	Pre-declared specification .....	141
5.4.2	Calculation domain .....	143
5.4.3	Wave conditions.....	143
5.4.4	Mesh distribution .....	144
5.5	Results .....	145
5.5.1	Mesh sensitivity study.....	146
5.5.2	Uncertainty.....	148
5.5.3	Result comparison and discussion .....	149
5.6	Chapter remarks .....	175
<b>6.</b>	<b>Conclusions and recommendations .....</b>	<b>177</b>
	<b>Reference.....</b>	<b>181</b>
	<b>Appendix.....</b>	<b>198</b>
	Appendix 1 .....	198
	Appendix 2 Runge-Kutta method and $I_{xx}$ approximation by CFD.....	200
	A2.1 Methodology .....	200
	A2.2 2-Dimensional validation.....	201
	A2.3 Estimation on mass moment of inertia about ship' s roll motion .....	205
	Appendix 3 Transformation of reference frames and the application of Newton's law .....	209
	A3.1 Methodology .....	209
	<b>List of Figures.....</b>	<b>215</b>
	<b>List of Tables .....</b>	<b>221</b>
	<b>Abbreviations .....</b>	<b>222</b>
	<b>Nomenclature.....</b>	<b>223</b>



# 1. Introduction

## 1.1 Background

With the increasing demand for trade, transportation and national defence, maritime safety has been investigated for decades. Along with considerations of minimising cost of operation and maintenance as far as possible, stability and survivability for a ship continue to be priorities for research investigations, while maritime incidents continue to provide researchers and naval architects more and more incentives to improve safety and stability.

Local damage can create a risk of a failure to structural integrity of ship hull and may be further followed by water flooding into the compartments through the damaged opening, so that ship may change its righting situation and react corresponding to a range of flooding scenarios and sea states. Although damage flooding for a ship is a complicated mechanism, the ultimate target is to keep the damaged ship safe, thus, the maintenance of structural strength (avoiding global structure failure) is of significance. In the meantime, understanding of the behaviour of floodwater, even if flooding is massive and progressive, is the first priority to be considered.

As matter of fact, the response of the damaged ship to damage flooding is not independent from the loss of structural strength and the behaviour of floodwater. In other words, there is a strong coupling impact on the stability of the damaged ship. Structural damage especially at and below the waterline must result in a water flooding from the damaged opening, which drives the ship motion to react to the situation and varies ship inherent characteristics such as longitudinal distribution of draught and buoyancy along the ship. Further loads due to this process may be increased, and in turn lead to deteriorate structural strength to trigger further flooding. However, although the watertight integrity of the vessel has been compromised, it is a possibility to reach an ultimately stable state if the ship has been correctly designed to survive flooding and analysis of the impact of water loading has been predicted accurately.

At the beginning of the occurrence of damage on the ship hull, high hydrostatic pressure across the area of damage opening drives rapid sea water ingress into compartments and tanks. Since buoyancy at the flooded compartment is lost, the

damaged ship may sink with increasing floodwater. Meanwhile, due to the possibility that floodwater suddenly and violently impacts the flooded compartment, the damaged ship may instantaneously take up a heel angle. After the initial response the floodwater continuously ingresses and egresses from the damaged opening depending on the ship motions and wave conditions. During this stage, which is called the intermediate stage, the ship motions and wave conditions may both have an impact on floodwater dynamics. If the frequency of the encountered wave is close to the natural frequency of response of the ship, even a small magnitude of excitation may result in a violent amplitude of response, which in turn may lead to consequent drastic interaction between ship motions and floodwater. Although a substantial body of research has been carried out on the behaviour and performance of the damaged ship considering the floodwater dynamics, the fundamental mechanisms are still not completely understood due to the highly coupled and complicated dynamics and interactions between floodwater and the damaged ship.

In this chapter, a series of maritime accident involving both commercial and naval vessels are reviewed. Several physical hydrodynamic test tanks/basins that have been used to carry out model tests of damaged ships will be described, by a brief description of the development of numerical wave tanks. Finally, the last section in this chapter sets out the aims and objectives of the present work and outline of the dissertation.

## **1.2 Motivation**

For millennia, ship building and maritime transportation have developed for decades as technologies have developed. Although the loss of Titanic shocks and leaves a lesson to the world even now, driving researchers to investigate the damaged stability of ships, accidents still occur on the ocean.

Ships sailing on the ocean may suffer several types of damage, such as ship-to-ship collisions, raking or grounding, and overload or cargo shift that may result in structure fracture. This section gives a brief description about damage cases for commercial ships and naval vessels due to the collisions, groundings and combatant trauma.

Ship collision and grounding accidents can cause serious damage to the ship hull. Consequently, a large amount of sea water can flood into the compartments from the

damaged opening and the damaged ship can lose her buoyancy and stability gradually. Table 1.1 gives instances of maritime fatalities during the past decades.

Table 1.1 Maritime accidents

<b>Type of damage</b>	<b>Cases(Year)</b>
Collision	Lamma IV(2012)
Grounding	Costa Concordia(2012)
Fire & Explosion	Al Salam Boccaccio 98(2006)
Fracture & Overload	Le Joola(2002)
Severe Weather	Eastern Star(2015), MS Estonia(1994)

- RMS Titanic (1912)

As one of the most famous disasters, the Titanic accident undoubtedly prompted the early development of safer ship design and building technology. The collision between the ship and the iceberg on a morning of April 1912 made it clear to naval architects that safety should be an increased priority for a vessel and that understanding on the stability of a ship is of huge importance.

- Costa Concordia (2012)

Just 100 years after the Titanic sank, a cruise ship, the Costa Concordia, collided with an underwater rock off Italian coast causing massive water flooding into the ship and ultimately capsizing the vessel. The incident indicates that, even with advanced technology and experience gained since the Titanic, accidents can still challenge maritime safety.

- M.V. Derbyshire (1980)

M.V. Derbyshire sunk in the Pacific Ocean as she set course to Japan from Canada encountering Typhoon Orchid at September 1980. According to the investigation report, she was one of the largest UK vessels sunk without giving any distress signal (Heffernan and Tawn, 2003). The ship sank after large loads were exerted on the hatch cover by strong wave impact during the typhoon and, which combined with a basic structural weakness caused structural failure and flooding into the hold. Consequently, flooding led to further damage and a series of flooding and structural failures making sinking unavoidable (Faulkner, 1998; Heffernan and Tawn, 2003). During a lengthy

period of investigation and research, it was found that the design standard for bulk carriers at that moment was not sufficient and should be improved about 35% (Heffernan and Tawn, 2001; Research Excellence Framework, 2014). This tragedy prompted a change in the SOLAS treaty applicable to ships from all the countries in United Nations (Maritime Safety Committee, 2004) to prevent similar tragic accidents happening again.

Combatant vessels are usually treated differently from commercial ships. Combatant ships are needed to be operated as long as possible and must keep a high degree of manoeuvrability and vigilance especially under hostile circumstances. Combatant ships experience some risks different to that experienced by commercial ships such as combatant traumas, from the threats of weapons and attacks that ship may encounter, such as launched weapon (missile and torpedo), underwater explosion, aerial attack and terrorist attack (Brown, 2004 and Hawass, 2015). Table 1.2 presents accidents that occurred on the combatant vessel.

Table 1.2. Naval combatant ship accidents

<b>Naval ship</b>	<b>Causes</b>
USS Cole (DDG-67)	Terrorist Attack
USS Stark (FFG-31)	Missile
USS Liberty (AGTR-5)	Torpedo
USS Higbee (DD-806)	Aerial Attack
USS Tripoli (LPH-10)	Mine
USS Fitzgerald (DDG-62)	Collision
USS John S McCain (DDG-56)	Collision
HMS Nottingham	Grounding

- USS Cole (DDG-67)

USS Cole is a commissioned Arleigh Burke Class destroyer serviced in U.S. Navy. On 12th October 2000, USS Cole was damaged in Aden harbour at Yemen by explosion from a small boat carrying explosives. A large hole at the waterline of the ship was caused by the explosion from the boat through which a large amount of water flooded, and the ship presented an obvious heel to the damaged side. Figure 1.1 and

Figure 1.2 indicate the damage caused by explosion at the waterline, and Figure 1.3 shows water flooding from the damage opening (Brown, 2004).



Figure 1.1 Damaged hole at waterline (Brown, 2004)



Figure 1.2. Damaged hole at waterline (Brown, 2004)



Figure 1.3. Water inflow from damaged opening (Brown, 2004)

- USS Stark (FFG-31)

During the Iran-Iraq War, an armed conflict between Iran and Iraq since September 1980, international shipping lanes and oil marine transportation were threatened by attacks from both Iran and Iraq. To protect the shipping lanes and maritime transportation, naval ships including USS Stark were positioned in Persian Gulf. On the evening of May 17, 1987, two Exocet AM-39 anti-ship cruise missiles launched from an Iraqi F-1 Mirage fighter hit the USS Stark followed by detonation and flame so that USS Stark suffered severe damage (Miller and Shattuck, 2004). Figure 1.4 presents an obvious heel angle after the attack by missiles.





Figure 1.4. Heel after damage (Miller and Shattuck, 2004)

- HMS Nottingham

In July 2002, HMS Nottingham, a Type-42 destroyer built in 1978 belonging to British Royal Navy, grounded on Wolf Rock near Lord Howe Island at north east of Sydney while heading to New Zealand from Australia. A large raking damage at most of the bow led to substantial flooding in the ship. Figure 1.5 and Figure 1.6 show the severe raking damage to the forward part of the hull. Figure 1.7 presents a flooding scenario in forward machinery room (Bole, 2007).



Figure 1.5. Tear damage (Bole, 2007)

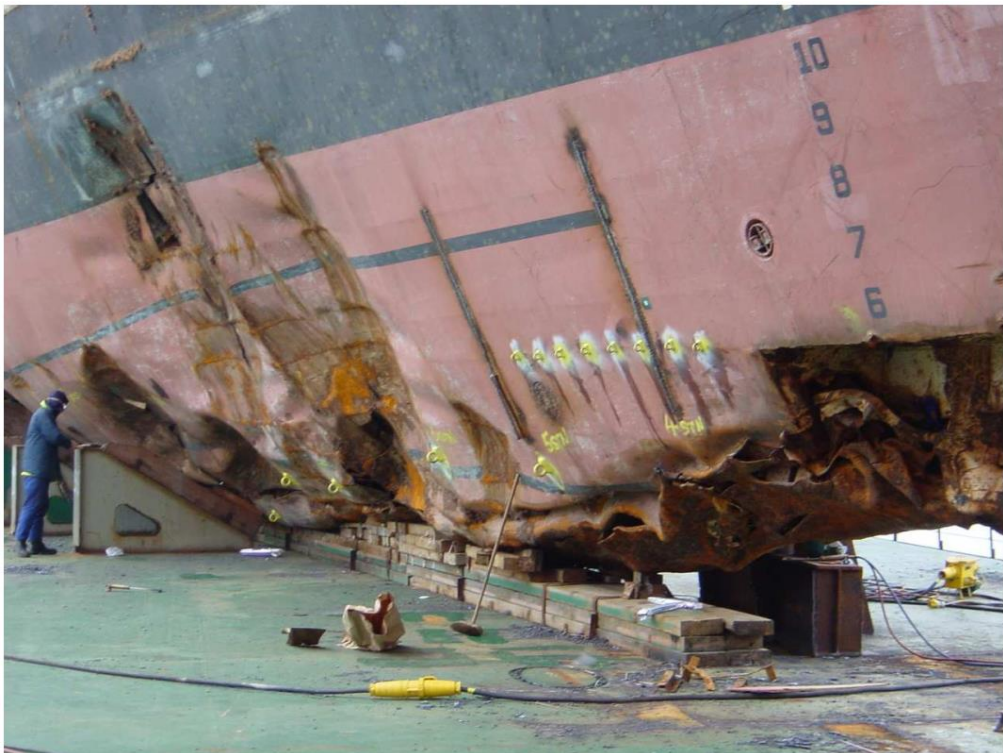


Figure 1.6. Severe damage (Bole, 2007)



Figure 1.7. Flooding into engine room (Bole, 2007)

- USS Fitzgerald (DDG-62) and USS John S McCain (DDG-56)

USS Fitzgerald (DDG-62) and USS John S McCain (DDG-56) are both Arleigh Burke Class destroyers in U.S. Navy. Fitzgerald suffered a collision at June 2017 with a container ship at Sagami Wan, while John S McCain collided with an oil and chemical tanker in the straits of Singapore at August 2017. According to the report by Department of the Navy of USA (2017), collisions occurred at the forward of the middle part of USS Fitzgerald on the starboard side and a hole below the waterline that allowed water to flood into the compartments was caused by the hit from bulbous bow. Due to the damage flooding, USS Fitzgerald presented a 7-degree heel angle to starboard, while draught had also increased. Figure 1.8 shows the collision damage to the starboard of Fitzgerald. The collision for USS John S McCain occurred at the port aft portion; the impact of the collision produced a large hole at the waterline causing serious flooding due to the bulbous bow, so that it is reported that McCain presented a 4-degree heeling to the portside within 15 minutes after damage. From Figure 1.8, it can be clearly seen that a large hole above and below waterline located at the portside of John S McCain due to collision.



Figure 1.8. A large damaged opening causing flooding (Department of the Navy of USA, 2017)

### 1.3 Damaged ship stability

It is critical to the design of safe and effective ships that they can withstand sudden and progressive external and internal loads acting on it after suffering a structural damage. Damage stability is therefore a critical attribute of ship design. Damage may occur due to several reasons, including:

- Collisions:  
Collision is a common phenomenon associated with maritime accidents occurring on busy sea routes.
- Grounding:  
Grounding typically occurs due to crew error in estimating clearance between lower part of the ship hull and the sea bed or rocks.
- Structural damage:  
Structural damage may involve many aspects, which may be caused by the loss of structural integrity due to damage or corrosion or local excess stress due to inappropriate loading.
- Environmental condition:

Rogue waves, storms, heavy weather, strong wind, etc. are all demanding conditions for leading to extreme loads on a ship navigating in a seaway.

If a ship is damaged seriously due to one or more of the above causes, the ship hull is usually breached, and therefore, the ship's watertight integrity will be affected. This in turn will lead initially to water flooding into damaged internal compartments, especially when the breach is located below the waterline. Further progressive flooding may then occur, which can ultimately lead to the total loss and capsize of the ship. This process becomes more complicated if we take the dynamic behaviour of the ship into consideration.

The effect of water flooding on the damaged ship can be considered as:

- Hydrostatic change

When water floods into the compartment, the damaged ship loses buoyancy which causes an increase of the draft, until a new equilibrium is reached. The increase in draft also drives the reduction of freeboard.

- Stability

Due to flooding the centre of buoyancy (KB) typically rises, and the damaged ship may have a different waterplane area ( $A_w$ ), and consequently a new BM. Hence the metacentric height of the ship changes. At the same time, dynamics of floodwater can also be considered as a load that drives ship behaviour, especially during transient and progressive flooding stages.

- Attitude

If the compartment that water floods into is not symmetric about the centreline of the ship, the ship will heel, and the trim of the ship may be changed. This is especially problematic when combined with the reduction of freeboard as mentioned above, since a low freeboard combined with a heel angle may trigger large amount of water to submerge the deck, with a resulting loss of stability.

The modelling for the damaged ship stability in this study can be decomposed and categorized into several aspects based on the key elements of the problem the environmental conditions, the ship motions and the water dynamics in the flooded compartment. These three sub-problems form the subject of the current study for the

damaged ship in regular beam seas. Given the methods of modelling these individual problems characterize the different situations, the study of the intact and damaged ship in regular beam waves can be considered numerically and experimentally as related to:

- Wave generation in a water tank.
- Ship motions in the calm water and regular beam waves.
- Water dynamics in the flooded compartment, i.e. the sloshing phenomenon under the wave excitation.

There are two common methods to estimate damaged ship stability:

- Lost buoyancy method:

As mentioned above, the floodwater increases the ship's draft to compensate the loss of buoyancy. The ship buoyancy is redistributed as draft increases but most of the ship particulars (displacement, GM, KG, mass moment of inertia, etc.) remain the same as in the intact case.

- Added weight method:

The method takes the floodwater as an additional weight at a particular location in the ship, and thus, ship's particulars should be evaluated counting in the effect of floodwater in the compartment. However, since the water flooding varies from moment to moment, this method is iterative and can be time consuming compared with the other one.

## **1.4 Physical model test in water tank**

Physical model tests in water tank and basin can play a significant role for investigation into ship hydrodynamics. It is an important method to test the hydrodynamic performance of ships and offshore structures and provide information for the validation of theory and numerical prediction. This section briefly gives an introduction about model tanks and marine experiments.

The size of ships and offshore structures nowadays varies from a few tonnes (tug or yacht) to hundreds of thousands of tonnes (ULCC), and the process to bring ships and offshore structures from the initial design, through construction to come into service is a complicated process that needs substantial and long-term investment of time,

money and effort, physical experiments in model basins are often used to avoid and/or fix undesirable errors.

Due to the demand of physical model tests, many kinds of model basin and towing tanks are established among maritime states worldwide. Several well-known towing tanks and basins are listed in the Table 1.3 shown as below.

Table 1.3. Widely known water basin

<b>Tank / Basin</b>	<b>Location</b>	<b>Dimension</b>
MARIN	Netherlands	252m×10.5m×5.5m
QinetiQ	United Kingdom	270m×12.2m×5.4m
KRISO	South Korea	221m×16m×7m
SINTEF	Norway	260m×10.5m×5.6m
CSSRC	China	474m×7.5m×7m
VTT	Finland	130m×11m×5.5m

Model tests in physical model basin allow the dimensions of ship and offshore structure to be scaled based on a similarity law, while physical characteristics can be maintained. This allows visualisation to make model behaviour clear under the desired wave conditions. Meanwhile, measured data from model tests allows valuable validation for design, optimisation and numerical simulation.

Objectives of model tests can be listed as below:

- Seakeeping and manoeuvring performance
- Propulsion and resistance characteristics

Model tests for stability of a ship are carried out to determine ship model's behaviour and wave loads acting on the ship model. It includes investigation of loss of static and dynamic stability, as well as dynamic rolling, parametric excitation, resonance excitation and so on. Generally, it is expected that the damaged ship model will survive under the critical damage scenario and wave condition. Wave conditions such as regular and irregular waves, and even extreme waves are generated to establish thresholds for the ship's motions and loads that may result in capsizing.

## **1.5 Numerical investigation**

Although the physical model test plays a unique role in naval architecture, a large investment in facilities and models may be required. Accuracy and error due to the limitation of equipment and measurement are also factors that need to be considered. A numerical wave tank, however, may be a good alternative method with increasing feasibility and reliability. Use of a numerical wave tank to obtain required data for the whole flow field around structures in flow domain provides a good way to complement a physical experiment.

Water waves, as a gravity wave along the surface of liquid, can be taken as an interface between two kinds of fluid (or phase) with different densities, namely the liquid phase and the gaseous phase. Since many important hydrodynamic investigations require excitation of the ship by waves, researchers have developed numerical wave tank for the study of ship hydrodynamic performance with a range of wave generation methods such as wave-maker modelling method, momentum source method and velocity-inlet wave making method.

To model the complicated free surface problem of the interaction of waves in a numerical wave tank with a damaged ship, correct modelling of viscous effects is essential. With the dramatic development of computing technology, Computational Fluid Dynamics (CFD) becomes an attractive method to study complex fluid-structure interaction (FSI). Better insight into the mechanism of complicated fluid flow with prediction of hydrodynamic performance and analysis of fluid field can be helpful for ship design and optimisation.

## **1.6 Research aim and objectives**

The aim of the project is to gain insight into the non-linear behaviour of damaged ships in terms of motions and hull girder loads via physical experiments and to explore the capability of predicting these non-linear responses by using RANS CFD method. The main focus of this work is the estimation of the performance of the ship in the intact and damaged condition, and in particular, the influence of the damage on the ship motions and hull-girder loads.



The CFD method is adopted in order to allow detailed modelling of regions of flow for which viscous forces exert a substantial influence on the ship motions and hull girder loads, such as the flows in the region of the sonar dome, and the flows in and out of the damage compartment. The impact of these flows on the motions and loads could not be predicted accurately in a traditional seakeeping analysis using potential flow codes.

The CFD results can also yield insight into local flows in these areas, but the scope of the present study in terms of both simulation and physical measurement is focussed on the global responses.

The objectives of the project are:

- ❖ To identify key mechanisms associated with the behaviour of a damaged ship and model these mechanisms using RANS CFD method.
- ❖ To validate these models against published data
- ❖ To carry out a physical model test campaign of an intact and damaged Naval Combatant vessel in regular beam seas measuring non-linear behaviour in motions and hull girder loads
- ❖ To solve the intact and damaged behaviour of the ship using RANS CFD and compare with model test data in order to explore the capability of CFD as a seakeeping tool for assessment of stability and survivability of damaged ships.

## **1.7 Outline of the thesis**

This thesis is separated into six chapters. A brief introduction including cases of accidents and the use of physical and numerical tests has been given in Chapter 1. A critical review about the study of stability and survivability of ships and investigation on performance and wave induced loads of intact and damaged ships with physical experimental method and numerical calculation method are presented in Chapter 2. Chapter 3 mainly concentrates on the procedure of physical model tests carried out in the present study. The complicated damaged flooding problem can be decomposed into several individual 2-dimensional case studies, which is investigated using CFD-based unsteady RANS solver, Star CCM+ and demonstrated in Chapter 4. Adopted scheme with CFD method is described with general remarks for using unsteady RANS

solver with Star CCM+. Regular wave generation in numerical tank, water sloshing in a tank, free roll motion decay and wave excitation of a float body are investigated in two dimensions. Integrated investigation on performance of intact and damaged ship in calm water and regular beam waves are described in Chapter 5. Methodology is conducted and proposed to assess wave-induced loads acting on the intact and damaged ship, feasibility is verified with comparison between results obtained by numerical method and experiment. The conclusions of the whole work, and suggestions and comments about the further study on estimation of wave-induced loads by numerical and experimental method will be given in Chapter 6.

## 2. Literature Review

In this chapter, a critical review of the related studies about damaged ship stability is presented.

### 2.1 Inspiration for passenger ship safety investigation

In the past decades, Ro-Ro and cruise vessel accidents showed that stability of passenger ships was an important area for investigation for naval architects and researchers. Accidents to ships such as the European Gateway, the Herald of Free Enterprise, MV Estonia and Express Samina illustrate that potential danger still exists for capsize and loss of lives onboard. Driven by maritime accidents, investigations to develop knowledge on ship survivability and stability have accelerated since the 1980s.

The accident to the European Gateway occurred in 1982 when it suffered a collision with a ferry named Speedlink Vanguard. The official report based on the accident investigation was published by NMI (1983) (National Maritime Institute of United Kingdom, now named British Maritime Technology). Another technical report investigating the accident was published by Arndt (1983) on behalf of a German consultant company employed by the operator of European Gateway.

The idea of the transient asymmetric flooding phenomenon, which plays a significant role at the initial flooding stage, was firstly developed by Spouge (1985) through investigation into the sinking of European Gateway. The height of water was integrated to calculate the volume of floodwater in the flooded compartment, and the free surface inside the compartment was treated as an equilibrium surface. A quasi-static method was applied, and hence the ship was regarded as a static equilibrium system at each time step in calculation.

A study on European Gateway accident was also attempted by Santos et al. (2002) applying numerical modelling simulation and experiment to transient asymmetric flooding. Three obstacles were regarded as generators to divide generator room into sub-compartments in order to approach reality in the numerical simulation. Experiments showed that due to the obstacle inside the flooded compartment, floodwater could accumulate and result in a transient heel angle. By mathematical

modelling, a non-linear coupled equation set was employed to calculate the six degree of freedom motions while hydrodynamic force components were treated by a potential-flow method. Although the viscosity and water flow effect were taken into account, the water surface of floodwater inside the flooded compartment was forced to be horizontal. With the increasing damaged opening and further flooding, it was highlighted that accidents could potentially occur for a Ro-Ro ship under these circumstances.

The Ro-Ro passenger ferry Herald of Free Enterprise at Zeebrugge capsized on 6 March 1987, with the loss of 188 lives. Official investigation into the accident was reported by Department of Transport (1987). Vandeveld (2006) studied the accident, viewed from aspect of the maritime rescue. It is found that due to the complexity of ship structure rescue diving and medical aid were extremely difficult. Parker (1987) reviewed the capsizing of the ship considering factors that had influenced the sinking including ship structure, ship operations and manoeuvrability.

Dand (1989) reviewed the sinking of the passenger ferry Herald of Free Enterprise in order to investigate the influence of hydrodynamic aspects on the capsizing. The asymmetric flooding aspect was taken into consideration as the centre of gravity of floodwater was varied in the flooded compartment. The flooding process was simulated by a program NMIFLOOD, which was developed by NMI. The same program was also employed to study the European Gateway accident. A similar modelling method was employed by Sen and Konstantinidis (1987) to investigate the survivability of a Ro-Ro ferry under the damaged situation.

The accident to M.V. Estonia took place on 1994 on the Baltic Ocean because of severe weather and loss of structure integrity. The damaged bow visor was lost resulting in a large amount of sea water flooding into the vehicle deck through the opening. This accident was regarded as a typical case inspiring enormous effort into research on damaged stability and flooding of passenger/Ro-Ro vessels. Figure 2.1 shows the Estonia with bow visor opened. The accident was reconstructed by experts for investigation on the cause leading to the capsizing and loss of the ship by Kehren (2009) and Valanto (2009).

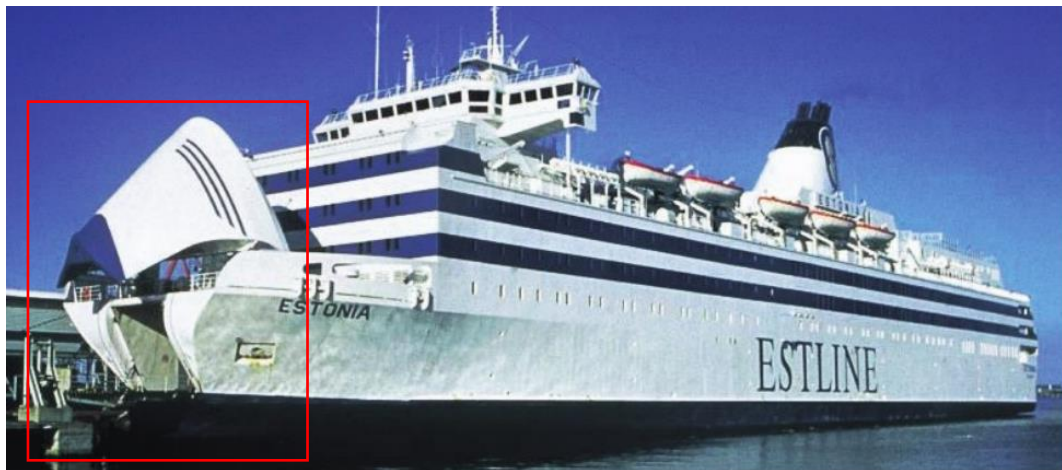


Figure 2.1. MV Estonia with bow visor opening (Jaeger, 2008)

A research report was published by SSPA Consortium (2008) (SSPA - the Swedish State Shipbuilding Experimental Tank) to investigate the sinking of MV Estonia experimentally. To take the progressive flooding inside the damaged ship into consideration, a model of the decks was made to fill with floodwater. In order to eliminate the effect of trapped air, ventilation pipes were installed as shown in Figure 2.2. A 40-scaled physical model was employed to investigate the sinking of Estonia with different Froude numbers, shown in Figure 2.3.

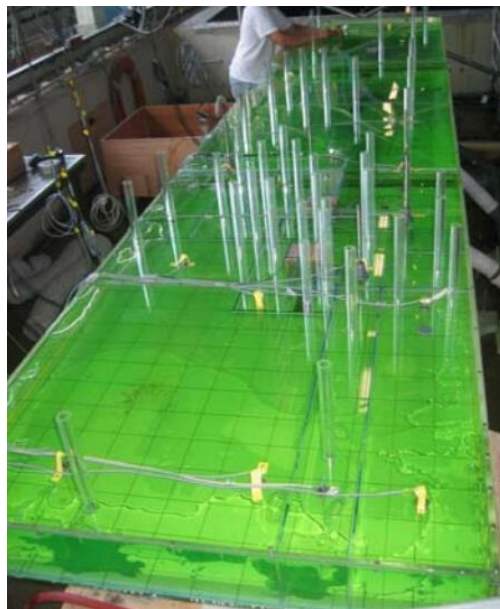


Figure 2.2. Flooded compartments during progressive flooding (SSPA Consortium, 2008)



Figure 2.3. Physical Ro-Ro ship model for reconstruction of Estonia (note the visor attached at bow) (SSPA Consortium, 2008)

A further numerical study was carried out by Jasionowski and Vassalos (2011) on the mechanism of the capsize of Estonia. Floodwater dynamics inside the ship and floodwater-ship interactions were taken into consideration. The sinking of the passenger ferry Express Samina after damage was investigated mainly by Papanikolaou et al. (2004) with a time domain simulation during the progressive stage of flooding.

## 2.2 Flooding procedure investigation

After a ship is damaged, it may suffer three main flooding stages, namely transient stage, progressive stage and final stage (Ruponen, 2007). Figure 2.4 shows the heel angle of flooded ship during the three main stages of flooding procedure.

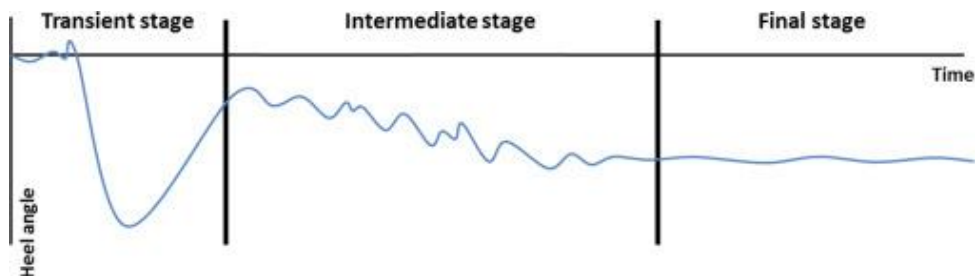


Figure 2.4. Main flooding process (Ruponen, 2007)

In the transient stage, due to sudden damage such as collision, grounding and explosion, ships lose their watertight integrity, and subsequent floodwater ingresses from the damaged opening. It is a complex flooding process that contains a wide range of factors to affect further behaviour of floodwater. If a large amount of water floods into a compartment after damage creation, a large heel angle may appear suddenly due to the added heeling moment and probable impact load acting on the damaged ship (Vermeer et al., 1994). In turn, the transient heel angle can have an influence on further flooding. Khaddaj-Mallat et al. (2011) stated that if the frequency of sloshing of floodwater in the flooded compartment was almost consistent with the frequency of the ship's roll motion, a large amplitude of floodwater behaviour could be produced, but on the other hand, it actually had a damping effect to decrease roll motions at other frequencies. In addition, during the transient flooding stage, other phenomena can occur due to the rapid heeling such as cargo shift, collapse of internal structure and cross-flooding, which can have an impact on further flooding. So that in this stage, dynamic behaviour cannot be ignored as the transient heel angle may directly cause the ship to be non-recoverable. Vassalos et al. (2004) found that stability could be lost, and ship might sink during the transient stage of flooding for a damaged large passenger ship.

A quasi-static method was used by Vredeveldt and Journée (1991) to investigate the roll motion of a damaged ship after sudden flooding. Heave and pitch motions were treated quasi-statically, but the dynamic effect on roll motion was taken into consideration. The study revealed that dynamic effect on damaged ship's roll motion caused by transient water flooding should be considered.

Spanos and Papanikolaou (2001a) numerically and experimentally investigated damaged ship motions as floodwater suddenly flowed into one compartment. The study considered the effect of a double bottom, and two model arrangements, one with single bottom and the other with double bottom, were employed both in numerical and experimental method. It was found that the transient flooding stage could be dominant to the whole flooding process as it determined the damaged ship's final equilibrium state including capsizing. The conclusion according to Spanos and Papanikolaou was made to emphasize the importance of investigation on initial flooding since it had a significant impact on estimation of damaged ship behaviour in waves. A similar

conclusion was made by Vassalos et al. (2004) based on the experimental and numerical investigation on a large passenger vessel. In their study, the mechanism of transient flooding in a large passenger ship with a virtual inner layout of compartments was simulated.

Transient asymmetric flooding, firstly proposed by Spouge (1985) as mentioned above, can suddenly result in an extremely large amplitude of roll motion because of the obstacles in the flooded compartment. An experimental study by Santos et al. (2002) showed that a damaged ship could capsize due to the transient asymmetric flooding. A similar conclusion was made according to the studies by Vredeveltdt and Journée, (1991) and Macfarlane et al. (2010).

Since water suddenly ingresses via damaged opening, floodwater can continue flooding into the adjacent compartments via internal non-watertight openings such as windows, doors, pipes and vents. This stage of flooding is named the progressive phase, and it is of significance for damaged ship survivability as progressive flooding may result into capsizing (IMO, 2003). Sometimes, a so-called intermediate flooding stage is alternatively used to describe the transient stage and the progressive stage, and it is meaningful to investigate flooding mechanism on intermediate or progressive stage for damaged ship.

During the intermediate stage, floodwater may uninterruptedly ingress and egress through the damaged opening. At this stage, floodwater affects ship motions so that the interaction results in a highly nonlinear behaviour of the ship (De Kat et al., 2000; Santos and Guedes Soares, 2008a and Vassalos, 2000). Taking the effect of progressive flooding into account, leads to much more complicated behaviour of damaged ships since progressive flooding and floodwater dynamics are highly coupled and can have a significant impact on each other (Khaddaj-Mallat et al., 2009; Palazzi and De Kat, 2004; SSPA Consortium, 2008). In addition, according to Journée et al. (1997), the impact of the inflow momentum and the flow propagation inside the flooded compartment should also be considered when investigating the intermediate flooding for a damaged ship.

Kim et al. (2017) developed a time-domain method to simulate intermediate flooding and capsizing of a damaged ship. A box-barge hullform was utilized to validate



feasibility of the method considering the intermediate flooding stage and the final equilibrium situation. According to the study the intermediate stage required extensive investigation to assess the motions of flooded ship and was more challenging and fickle than other stages. Damage creation is not taken into consideration, and the sea state was assumed to be calm during simulation. Another aspect neglected in the simulation which might affect flooding and behaviour of the damaged body was the hydrodynamic effect of floodwater inside the flooded compartment. Since quasi-static method was applied to floodwater, fluid flow was treated based on potential theory, and dynamics of free surface was ignored.

An experimental investigation on a passenger ship model was carried out by Ikeda and Ma (2000) addressing the large amplitude of rotation angle occurring after sudden flooding. A double bottom was created, and obstructions were placed inside the flooded tanks. It was noted that the amount of floodwater flooding into the damaged compartment from the beginning until the damaged opening was completely submerged may play a significant role to determine the angle of inclination of the damaged ship. They also concluded that during the intermediate flooding stage, the damaged ship's roll motion could be decided by many aspects such as the arrangement inside the flooded compartment and the size and location of the damaged opening. It was found that the floodwater flow forced a heeling to the undamaged side, and roll motion, on the other hand, could slow down the flow of water into the flooded compartment by lifting the damaged opening above the water surface when it rotated to the undamaged side. Similar phenomena were observed by De Kat and Van't Veer (2001), Ikeda and Kamo (2001), and Ikeda et al. (2003).

### **2.3 Experimental investigation**

Model tests have been carried out by many researchers and institutes on the damaged stability of vessels. Reliable physical tests are indispensable for validation of numerical methods. There have been several representative attempts to investigate damaged ship behaviour with physical ship model tests, taking the interaction between damaged ship motions and floodwater dynamics, internal tank arrangement and so on into consideration (Cotton and Spyrou, 2001; Palazzi and De Kat, 2004; Chan et al, 2002).

A simplified 4-metre box shape barge (firstly developed by Ruponen, 2006) was employed by Manderbacka et al. (2015a and 2015b) for investigation of the transient motion of a damaged vessel during flooding. Two flooded compartments were installed in the midship of the ship model and tested separately with divided (Room 21 on the right) and undivided (Room 11 on the left) spaces, as shown in Figure 2.5. A square damaged opening was placed at each flooded compartment, which controlled the different flooding case, to investigate the effect of divided and undivided compartments during flooding, shown in Figure 2.6. During the physical tests, different amount of water within the different flooded compartment were investigated, in free roll decay tests. Experimental results showed that the internal layout of the flooded compartment had a significant influence on the damping of rotational motion, and consequently the period of motion. The same conclusion was made by Van't Veer et al. (2011). However as mentioned above, the tests were carried out in calm water so that the effect of wave excitation was not considered. Another point highlighted from the tests was the role played by floodwater as a non-rigid body inside the flooded compartment with the different centre of mass and with inertia varying with time. Therefore, floodwater had to be treated as another degree of freedom motion when investigating damaged flooding for a ship.

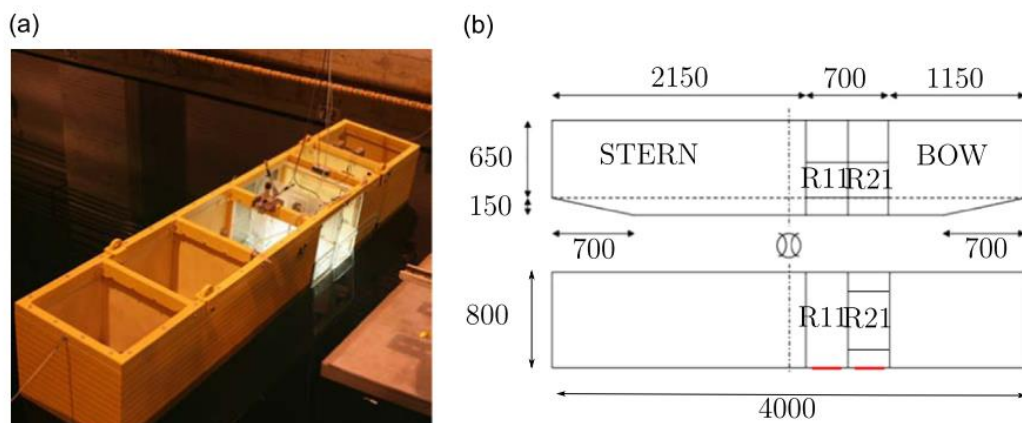


Figure 2.5. Experiment setup. (Ruponen, 2006)

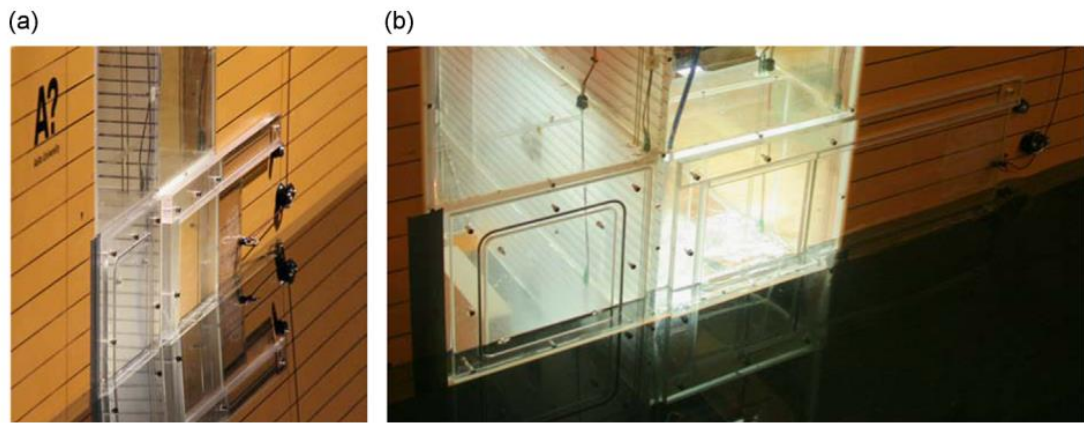


Figure 2.6. Flooding control mechanism (Manderbacka et al., 2015b)

A similar model test was performed by Ruponen et al. (2007) for validation of a numerical method. In their test, water flooded into the model via one damaged opening and the sea state was kept calm during the intermediate flooding stage. A bottom damage scenario was tested with a box barge model by Santos et al. (2009). The damaged opening was located at the bottom of the physical model. Besides, double bottom and trapped air compression were considered.

It was presented by studies that the difference in flooding and ship behaviour between undivided compartment and divided compartments was obviously large, and flooded compartments had a significant effect on floodwater and ship motions (Acanfora and Cirillo, 2017; Gao et al., 2011; Manderbacka and Ruponen, 2016 and Strasser et al., 2009).

Lee et al. (2016) employed an experimental study on damaged ship motions with a scaled passenger ship model. A square damaged opening was positioned at the midship of starboard side, and two tanks could be flooded due to damage, as shown Figure 2.7. The experiment aimed to provide a benchmark database study for validation of further numerical methods, and many aspects could be used for reference and simulated from the experimental investigation. It should be noted that the bow and stern of the ship model were moored, therefore, the ship model was not free to drift; however, the mooring force acting on the ship model was measured. Another highlighted point was the damage creation. As shown in Figure 2.8, an opening gate was controlled by an air cylinder so that measurement could be carried out immediately after the gate was opened to simulate a rapid damage on the ship hull. Therefore, in this case, the whole

flooding process could be studied. However, regular beam waves generated by the wave maker encountered the ship on the undamaged side, which indicated that the beam waves did not directly flood into damaged compartment through the damaged opening, so that transient heel angle did not appear.

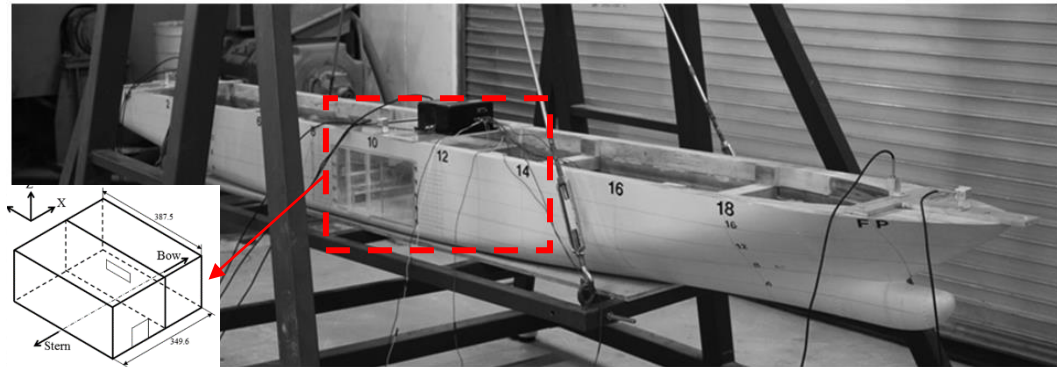


Figure 2.7. Ship model with a sketch of internal flooded compartments (Lee et al., 2016)

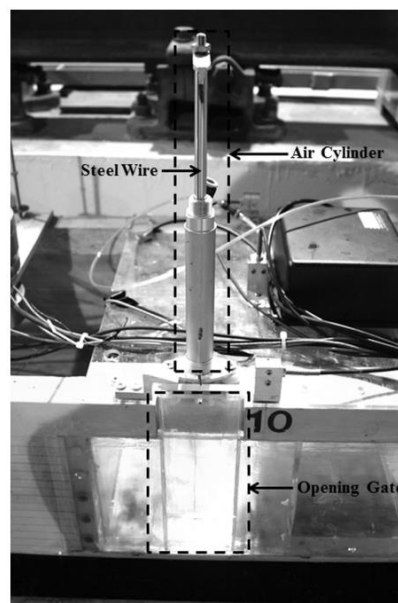


Figure 2.8. Rapid damage opening indication (Lee et al., 2016)

The same ship model was also tested by Lee et al. (2012a) and Cho et al. (2010). It was found in free roll decay tests that for the damaged ship the floodwater dynamics acted as a damper to increase the period of ship's roll motion, as also concluded by De Kat et al. (2000), Papanikolaou (2001) and Papanikolaou and Spanos (2004).

A series of tank model tests of a damaged Ro-Ro ship model were carried out by Spanos et al. (2002a). During the tests, different damaged locations (intact or damaged vehicle compartment) and various sea conditions (regular or irregular beam seas) were chosen depended on the damaged cases. It was found that the amount of water accumulated in the damaged compartment had little impact on the heave motion.

The behaviour of a large passenger ship was investigated experimentally by Ikeda et al. (2003). The roll motion due to the transient flooding in the intermediate stages was monitored and various flooding cases due to the different flooded compartments were taken into consideration. It was found that not only the amplitude of transient roll motion, but also the time to arrive at final equilibrium state could be strongly affected by the internal arrangement.

For passenger Ro-Ro ships, violent motions of the floodwater can appear especially during flooding on the vehicle deck as there are typically no substantial barriers at vehicle deck level, e.g. watertight bulkhead or divided compartments to prevent the flows of floodwater and decrease the effect of free surface. These phenomena can be observed by experimental investigation on passenger ship models that employed by Chang and Blume (1998), Dand (1994), Ishida and Murashige (1997), Molyneux et al. (1997) and Stubbs et al. (1996).

To study the dynamic effect of the floodwater on deck, a model experiment was carried out on a scaled passenger Ro-Ro ship model by Fujiwara and Haraguchi (2002). As shown in Figure 2.9, the ship model was softly constrained. Vertical and longitudinal translational movements were restricted by lines and springs, but the ship model could freely roll and drift due to the wave excitation. A damage opening was located at the starboard amidships, and two decks were installed to model the vehicle decks typically found in modern Ro-Ro vessels. In two free decay tests with and without floodwater on deck, to give a better insight at the effect of floodwater, the amount of floodwater on deck was varied. Experimental results indicated that floodwater on deck could have a non-linear effect on the damaged ship's roll motion. It was also noted that to investigate behaviour of damaged ship in beam waves, the dynamic effect of floodwater must be taken into consideration as it significantly influenced damaged ship motion.

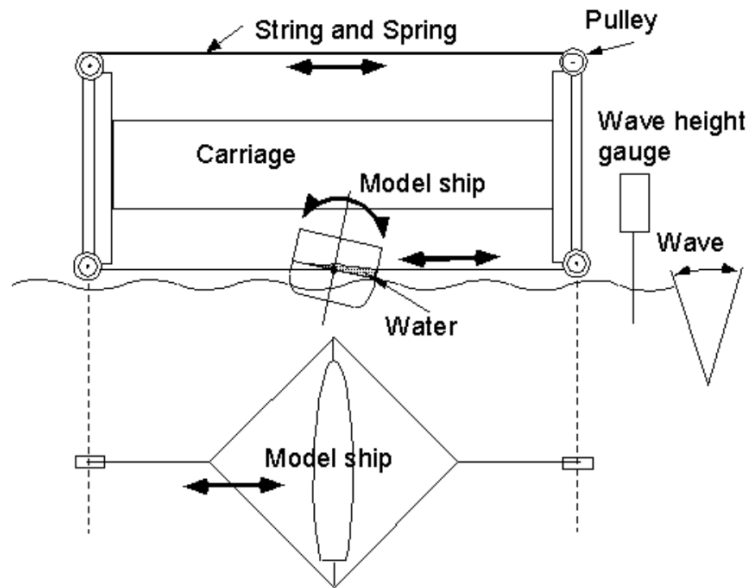


Figure 2.9. Sketch of experimental settings by Fujiwara and Haraguchi (2002)

More physical model tests to investigate the dynamic effect of water on deck on damaged ship behaviour can be seen in Papanikolaou et al. (2000 and 2004), Santos and Guedes Soares (2008b).

On the other hand, flooding into compartments has also attracted attention, and research on the different conditions of flooding into different compartments has been carried out with both experiments and numerical methods. It is worth mentioning an experimental investigation on flooding mechanism by Khaddaj-Mallat et al. (2012). A complex but more realistic damaged scenario was reconstructed – complicated flooded compartments including generators and engines, shown in Figure 2.10. A damaged opening mechanism was also contained. Intermediate flooding with the effect of double bottom, the internal layout of compartments, obstructions in flooded space and trapped air compression were taken into consideration. The experimental results revealed a high coupling effect between floodwater dynamics, trapped air and damaged ship behaviour, which dominated the flooding physics of a damaged passenger ship.

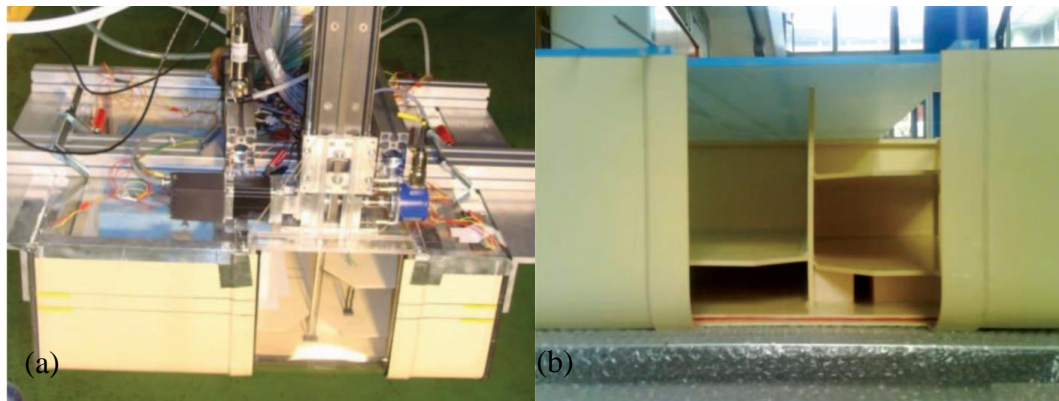


Figure 2.10. (a) Flooded compartment with opening system; (b) Internal view at flooded compartment (Khaddaj-Mallat et al., 2012)

An engine room was physically modelled, and progressive flooding was investigated by Veer and De Kat (2000). Blocks replaced engines and gearboxes as obstructions in the flooding tests shown in Figure 2.11. Result indicated that large obstructions played an important role to the transient flooding. Moreover, obstructions could significantly affect floodwater dynamics in flooded compartment, and thus needed to be carefully modelled. A similar conclusion was reached by Armenio et al. (1996a and 1996b) based on experimental investigation of a baffled and unbaffled tank.

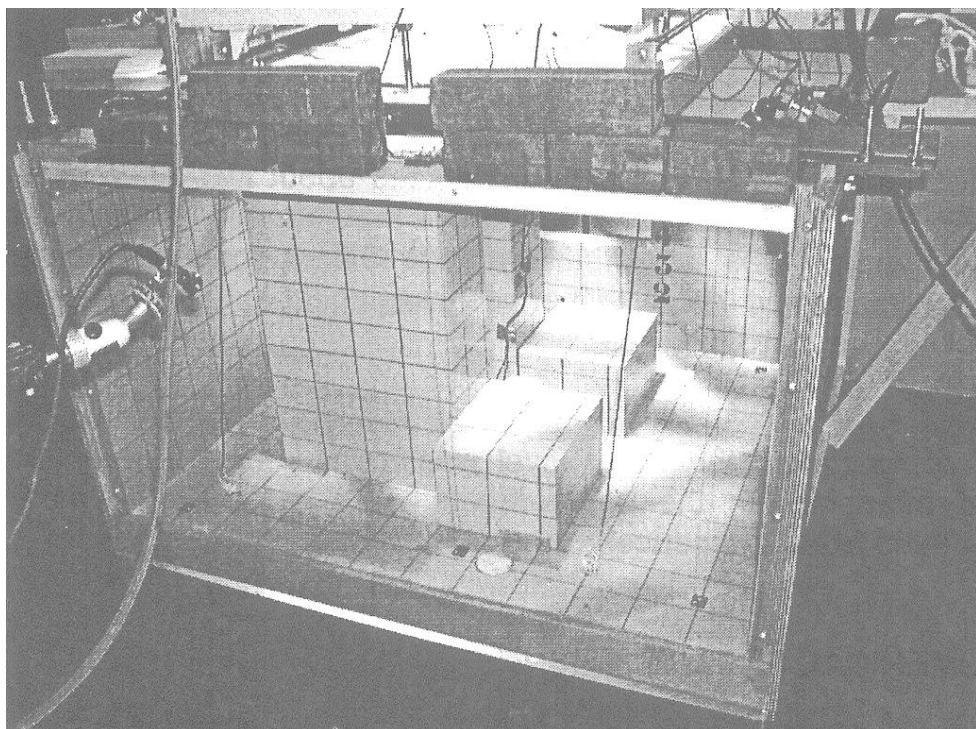


Figure 2.11. Large flow obstructions in flooded compartment (Veer and De Kat, 2000)

Warships, different from commercial ships, may have a high possibility of experiencing another type of damage, i.e. trauma from launched weapons such as torpedoes and missiles; therefore, investigation of the stability and survivability of damaged combatant ships is of current relevance. The transient effect of floodwater on a frigate model was investigated by Macfarlane et al. (2010). A 1/45-scale frigate model was used with a latex membrane material on the damaged opening to allow simulation of transient damage. Domeh et al. (2015) carried out experiments with a Leander class frigate model in a towing tank to study the damaged ship motions in waves considering different compartment permeability. Equipped with full appendages, a 5-metre-long Leander class frigate model with relatively complex layout of the internal compartments was presented in experiments under the different loading conditions and sea states (De Kat and Peters, 2002 and Palazzi and De Kat, 2004). Other towing tank tests were undertaken with Leander class frigate models to investigate the performance of damaged combatant ship considering the effects of regular and irregular waves, different damage positions and forward speeds (Bennett et al., 2013 and 2014, Bennett and Phillips, 2017).

## **2.4 Sloshing and its coupling effect combined with behaviour of water tank**

After a damage event which results in floodwater entering into internal compartments, the dynamic behaviour and loads that the damaged ship experiences are not only due to the external hydrodynamics and the solid inertia, but also the dynamics of the water sloshing in the flooded tanks. In this section liquid sloshing and its coupling effect with ship motions are addressed.

Liquid sloshing in the water tank may be regarded as a type of wave motion. The dynamics of the water sloshing is a complicated, and sometimes unpredictable phenomenon itself. Therefore, it is desirable to investigate the sloshing by physical experiment. To test water sloshing effect on partially water-filled tanks, experiments were developed by Mikelis (1984), Akyildiz and Ünal (2005 and 2006) and Nasar et al. (2010). Ji et al. (2012) investigated the two-dimensional fluid behaviour in a rectangular tank, shown in Figure 2.12, with the aid of the time history of wave elevation and surface profile captured by a high speed camera. Experiments considered



a nonlinear system that frequency of the tank is different from the resonant frequency of water inside. An easy-to-visualize water container was driven by a crank system, which was rotational and powered by a motor. Therefore, the tank could move harmonically to produce lateral water sloshing movement. PIV (Particle Image Velocimetry) technique was also applied to obtain the flow field in the tank.

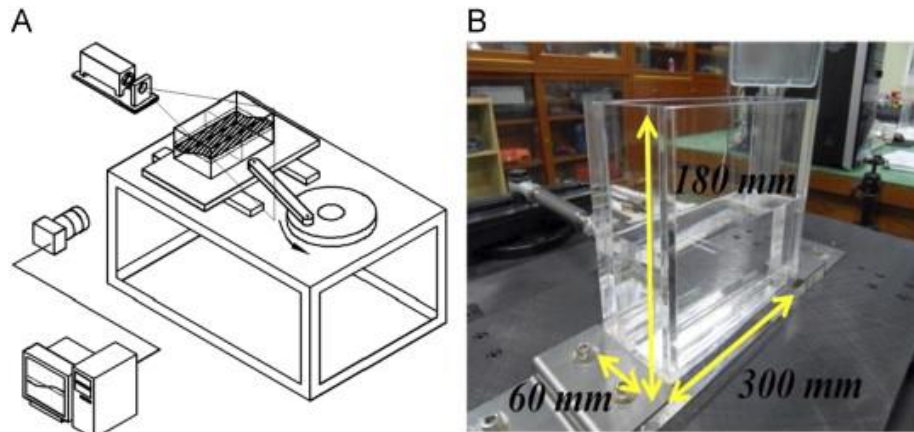


Figure 2.12. Model tests setup by Ji et al. (2012)

A scaled LNG-FPSO model was equipped with two partially water-filled tanks as shown in Figure 2.13 in a series of model tests by Nam and Kim (2007). The three-dimensional coupling effect between water sloshing and model behaviour was investigated and it was observed that liquid sloshing effect on pitch and heave motions was not extreme in head seas. It was also found that the impact pressure due to the coupling effect between liquid sloshing and ship motions was dependent on the natural frequencies of sloshing and wave excitation. Compared with Nam and Kim's results, Zhuang et al. (2016) further investigated modelled the fully coupling dynamics numerically via a CFD method considering five different filling levels (including empty tank), and observed that amplitudes of heave and pitch motions were both increased due to the water sloshing in the tank.



Figure 2.13. LNG-FPSO model (Nam and Kim, 2007)

The interaction between liquid sloshing and ship behaviour has been studied by many researchers. An experimental investigation of coupling effects was carried out by Rognebakke and Faltinsen (2003) and Nasar et al. (2008). The interaction between liquid and ship motions was investigated by Mikelis and Journee (1984) experimentally and numerically. Zhao et al. (2014a) coupled nonlinear sloshing dynamics with linear ship motions based on experiments with a FLNG tank model and a boundary element method. A similar result was obtained by Francescutto and Contento (1994), Lee and Kim (2010) and Zhao et al. (2014b). They pointed out that sloshing effect on the ship motions, especially on roll motion, could act as a damper and can be designed to achieve an anti-rolling damping effect on ship motions. The coupling effect between liquid motion and ship behaviour was studied using potential theory considering linear sloshing and nonlinear ship motions (Wang and Arai, 2011), nonlinear water dynamics in the tank with linear ship behaviours (Kim et al., 2007 and Malenica, 2003) and fully nonlinear coupling system (Chen and Chiang, 2000 and Mitra et al., 2012). Tang (1991) developed a method to estimate 2-dimensional forced roll motion in beam seas based on the potential theory. Four different types of two dimensional hullform were used to investigate the effect of nonlinear variation of wave damping and restoring moment. Nonlinearity within wave excitation, added mass, damping and restoring moment was investigated and it was pointed out that if large amplitude of ship motions was taken into account nonlinear system should be deployed. It was also reported by Lee et al. (2007a) and Bass et al. (1985) that the effect of the turbulence and viscosity of the water in the tank was not influential on impact pressure.

A number of researchers have investigated the impact of sloshing on the floating body motion by numerical and experimental methods. Numerical methods, such as potential theory (Kim et al., 2003; Lee and Choi, 1999; Zhang and Sun, 2014), CFD method (Eswaran et al., 2009; Godderidge et al., 2006, 2009a and 2009b; Lee et al., 2007a; Liu and Lin, 2008; Loots et al., 2004; Rhee, 2005), FVP (Finite Volume Particle) method (Guo et al., 2012), MPS (Moving Particle Semi-Implicit) method (Zhang et al., 2014) and SPH (Smoothed Particle Hydrodynamics) method (Colagrossi et al., 2004; Delorme et al., 2009; Iglesias et al., 2004 and 2006; Landrini et al., 2003; Shao et al., 2012a and 2012b) have been adopted in the study of the effect of liquid-sloshing taking account of different fill levels simultaneously accompanied with validation of experimental results.

A numerical study by Li et al. (2014) addressed the variation of the water surface under low fill levels (28% and 41%). To validate the numerical results, a series of model tests were applied with a rectangular tank placed on a platform driven by a gearbox and a motor. Wave elevation and pressure on the sidewall were monitored and recorded. They found that the loads due to the impact pressure at lower fill levels could be larger than those at higher fill levels; this result was more pronounced under resonant excitation.

Lee et al. (2007b) investigated the coupling effect with CFD method. Numerical results revealed that due to the coupling effect between water and ship motions, the resonant frequency of roll motion was shifted and a second resonance appeared around the natural frequency of sloshing.

Fluid sloshing behaviour in a rectangular tank was investigated by Rafiee et al. (2010) both numerically with SPH method and experimentally with a physical rectangular water tank. Impact pressure was evaluated according to the 3-D SPH technique and good agreement was obtained with experiment results. However, it was seen from the two dimensional and three dimensional studies that three-dimensional simulation could further improve the accuracy compared to two dimensional approach, since the 2D approach was found to overestimate the pressures. The authors also highlighted a shortcoming of the approach, related to the neglect of trapped air effects in their numerical method.

An improved SPH method was raised by Chen et al. (2013) to investigate the pressure on the sidewall, and the predictions were compared with experiments. Severe water impact behaviour was observed in both experiments and numerical simulations and it was concluded that severe liquid sloshing could have a significant influence on the stability of the ship with partially filled tanks due to the great loads.

Similar risk to the stability of ships with liquid tanks was also addressed by Lee et al. (2007a). In their study, the CFD method was adopted and water surface in the liquid tank was handled by Volume-of-Fluid method. They mentioned that compressibility of the air phase should be taken into consideration.

The use of baffles, to impose restriction on the water dynamics in the tank, has attracted much attention by researchers (Akyildiz, 2012; Biswal et al., 2006; Xue et al., 2012 and Younes et al., 2007). Akyildiz and Ünal (2006) studied sloshing loads acting on the liquid tank with and without baffles both numerically and experimentally. They concluded that the baffles could significantly damp liquid dynamics and loads via a range of liquid phenomena including hydraulic jumps, wave breaking, turbulence and vorticity. Similar effects of baffles on water sloshing was mentioned by Armenio and La Rocca (1996), Liu and Lin (2009) and Panigrahy et al. (2009). Jung et al. (2012) investigated the effect of the baffle height on the sloshing by CFD method and compared their results with physical model tests by Kang and Lee (2005). They obtained the similar conclusion that baffle could mitigate water dynamics in the tank through energy dissipation. They also highlighted that when the height of baffle was more than the initial height of inner-water elevation filling in the tank, the baffle could block water behaviour separately into each subdivision, and in doing so, water surface exhibited a more linear behaviour.

## **2.5 Numerical study on behaviour of a damaged ship and floodwater**

Although physical experiment can provide valuable data for investigation of damaged ship behaviour, both the expense and the measurement uncertainties due to accuracy of equipment may limit investigations. Vassalos and Turan (1994) developed a semi-empirical approach to study the behaviour of a damaged passenger Ro-Ro ship accounting floodwater dynamic in the flooded compartment. However, Gao et al.,

(2011) suggest that an empirical method is not sufficient to describe a complex coupling consequence among floodwater dynamics, water flow and ship motions since the behaviour of floodwater inside compartment may “become totally out of phase with the exciting motion”, and hydrodynamic components (added mass and damping effect) obtained from empirical method can be useless. Hence, a number of numerical methods have been proposed to study damaged ship behaviour considering flooding physics.

Numerical studies based on a potential flow method were applied to the investigation on the stability of a damaged ship by Lee et al. (2007a), Letizia (1996), Palazzi and De Kat (2004), Santos and Guedes Soares (2009) and Spanos and Papanikolaou (2001b). The potential flow method is taken to calculate hydrodynamic components due to wave excitation, and effects of viscosity are replaced by an empirical method. Water flow dynamics are based upon Bernoulli's equation but floodwater surface inside the compartment is assumed to be horizontal and behaviour of floodwater is even neglected. Therefore, based on these assumptions and conditions, potential theory is difficult to use to accurately estimate damaged ship behaviour, especially when sloshing effect is dominant and must be taken into consideration.

The intact and damaged ship's behaviour was investigated by Hearn et al. (2008) by numerical models in relation to the sinking of M.V. Derbyshire. Although the research applied potential theory, which took water as an incompressible and inviscid flow, it took air effect and internal free surface in consideration, could assess the influence due to the interaction between internal free surface and ship motions. An oblique wave was chosen and the ship model was stationary without any forward motion. However, only ship's behaviour was presented considering heave, pitch and roll motions without estimation of wave loading acting on the intact and damaged ship. Another research based on the bulk carrier vessels (such as Derbyshire) aimed to develop a new way to estimate the cross-product of the inertia of the intact and damaged ship as 6-DOF motions are taken into consideration by Saydan (2006). In this study, the cross-product between different degree of freedom motions was conducted in detail with potential fluid theory applied, and internal fluid dynamic influence was also neglected.

Time domain simulation, as a numerical method, has been widely applied to investigation of damaged ship motions with floodwater behaviour in the flooded compartment by Chan et al. (2002), Dand (1989), De Kat and Paulling (1989), Fujiwara and Haraguchi (2002), Santos et al. (2002), Sen and Konstantinidis (1987) and Vassalos and Turan (1994). A range of approaches have been used to consider water behaviour inside the flooded compartment. Spanos and Papanikolaou (2001a) and Papanikolaou et al. (2000) treated floodwater with “lump mass concept”, while Santos and Guedes Soares (2008b) regarded floodwater as an additional load acting on the damaged ship and did not take ingress and egress of water flow impact into account. Ruponen (2007) developed a pressure-correction method in time domain simulation to deal with floodwater dynamics. Although the air compression was taken into consideration the inertia of floodwater was neglected. Palazzi and De Kat (2004) studied flooding mechanisms with time domain simulation considering trapped air effect. They treated water and air inside the compartment with different spring systems to investigate air compression inside the tank. It was found that air flow had little impact on damaged ship behaviour, but that air compression significantly influenced damage flooding. It was also noted that to precisely estimate the behaviour of a damaged ship, the prediction of floodwater dynamics inside the compartment was a determinant factor since floodwater behaviour was influenced by a binding effect that composed of the variation of pressure and velocity, ship motions and trapped air. Cross-flooding arrangements were also taken into consideration in the time domain simulation, which had been also studied by Peters et al. (2003), Vredeveldt and Journée (1991) and Xia et al. (1999).

With rapid increasing development of computing equipment, the capability of Computational Fluid Dynamics (CFD) method has been improving rapidly. In order to estimate more realistic behaviour of floating body and water dynamics, Reynolds Averaged Navier-Stokes (i.e. RANS) equations with the Volume of Fluid (VOF) method, which was developed by Hirt and Nichols (1981), are widely used to study damaged ship stability as they have the ability to tackle complicated flow problem such as viscous flows, violent sloshing with highly nonlinear surface, and wave conditions coupled with complex ship motions. in regular or even irregular waves (Gao and Vassalos, 2011; Lee et al., 2012a; Sadat-Hosseini et al., 2016 and Woodburn, 2000)

Nabavi et al. (2006) applied a CFD method to investigate the fluid dynamics of floodwater through different sizes of damaged openings. Similar research was also carried out by Wood et al. (2010). Gao et al. (2011) applied the VOF method to simulate the flooding of a damaged ship combined with a dynamic mesh, which was used to capture transient ship motions. Spanos et al. (2002b) investigated the effect of floodwater inside a compartment on the behaviour of a damaged ship. Since high computational cost is a challenge for the CFD method, Kim et al., (2017), developed a combination between CFD and other numerical method to estimate damaged ship behaviour in waves. Strasser et al. (2009) coupled CFD method with potential theory as CFD method had a good ability to deal with dynamic effect of floodwater inside the compartment, while the potential method could be able to predict ship motions. Gao et al. (2013) developed a seakeeping solver that coupled potential flow method and CFD method for its feasibility on estimation of behaviour of a damaged ship in regular beam waves.

Another method adopted by researchers for studies on numerical simulation of the behaviour of a damaged ship under flooding condition is Smoothed Particle Hydrodynamics (SPH) method, which was first developed by Monaghan (1994). Unlike CFD method that relies on grid quality, SPH is a meshless method with a good ability to simulate complicated floodwater dynamics through damaged opening and inside the flooded compartment (González et al., 2003; Skaar et al., 2006 and Zhang et al. 2013). However, SPH method is generally used only to simulate the internal flows but not reflect the coupling between ship motions and floodwater, whereas this coupling effect is necessary for investigation on assessment to damaged ship in waves. Since CFD and SPH methods both require large amount of computational contribution, MPS (Moving Particle Simulation) method can alternatively reduce time cost, but the method cannot solve multi-phase problem (Hashimoto et al. 2017).

## **2.6 Study on loads acting on intact and damaged ship**

After ship suffering damage, wave loads acting on the damaged ship is another factor that attracts attention, and the motion of the damaged ship will not be the only aspect that naval architects need to consider but also the force and moment caused by waves and floodwater also should be addressed. Considering structural strength of damaged

ship, investigation on global loads of the intact and damaged tankers and bulk carriers was assessed by researchers with numerical and experimental methods (Dalzell, 1964; Eward et al., 1954; Kukkanen 2010, Lutzi, 1957 and Salvesen et al., 1970). A detailed ship model test was proposed by Chan et al. (2003) with intact and damaged scenarios at different wave headings. Global wave loads assessment was evaluated by a nonlinear time-domain method. Wu and Hermundstad (2002) and Santos and Guedes Soares (2008a) also applied a nonlinear time-domain simulation on a container ship model to study the effect of wave on the motions and loads that distributed along the ship. Detailed studies on structural strength analysis with evaluation of the vertical and horizontal bending moments on intact and damaged ships under the different damage scenarios were focused on by Khan and Das (2008) and Rodrigues and Guedes Soares (2017). Two comprehensive investigation on prediction of loads acting on ships are referred to Hirdaris et al. (2014) and Temarel et al. (2016).

For large ships, particularly for slender hull forms of naval combatant ship, wave-induced loads, composed of shear forces and bending moments acting on the hull girder play a significant role. Brown et al. (1991) and Brown and Clarke (1993) suggested that for the purpose of design of naval ships, it was essential to predict the maximum wave-induced loads acting on the ship and monitor the variation of the loads in time that ship experienced. Investigation on wave loading acting on warships were carried out by Clarke (1986) with many factors such as nonlinear ship motion, bow slamming taken into consideration.

As a well-known benchmark hull form, US Navy Destroyer model DTMB 5415 has been widely tested in model basins. Lee et al. (2012b) carried out small-scale experimental tests at Newcastle University. With detailed arrangement of each compartment global wave loads acting on the intact and damaged 1/100-scale ship hull are investigated under the different wave conditions and damaged scenarios, as well as wave-induced loads. Although extensive experimental records were provided, the ship model was too small for range of some measurement devices so that some variation of physical parameters and nonlinear behaviour were not observed.

Begovic et al. (2017) carried out an experimental study on a 1/51 scaled DTMB 5415 at Kelvin Hydrodynamics Laboratory, University of Strathclyde, Glasgow, UK.



Motions and wave loading acting on the intact and damaged ship model without forward speed were investigated in head and beam seas. However, in the physical tests, only the virtual mass moment of inertia of the ship model was obtained by free roll decay test in calm water, which leads to challenges for simulation in which the solid mass moment is required. The experimental results did not address in detail the nonlinear effect on the wave-induced loads on the damaged ship.

## 2.7 Chapter remarks

This chapter mainly addresses research and methodology into the influence of flooding on stability and behaviour of damaged ships. From this review, factors that can be dominant or have an impact on the stability of a damaged ship may be categorized as:

- Geometric features
  - Ship hull
    - Inner structure: multiple decks, bulkheads, sub-compartments, double bottom, etc.
    - Internal layout: obstruction, cross flow arrangement, air pipes/ventilation, etc.
  - Dimensions, locations, shapes, etc. of damaged opening.
- Hydrostatic characteristics
  - Metacentric height, initial intact condition and initial heel angle, etc.
- Fluid dynamic characteristics
  - Damage related
    - Flow rate (time varying), time of damage creation, water accumulation, etc.
  - Hydrodynamic
    - Floodwater behaviour inside compartment, transient flooding effect, sloshing effect, cross-flooding effect, etc.
    - Coupling effect or interaction between floodwater and ship motions
  - Air dynamic
    - Air flow behaviour, trapped air compression, air pocket
- Environment factor
  - Wave conditions, or calm water, with or without advanced speed, wave heading, etc.

Since damaged flooding a damaged ship is such an integrated problem containing many aspects, in this work, experimental and numerical investigation are applied to study on the behaviour and wave loads acting on an intact and damaged naval ship model with several of the factors highlighted above taken into consideration.

# 3. Experimental Investigation

## 3.1 Brief introduction

Since the damaged ship loses her segmental watertight and structural integrity, there is necessity to accurately predict ship motions and the loads acting on the damaged hull girder. In the present study an experimental assessment is carried out on a naval ship hull to show the effects of damage and water dynamics on ship performance. Ship motions and wave-induced loads acting on a combatant ship model are assessed by physical tests at Kelvin Hydrodynamic Laboratory. Results obtained from the present experimental investigation are compared with previous physical model tests by Begovic et al. (2017). A scaled naval ship model – DTMB 5415 – is utilized, which is a bare hull without any appendages such as fin stabilizers, bilge keels and propellers. A damaged opening is located at midships to starboard; two compartments can be flooded into once the cover on the damage opening is removed. Free rolling decay tests for the intact and damaged condition with and without mooring constraint are implemented in calm water, while the model is restrained by soft moorings at the bow and stern during the tests in regular waves. The test case is therefore an idealised representation of the behaviour of a damaged ship which has been disabled after an incident such as a collision.

In order to investigate the performance of the ship in the intact and damaged conditions in beam seas with zero forward speed the model is positioned perpendicular to the direction of wave propagation with the damaged opening facing the incoming waves so that floodwater can ingress and egress from the damage opening. To eliminate the influence on advanced speed of the ship, ship model is soft-moored at bow and stern. To set an actual situation on the damaged ship after sudden damaged flooding, the damaged opening is set to face to the incoming wave. The model motions are measured in a range of wave heights and frequencies in regular beam waves to investigate the influence of waves and damage on the ship. Results will be used to validate results from the CFD-based RANS solver.

## 3.2 Facilities

The experiment was carried out at the Kelvin Hydrodynamic Laboratory of the University of Strathclyde. A tank with 76-metre length, 4.6-metre width and 2.15-metre depth is used in the model tests. Figure 3.1 gives a view of the tank. It is equipped with a multi-flap force-feedback absorbing wave maker so that reflected and radiated waves from structures during the tests can be absorbed to make sure steady consistent waves can be generated. To eliminate effect of wave reflection from the end of the tank a high-quality sloping beach is installed at the far end of the tank. The wave maker and wave-absorbing beach are shown in Figure 3.2 and Figure 3.3.



Figure 3.1 Kelvin Hydrodynamic Tank at University of Strathclyde (URL.1)



Figure 3.2. Wave maker



Figure 3.3. Wave absorbing beach

### 3.3 Ship model

A model of the naval ship DTMB-5415 of overall length 3.0m is used during the tests. It is an open-to-public early concept of the DDG-51 known as the Arleigh Burke class destroyer. This was commissioned by the U.S. Navy for hull-form optimization (Senari, 2016). Since conceived as a preliminary design in 1980s, DTMB-5415 is now widely used for investigation in hydrodynamic and resistance experiments (Larsson, 2013) as a benchmark ship model. Particulars of the ship model used in the present test are given in Table 3.1. Figure 3.4 shows the lines plan hullform of DTMB-5415.

Table 3.1. Particulars of the ship model

Particulars	Full Scale	Model Scale	Particulars	Full Scale	Model Scale
Scale factor	1	51	$C_M$	0.818	0.818
$L_{OA}$	153m	3m	$C_P$	0.61	0.61
$L_{WL}$	142m	2.784m	$C_{WP}$	0.76	0.76
$B_{OA}$	20.5m	0.402m	$KM$	9.486m	0.186m
$B_{WL}$	19.1m	0.374m	$KG$	7.548m	0.148m
$D$	19.2m	0.376m	$GM$	1.938m	0.038m
$T$	6.16m	0.12m	$LCG$	70.125m	1.375m
$\nabla$	8423.3m <sup>3</sup>	0.0635m <sup>3</sup>	$k_{xx}$	-	-
$\Delta$	8423.3ton	63.5kg	$k_{yy}$	0.25L	0.25L
$C_B$	0.498	0.498	$k_{zz}$	0.25L	0.25L

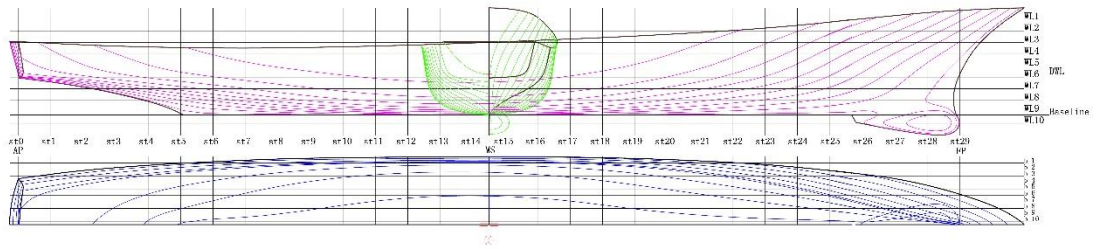


Figure 3.4. Hullform of DTMB-5415

It should be noted that the model used in the tests is a double-bottom bare hull without any appendages. The whole ship model includes a sonar dome and a transom stern, and it is divided into several compartments by 7 watertight bulkheads shown in Figure 3.5. The damaged opening is located at the midship to starboard, facing the incoming direction of waves; two compartments can be flooded into when the cover on the damage opening is removed. Figure 3.6 shows the layout of the flooded compartments.



Figure 3.5. Physical naval combatant ship model



Figure 3.6. Internal view at flooded compartments

The ship model is moored at the bow and the stern by soft elastic moorings in water so that the ship is not free to drift. Therefore, the model ship encounters beam waves with zero speed. It should be noted that the flooded compartments are ventilated by two pipes so that air compression effect can be eliminated when water floods into the damaged compartments from the opening shown in Figure 3.7.

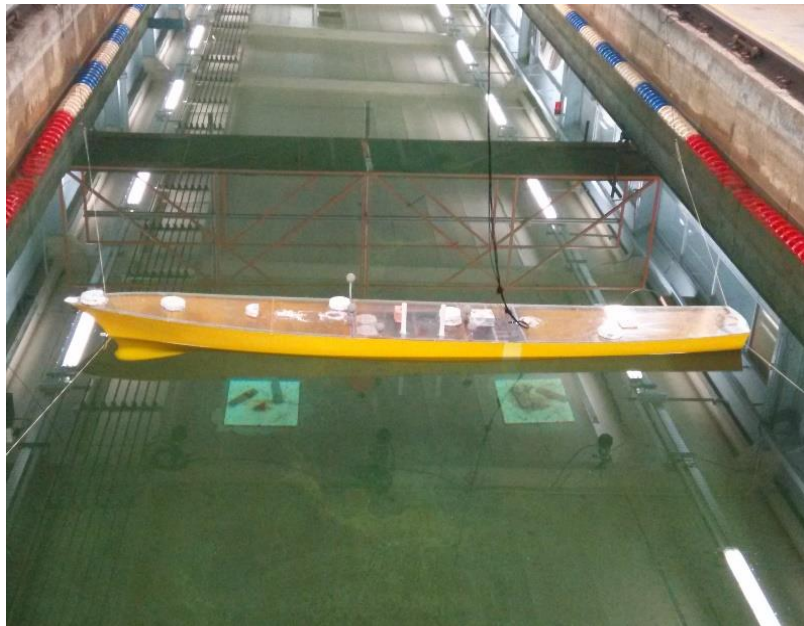


Figure 3.7. Stationary model in calm water with moorings

Table 3.2 gives the particulars of damaged ship model after the cover on the damage opening is removed and the ship reaches the equilibrium condition in calm water. The main particulars of damaged ship model remain the same as those of the intact model, but draft and buoyancy distribution are changed, since draft is increased and buoyancy in the flooded compartments disappears due to the water flooding. Dimensions of flooded compartments can be shown with a CAD model in Figure 3.8.

Table 3.2. Particulars of the damaged ship

Particulars	Dimensions
$L_{flooded}$	0.4685m
$T_{damaged}$	0.145m
$B_{WL}$	0.382m

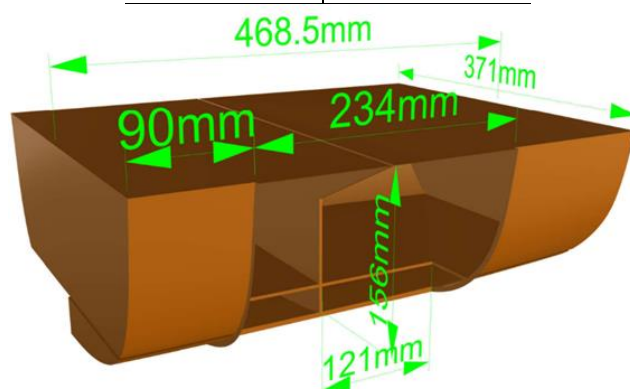


Figure 3.8. Dimensions of the flooded compartments



### 3.4 Experimental setup

#### 3.4.1 Waves

During the tests, a regular beam wave is generated by the wave maker based on pre-set values of wave height and wave frequency. Wave heights are varied from 10mm to 25mm, and frequency is changed in the range from 0.446Hz to 1.19Hz, as shown in Table 3.3.

Table 3.3. Wave settings

$f$ (Hz)	$T_w$ (s)	$H$ (m)		$f$ (Hz)	$T_w$ (s)	$H$ (m)	
1.19	0.84	0.02		0.664	1.505	0.02	Deep
1.02	0.98	0.02		0.649	1.54	0.02,	water
0.893	1.12	0.02		0.639	1.565	0.015,	
0.8	1.249	0.02				0.02,	
0.794	1.26	0.02				0.025,	
0.752	1.33	0.02				0.030	
0.733	1.365	0.02	Deep	0.635	1.575	0.02	Finite
0.717	1.394	0.01,	water	0.621	1.61	0.02	water
		0.015,		0.595	1.68	0.02	depth
		0.02,		0.549	1.82	0.02	
		0.025		0.51	1.96	0.02	
0.714	1.4	0.02		0.476	2.1	0.02	
0.697	1.435	0.02		0.446	2.24	0.02	
0.68	1.47	0.02					

#### 3.4.2 Instrumentation

A wave probe is positioned in front of the ship model to measure the elevation of the generated waves over time. According to Dai (2016), the uncertainty of these wave probes that yields a 95% confidence level is about 0.6mm. The six-DOF motions of the ship model in calm water and beam waves during tests are measured by QUALISYS motion capture system.

As shown as Figure 3.9, five reflective markers installed on the ship model are detected by the QUALISYS cameras and used to calculate the six-DOF motions of ship model in a global coordinate system. These five markers are installed on one side of the cut section (which can be seen at the midship in Figure 3.9) so that any bending or twisting of the ship due to the load cell can be neglected. Typically, the 95% uncertainty of QUALISYS measurements is less than 1mm.

Wave-induced loads, which can be taken as loads acting on the hull girder, are measured by a type 206/5C five-component force gauge manufactured by DHI (Danish Hydraulic Institute). As shown in Figure 3.10, the force gauge includes two vertical end pieces joined by four aluminium beams. It is installed at a cross section at which the whole ship hull is cut into two portions. All available data including wave heights, six DOF motions and five wave-induced loads acting on the ship model varying over time is acquired through a CED 1401 A/D converted using the *Spike* data acquisition software.

During each test, acquisition of all data, including waves, ship motions and wave-induced loads, runs until the ship's behaviour reaches a stable periodic state and more than ten stable oscillations have been completed. Between tests, two sets of side markers installed at each side of the tank are lifted to the surface to accelerate damping effect on waves and calm the water quickly after each test so that the next test should not be affected.

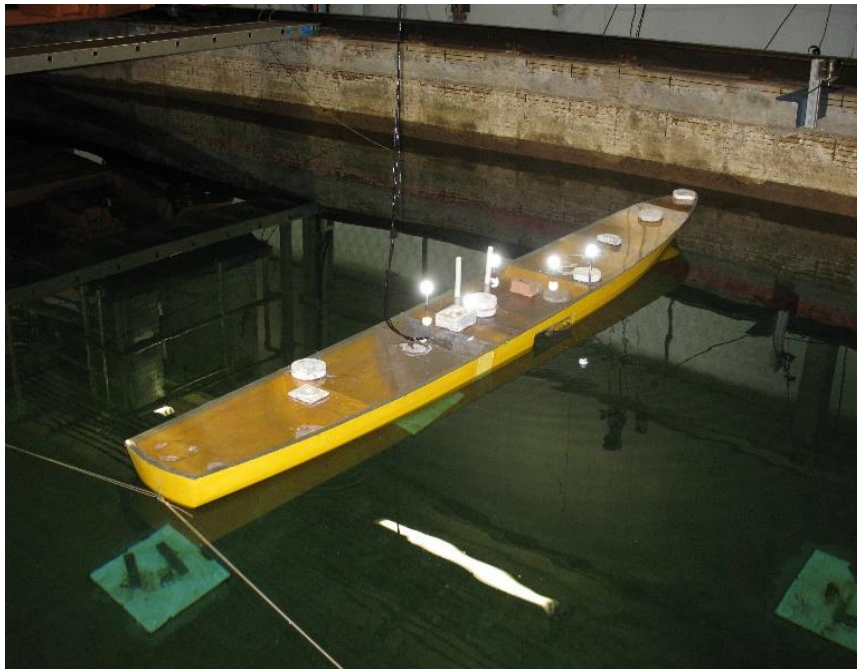


Figure 3.9. Infra-red markers and force gauge installed on the ship



Figure 3.10. Type 206/5C 5-Component force gauge by DHI

## 3.5 Test procedure

### 3.5.1 Force transducer (load cell) calibration and uncertainty analysis.

#### 3.5.1.1 Calibration

A five-component force transducer (also called load cell) is used in this study based on the process of transforming signals between voltage (V) and load (force (N) or moment (Nm)). Calibration to validate the relation of the transformation for the

transducer is carried out with five sets of loads: forces along X and Y axes and moments around the X, Y, Z axes. Figure 3.11 to Figure 3.14 illustrate calibration for the force transducer. As shown in Figure 3.11, loads are applied vertically at positions 1, 2 and 3, respectively. Then forces acting in that direction and the associated moments due to these forces acting on the transducer can be measured.

Similarly, forces acting in an orthogonal direction and related bending moments are measured by rotating transducer with 90 degrees, as seen from Figure 3.12. Therefore, forces and bending moments about two axes – X and Y may be obtained. To measure torsional moment ( $M_z$ ) via force transducer (as marked in

Figure 3.13), forces are imposed at both sides simultaneously as shown in Figure 3.14. As demonstrated in Figure 3.15 and Figure 3.16, increasing force presents a linear increase in voltage so that the slope of the line can be taken as the transformation factor between voltage and load (force or moment), which is directly used in the tests of the ship model.

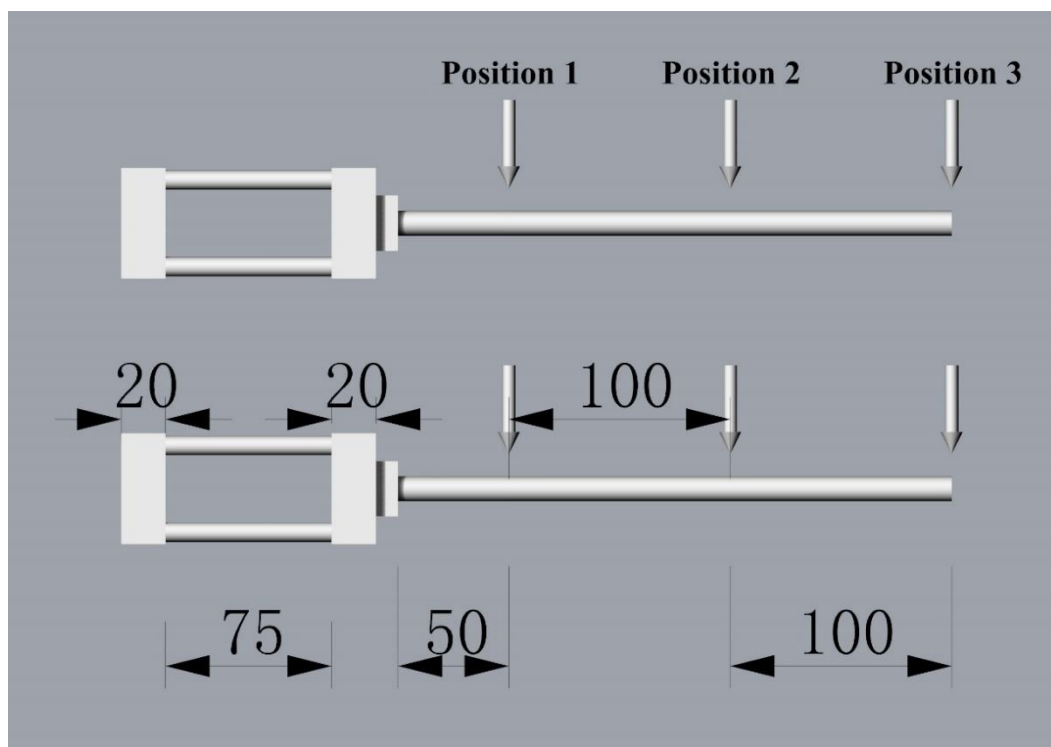


Figure 3.11. Sketch of transducer calibration setup with dimensions (unit: mm)

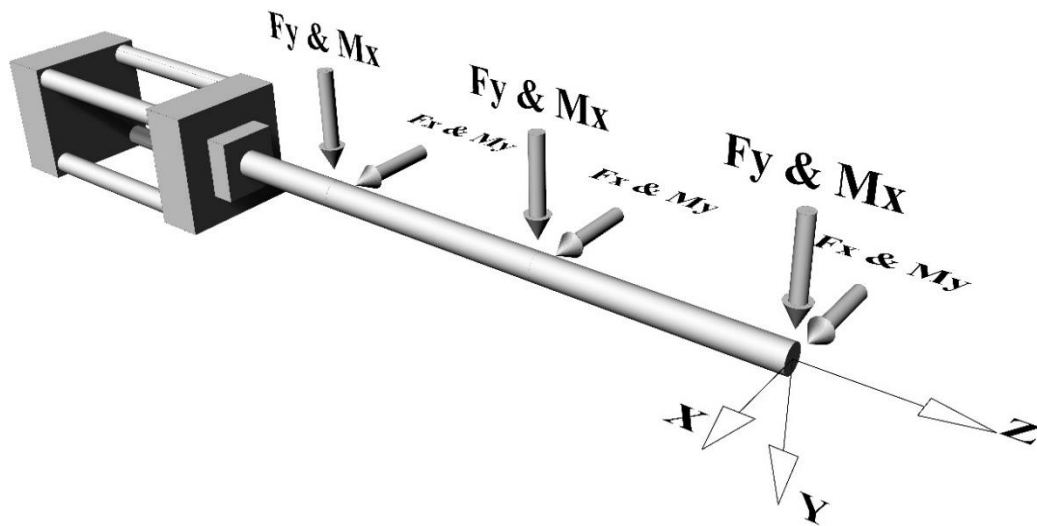


Figure 3.12. Illustration of load cell calibration in two directions



Figure 3.13. Torsional moment ( $M_z$ ) marked on transducer

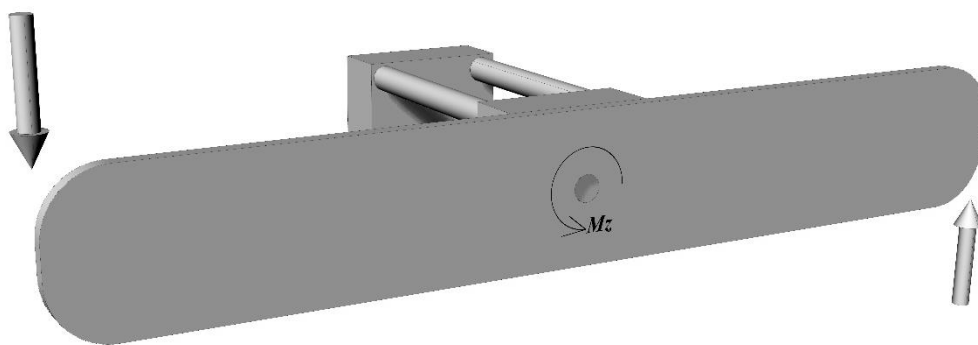


Figure 3.14. Sketch of transducer's calibration for  $M_z$

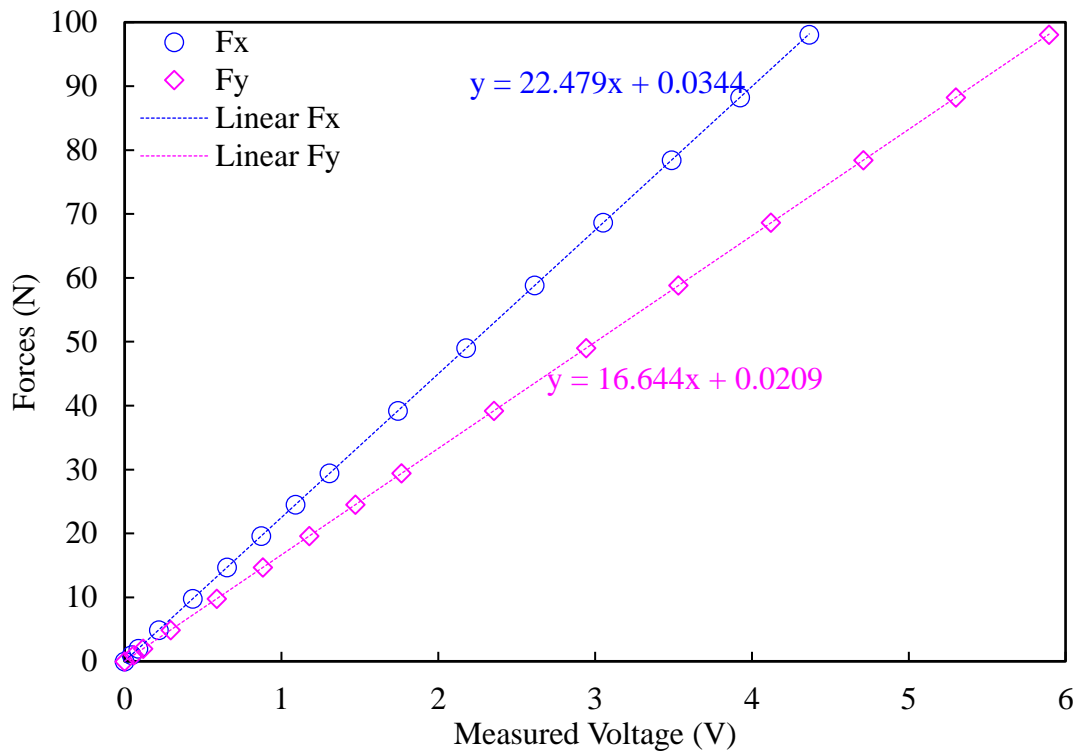


Figure 3.15. Calibration for forces acting on the load cell

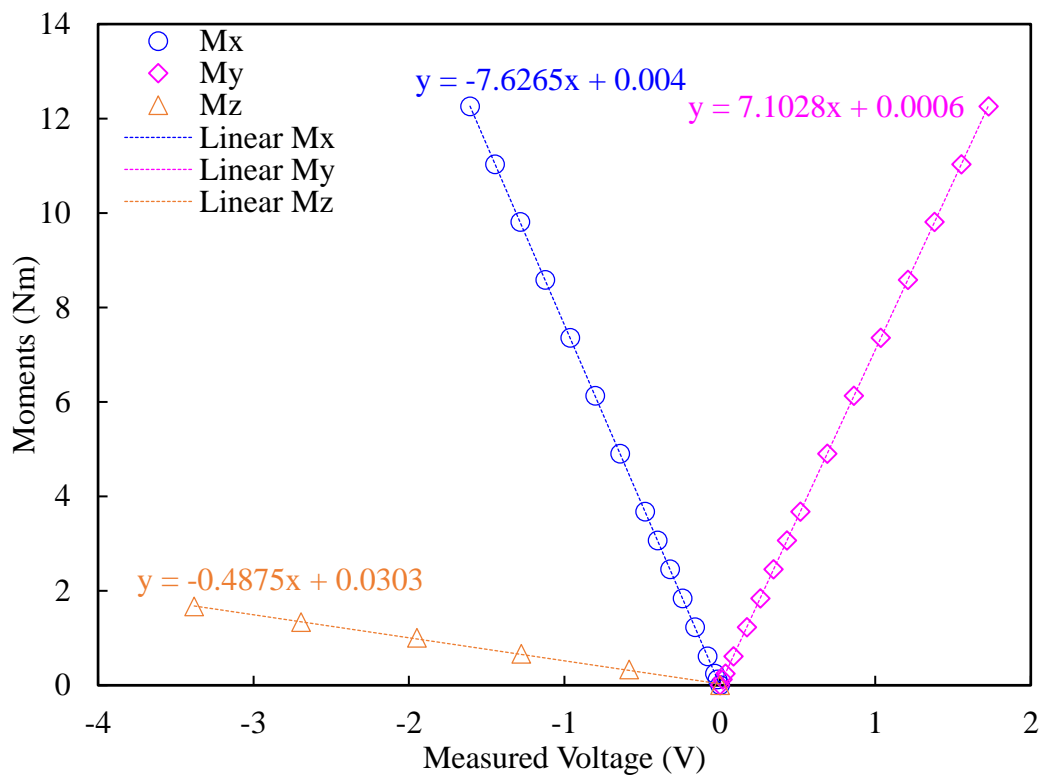


Figure 3.16. Calibration for moments acting on the axes of the load cell

### 3.5.1.2 Uncertainty analysis

The calibration uncertainty at the 95% confidence level, related to the slope and intercept of the regression line, is taken as three times the value of the Standard Error of Estimate (SEE), as recommended by ITTC procedure (2014a). The SEE can be expressed by

$$SEE = \sqrt{SS_R / (n - 2)} \quad \text{Equ. 3.1}$$

where  $SS_R$  is the sum of the square of residuals, which means the sum of the difference between measured data and the fitted curve. Then  $SS_R$  can be expressed by

$$SS_R = \sum_{i=1}^N (Residual_i)^2 \quad \text{Equ. 3.2}$$

Here, residual can be defined as

$$Residual_i = y_i - a - bx_i \quad \text{Equ. 3.3}$$

where

$y$  is the measured value in Volts

$x$  is the independent variable, which represents force or moment in this section.

$a$  is the intercept of fitted curve

$b$  is the slope of fitted curve

Table 3.4 shows the uncertainties of five-component force gauge at the 95% confidence level as below.

Table 3.4. Uncertainty analysis of the five-component loads

<b>Loads</b>	<b>SEE</b>	<b>Uncertainty</b>
Fx (N)	0.001	0.004
Fy (N)	0.002	0.005
Mx (Nm)	0.006	0.017
My (Nm)	0.002	0.005
Mz (Nm)	0.009	0.027

### 3.5.2 Cross coupling

During calibration the cross-coupling between different forces and moments has to be investigated. The coupling mechanism is observed when loading the transducer purely in X-direction results in non-zero force and moment measurements in other directions ( $F_y$  and  $M_x$ ). These non-zero measurements can be regarded as spurious readings, which ideally should be zero. Similarly, as  $F_y$  and  $M_x$  are applied to the load cell,  $F_x$  and  $M_y$  generate non-zero readings by load cell.

$F_y$ ,  $M_x$  and  $M_z$  are plotted against  $F_x$  shown in Figure 3.17 to Figure 3.19. It can be seen that a “spurious”  $F_y$  equals to about  $6.8\%F_x$  due to loaded  $F_x$ , but  $M_x$  and  $M_z$  do not reveal an apparent variation due to  $F_x$ . A similar coupling effect caused by  $F_y$  is shown in Appendix 1 .

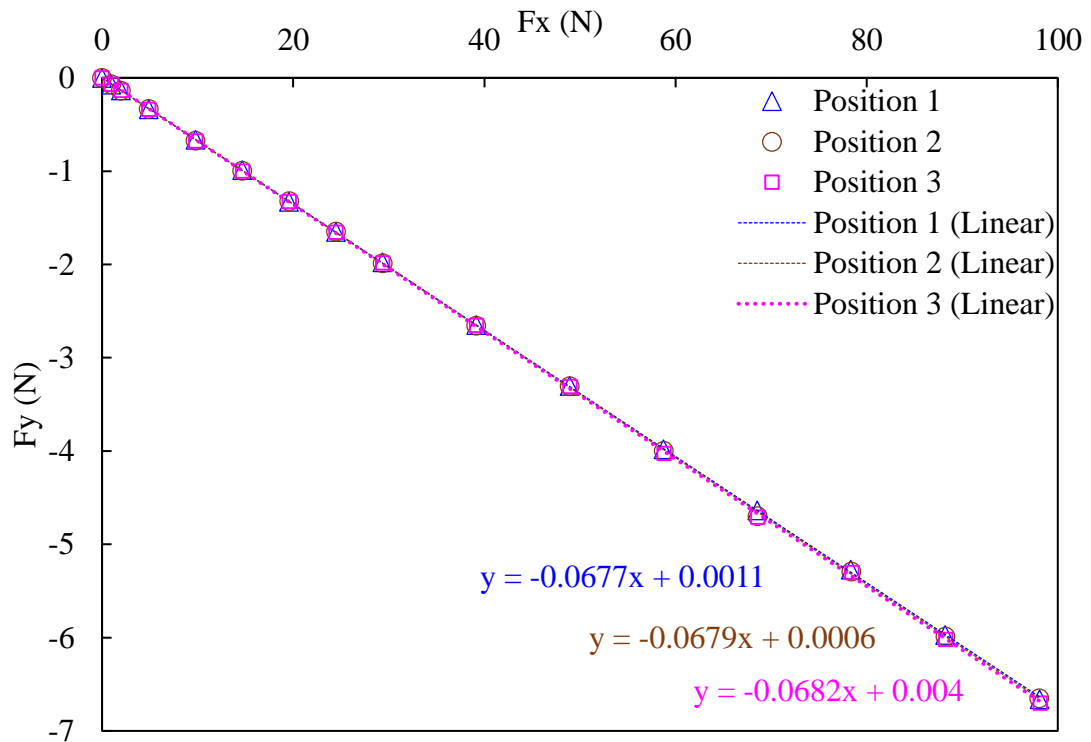


Figure 3.17.  $F_y$  triggered by  $F_x$



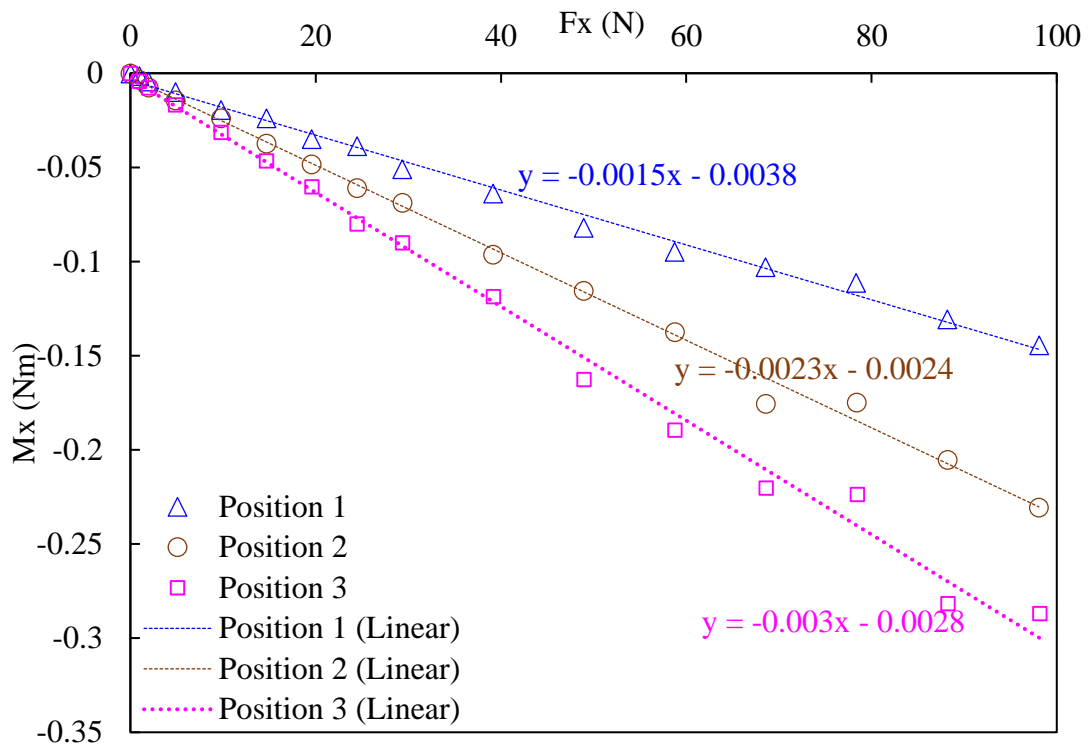


Figure 3.18. Mx triggered by Fx

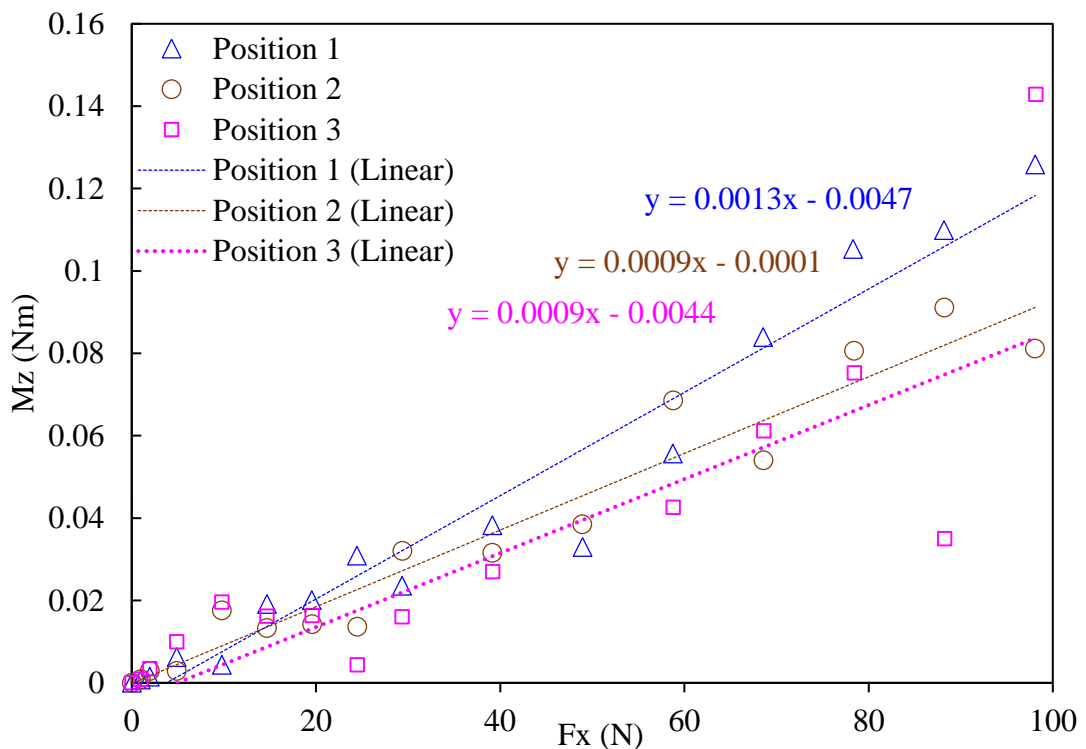


Figure 3.19. Mz triggered by Fx

Logically analysing, taking  $F_x$ ,  $F_y$ ,  $M_x$  and  $M_y$  into account, all four loads can have a cross coupling effect on each other. In other words, there is a matrix relationship

between loads measured by the load cell and true (applied) values. This can be expressed by

$$\begin{bmatrix} F_{xm} \\ F_{ym} \\ M_{xm} \\ M_{ym} \end{bmatrix} = \begin{bmatrix} 1 & r_{12} & r_{13} & 0 \\ r_{21} & 1 & 0 & r_{24} \\ r_{31} & 0 & 1 & r_{34} \\ 0 & r_{42} & r_{43} & 1 \end{bmatrix} \cdot \begin{bmatrix} F_{xt} \\ F_{yt} \\ M_{xt} \\ M_{yt} \end{bmatrix}$$

Where,

$F_{im}$  is measured force by load cell ( $i = x, y$ )

$M_{im}$  is measured moment by load cell ( $i = x, y$ )

$F_{it}$  is the true value of force ( $i = x, y$ )

$M_{it}$  is the true value of moment ( $i = x, y$ )

$R = r_{ij}$  ( $i, j = 1, 2, 3, 4$ ) is the matrix that describes the relation between measured and true values due to cross coupling. It was found that it can be expressed as

$$R = \begin{bmatrix} 1 & -0.0123 & 0.0006 & 0 \\ -0.0677 & 1 & 0 & -0.0002 \\ -0.0015 & 0 & 1 & -0.0007 \\ 0 & 0.0037 & -0.0009 & 1 \end{bmatrix}$$

Then inverse matrix of R is

$$R^{-1} = \begin{bmatrix} 1.0008 & 0.0123 & -0.0006 & 0 \\ 0.0678 & 1.0008 & 0 & 0.0002 \\ 0.0015 & 0 & 1 & 0.0007 \\ -0.0002 & -0.0037 & 0.0009 & 1 \end{bmatrix}$$

And hence the true values of forces and moments can be obtained from the measured values as:

$$\begin{bmatrix} F_{xt} \\ F_{yt} \\ M_{xt} \\ M_{yt} \end{bmatrix} = R^{-1} \cdot \begin{bmatrix} F_{xm} \\ F_{ym} \\ M_{xm} \\ M_{ym} \end{bmatrix}$$

### 3.5.3 Mass moment of inertia measurement

Traditional swing-type devices are normally used for measuring pitch moment of inertia of model ships; in this application the width of the device needs to be greater than the beam of the ship. In the present application, measurement of roll moment of inertia requires the width of the device to be greater than the overall length of the ship model (3 metres), which presents a challenge. An attempt was made to use a compound pendulum method in the present study. As shown in Figure 3.20, a wooden support is used to lift the ship model in and out of the basin to avoid the risk that the load cell is broken due to overload. The compound pendulum method was applied to measure the mass moment of inertia about the longitudinal axis of ship model ( $I_{xx}$ ). However, measurement was made just after the whole system (including ship model and wooden support) was pulled out of the tank when with the wooden support had absorbed some water. Therefore, the total mass of the whole system is wrongly taken into consideration (considering the water absorbed by the wood), and hence failed to obtain the accurate mass moment of inertia of the ship model's roll motion. Furthermore, even without this issue, the method did not prove to be able to determine with sufficient accuracy the relatively small moment of inertia of the ship about its own CG in the presence of the relatively large moment of inertia due to the rotation of the ship mass about the pendulum support.



Figure 3.20. Wooden support used to hold the ship model

When a specific ship rolls in calm water, one factor that has an influence on the (natural) period of roll motion (as obtained by decay tests) is the mass moment of inertia about longitudinal axis. Hence, an alternative way to obtain an approximate ship's mass

moment of inertia is to use a method based on CFD to fit the data from a free decay test, which will be explained in Appendix 2 .

### 3.6 Decay tests in calm water

#### 3.6.1 Free roll decay tests for the intact and damaged ship model

During the roll decay tests in calm water, both the intact case and the damaged case (obtained by removing the cover on damage opening) are tested. The rotational motion of the ship model is monitored and recorded. It should be noted that decay tests for both intact and damaged cases are both carried out ten times each to minimise the uncertainty in the natural periods obtained for the intact and damaged ship model much as possible.

As mentioned above, free rolling decay tests are undertaken with and without mooring restraints in still water. The roll motions of the intact and the damaged ship models are presented in Figure 3.21. It is clearly observed that the equilibrium of damaged scenario is at approximately 2 degrees of heel. The reason for this can be explained that when water floods into the compartments, the double bottom is not fully filled with floodwater, instead, only half (starboard side) of bottom space can be flooded due to the damage. Finally, when ship reaches its upright state it heels to the damaged side.

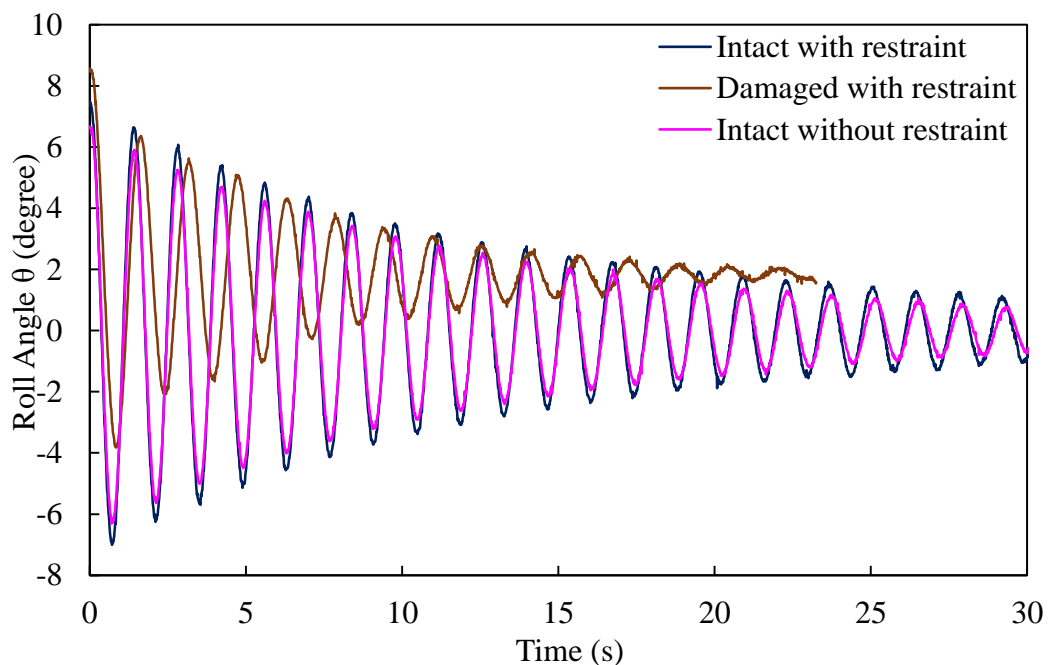


Figure 3.21. Decrement curves of free decay tests

To determine the natural frequency of roll motion of ship model, free decay tests on roll motion are carried out by imposing a rotational angle on the ship hull. A Fast Fourier Transform (FFT) algorithm is used to determine the natural frequency of the ship's roll motion as shown in Figure 3.22. The natural frequencies for three cases are given by Table 3.5. It can be noted that natural frequency under the damaged condition is lower than that in the intact condition and that the water surface effect in the damaged compartment under the damaged condition increases the damping to ship motions, as highlighted also by De Kat (2002), Lee et al. (2012b), Manderabacka et al. (2015b) and Papanikolaou and Spanos (2004).

	Natural Frequency (Hz)	Natural Period (s)
Intact (restrained)	0.7194	1.39
Intact (not restrained)	0.7173	1.394
Damaged (restrained)	0.6391	1.565

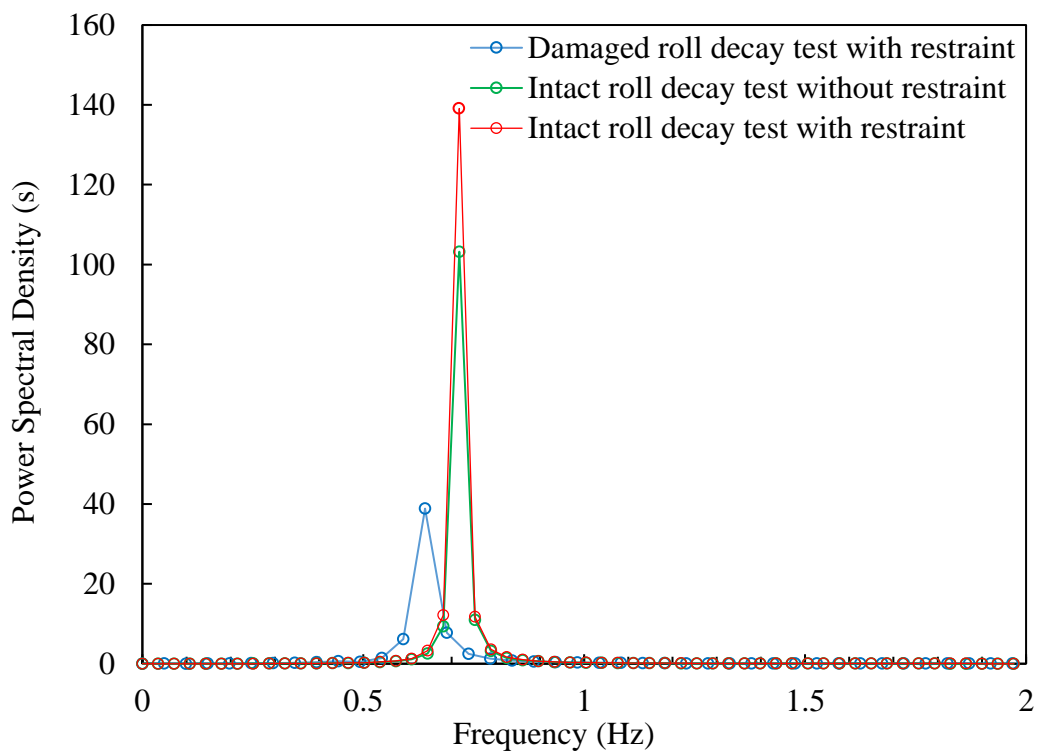


Figure 3.22. Natural frequency analysed by FFT

### 3.7 Tests in regular beam seas

The ship motions and loads acting on the ship model are measured for all the intact and damaged cases in regular beam waves. A wave of height 20mm is created for the full range of frequencies; a further set of waves of 10mm to 25mm wave heights are also tested around the natural frequency as shown in Table 3.3 at Section 3.4.1.

The intact ship is tested first followed by the damaged cases. Figure 3.23 presents a sample of measured data acquisition that is represented by the *Spike* data acquisition software for the wave elevation and ship motions (rotational angle and heave motion) responding to the encountered wave. Valid data can be taken during a period of steady periodic fluctuation and should be averaged over several cycles to minimize the probability of superfluous errors or peaks. It should be mentioned that the wave probe is positioned between the wave maker and the model, around 10m from the wave maker and 20m from the model so that wave elevation is unaffected by the ship's movement. The time required for the wave to propagate from the probe to the ship is calculated for each case, and the section of the time history over which the ship motion and load data is analysed is offset by this period as shown in Figure 3.23, in order to ensure that the measured responses correspond to the measured waves.

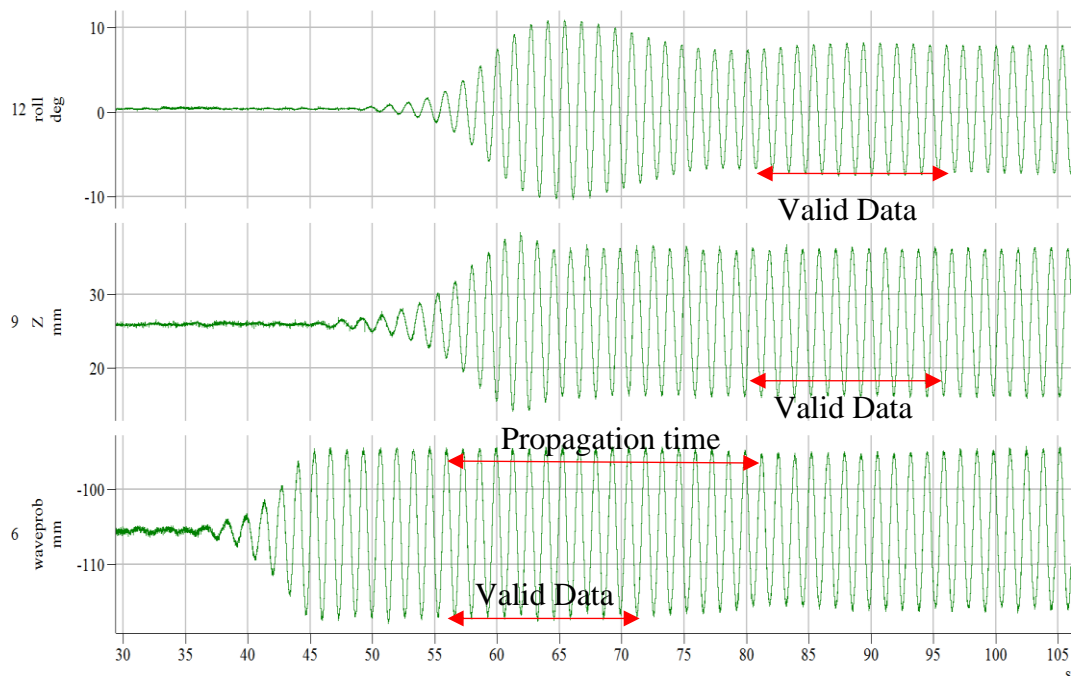


Figure 3.23. A sample of data acquisition by Spike

### 3.7.1 Ship motions

In regular beam waves, the model is restrained at each case by soft elastic moorings. Although six DOF ship motions are captured by QUALYSIS system, roll and heave motion are the focus in this section under the intact and damaged scenarios. The amplitudes of roll and heave oscillation are non-dimensionalized by  $kA$  (wave number times wave amplitude) and  $A$  (wave amplitude). To uniform the non-dimensional demonstration shown in the plots between frequency and amplitude of motion, frequency is also non-dimensionalized by multiplying by  $(L/g)^{0.5}$ , where  $L$  means the length of the ship model. Figure 3.24 captures the motions of the intact ship during one period excited by a regular beam wave. A particular view at free surface in the vicinity of the damaged opening is shown in Figure 3.25 during a period of one cycle for the damaged ship. It is interesting to see that due to the complicated geometry of the flooded compartments as well as floodwater effect, the free surface presents a perturbed dynamic effect in the flooded compartments. To give a demonstration about how damage can affect the ship motions, Figure 3.26 and Figure 3.27 illustrate the non-dimensional Response Amplitude Operators (RAOs) of the intact and damaged ship motions in regular beam waves relative to non-dimensional frequencies respectively.

It can be clearly observed that roll motion resonance for the intact ship occurs at a higher frequency than that for the damaged ship. The non-dimensional natural frequency of the damaged ship (about 2.2), is obviously lower than that of the intact ship (2.5 approximately). The amplitude of the intact ship roll motion is lower than the damaged ship when non-dimensional frequency is less than 2.3. In contrast, when the non-dimensional frequency is greater than 2.3, the intact ship has large motions while the damaged ship roll motion is reducing rapidly. As non-dimensional excitation frequency is higher than 3.5, the roll amplitudes are small in both situations. The floodwater not only increases reactive time in roll but also imposes extra damping on the peak of ship roll motions. At the resonance frequency the peak amplitude of damaged ship (8.3) is clearly much lower than that of the intact ship (13) due to the free surface effect of floodwater in the flooded compartments.

As seen from Figure 3.27, the resonance frequencies of heave motion for the intact and damaged cases do not reveal clear differences. Furthermore, there is no obvious difference in magnitude of heave RAOs between intact and damaged cases as well.

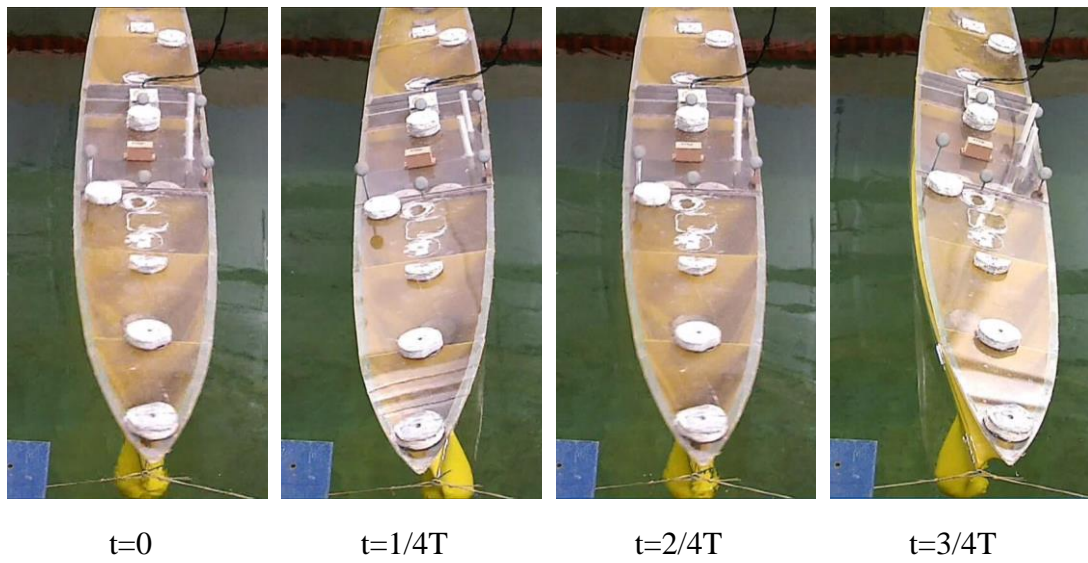
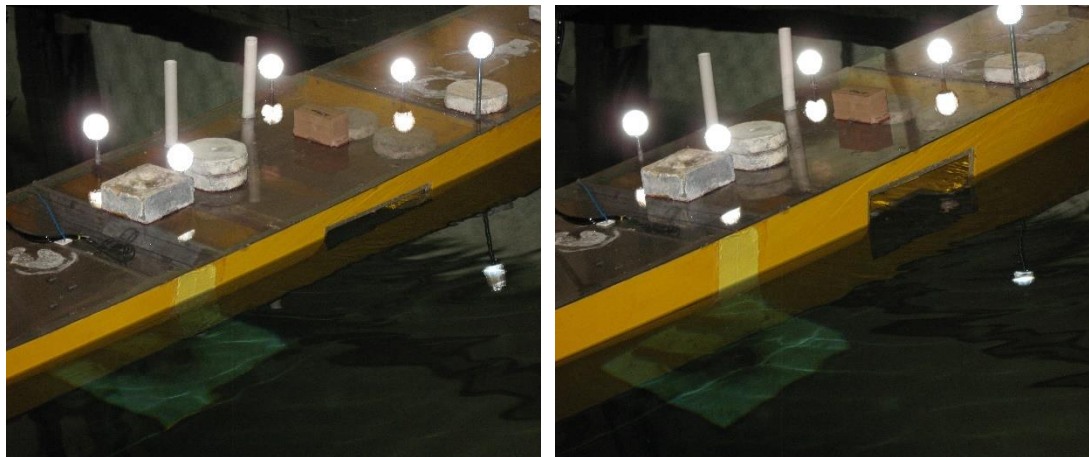


Figure 3.24. Intact ship motion in beam waves





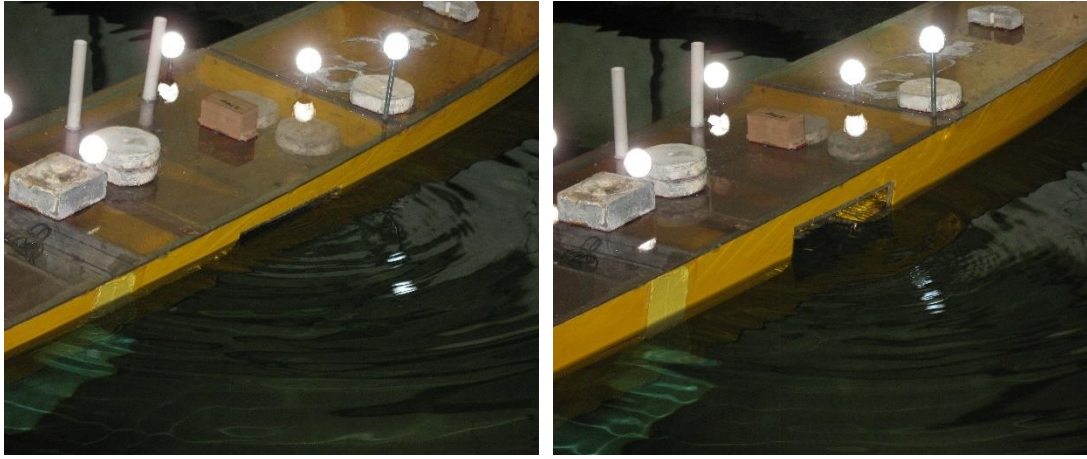


Figure 3.25. Free surface near the damaged opening under damaged condition

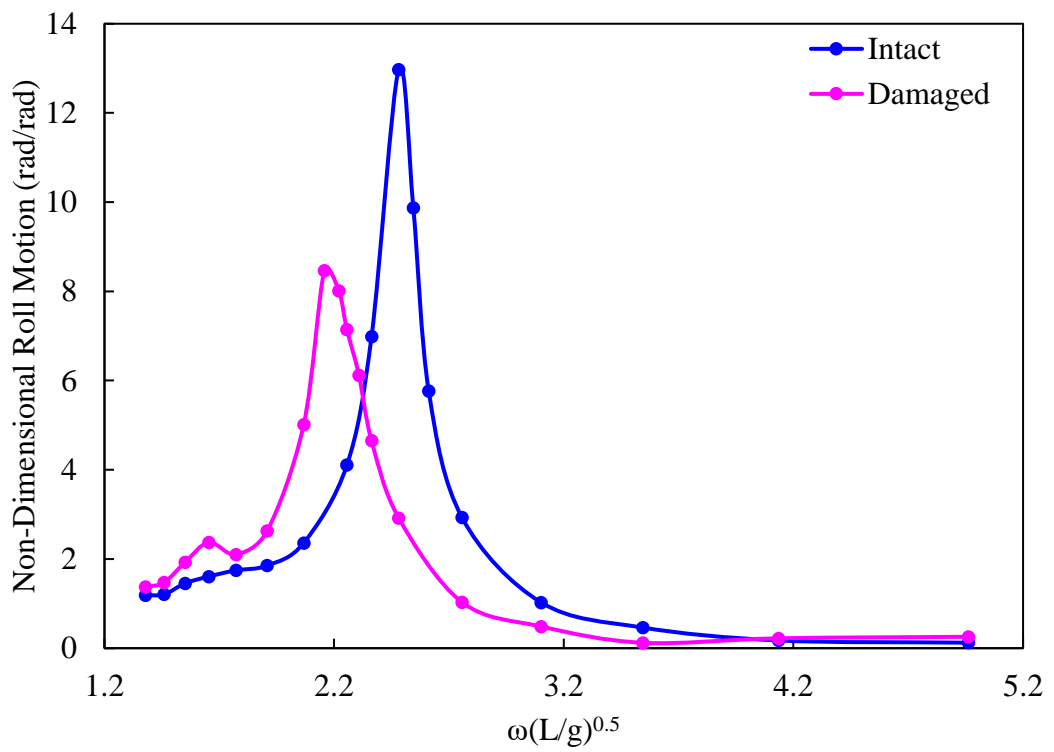


Figure 3.26. Non-dimensioned roll motion against non-dimensioned excitation frequency

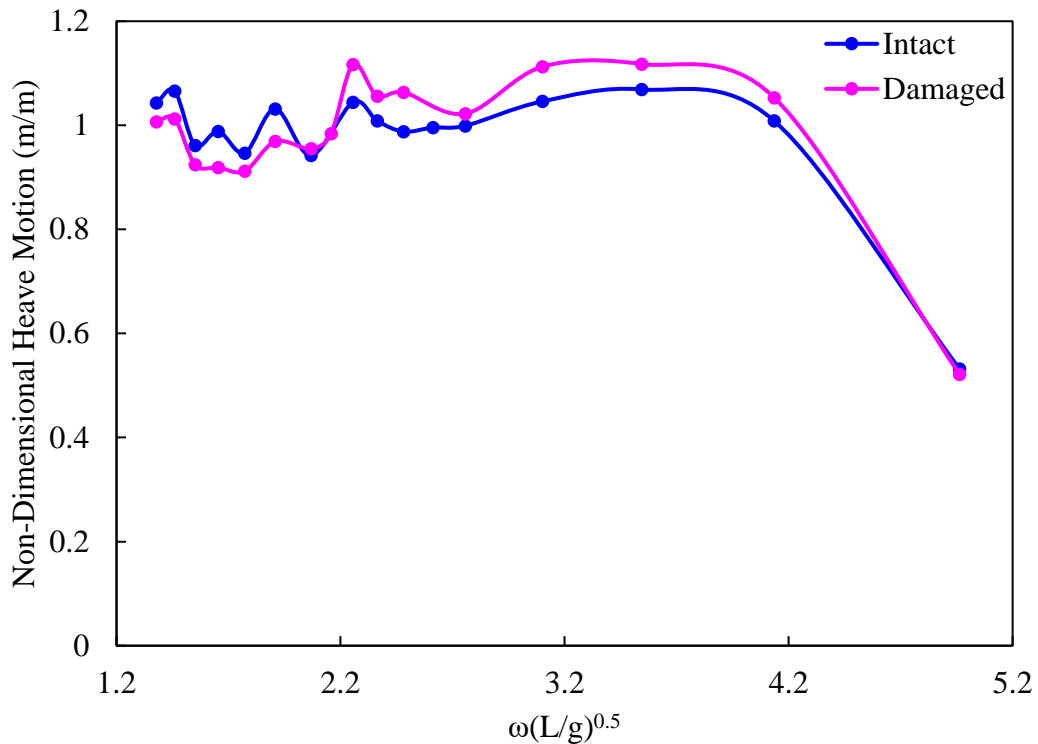


Figure 3.27. Non-dimensioned heave motion against non-dimensional excitation frequency

### 3.7.2 Wave-induced loads

Wave-induced loads acting on the intact and damaged ship model are of significance for stability and survivability of a vessel. Specifically, during the physical model tests, five components of loads including two shear forces – vertical shear force and horizontal shear force, and three moments – vertical bending moment, horizontal bending moment and torsional moment - are measured under both intact and damaged scenarios. Definitions of the five-component wave-induced loads acting on the ship are shown in Figure 3.28. These loads are obtained by a five-component force gauge (also called load cell) manufactured by the Danish Hydraulic Institute (DHI). A sample of measured wave-induced loads on a damaged hull is given as Figure 3.29. It can be seen clearly that due to the floodwater an obvious nonlinearity shown on the loads acting on the damaged ship (Mx at row 3).

Through motion analysis shown in Section 3.7.1, resonant frequencies can be recognized by peak values. They are labelled as “first-order” and “second-order” frequency shown in the plots below accompanied with corresponding wave-induced

loads, such as SF (shear force), BM (bending moment) and TM (torsional moment), and directions like V (vertical) and H(horizontal). Amplitudes of wave induced loads, including forces and moments, at the resonant frequencies are presented against non-dimensional resonant frequencies.

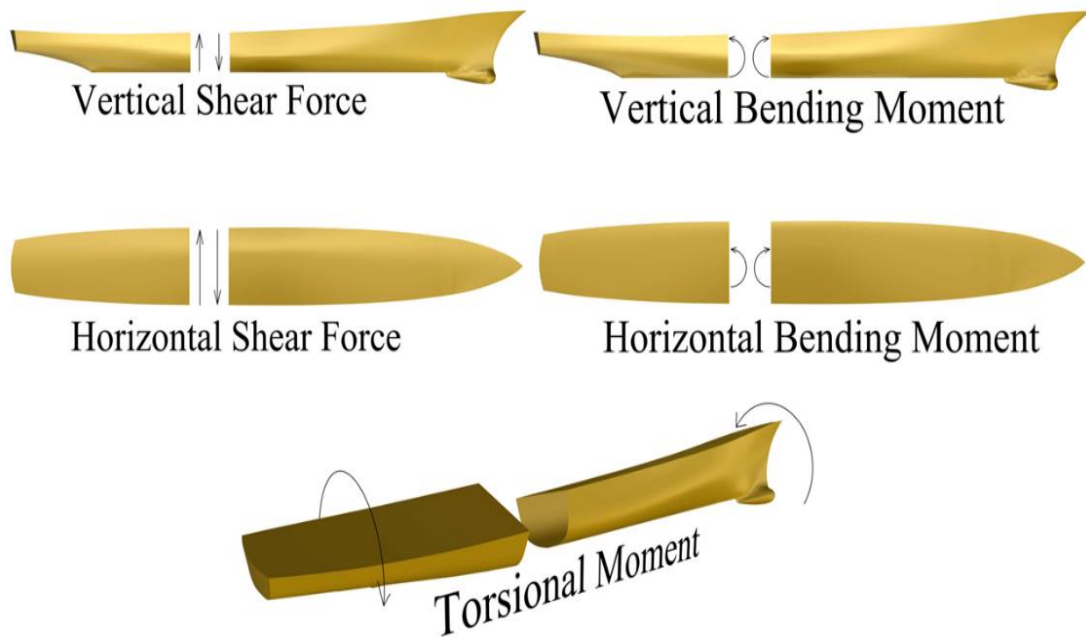


Figure 3.28. Definition of wave-induced loads on the ship hull

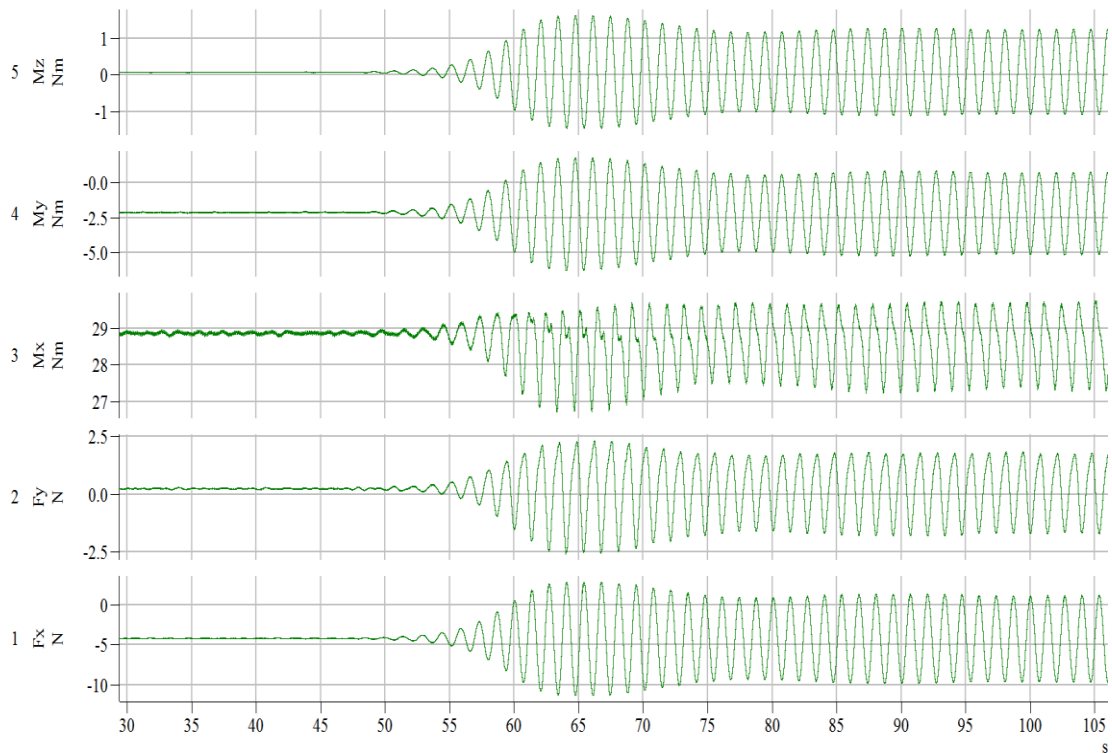


Figure 3.29. 5-component wave-induced loads acting on the damaged ship

### 3.7.2.1 Shear Forces

Figure 3.30 to Figure 3.31 illustrate non-dimensional vertical and horizontal shear forces acting on the intact and damaged ship hull in beam waves including first- and second- order study. The shear force, acting at the cross-section where the force gauge is located, is non-dimensionalized by  $\rho g A B L$ , where  $A$  is the amplitude of the incident wave,  $B$  is the breadth of ship model, and  $L$  is the ship length. Frequency is non-dimensionalized by  $(L/g)^{0.5}$ . It can be clearly seen that as the resonance frequency decreases due to floodwater the magnitude of vertical shear force raises by approximately 26%, while that of horizontal shear force grows up to 22% compared to the intact scenario.

At the resonance frequency of roll motion, the vertical shear force of the intact ship presents a relatively high second-order response, which takes magnitudes up to 30% of the first-order, while the second-order response of vertical shear force for the damaged ship and the horizontal shear force for both intact and damaged ship are small. It can be observed that there is a clear increase of vertical shear force acting on the damaged ship and it seems that there may be another peak in response with non-dimensional frequency over 5 due to floodwater dynamics.

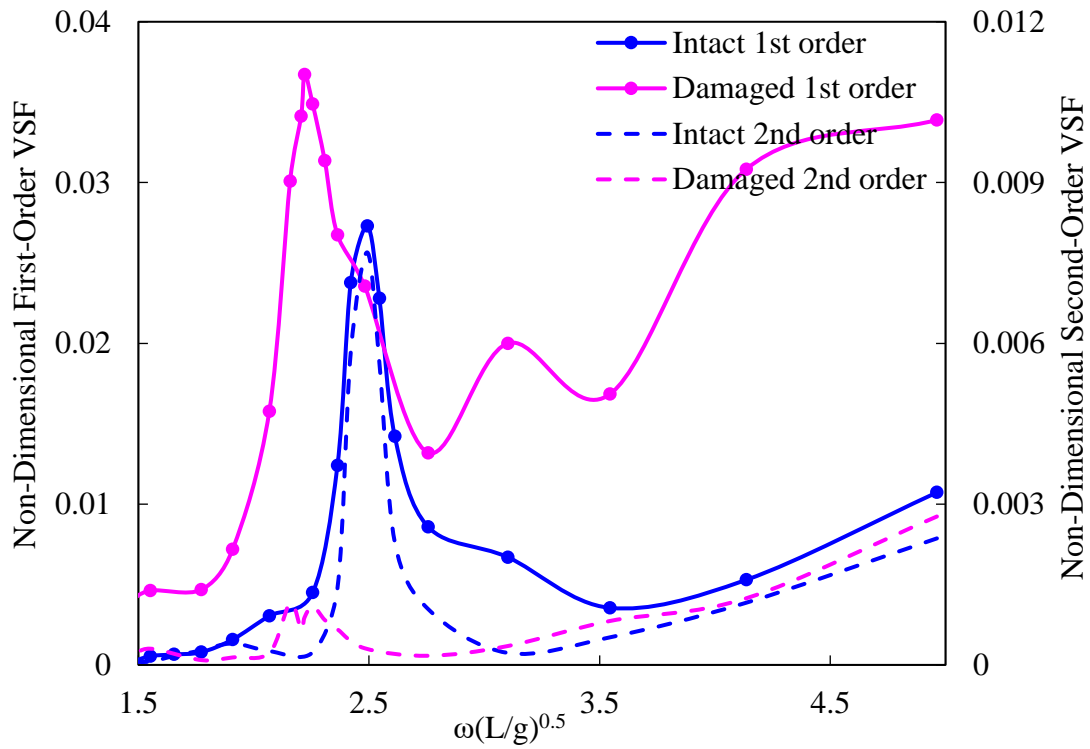


Figure 3.30. Non-dimensional vertical shear force against non-dimensional excitation frequency

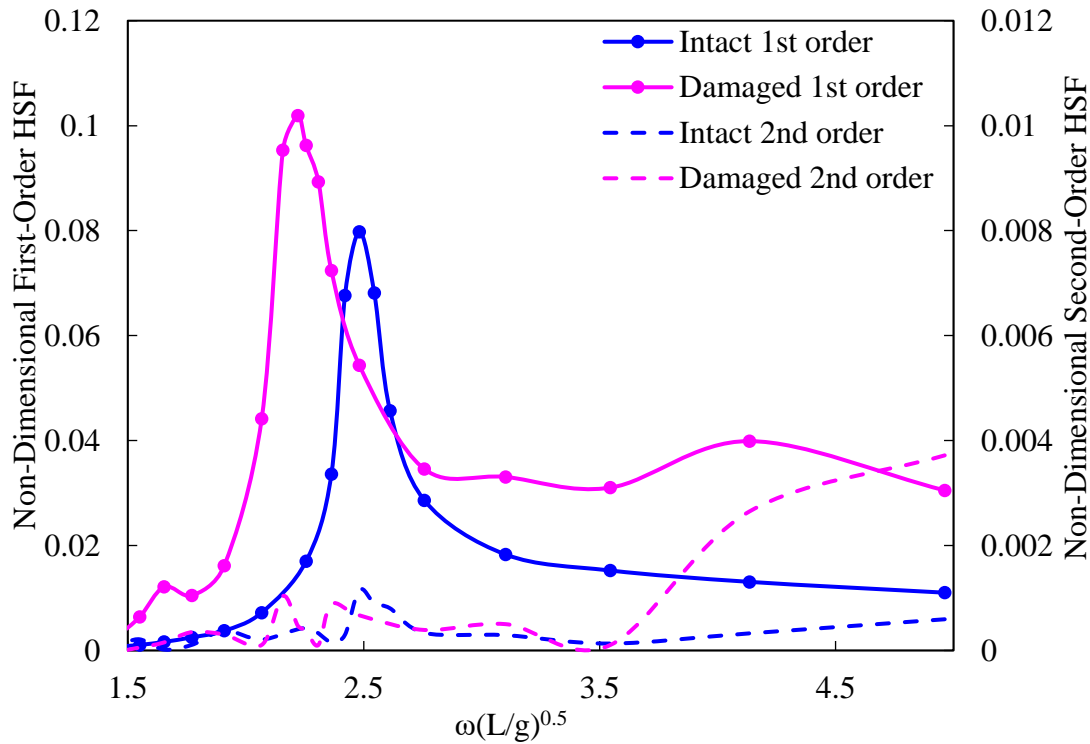


Figure 3.31. Non-dimensional horizontal shear force against non-dimensional excitation frequency

### 3.7.2.2 Moments

The bending and torsional moments acting on the intact and damaged ship hull are shown in Figure 3.32 to Figure 3.34. It can be highlighted that the free water surface inside the flooded compartment plays a significant role to reduce bending moments and torsional moment acting on the damaged ship, and it can be seen that a substantial decrease shown in vertical bending moment and horizontal bending moment by 16% and 86% respectively, and in torsional moment by 36% at the damaged resonance frequency.

Vertical bending moment acting on the intact ship presents a strong nonlinearity with the second-order response almost the same as the first-order amplitude. In contrast the damaged ship's vertical bending moment does not demonstrate a significant nonlinearity. It is interesting to find that the first-order vertical bending moment acting on the intact and damaged ship seems to reveal another peak apart from the resonance frequency. As non-dimensional frequency reaches about 3.5, the intact vertical bending moment appears to reach a peak amplitude. The vertical bending moment acting on the damaged ship also increases in this region as shown in Figure 3.32. This is similar to the vertical shear force acting on the intact and damaged ships, which also reveals another peak as non-dimensional frequency is greater than 5.

As shown in Figure 3.33, the horizontal bending moment acting on the damaged ship presents a substantial drop compared to the intact case. The free surface of floodwater in the damaged compartment also has an impact on the nonlinearity of horizontal bending moment. At resonance frequency of the damaged ship a second-order response can be seen in the horizontal bending moment (20% to first-order) while the horizontal bending moment at resonance frequency of the intact ship seems to be linear. When the non-dimensional frequency is greater than 5, horizontal bending moment on the damaged ship tends to show another peak response with relatively higher nonlinearity.

The damaged ship experiences a larger torsional moment than the intact ship when non-dimensional excitation frequency is less than 2.4, while the reverse is true between non-dimensional frequency from 2.4 up to 3.1. As non-dimensional frequency increases beyond 3.1, there is almost no difference between intact and damaged

torsional moment on the intact and damage ship. The second-order torsional moment acting on the intact and damaged ship is small.

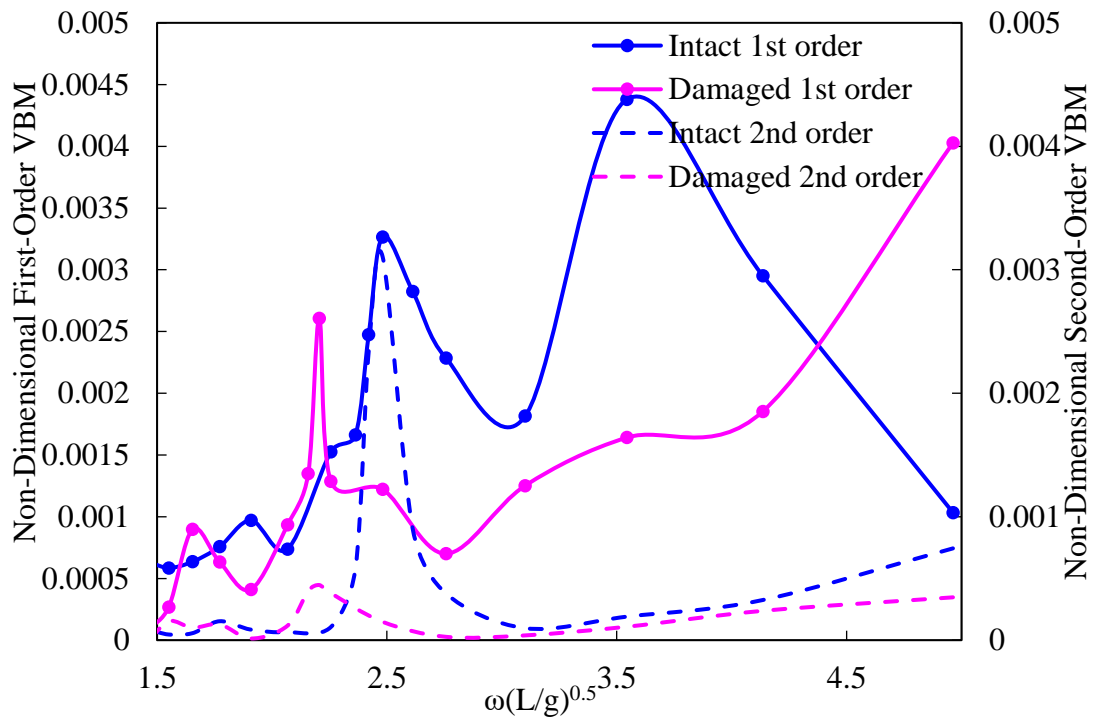


Figure 3.32. Non-dimensional vertical bending moment with non-dimensional frequency

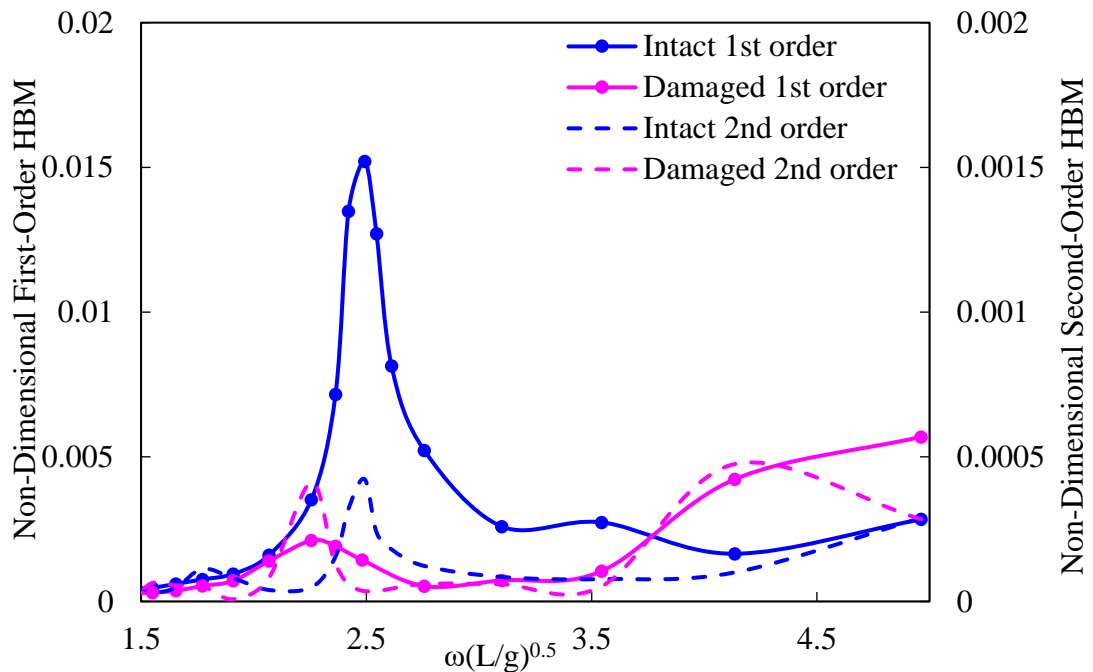


Figure 3.33. Non-dimensional horizontal bending moment with non-dimensional frequency

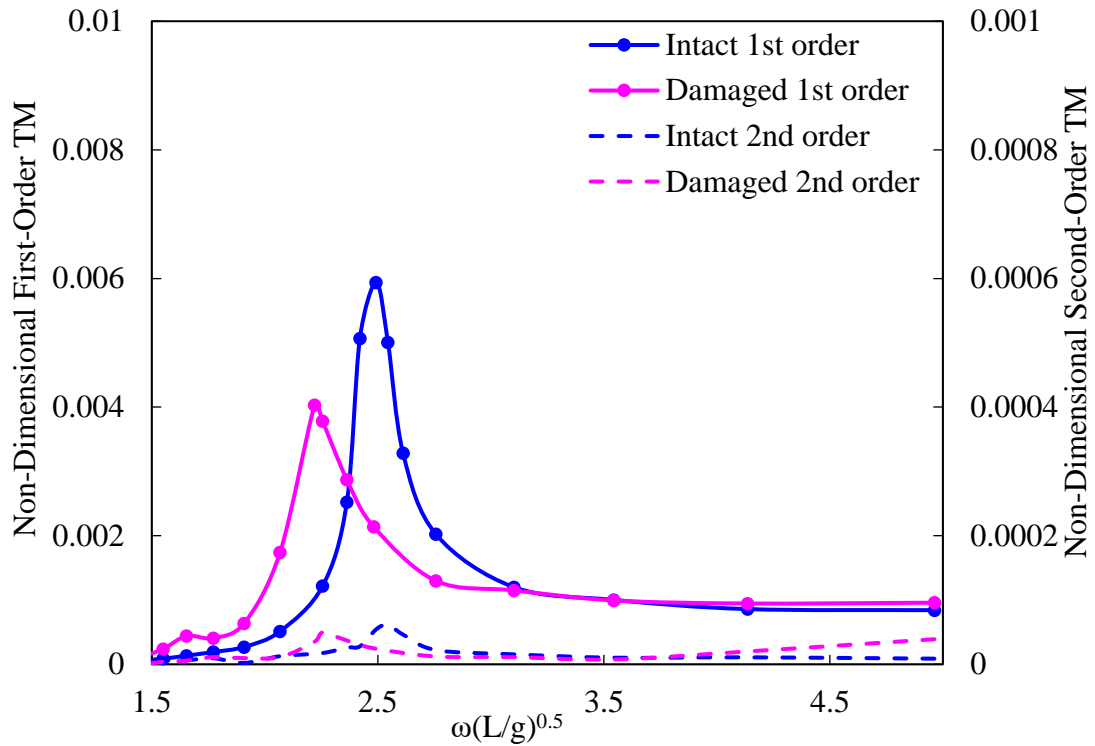


Figure 3.34. Non-dimensional torsional moment with non-dimensional frequency

### 3.7.3 Comparison between two experiments

As a comparison with the present tests, the previous measurements by Begovic et al. (2017) are shown. Table 3.6 gives the natural period and frequency of the intact and damaged ship's roll motion compared to the former work.

	Intact		Damaged	
	Present work	Begovic et al., 2017	Present work	Begovic et al., 2017
$T_N$	1.394 s	1.370 s	1.565 s	1.525 s
$\omega_N$	4.507 rad/s	4.586 rad/s	4.015 rad/s	4.120 rad/s

Figure 3.35 and Figure 3.36 compare the intact and damaged ship roll motion between the two model tests. Although the roll motions of the intact and damaged ship at lower and higher frequencies between two tests reveal a general agreement, it is obvious that a substantial difference can be observed around the resonance frequency of the intact and damaged ship's roll motion.



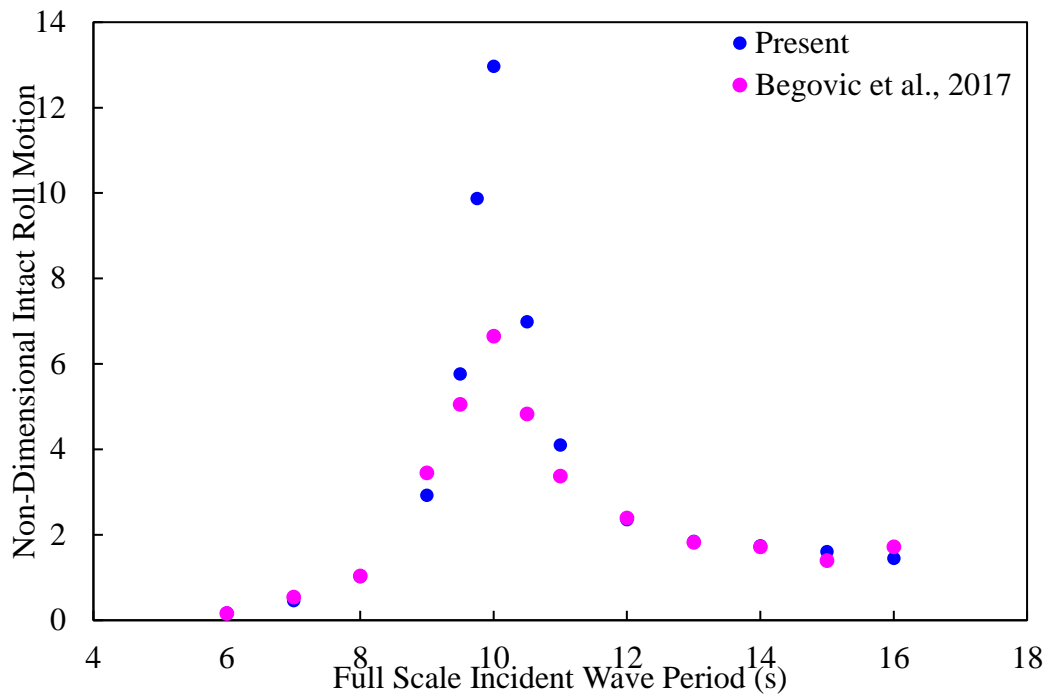


Figure 3.35. Comparison of the intact ship's roll motion

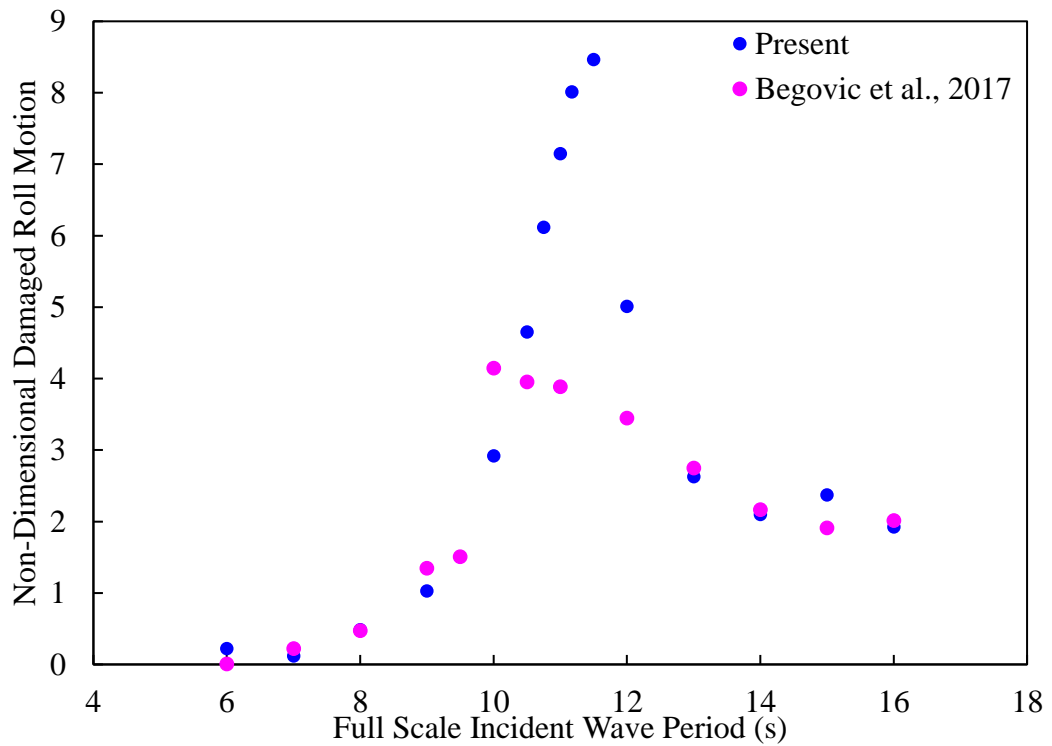


Figure 3.36. Comparison of the damaged ship's roll motion

There are several factors which contribute to this difference.

Begovic et al. (2017) presents results obtained from the model test at Kelvin Hydrodynamic Laboratory with the same ship model – DTMB 5415 with scale factor

51. The present experiment attempted to keep the main particulars of the ship model the same as in the previous experiment. However, it proved hard to repeat the ballast condition of the ship model precisely and key factors of the present ship model, in particular  $I_{xx}$  and the distribution of mass within each of the cut sections are approximations. A related problem is found in relation to the radius of gyration,  $k_{xx}$  (or  $I_{xx}$ , the mass moment of inertia of ship's roll motion); the value for the radius of gyration given by Begovic et al. (2017) is that obtained directly from free decay tests in calm water (marked as " $k_{xx-water}$ "). This means that the value of  $k_{xx}$  provided by the former experiment, includes hydrodynamic effects and should not be directly compared with the value from the present tests, which are for the solid mass only. This is especially relevant when considering numerical simulation with CFD method for which  $k_{xx}$  is a crucial input parameter. Therefore, it is expected that there is a difference between the two mass moments of inertia of the ship's roll motion from the two experiments. This contributes to the (relatively small) difference in natural frequency seen from the free decay tests.

Another key factor that triggers this difference between two experiments is the choice of wave settings. Begovic et al. (2017) used waves of constant steepness (defined as the ratio of wave height and wave length,  $H/\lambda_w$ ). The steepness is kept constant as 0.02 under the most wave conditions, and hence wave height grows with increasing wave period. In the present test wave height is mainly kept constant at 0.02m at the most of wave frequencies, but several different wave heights are also chosen for nonlinear investigation. This difference in approach has particular significance for the roll motion of this vessel, which is highly non-linear with wave height, presumably due to the non-linearity of viscous roll damping for this round-bilged vessel. To investigate the different wave heights on the intact and damaged ship's roll motion, different wave heights were generated at the resonance frequency of the intact and damaged ship's roll motion, which is 0.72 Hz and 0.64 Hz respectively under the intact and damaged condition for both works. The values chosen 10mm, 15mm, 20mm, 25mm and 30mm in the present study. In the previous study the wave heights adopted are equal to 0.03m, 0.04m and 0.062m at the intact resonance frequency and 0.074m at the damaged resonance frequency respectively. Figure 3.37 and Figure 3.38 show non-dimensional wave heights (non-dimensionalised as  $H/L_{oa}$ ) against non-dimensional intact and

damaged roll motion respectively obtained in both works. It is clear to see that results obtained by both tests show a consistent decreasing trend as wave height increases. Since data about heave motion by Begovic's work is not available in beam sea tests, and the roll motion is the point that we mainly concerned, heave motion is not to be presented here.

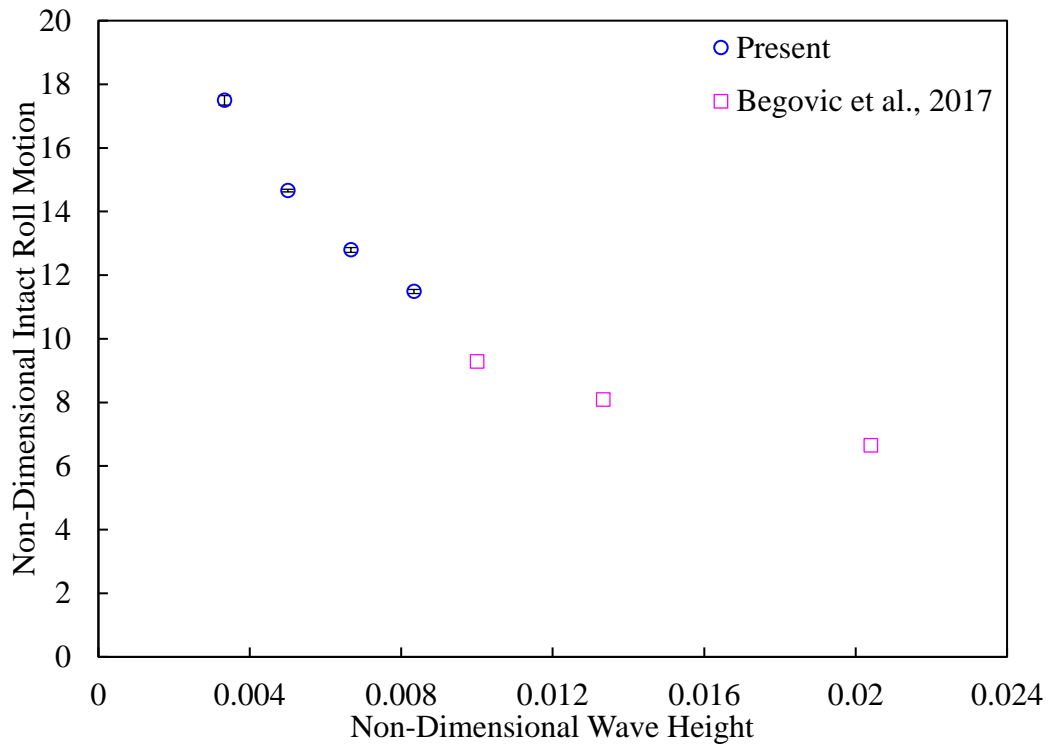


Figure 3.37. Roll motion of the intact ship at the resonance frequency of roll motion

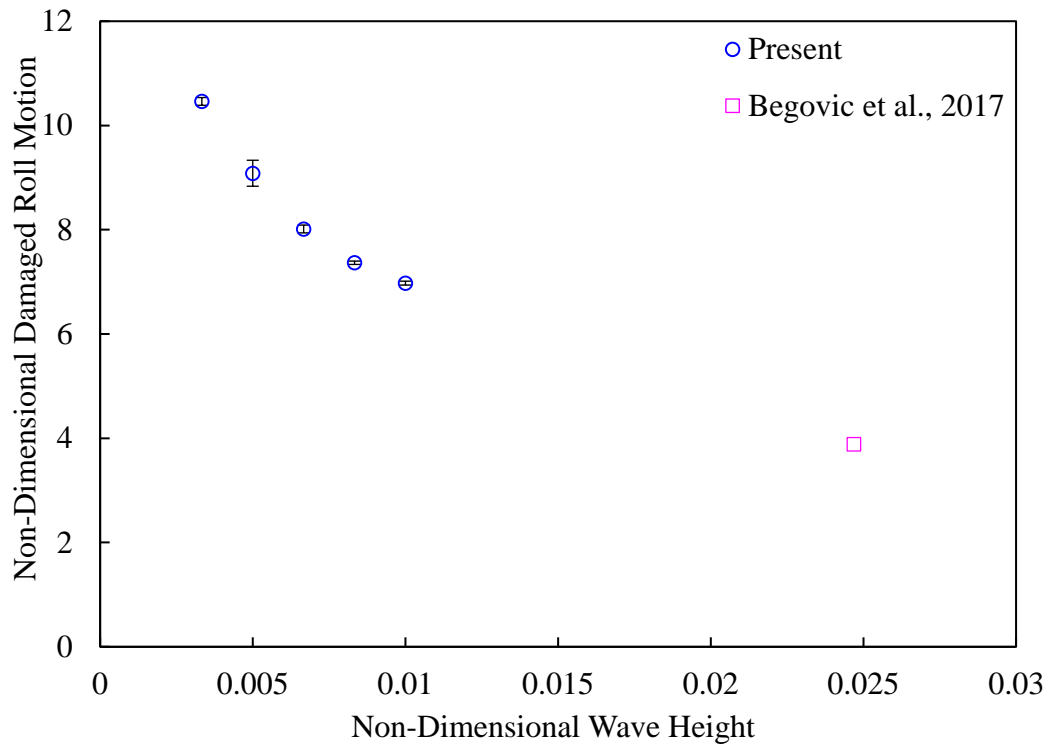


Figure 3.38. Roll motion of the damaged ship at the resonance frequency of roll motion

Figure 3.39 and Figure 3.40 compare the measured vertical shear force by the present physical model test and Begovic et al. (2017). It is once again clearly seen that differences can be observed between both experiments' results especially at the resonance frequencies. Figure 3.41 to Figure 3.42 illustrate the variation of non-dimensional vertical shear force acting on the intact and damaged ship with wave height, at the resonance frequency of the intact and damaged ship's roll motion. With increasing incident wave height, the non-dimensional vertical shear force acting on the intact and damaged ship all decrease in a manner similar to that seen for the roll motion.

It can be inferred from this analysis that the difference in wave height between the two sets of tests, allied to the highly non-linear roll of the vessel, is the main reason for the difference in results between the present and previous tests, especially at the resonant frequency. Similar studies for horizontal shear force, vertical and horizontal bending moment and torsional moment are shown in Figure 3.43 to Figure 3.58, respectively. Again, it is interesting to see that when full-scale incident wave period is smaller than 7s (i.e. non-dimensional frequency is greater than 3.5), vertical shear force, vertical

bending moment and horizontal bending moment acting on the damaged ship show a rise due to the damaged floodwater dynamics. To characterize wave-induced loads acting on the damaged ship at the non-dimensional frequencies greater than 3.5 (model-scale frequency equals to 1Hz), more investigation should be focused in the further study.

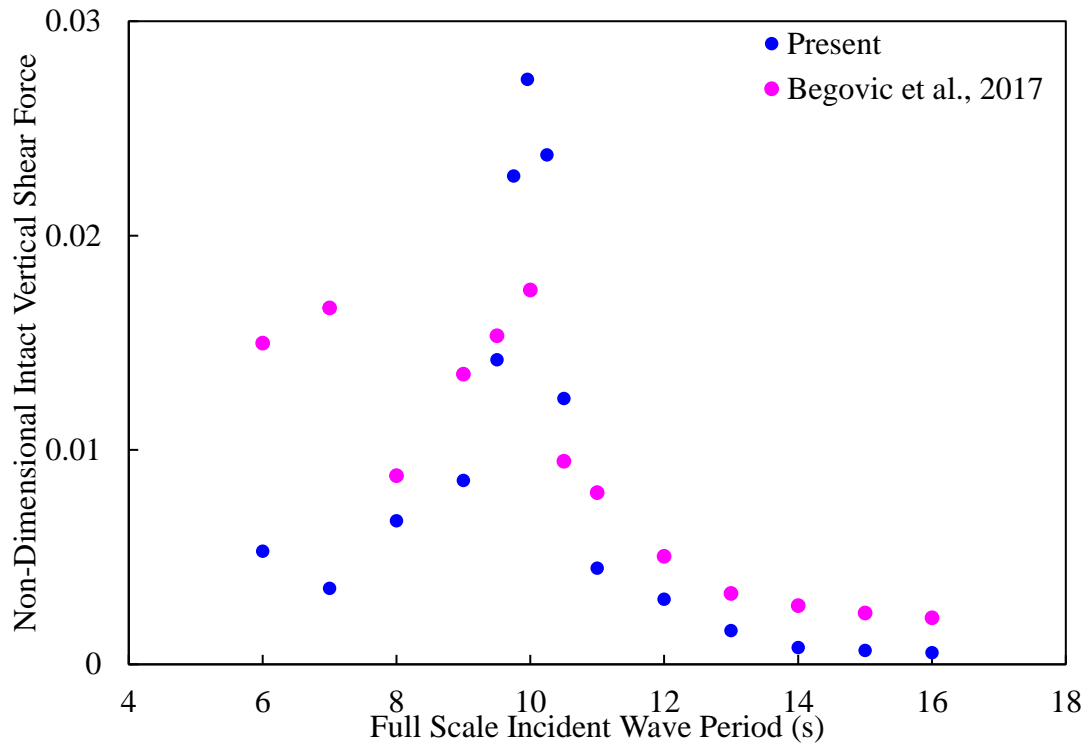


Figure 3.39. Comparison of the intact ship's vertical shear force

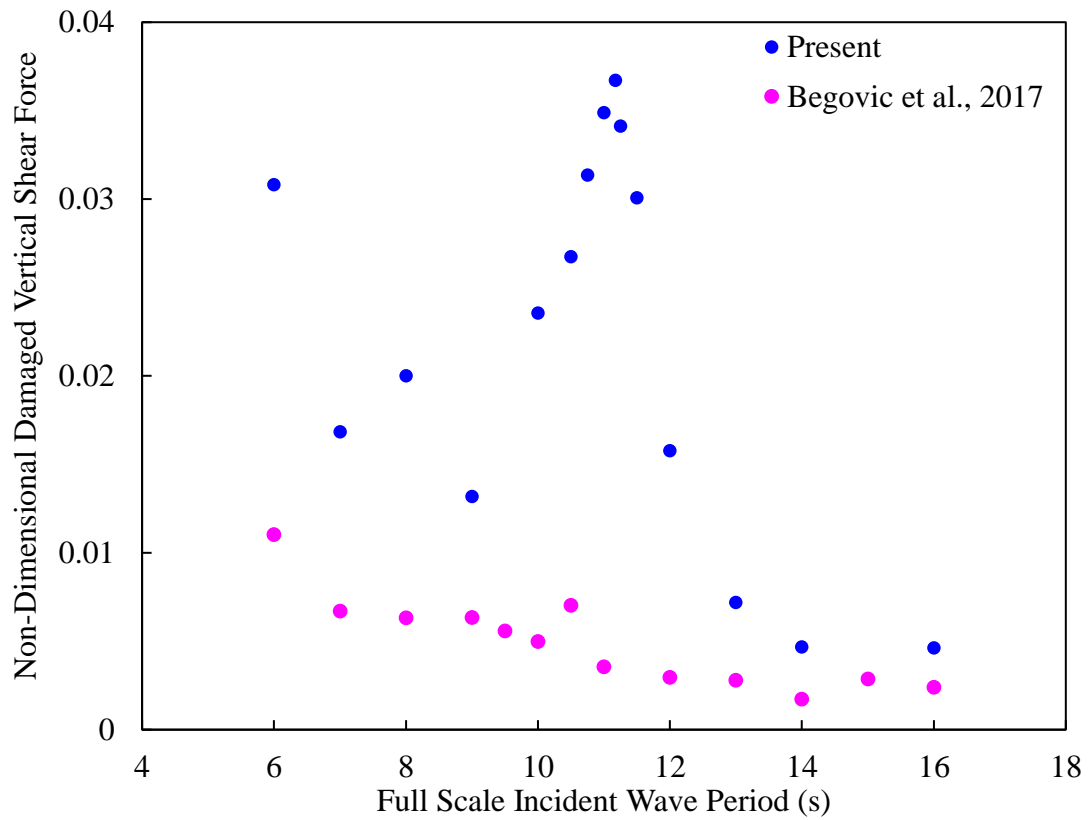


Figure 3.40. Comparison of the damaged ship's vertical shear force

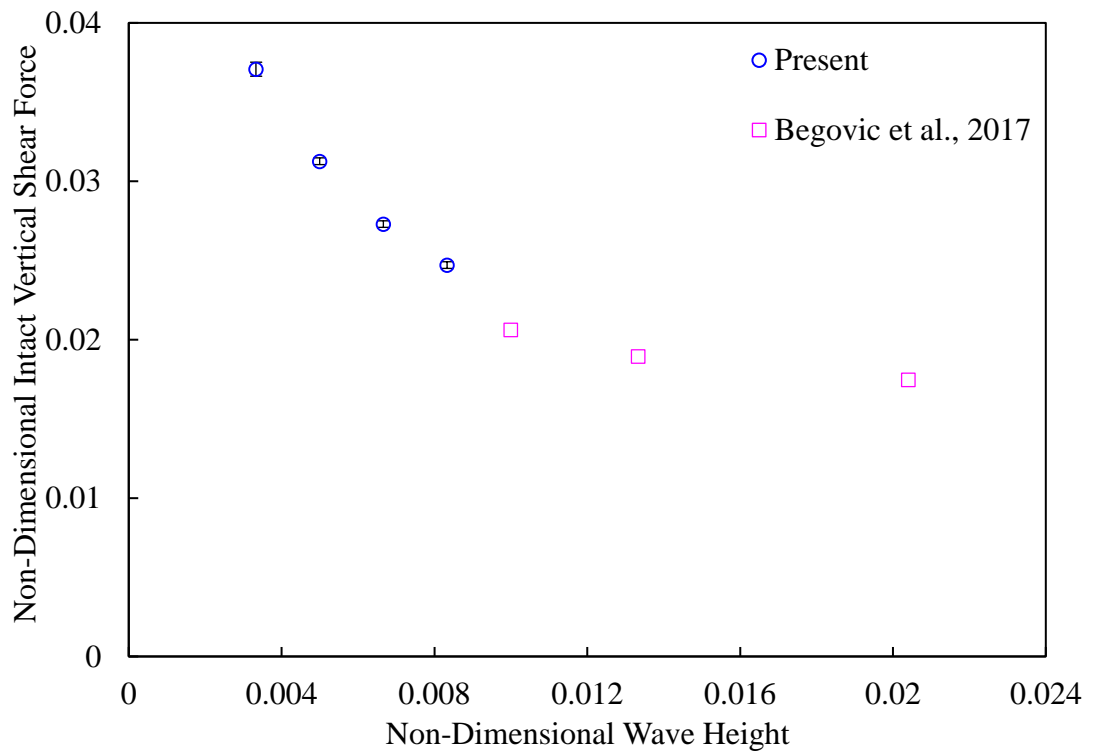


Figure 3.41. Vertical shear force acting on the intact ship at the resonance frequency

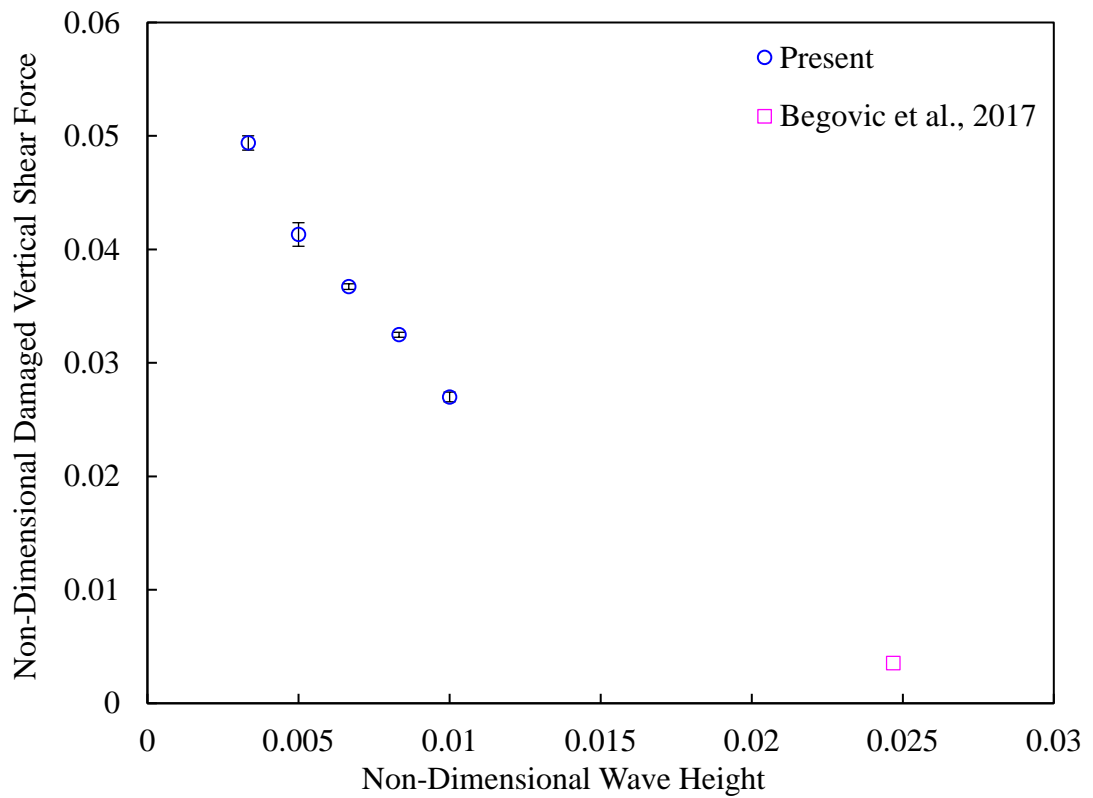


Figure 3.42. Vertical shear force acting on the damaged at the resonance frequency

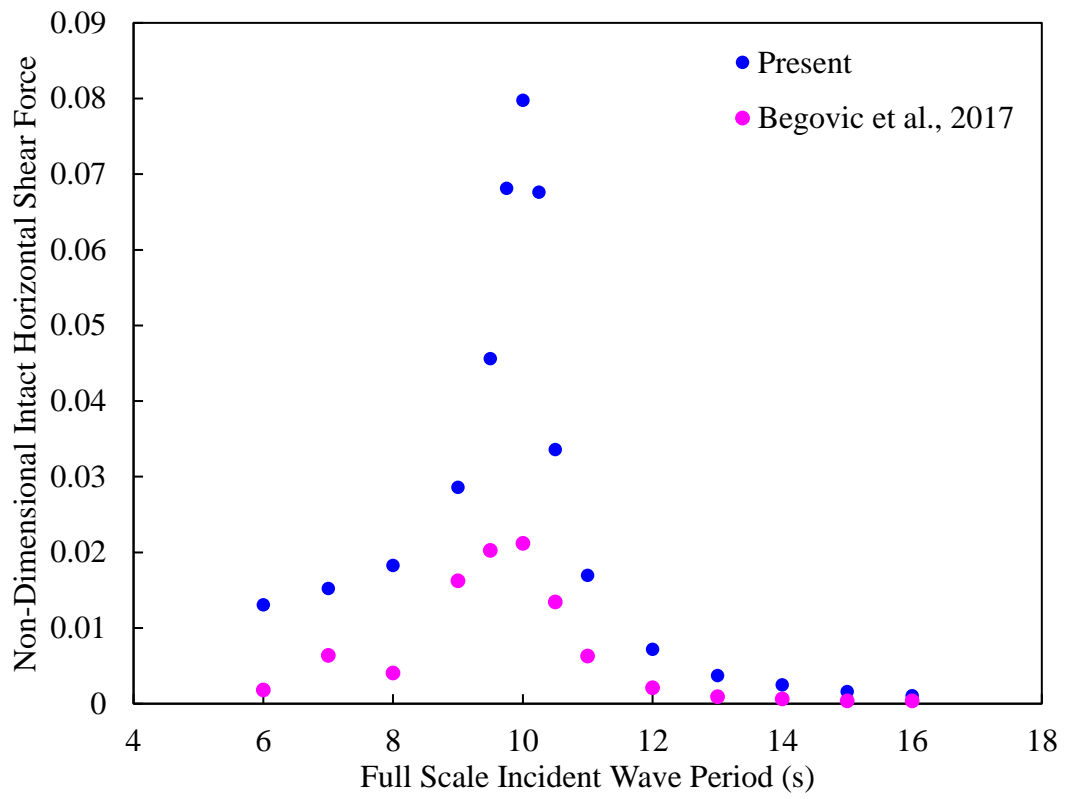


Figure 3.43. Comparison of the intact ship's horizontal shear force

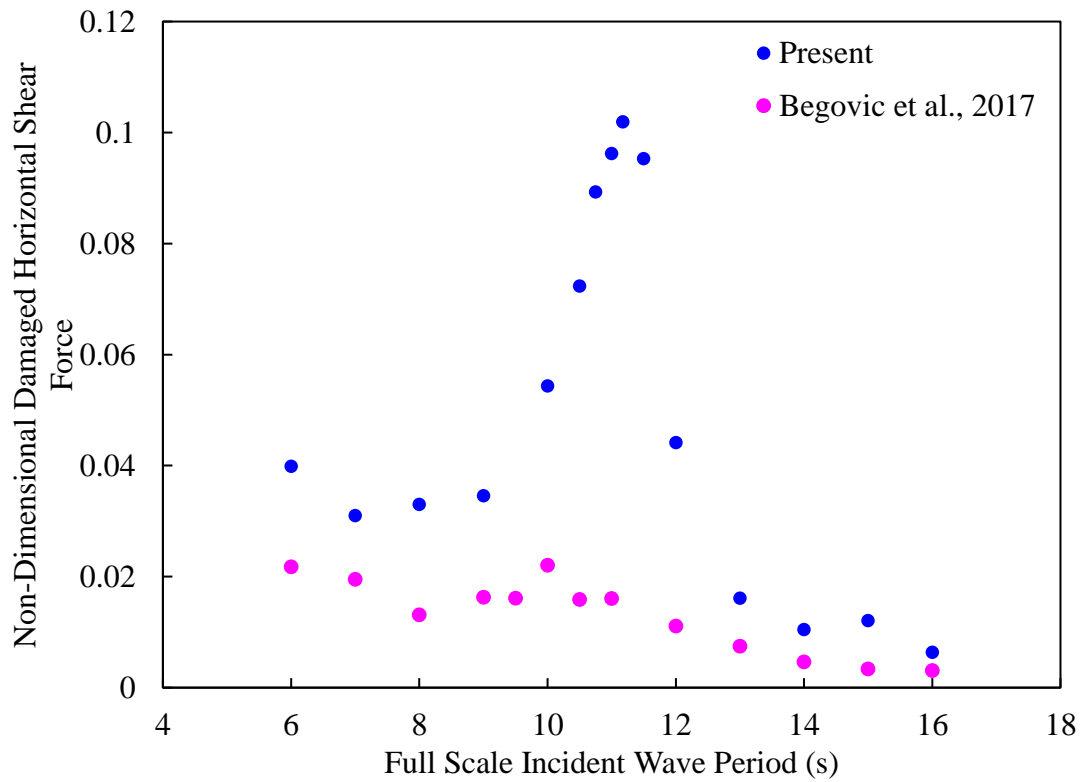


Figure 3.44. Comparison of the damaged ship's horizontal shear force



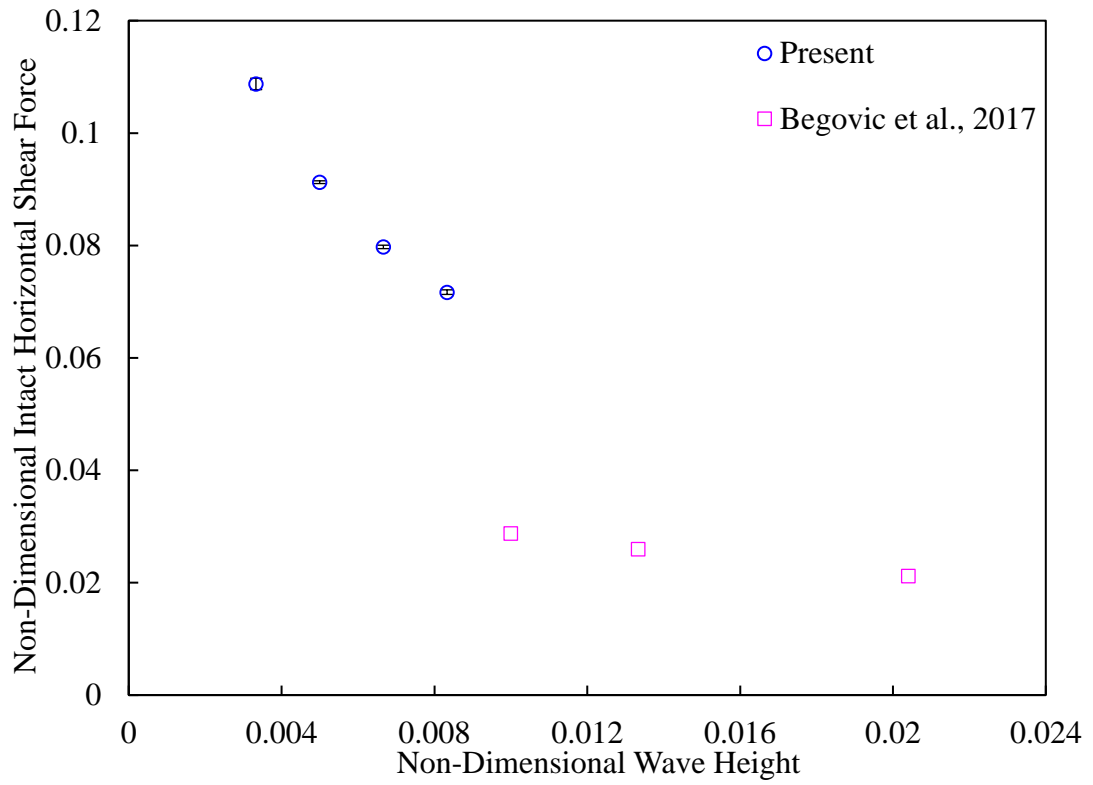


Figure 3.45. Horizontal shear force acting on the intact ship at the resonance frequency

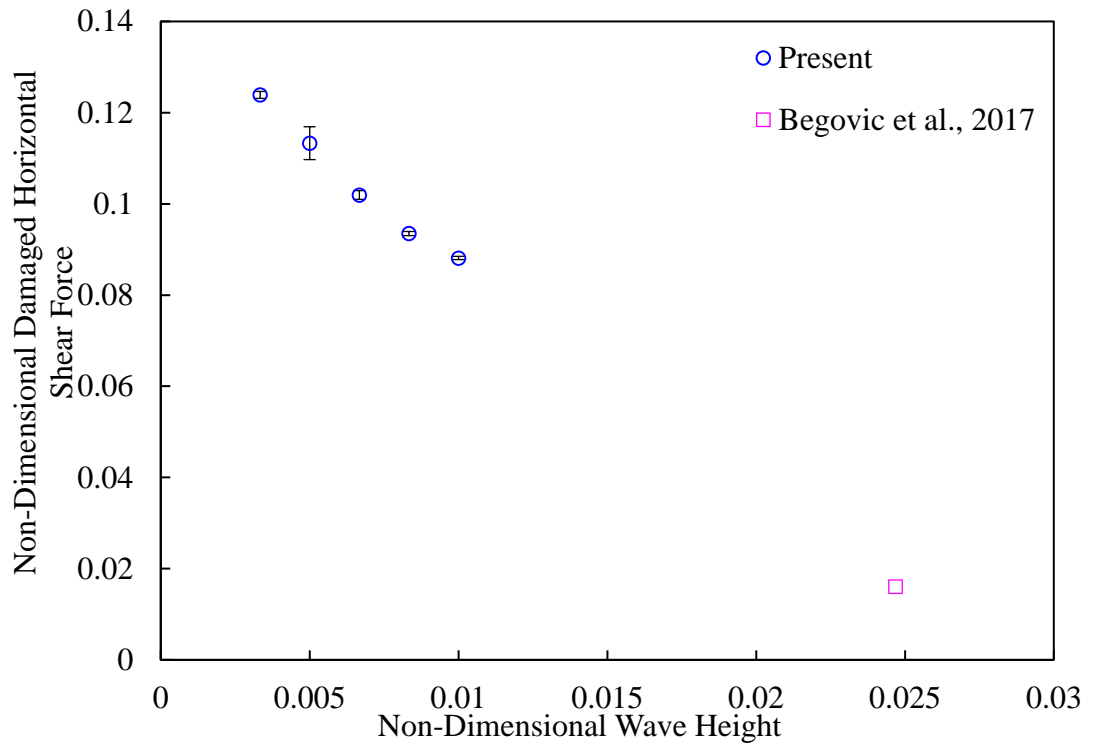


Figure 3.46. Horizontal shear force acting on the damaged ship at the resonance frequency

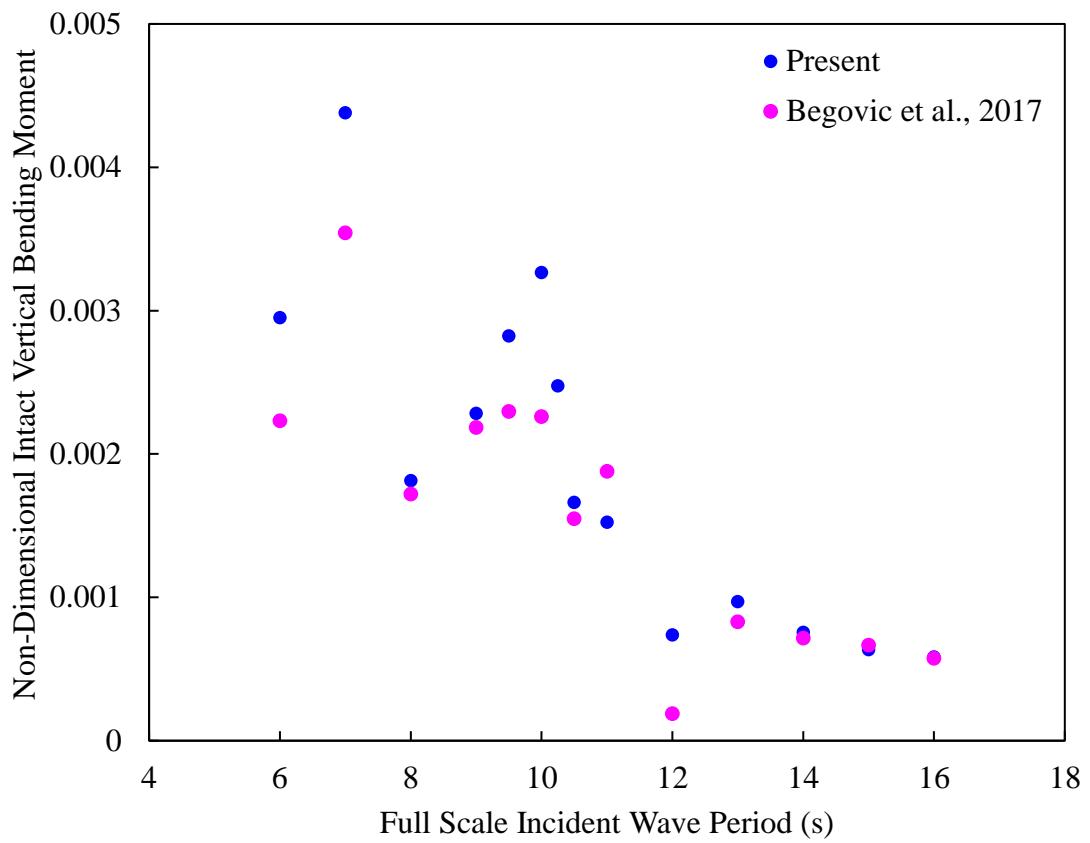


Figure 3.47. Comparison of the intact ship's vertical bending moment

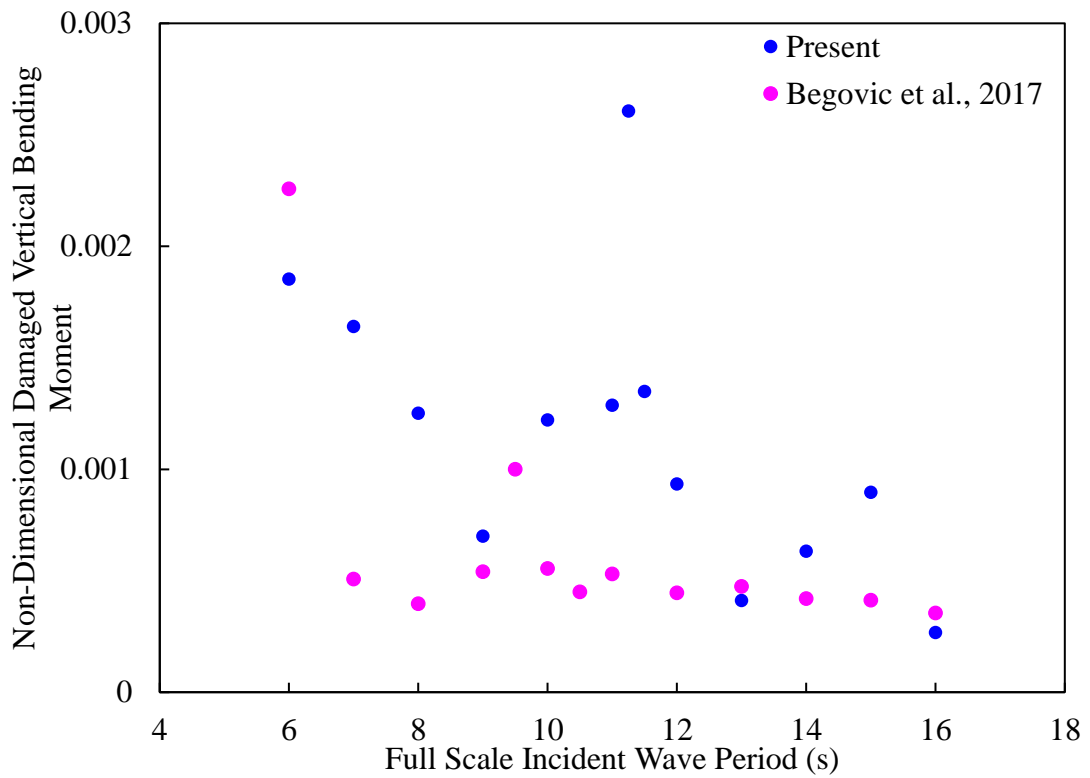


Figure 3.48. Comparison of the damaged ship's vertical bending moment

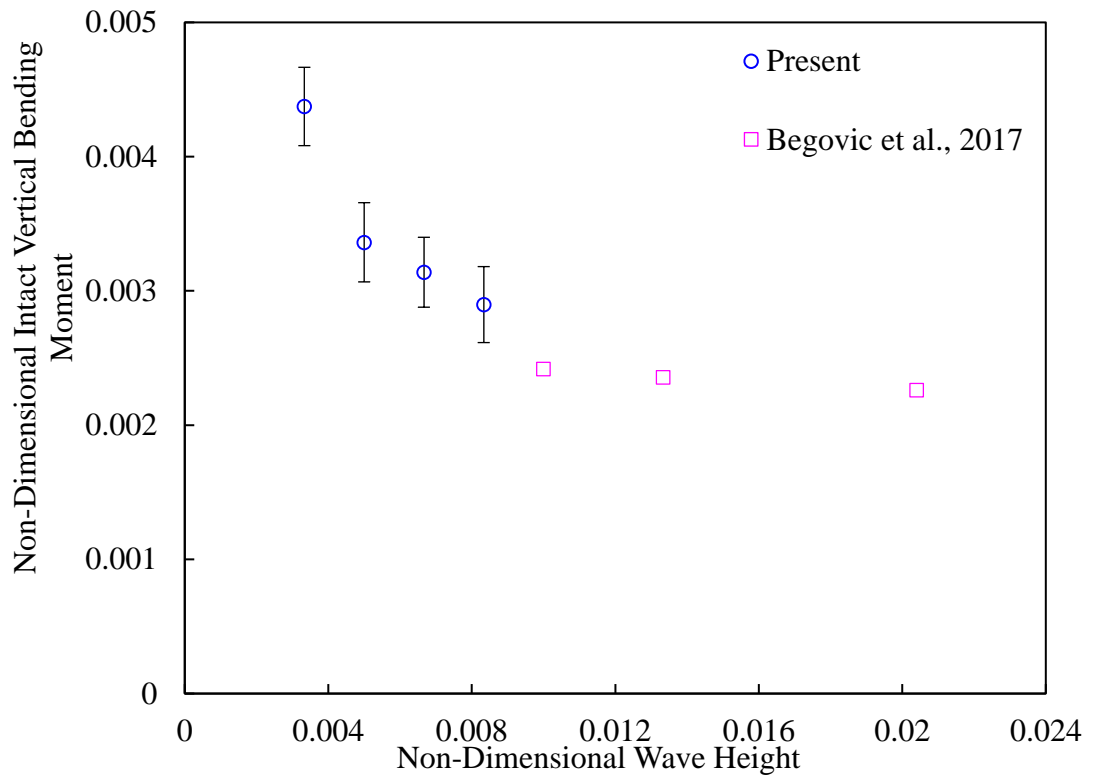


Figure 3.49. Vertical bending moment acting on the intact ship at the resonance frequency

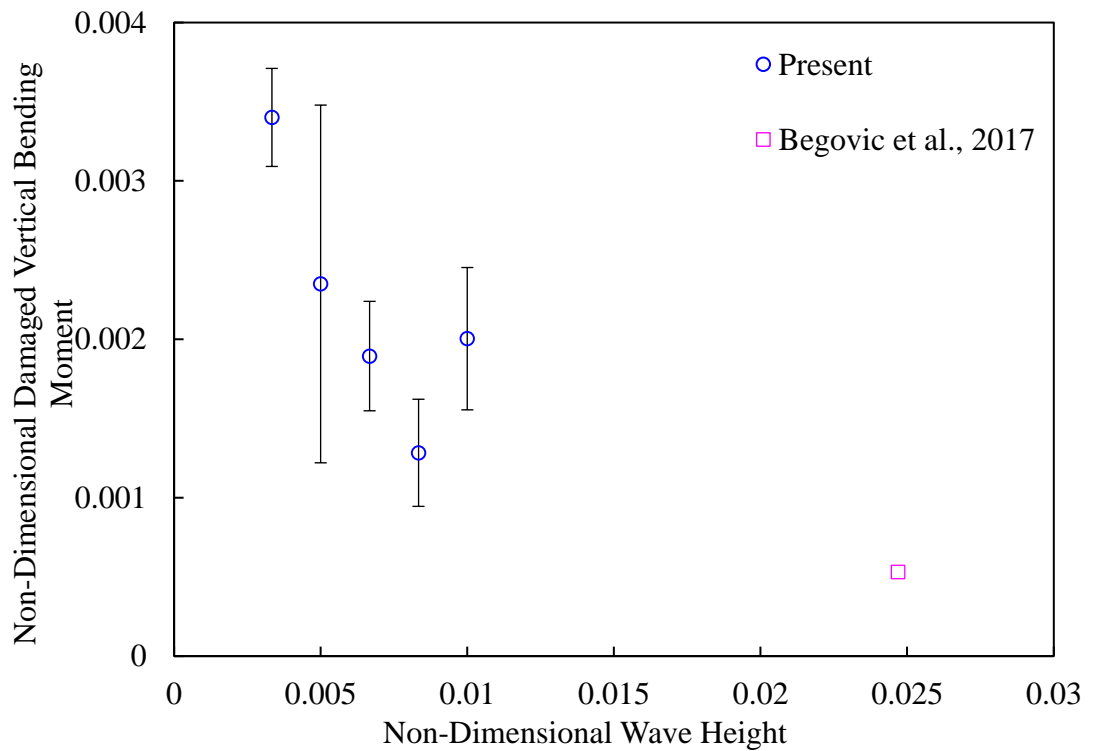


Figure 3.50. Vertical bending moment acting on the damaged ship at the resonance frequency

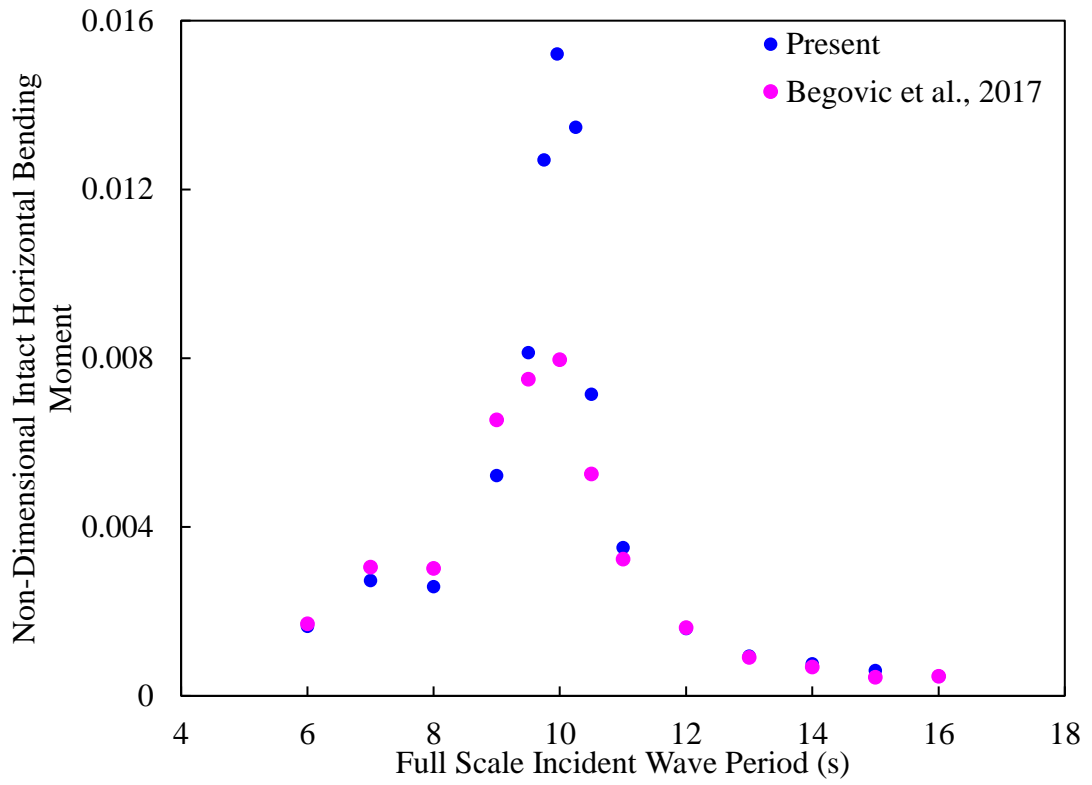


Figure 3.51. Comparison of the intact ship's horizontal bending moment

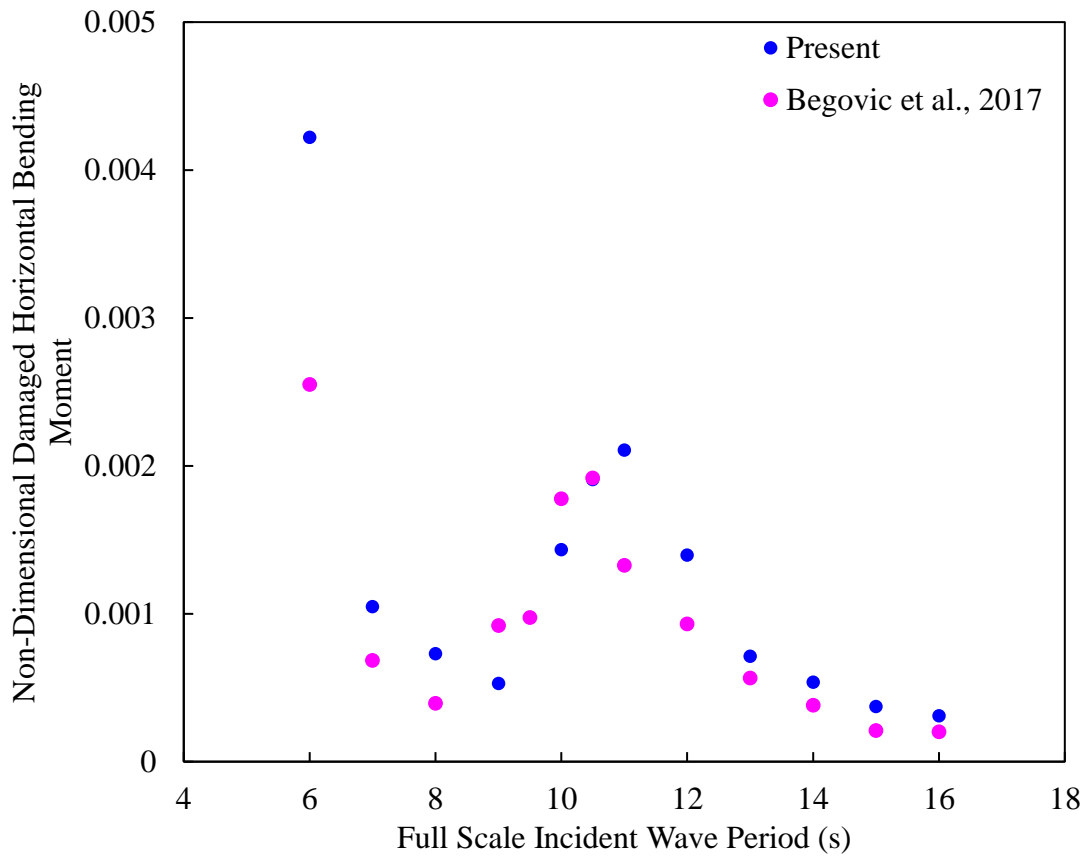


Figure 3.52. Comparison of the damaged ship's horizontal bending moment

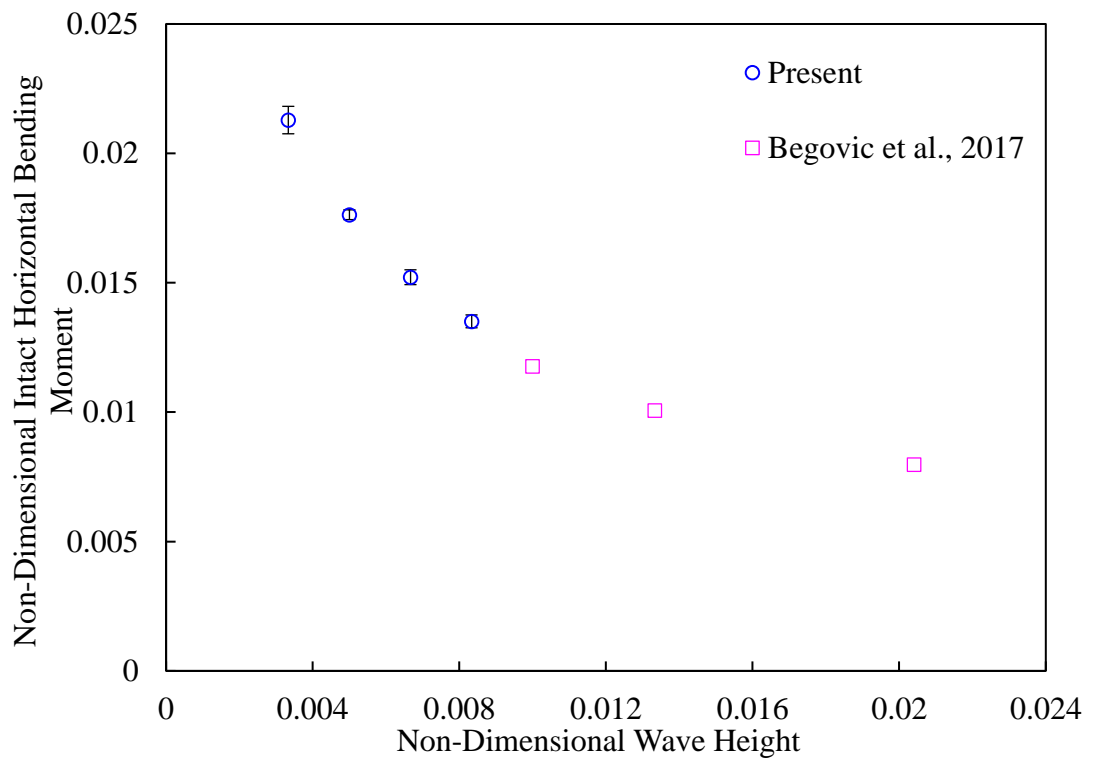


Figure 3.53. Horizontal bending moment acting on the intact ship at the resonance frequency

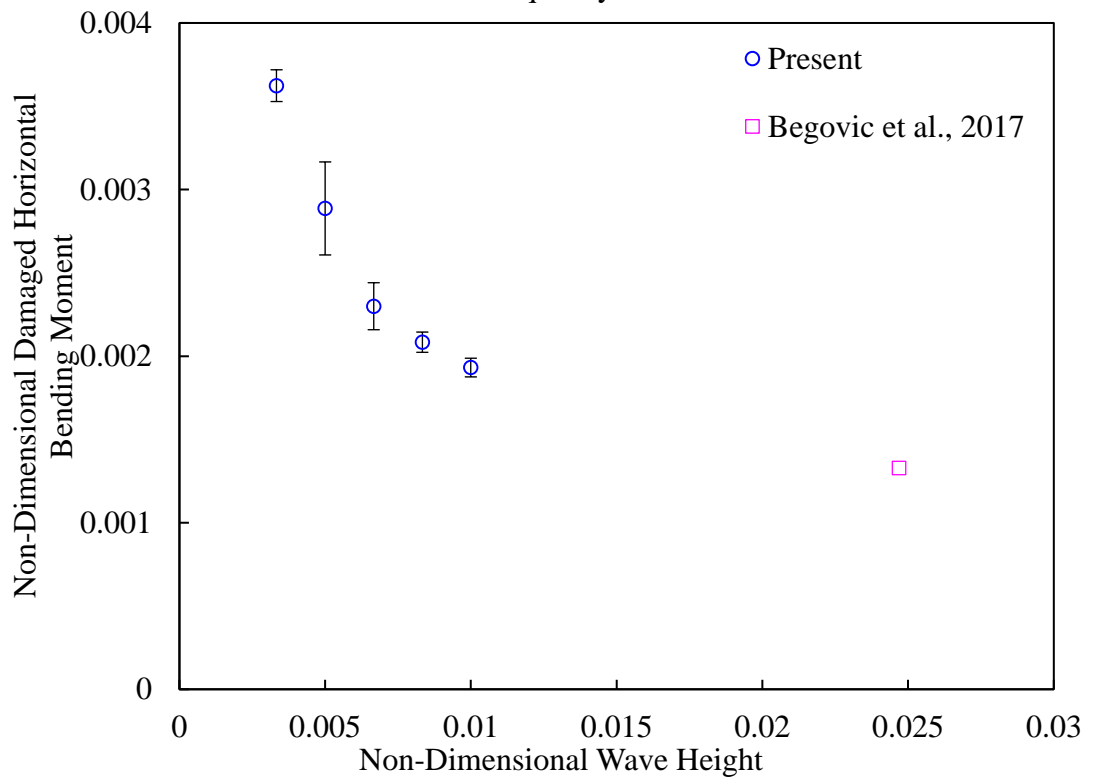


Figure 3.54. Horizontal bending moment acting on the damaged ship at the resonance frequency

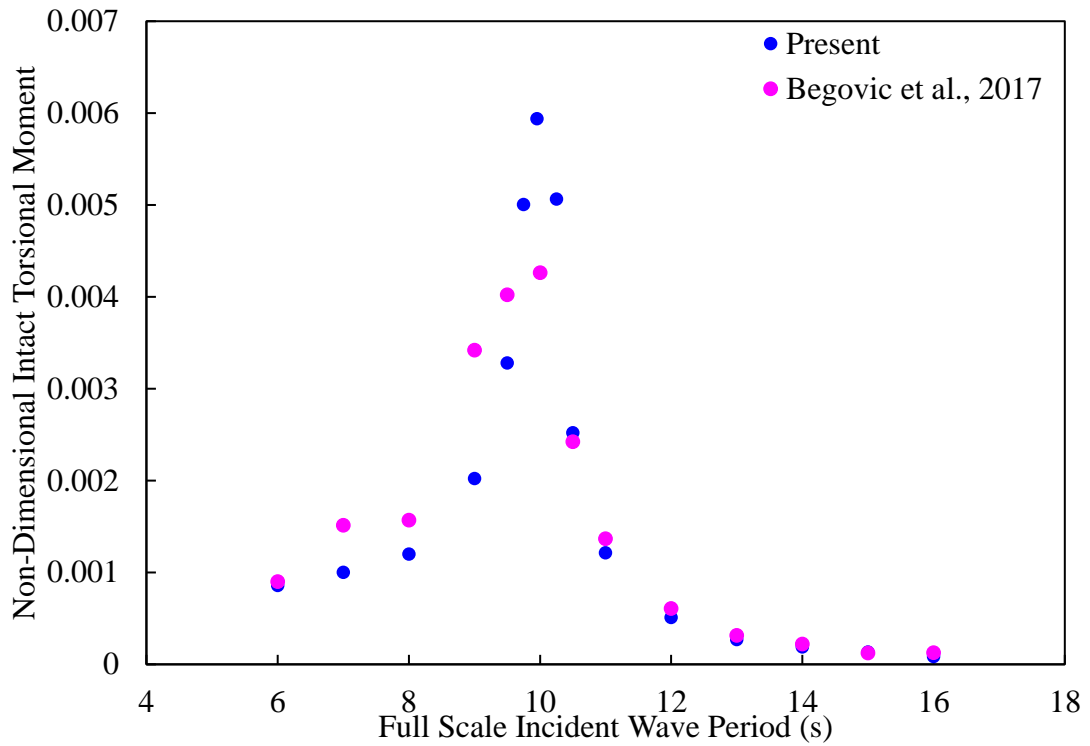


Figure 3.55. Comparison of the intact ship's torsional moment

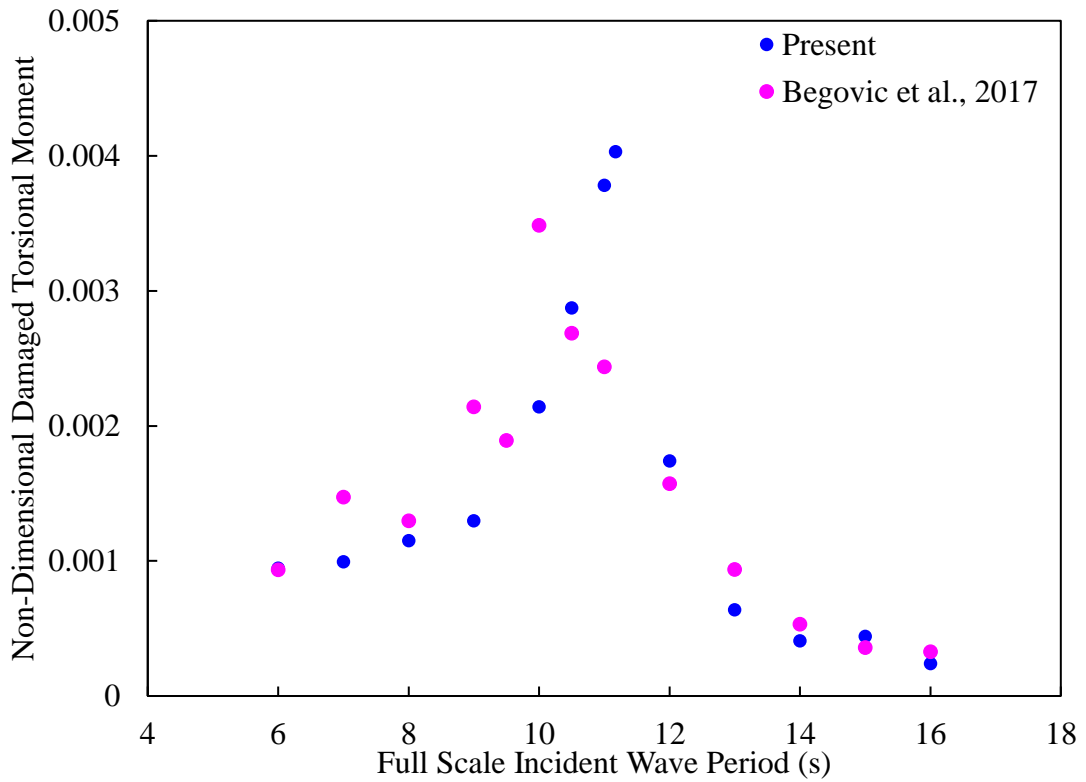


Figure 3.56. Comparison of the damaged ship's torsional moment

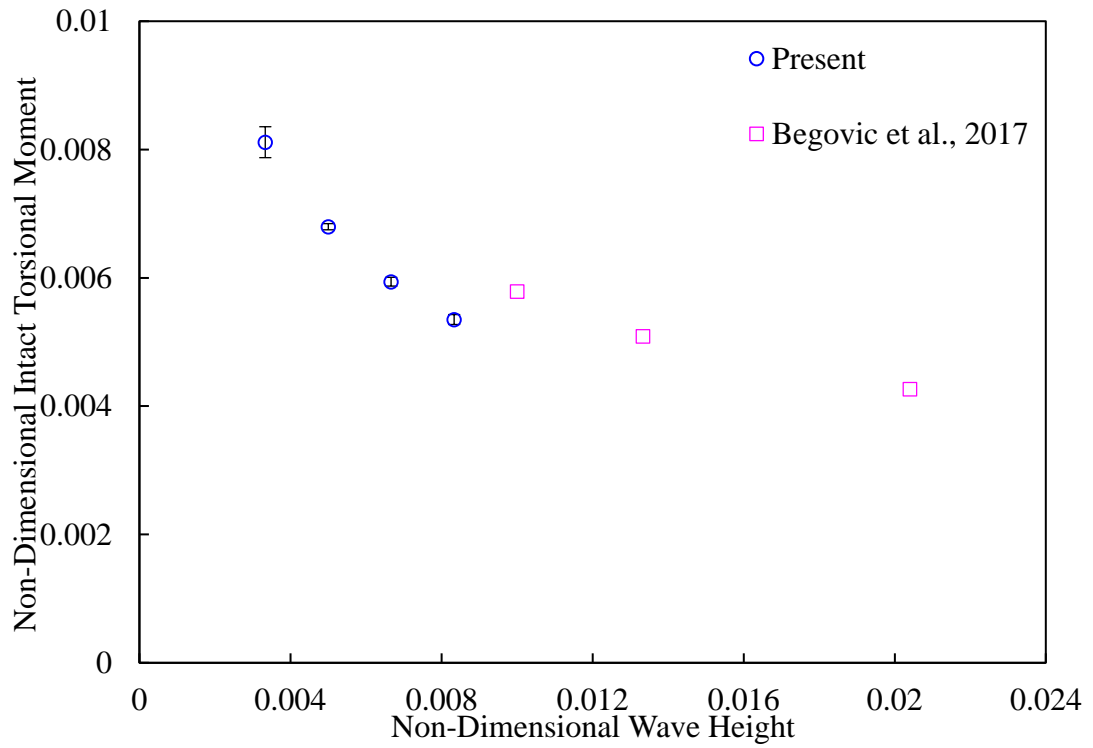


Figure 3.57. Torsional moment acting on the intact ship at the resonance frequency

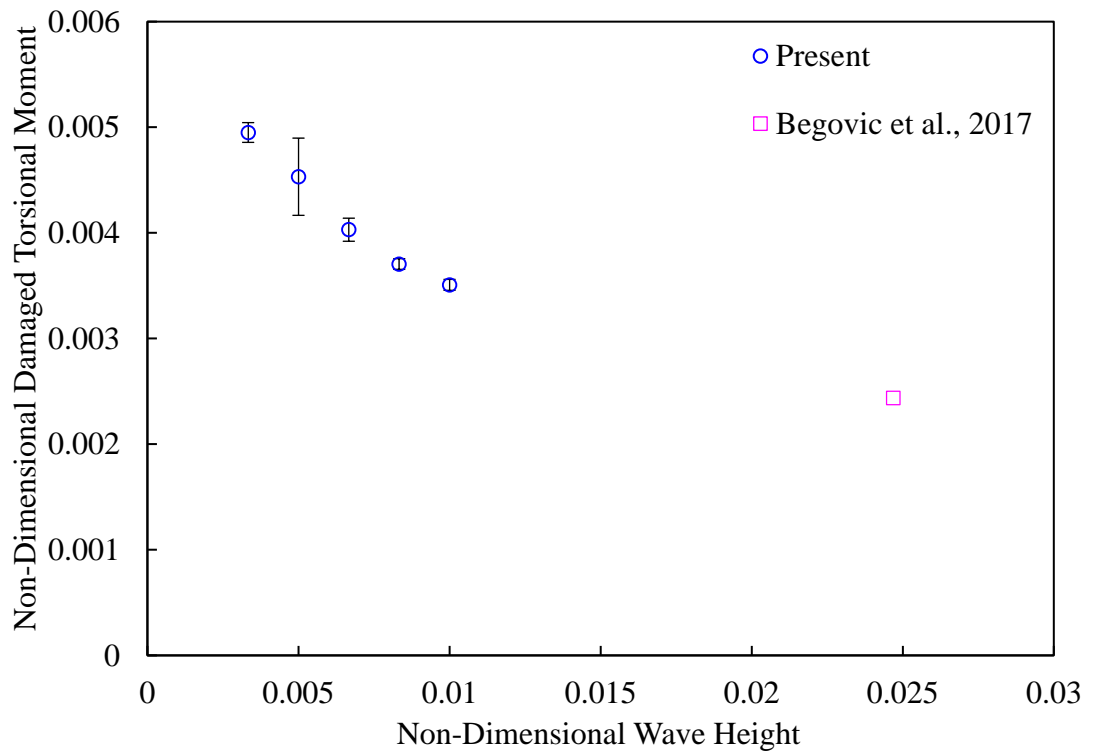


Figure 3.58. Torsional moment acting on the damaged ship at the resonance frequency

As a final comment, it is unclear as to how (or whether) Begovic corrected for cross-coupling in the load cell, which as shown previously, has a significant impact on some of the measured loads.

### **3.8 Chapter remarks**

An experimental investigation is carried out on the intact and damaged behaviour of a 1/51-scale model of a naval combatant in this Chapter. The ship motions and wave-induced loads acting on the intact and damaged ship hull are measured in calm water and beam seas with zero forward speed. Regular beam waves are generated by wave maker and ship hull is moored perpendicularly to the direction of wave coming. Damaged opening faces to starboard, where ship encounters the generated beam waves directly. Two compartments can be flooded but the entire flooding is asymmetric due to a half-unflooded double-bottom tank. To eliminate trapped air compression, a ventilation pipe is installed in each flooded compartment so that trapped air cannot influence floodwater inside the compartments. Experimental data obtained in this study including ship motions and wave-induced loads of intact and damaged combatant vessel in beam waves is provided to valid with numerical method.

The free decay motions in calm water and the motions excited by regular beam waves give the same conclusion that the water surface effect in the damaged compartments has an additional damping impact on ship behaviours, and the natural frequency of damaged ship is obviously smaller than that of the intact ship. However, damaged ship can reach the final stable state within a shorter time. In other words, damaged ship stabilizes more quickly than intact ship. Due to the free surface dynamics in the damaged compartments as well as its interaction with ship motions, highlighted nonlinearities can be obviously observed in roll motions and wave-induced loads, but linearity is shown in heave motions of the intact and damaged ship hull. According to the results of wave-induced loads acting on the intact and damaged ship hull, there is a remarkable reducing effect on wave-induced bending moments on the ship model due to existence of water surface in damaged compartments, however, in contrast, shear forces on damaged ship are higher than that on the intact ship.

The present experimental work is a further investigation from Begovic et al. (2017). In this work, cross-coupling effect of the force transducer on measured loads is



discussed as it may result in overestimation of the measurements, which should be corrected.

The ship's roll motion and measured loads obtained from two experiments are also compared. Although it can be seen that tendencies of RAOs for roll motion and wave-induced loads are reasonably similar, it seems that non-dimensional ship responses and measured wave-induced loads in this work are substantially larger near resonance. It is shown however that the difference in non-dimensional response can be largely explained by the different approach to setting wave height between the two works, since non-dimensional roll motion and subsequent non-dimensional wave-induced loads reduce substantially as wave height increases, due to the non-linearity of the roll response. It is interesting to find that some wave-induced loads that acting on the damaged ship can present a second peak response as wave frequency is greater than 1Hz, which should be carefully investigated in the further study.

Prior to testing the ship hull in water, the solid mass moment of inertia in roll, which is one of the most significant parameters of the ship model could not be measured reliably. The ship length is too large to allow use of the current conventional measurement method used to determine mass moment of inertia in pitch, while the compound pendulum method is not effective due to the limitation and error of the measurement devices. Therefore, an alternative way to reasonably obtain the mass moment of inertia of the ship model is to approach the ship's free decrement curve and varying the mass moment of inertia via an iterative numerical method. This provides a feasible way to estimate the actual mass moment of inertia of the ship model rather than using a total mass moment of inertia (including hydrodynamic effects) by testing in calm water as Begovic et al. (2017) presented.

Another factor that may have an impact on the damaged ship model's behaviour is the neglected damage creation. In this experimental investigation, the damage to the ship is created by removing the cover at the damaged opening, and hence the floodwater inside the compartments has been calm before testing. Therefore, the transient damage flooding effect on the ship hull is neglected, even if it can have a significant influence on ship's behaviour, and even on further flooding due to the interaction between ship motions and floodwater dynamics.

\* *This chapter has been modified and published as*

*Yue Gu, Alexander Day, Evangelos Boulougouris & Saishuai Dai (2018) Experimental investigation on stability of intact and damaged combatant ship in a beam sea, Ships and Offshore Structures, DOI: 10.1080/17445302.2018.146501. Online available:*

<https://www.tandfonline.com/doi/abs/10.1080/17445302.2018.1465012>

# 4.2D simulation by CFD-based approach

## 4.1 Computational fluid dynamic (CFD) approach

### 4.1.1 Basic theory of adopted CFD-based method

With the rapid development of computational technology, the computational fluid dynamic method becomes increasingly attractive to be an economic and powerful alternative to tank testing in naval architecture. With high performance computing techniques, parallel processing may be applied for CFD method efficiently and quickly. Although potential theory has been used widely in ocean engineering, it is unlikely to give reliable information about the fluid field in particular for the damage flooding due to the nature of the floodwater and the neglected effect of viscosity. Especially for vortex-shedding and other phenomena with strong nonlinearity of complex water surface evolution such as slamming, wave breaking, water on deck and damage flooding and sloshing in the compartment, potential theory lacks ability to handle these issues (Yeung et al, 2001). However, considering viscosity and nonlinear effect of water surface, RANS solver is a better approach to deal with the complicated hydrodynamic fluid problem. In the present study, with CFD-based RANS solver, a commercial CFD package called STAR-CCM+ is used to investigate behaviour of the intact and damaged ship in wave conditions. At the same time, structural loads acting on the intact and damaged ship hull in beam waves are solved by applying RANS solver. As the present work is mainly concentrated on application of CFD-based RANS solver on hydrodynamics of ships in waves, methods and algorithms adopted are introduced in this section. For further information, Versteeg and Malalasekera (2007) provide a detailed specification about methodology with computation fluid dynamics.

STAR-CCM+ as a comprehensive CFD solver package provides an entire procedure for solving multiple objects including pre-processing (CAD geometry, mesh generation), solving with physical models, and post-processing (optimisation and analysis) with plots. Through the contribution of high-performance computing technology, parallel calculation in STAR-CCM+ can efficiently and quickly solve the

complicated hydrodynamic problems. Figure 4.1 illustrates a general workflow for solving with STAR-CCM+.

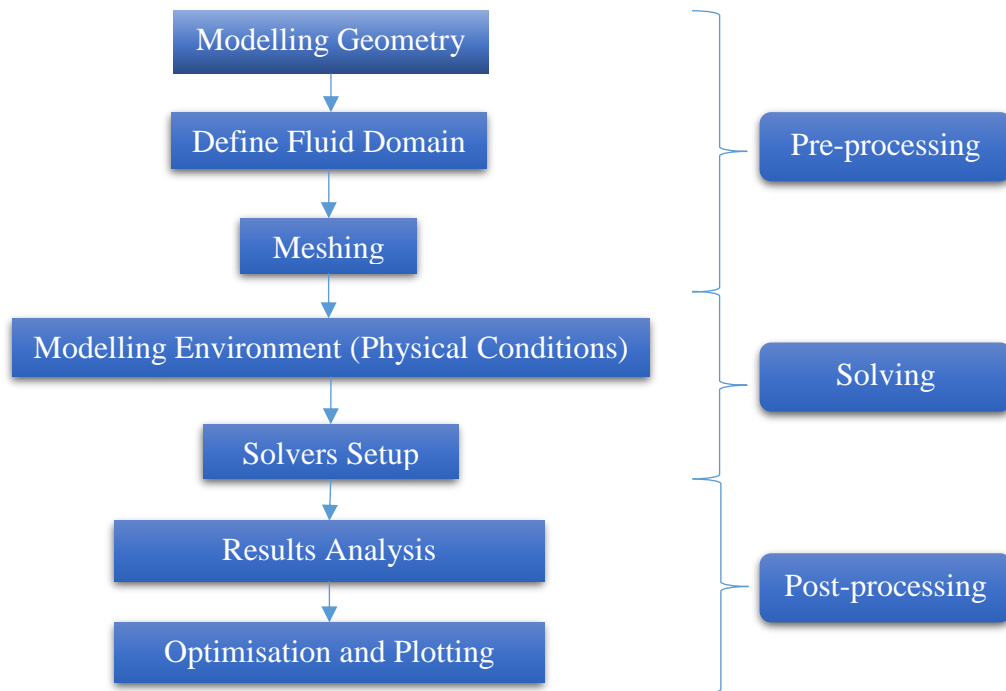


Figure 4.1. Workflow with STAR-CCM+

#### 4.1.2 Governing equations

The characteristics of motion of a fluid can be described by five equations, which are the fundamental governing equations of fluid dynamics, also known as conservation equations of mass, momentum (in three directions) and energy.

Mass conservation equation, as known as the continuity equation, states that the mass of a fluid is conserved:

$$\frac{\partial \rho}{\partial t} + \text{div}(\rho \mathbf{u}) = 0 \quad \text{Equ. 4.1}$$

where  $\rho$  is the fluid density.

If applied for an incompressible flow, the density of each phase is kept constant, which means density does not vary with time, so that mass conservation equation becomes:

$$\nabla \mathbf{u} = \frac{\partial u}{\partial x} + \frac{\partial v}{\partial y} + \frac{\partial w}{\partial z} = 0 \quad \text{Equ. 4.2}$$

According to Newton's second law, the rates of increase of momentum of fluid particle is equal to the sum of forces on the fluid particle including pressure forces, viscous forces and gravity force as well as body forces. Considering applied to an incompressible fluid in finite volume method, conservation equation of momentum, or here we call it the Navier-Stokes equations can be expressed in  $i$ -th direction as

$$\frac{\partial(\rho u_i)}{\partial t} + \frac{\partial}{\partial x_j}(\rho u_i u_j) = \frac{\partial(-P)}{\partial x_i} + \mu \nabla^2 u_i + \rho g_i \quad \text{Equ. 4.3}$$

where

$p$  is the pressure

$\mu$  is the dynamic viscosity of fluid

$\nabla^2$  is the Laplace Operator

$\rho g_i$  indicates the gravity force on the fluid

### 4.1.3 Reynolds-Averaged Navier Stokes (RANS) equations

Reynolds-averaged concept refers to a decomposition of an instantaneous variable  $\phi$  that can represent velocity, pressure or energy in Navier-Stokes equations into its time averaged value ( $\bar{\phi}$ ) and fluctuating value ( $\phi'$ ), which can be expressed as

$$\phi = \bar{\phi} + \phi' \quad \text{Equ. 4.4}$$

Therefore, RANS can be given as

$$\frac{\partial \bar{u}}{\partial x} + \frac{\partial \bar{v}}{\partial y} + \frac{\partial \bar{w}}{\partial z} = 0 \quad \text{Equ. 4.5}$$

$$\rho \left[ \frac{\partial \bar{u}_i}{\partial t} + \frac{\partial}{\partial x_j}(\bar{u}_i \bar{u}_j) \right] = -\frac{\partial \bar{P}}{\partial x_i} + \mu \nabla^2 \bar{u}_i + \rho g_i - \frac{\partial(\rho \overline{u'_i u'_j})}{\partial x_j} \quad \text{Equ. 4.6}$$

where  $\rho \overline{u'_i u'_j}$  is defined as Reynolds stress tensor, which makes the governing equations unclosed for turbulence so that additional equations are required to close the RANS equations. In the present work,  $k$ - $\omega$  turbulence model including two transport equations is used.

#### 4.1.4 Shear Stress Transport (SST) $k$ - $\omega$ turbulence model

The SST  $k$ - $\omega$  turbulence model with two transport equations for the kinetic energy  $\kappa$  and the specific dissipation rate  $\omega$  was developed (Menter, 1994) to be a general-purpose suitable model in CFD calculation.

#### 4.1.5 Boundary conditions

Correct Boundary conditions are critical for accurate solution with CFD method as boundaries define fluid flux in and out of the computational domain as physical conditions. It is essential to specify the correct boundary conditions for the flow characteristics. Here boundaries that applied in present work can be catalogized given as follow

- Velocity inlet:

For the velocity inlet boundary in the computational domain, flow velocity is specified, and the pressure is extrapolated from the neighbour cell with reconstructed gradients.

- Pressure outlet:

In a pressure outlet boundary pressure is specified while velocity is extrapolated from adjacent cells.

- Symmetry boundary:

By definition, symmetry boundary condition refers to the expected flow pattern, which contains mirror symmetry. It can be used to model zero-shear slip walls in viscous flows.

- Wall boundary:

Wall boundary with non-slip condition is commonly used to represent the surface of a body or a physically confine.

- Near-Wall treatment:

Velocity distribution near to the wall boundary is tangential. For instance, considering a flow over a flat plate, the velocity development along the plate can be shown in Figure 4.2. Especially for turbulent boundary in an incompressible flow,  $y^+$  value (Figure 4.3) clearly effects turbulent flow, and determines the definition of layers

(Pope, 2001). In STAR-CCM+, the  $k-\omega$  turbulence model for RANS solver has good ability to treat all  $y^+$  value (STAR-CCM+, 2017).

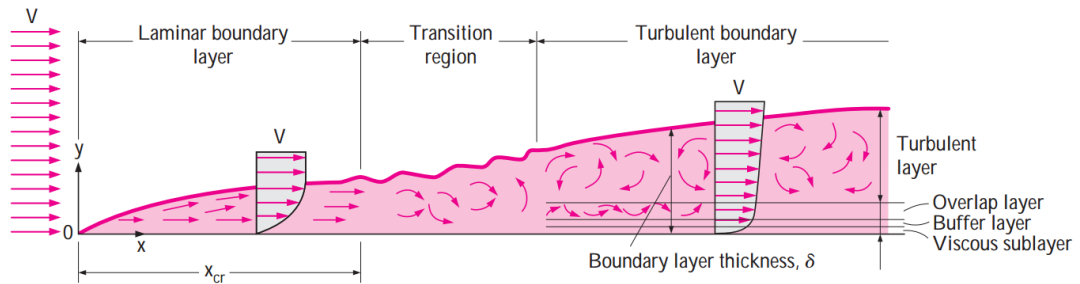


Figure 4.2. The flow of a fluid over a flat plate (Yunus and Cimbalá, 2006)

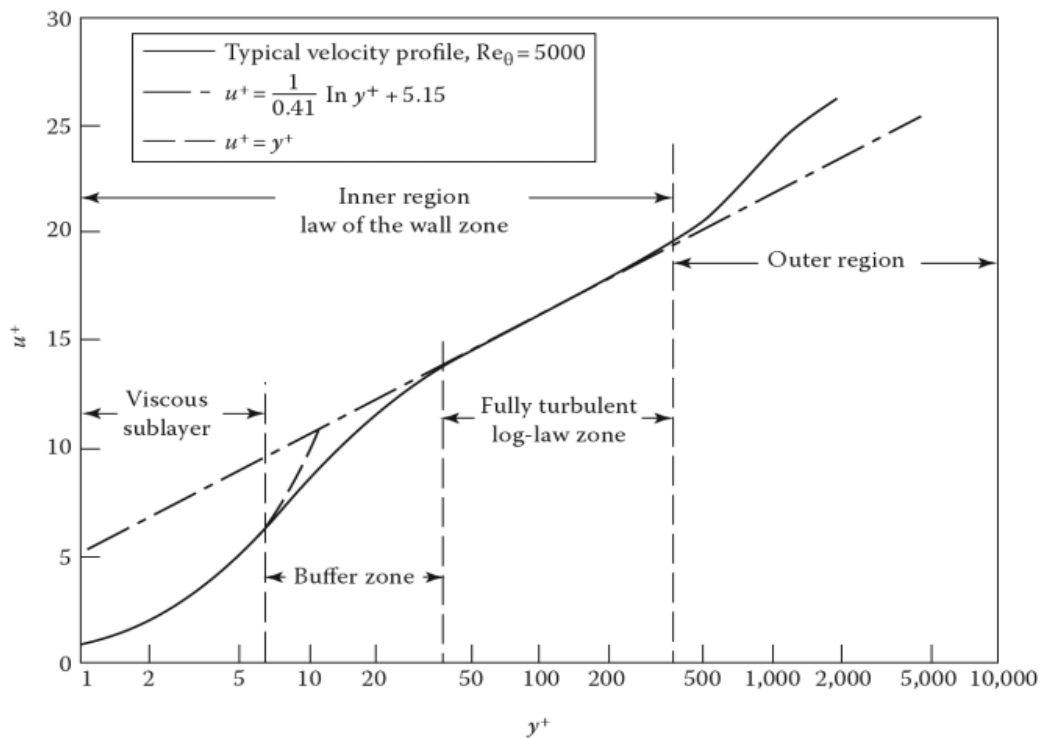


Figure 4.3. Turbulent boundary layer for a typical incompressible flow over a smooth flat plate (Pletcher et al., 2012)

#### 4.1.6 SIMPLE

To solve the discretized governing equation in a segregated way, the SIMPLE (Semi-Implicit Method for Pressure-Linked Equations) algorithm is applied in segregated solver for pressure-velocity coupling, which is suitable for long time-steps calculation with steady-state solution. The calculation iteration is repeated within a single time step until the difference between the solution and actual solution is under the limitation of tolerance.

#### 4.1.7 Volume of Fluid Method

Volume of Fluid (VOF) Method is used to capture the interface between two phases. In the present study, interface between water and air can be captured by VOF method with a concept of volume fraction  $\alpha$ . A volume fraction of a phase in a cell indicates the distribution of the specific phase in a control volume. For each single control volume, the sum of volume fractions for air and water must be 1, which can be expressed by

$$\sum \alpha = \alpha_{air} + \alpha_{water} = 1 \quad \text{Equ. 4.7}$$

- $\alpha_{water} = 1$  ( $\alpha_{air} = 0$ ) means the volume is full of water (air) phase.
- $\alpha_{water} = 0$  ( $\alpha_{air} = 1$ ) means there is no water (air) phase in the cell.
- $0 < \alpha_{water} < 1$  means the cells include the interface between air and water.

VOF as a homogeneous multiphase fluid method that used in CFD simulation for fluid dynamics in the water tank is considered to be less suitable for the violent sloshing problem than an inhomogeneous model (Godderidge et al., 2009b). However, the present work aims to investigate the application of CFD method to estimation of motions and wave induced loads acting on the intact and damaged ship, and hence the VOF method is adopted; inhomogeneous multiphase model may be studied in the future work.

#### 4.1.8 $Y^+$

As one of the most prominent parameters in CFD method  $y^+$  is a dimensionless wall distance. It is often used to indicate mesh quality for a particular viscous flow along body surface. It is significant in turbulence modelling to determine the proper size of the adjacent cells around the body surface.

## 4.2 Numerical wave tank

In naval architecture and ocean engineering, a numerical wave tank is an alternative significant tool to investigate on hydrodynamics of structures and interaction between structures and waves. With the development of high-performance computing technique, the numerical wave tank is increasingly attractive to be applied to simulate physical model in waves. In this chapter, a numerical wave tank is simulated without any structure in water to investigate the scheme for wave generation and absorbing by



CFD method. A two-dimensional calculation domain with XOZ plane is established, where the wave propagates along X-direction and gravity is set to be in the direction of the minus Z-axis ( $g_z = -9.81 \text{ m/s}^2$ ), while there is only one-cell thickness along Y axis to avoid needless calculation cost.

#### 4.2.1 Calculation domain dimensions and boundaries

In this study, a deep-water 1<sup>st</sup>-order Stokes wave is generated with period=0.84s and height=0.02m as the matter of fact that it is actually generated in physical tests (which is coincided with the resonant condition of the intact ship's roll motion). Since water depth for physical tank is constant (2m) during all the physical tests, water depth remains 2m for all the CFD simulations. The length of domain along X-direction is six times wave length ( $\lambda$ ) that contains  $4\lambda$  for wave propagation and  $2\lambda$  for wave absorbing (damping). With boundaries the whole calculation domain can be shown in Figure 4.4 and Figure 4.5.

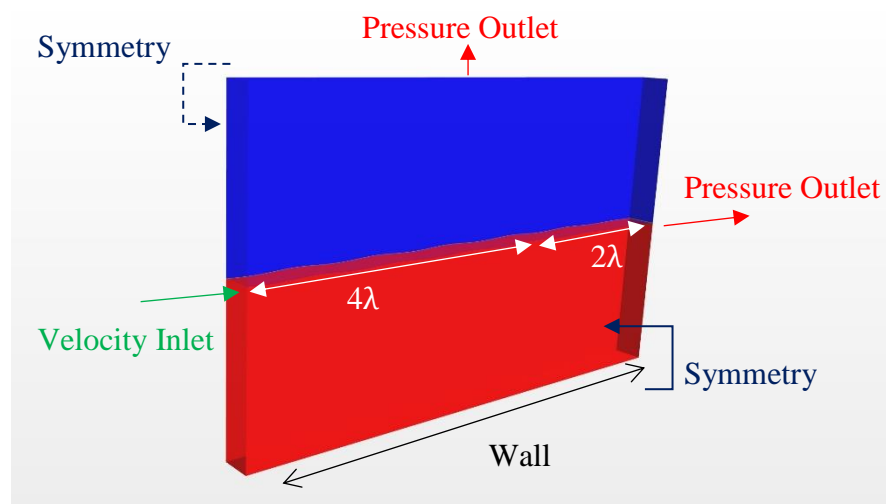


Figure 4.4. Boundary conditions of the fluid domain

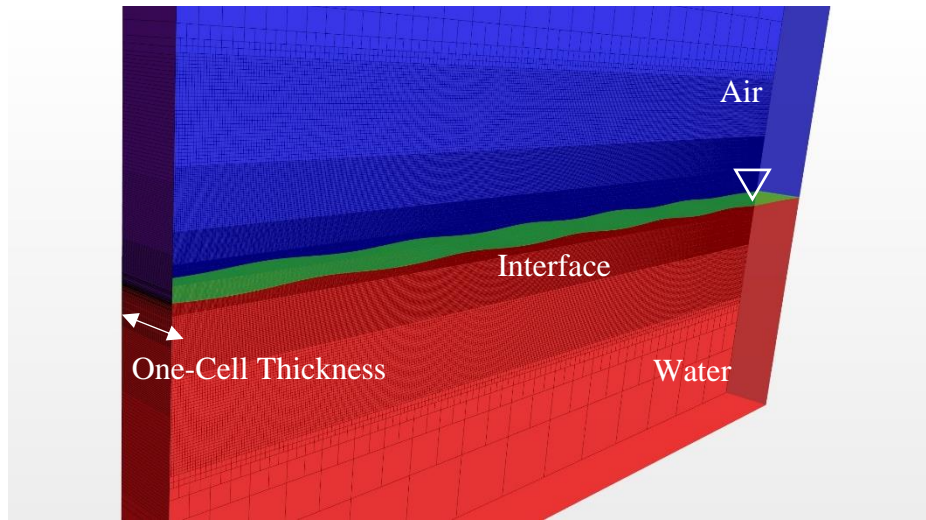


Figure 4.5. Free surface (interface) between air and water

#### 4.2.2 Physical modelling

Taking air and water as two phases treated by VOF method, Standard  $k-\omega$  SST (since standard  $k-\omega$  SST turbulent model is applied for the intact and damaged ship in beam seas stated in Chapter 5) is selected as the turbulence model with segregated flow solver and segregated VOF solver. To identify the interface between air and water, VOF is set to be 0.5 to visualize the free surface. The segregated flow solver controls the solution update for the Segregated Flow model according to the SIMPLE algorithm. Volume of Fluid (VOF) is a simple multiphase model. It is suited to simulating flows of several immiscible fluids on numerical grids capable of resolving the interface between the phases of the mixture. Second-order temporal discretization accuracy is chosen to update the solution at each time step for a high accuracy of calculation.

#### 4.2.3 Mesh sensitivity

Under the consideration of economic cost in calculation, an understanding of mesh sensitivity is essential, and the summary of mesh schemes can be given in Table 4.1. According to ITTC recommendation (ITTC, 2014b), a constant refinement ratio  $\sqrt{2}$  is suggested as the ratio for mesh refinement so that refinement is applied based on the number of cells in a wave height (S1 to S5). An aspect ratio means the ratio of length and width of a cell that contains the interface. A sample of mesh scheme (S3) is shown in Figure 4.6. In this section, the effect of cell's aspect ratio is also taken into consideration. A wave probe is positioned at four times wave length ( $x=4.422\text{m}$ ) and wave elevation is obtained and compared with desired value (wave height = 0.02m).

Table 4.1. Wave properties with mesh dependence

Wave properties					
	Height (H)	Length ( $\lambda$ )	Period (T)	Depth (d)	H/ $\lambda$
Value	0.02m	1.1057m	0.84s	2m	1/55
Scheme	Cells in height	Cells in length	Aspect ratio	Error	Total No.
S1	H/5	$\lambda/69$	4	-4.292%	24544
S2	$H/5\sqrt{2}$	$\lambda/69\sqrt{2}$	4	-2.914%	38611
S3	H/10	$\lambda/138$	4	-1.981%	52306
S4	$H/10\sqrt{2}$	$\lambda/138\sqrt{2}$	4	-1.734%	87465
S5	H/20	$\lambda/276$	4	-1.413%	123076
S6	H/10	$\lambda/69$	8	-4.384%	33280
S7	H/10	$\lambda/276$	2	-2.615%	77346

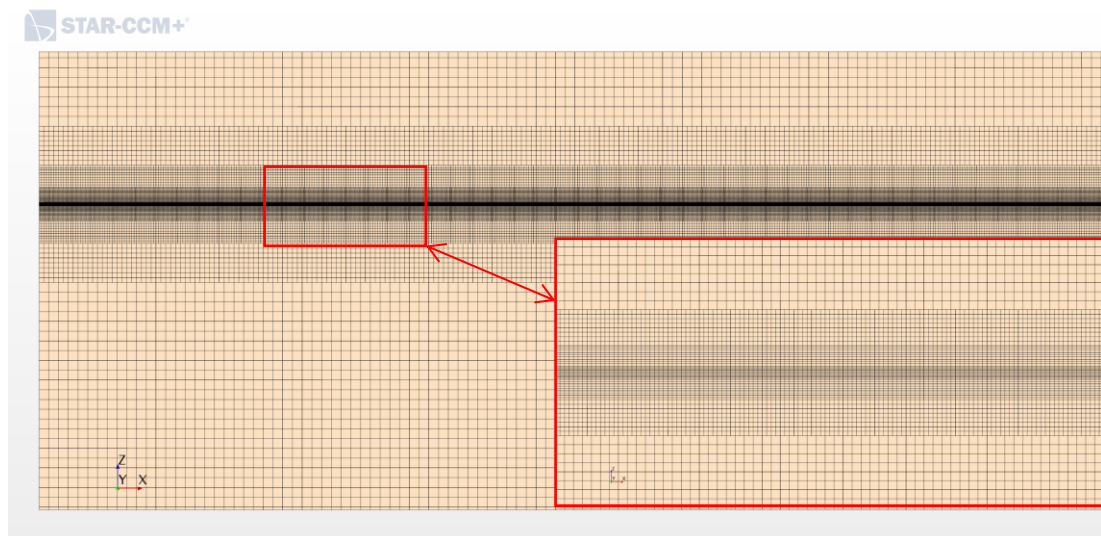


Figure 4.6. Generated mesh for fluid domain

Figure 4.7 indicates the wave elevation in Z-axis at X=4.4m where the structure will be positioned at 35<sup>th</sup> period (t=30s). Figure 4.8 shows the wave elevation detected by the wave probe at 4<sup>th</sup> wave length position (x=4.4m) over time. It seems that generated waves can have a good match to the desired requirement. Apart from two cases that 69 cells in one wave length (S1 and S6) where errors are over 4%, deficiencies are no more than 3%. As shown in Figure 4.9, error decreases rapidly from S1 to S3, while from S3 to S5, the decrease is not so distinct with further refinement of the mesh but

total number of cells in the whole calculation domain dramatically increases. For aspect ratio refinement (S3, S6 and S7), compared to S3, double aspect ratio (S6) deteriorates the elevation that obtained, however, reduced aspect ratio (S7) does not reveal an obviously improvement.

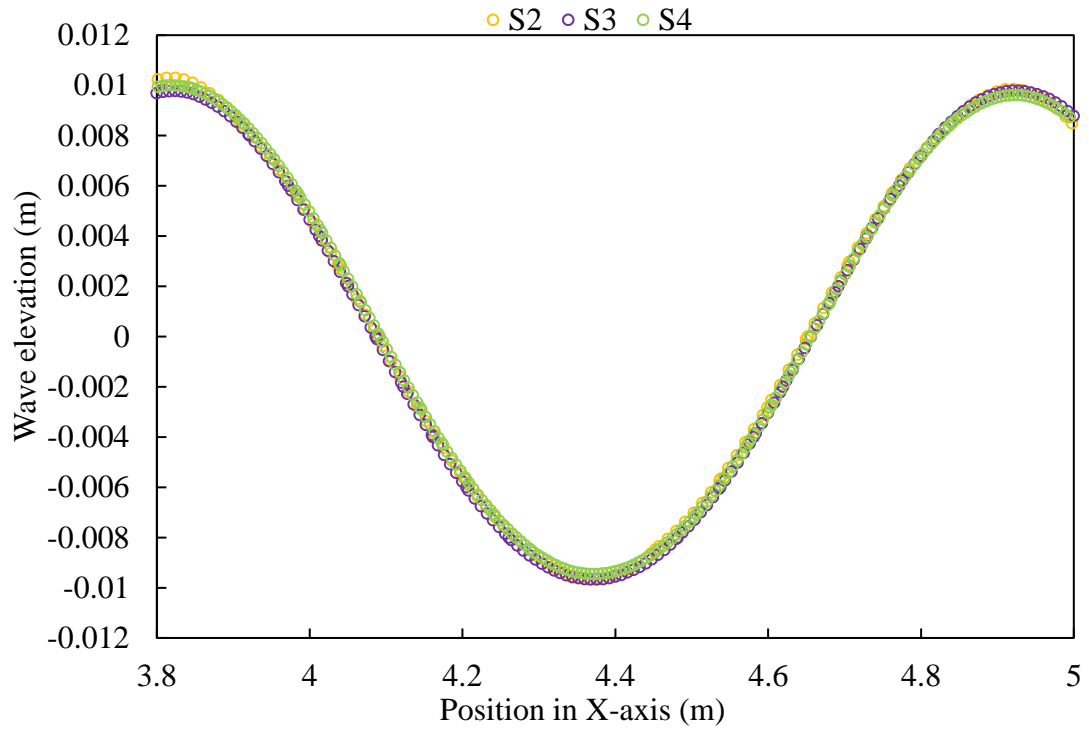


Figure 4.7. Wave elevation at t=30s

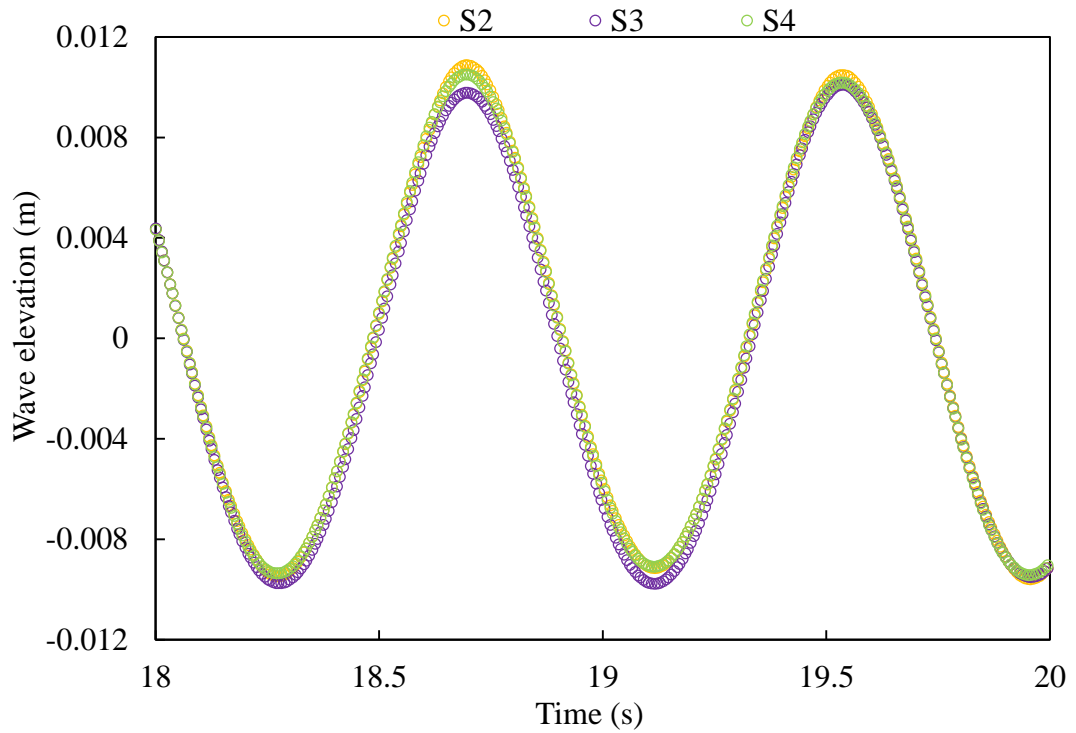


Figure 4.8. Wave elevation against time history

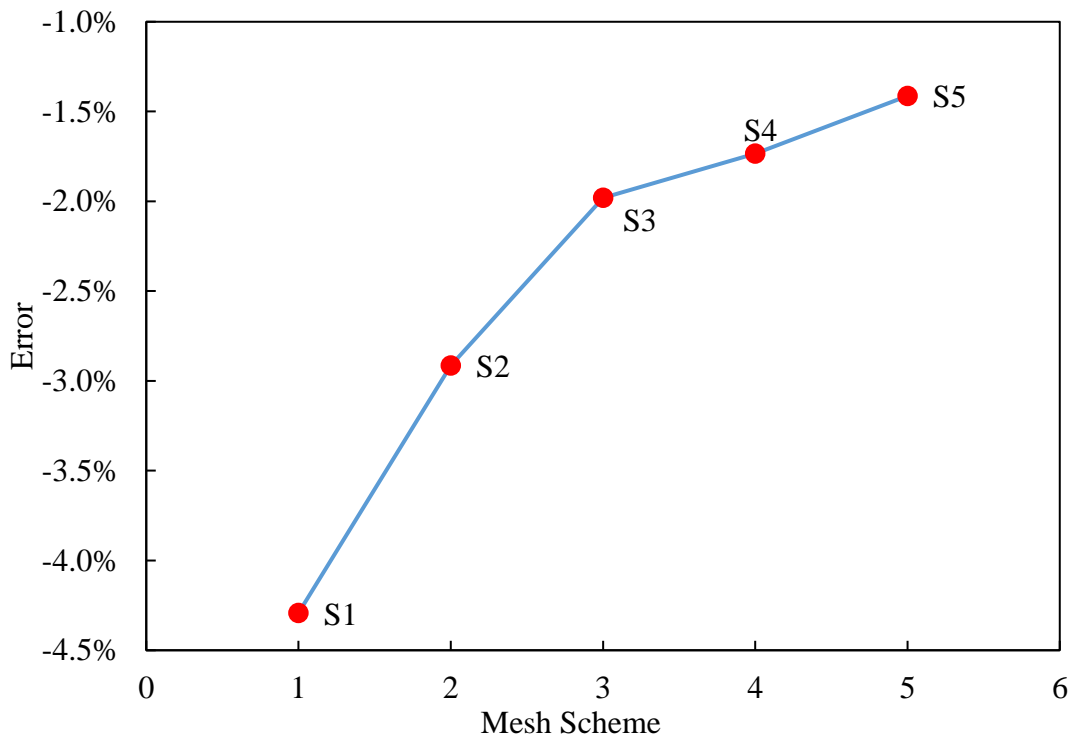


Figure 4.9. Mesh dependence verification

#### **4.2.4 Nonlinearity of generated waves**

In this section, the nonlinearity of the generated wave, i.e. first and second order wave frequency and amplitude is investigated in order to recognize the nonlinear effect of regular waves on a ship.

Figure 4.10 shows a time history of generated wave by CFD method compared with experimental measurement by a wave probe. The wave frequency is chosen to coincide with the resonant frequency of the intact ship roll motion. A Fast Fourier Transform is applied to demonstrate the first and second order amplitudes and frequencies of the generated wave as illustrated in Figure 4.11. It can be observed that the wave includes the first order component at 0.73Hz, with amplitude of approximately 11mm and a second order component at 1.47Hz, with amplitude of 0.2mm. Thus, the amplitude of the second order component of the wave is less than 2% of the first order amplitude. Although in most of the wave experiments the second order amplitude of wave is less than 5% of the first order amplitude (Fonseca and Soares, 2004), it still has an effect on ship behaviour and the wave loads acting on the ship, since the second order resonance can trigger serious stability problem (Fujino and Yoon, 1985).

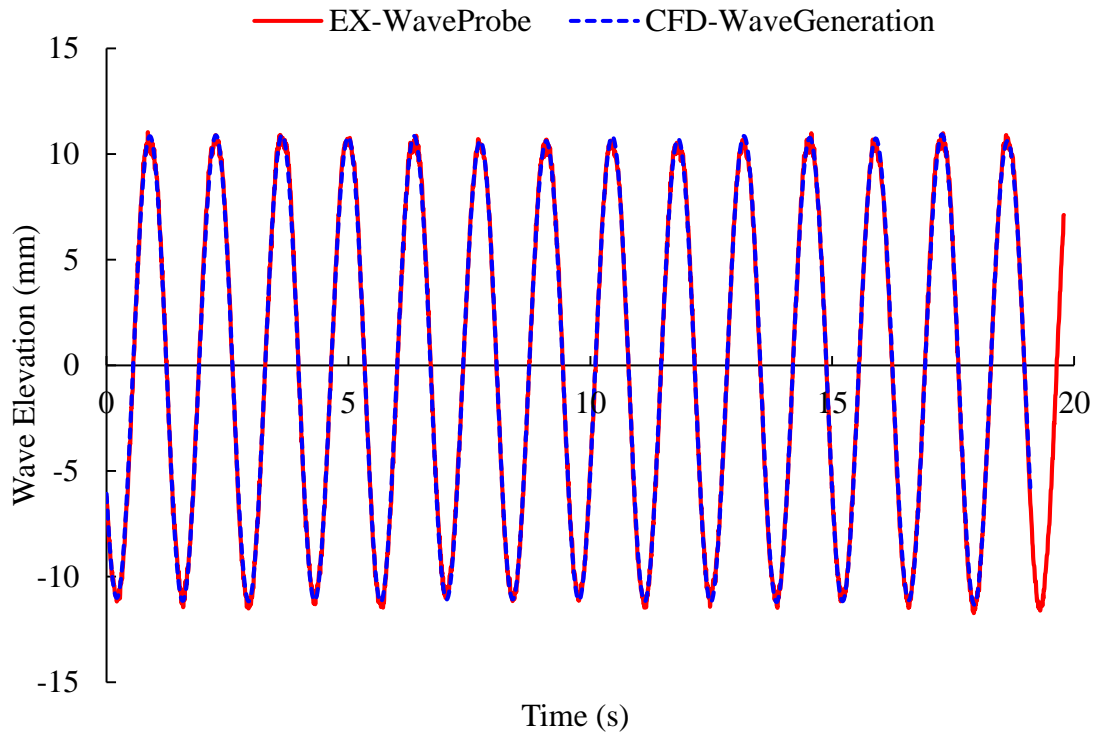


Figure 4.10. Generated wave by CFD compared with the wave in the tank

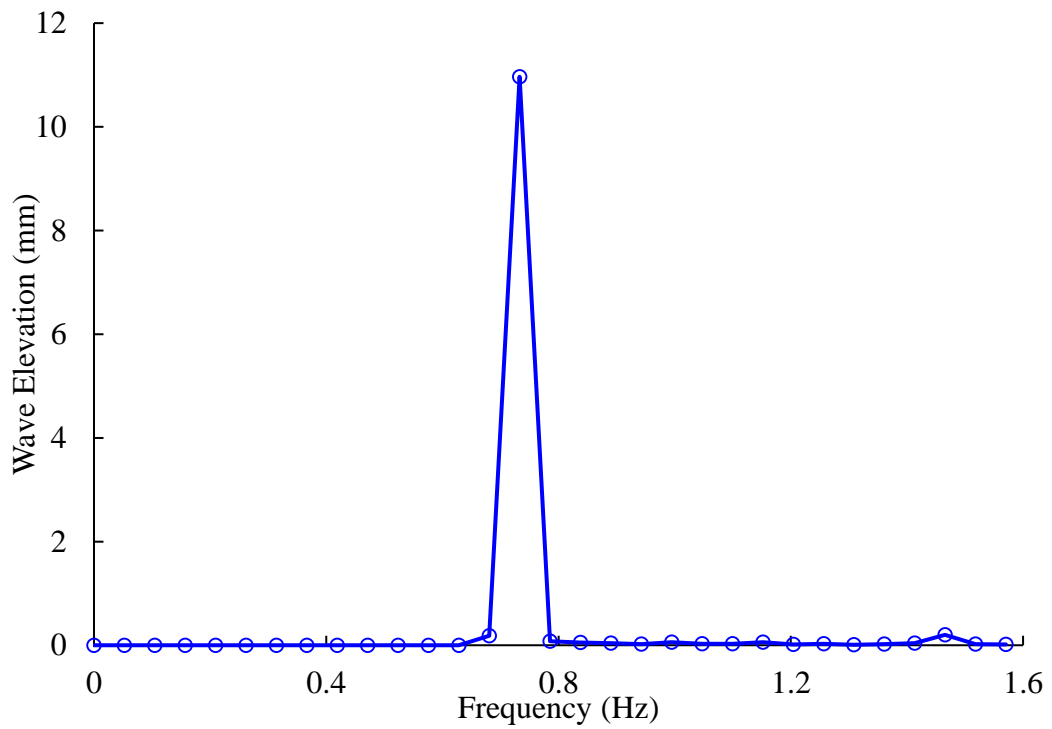


Figure 4.11. First and second order frequencies and amplitudes of the generated wave by FFT

### 4.3 2-Dimensional investigation on free rolling decay

In this section, two free rolling decay simulations are carried out based on two experimental campaigns that provide valuable data for validation with CFD method.

#### 4.3.1 Rectangular structure roll-decay study in 2-dimensional

##### 4.3.1.1 Geometry

An experimental study on viscous effect is carried out on a rectangular structure by Jung et al. (2006). With 0.9-metre length, 0.3- metre breadth and 0.1- metre height the rectangular structure is installed in a 0.9- metre wide wave tank, which is just equal to the length of the structure so that the whole system can be taken as a 2-dimensional investigation. A pair of hinges goes through the centre of gravity of the structure so that the structure rotates around its COG. Figure 4.12 shows a simple diagram of experimental layout. With 2-dimensional geometry in CFD solver, one-unit thickness (29mm) mesh is established to simplify the physical test into 2D problem and main particulars are shown in Table 4.2.

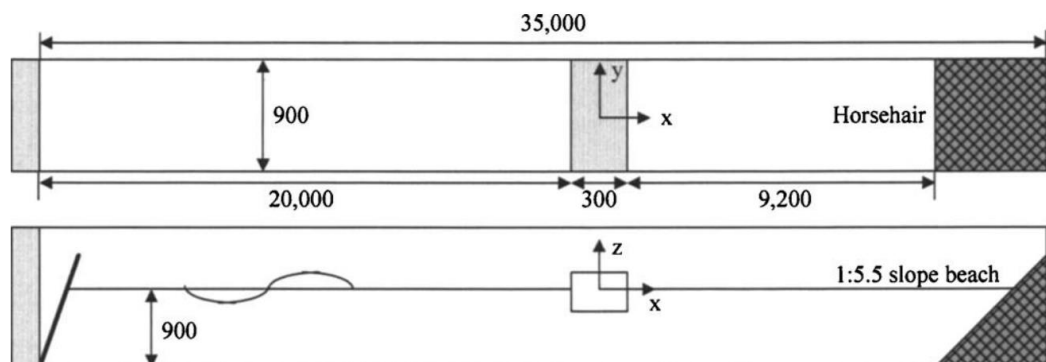


Figure 4.12. A sketch of experiment (Jung et al., 2006)

Table 4.2. Main characteristics of structure

Particulars	Physical model	2D geometry
Length	0.9m	0.009m
Width	0.3m	0.3m
Height	0.1m	0.1m
Draught	0.05m	0.05m
GM	0.125m	0.125m
Water depth	0.9m	0.9m



Natural period (roll)	0.93s	0.93s
Mass moment of inertia (roll)	0.236 kgm <sup>2</sup>	0.00236 kgm <sup>2</sup>

#### 4.3.1.2 RANS solution

A 2-dimensional calculation domain is generated in CFD solver with STAR-CCM+. Mesh distribution in fluid domain can be shown in Figure 4.13. Again, it can be seen that 2-dimensional presentation is expressed by one single layer of mesh (0.009m thickness). Results shown in Figure 4.14 are compared with experimental data as well as the numerical solutions from other works (Ghasemi et al., 2014 and 2017 and Nematbakhsh et al., 2013). It seems that results in the present study give a fair (perhaps even better) agreement compared to the other numerical methods. The amplitude of inclination angle in model test exhibits a higher damping effect on the structure during decrement. One of the common possible reasons to explain this over-estimation is due to the additional frictional loss from the physical devices (Chen et al., 2016 and Ghasemi et al., 2014).

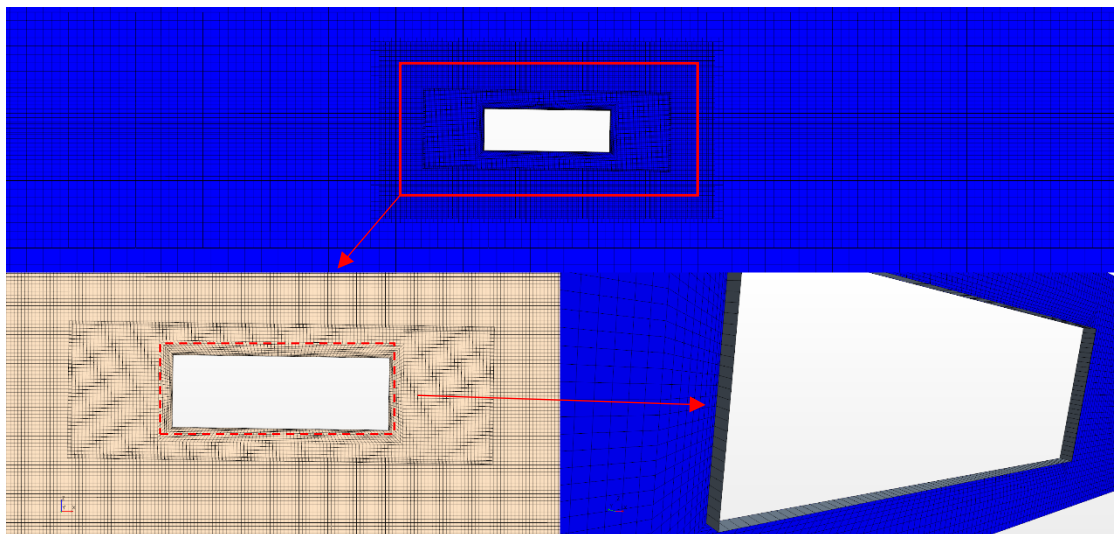


Figure 4.13. Mesh distribution in fluid domain

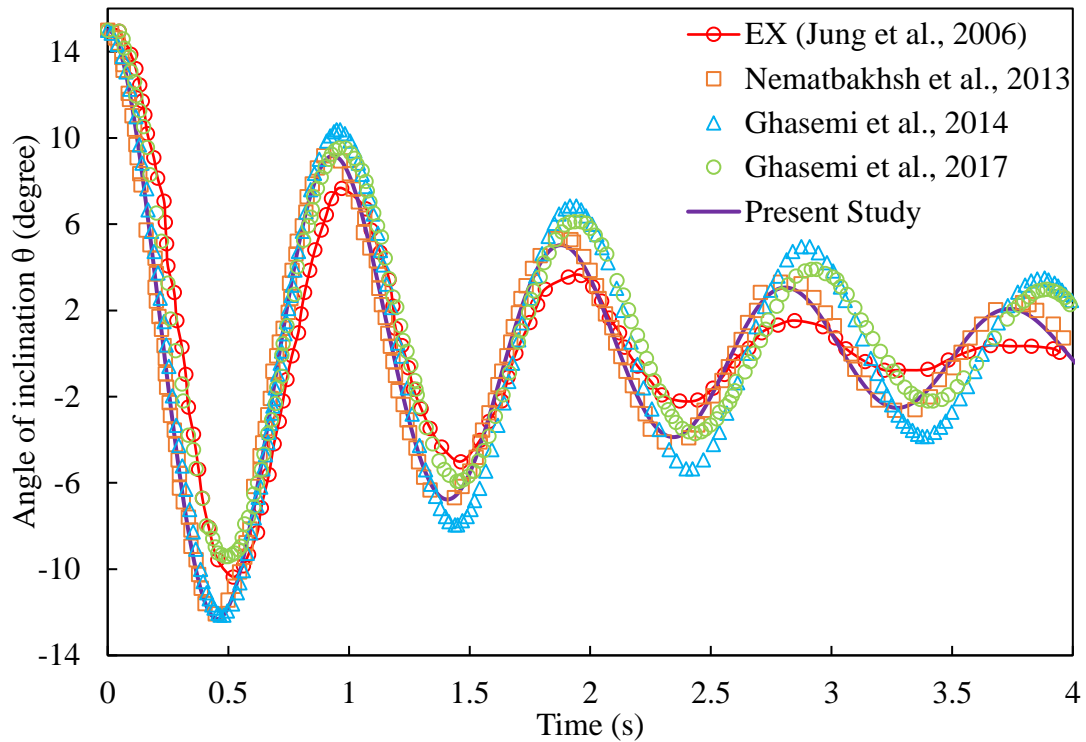


Figure 4.14. Roll decrement results comparison

### 4.3.2 Ship-like body rolling decay study in 2-dimensions

#### 4.3.2.1 Geometry

A typical Panamax ship is simplified by Irkal et al. (2016) to investigate on a 2-dimensional ship-like body's roll motion by model tests and CFD method. With a pair of bearings across the centre of gravity of the structure, the length of the structure (580mm) crosses the entire width of the tank (600mm) so that the whole system can be taken as a two-dimensional rotation system with beam seas. Setup of structure in the physical tank is shown in Figure 4.15. A sketch of the whole system is demonstrated in Figure 4.16. It should be noted that, different to the structure used in physical test of Section 4.3.1, round bilges with 25mm radius are presented at the corners under the water. The summary of particulars of the structure and CFD model can be given in Table 4.3. A sketch that describes the calculation domain with boundary conditions is illustrated in Figure 4.17.

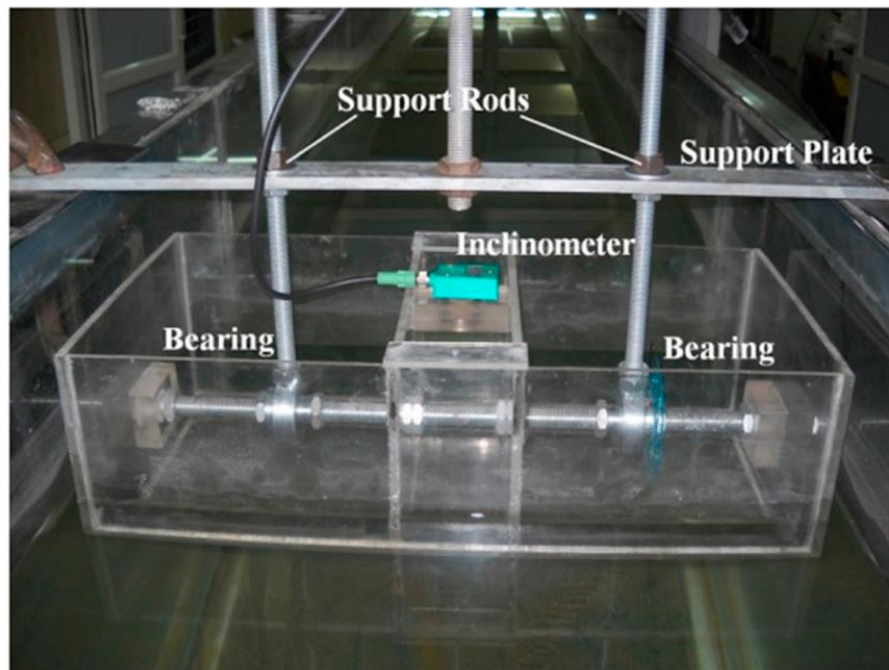


Figure 4.15. Physical model (Irkal et al., 2016)

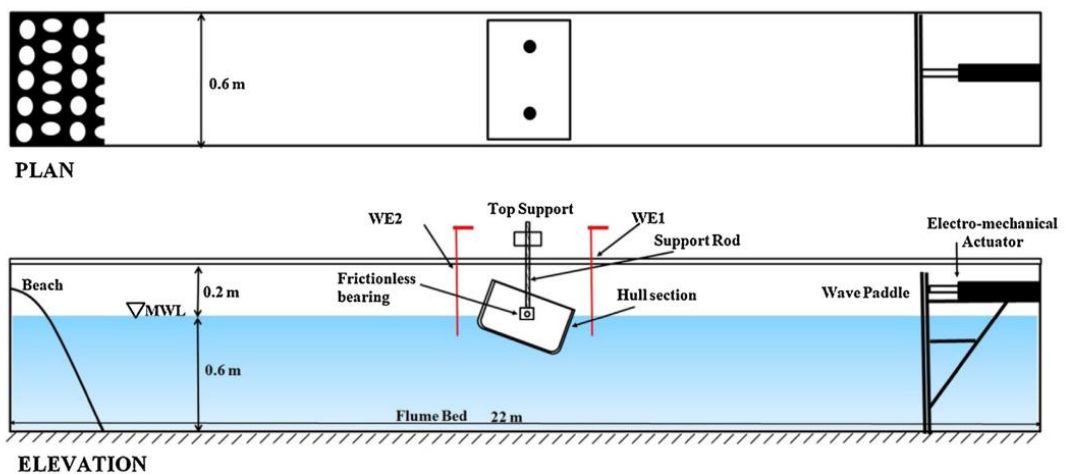


Figure 4.16. A sketch of experimental setup

Table 4.3. Summary of geometry used in physical test and CFD simulation

Particulars	Physical model	2D geometry in CFD
Beam	0.3m	0.3m
Height	0.2m	0.2m
Length	0.58m	0.029m
Mass	20.88kg	1.044kg
Draft	0.12m	0.12m

KG	0.08m	0.08m
$I_{xx}$	0.2244 kgm <sup>2</sup>	0.01122 kgm <sup>2</sup>
Water depth	0.6m	0.6m
GM	0.0425m	0.0425m

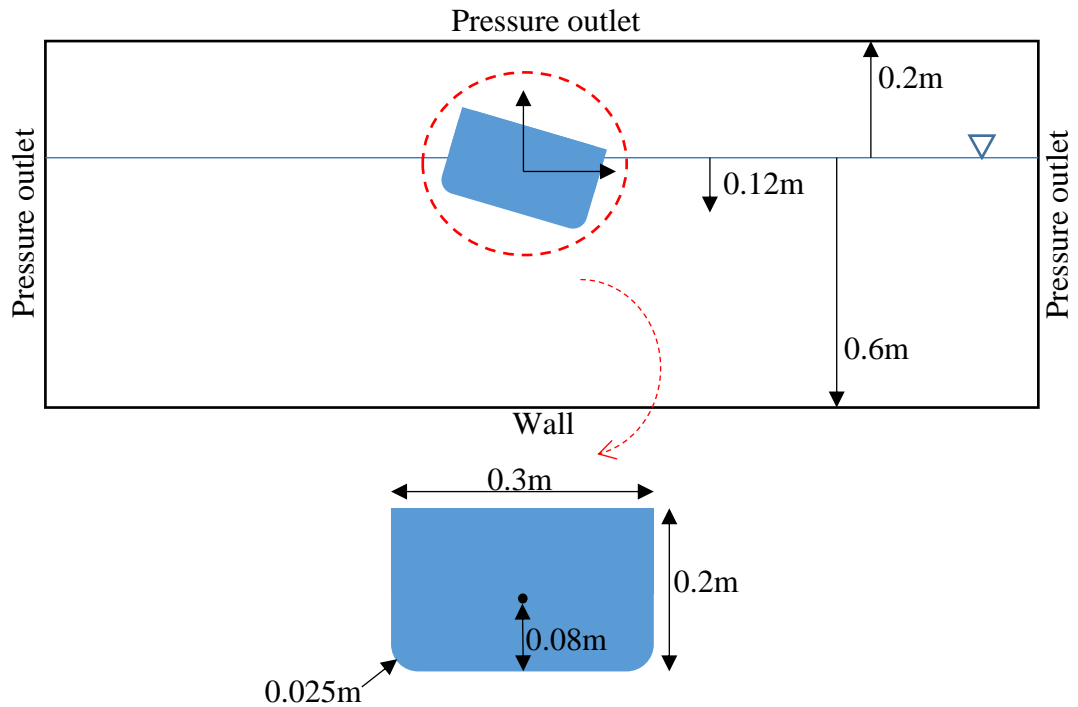


Figure 4.17. Geometry and boundary conditions of calculation domain

#### 4.3.2.2 Mesh and time-step sensitivity

According to the recommended procedure for mesh refinement given by ITTC (2014b), a refinement ratio  $\sqrt{2}$  is applied and mesh scheme is given in Table 4.4. A refined time step is applied by 2 from 0.0005s.

Table 4.4. Mesh and time step dependence

Scheme	Cell Size	Total No.	Time step
S1	5mm×5mm	78506	0.0005s
S2	7mm×7mm	40924	0.0005s
S3	10mm×10mm	16540	0.0005s
S4	10mm×10mm	16540	0.001s

S5	10mm×10mm	16540	0.00025s
----	-----------	-------	----------

Curves of decrement angle for mesh sensitivity is shown in Figure 4.18 compared with experimental data. Even though generally good agreement with experimental data appears in S1, S2 and S3, it seems that the amplitude of oscillation in physical test decay faster than numerical solutions. One of the possibilities can be considered that additional damping effect due to the friction loss of physical devices is inevitable, and to some extent, cannot be completely eliminated during the tests as matter of fact. Unfortunately, none of uncertainty is analysed from physical tests so that further accuracy and reliability of the results are unknown. As shown in Figure 4.19, phase deviant of decrement curve in S3 is slightly larger than S2 and S1, while there is nearly no difference between S2 and S1. Fast Fourier Transformation is used to analyse the natural period (or frequency), which is shown in Figure 4.20 and Table 4.5 specifically. Figure 4.21 illustrates time-step sensitivity. With 0.001s time step, amplitude of rotation decrement decays more slowly, while with further decrease of time step, there is no clear improvement.

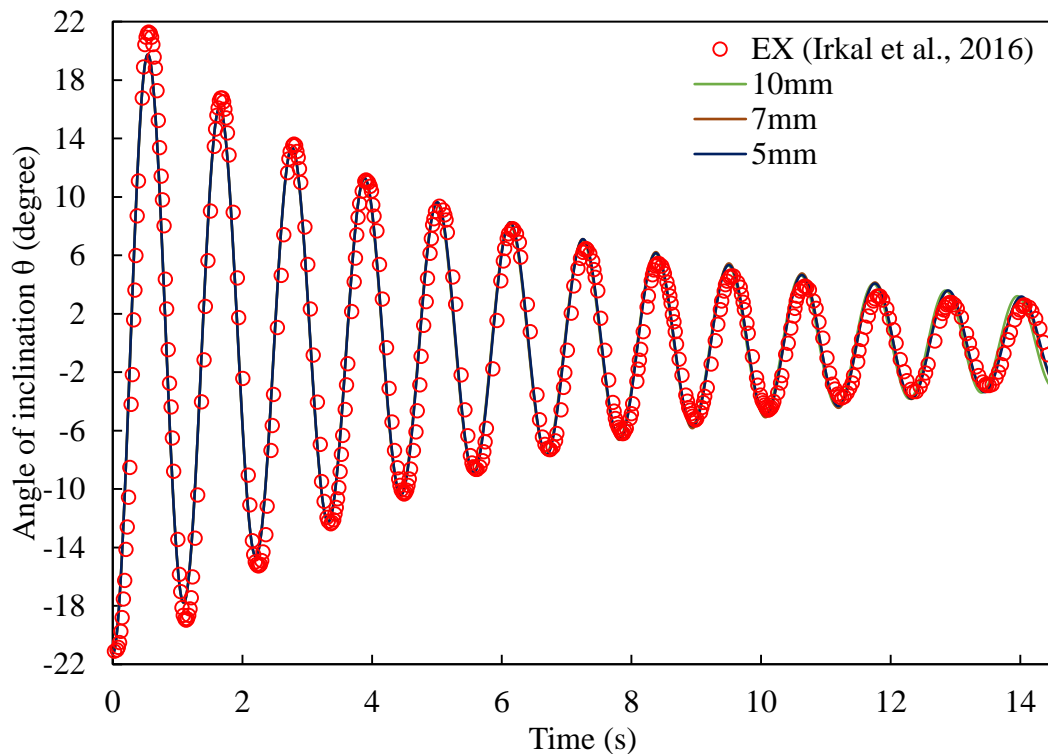


Figure 4.18. Decrement curves of mesh sensitivity compared between CFD method and physical test

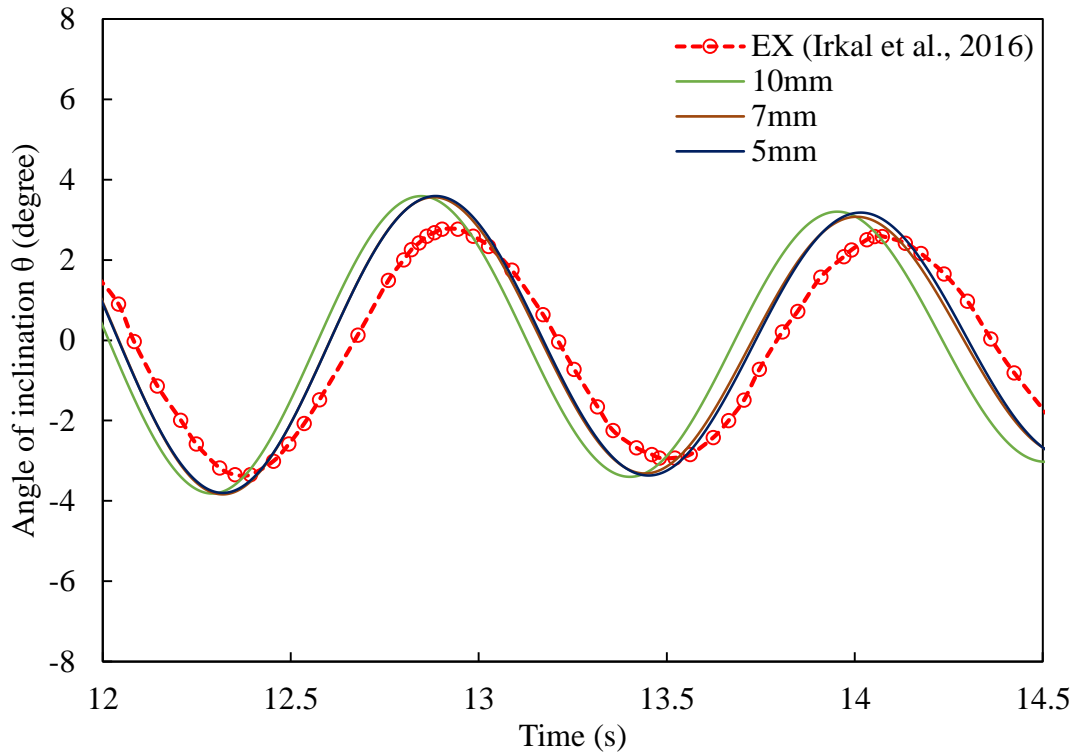


Figure 4.19. Results for mesh dependence

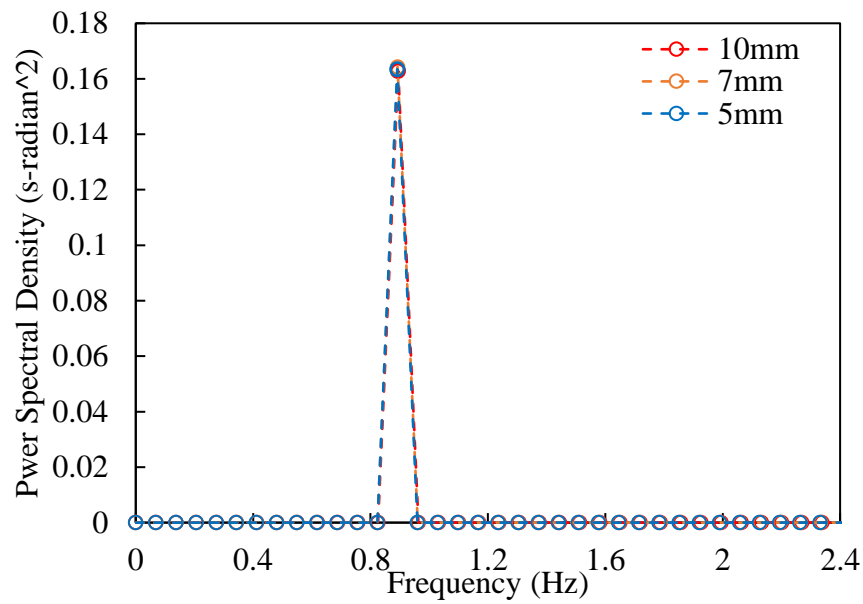


Figure 4.20. Frequency obtained by FFT method

Table 4.5. Summary of results for mesh dependence

	Size	Natural Period	Error
S1	10mm	1.118s	0.4%
S2	7mm	1.121s	0.61%

S3	5mm	1.122s	0.68%
EXP	-	1.114s	-

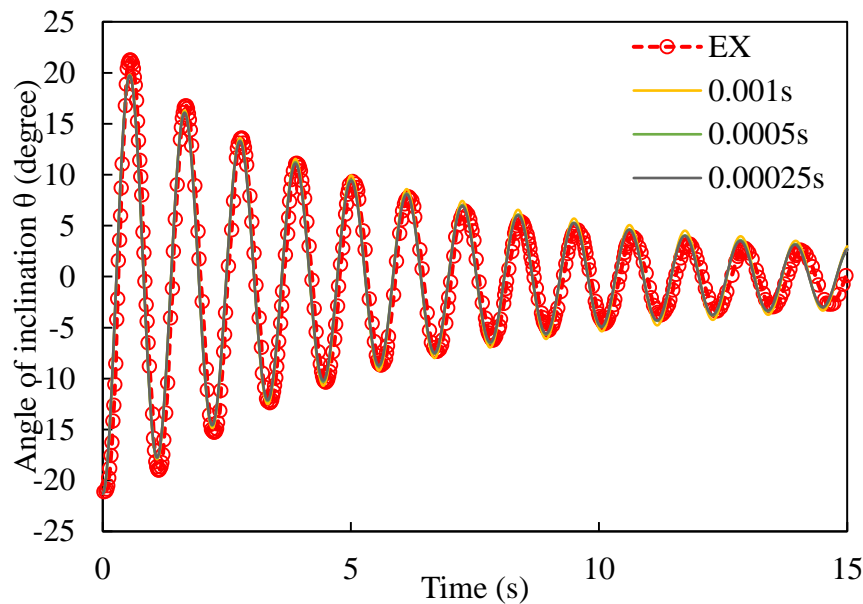


Figure 4.21. Comparison presented for time-step sensitivity

## 4.4 2-Dimensional structure in regular beam seas

To investigate the motion of structure in regular beam seas, a ship-like rectangular structure with round bilge was tested by Irkal et al. (2014) in a physical tank. It is the same model that described in Section 4.3.2. As regular waves are generated from velocity inlet boundary, the 2D simplified structure is excited by and reacts to the incoming waves. The structure is located four wave lengths away from the inlet boundary.

### 4.4.1 Geometry and boundary conditions of calculation domain

The sketch of entire calculation domain can be shown in Figure 4.22. Regular beam wave is generated by defining the velocity and pressure of the boundaries and volume of Fluid (VOF) method is used to capture the interface (water surface) between two phases (i.e. water and air). The model is positioned at four times wave length away from boundary A, where the regular waves come from and two times wave length to the boundary B, which is used for wave damping. To be the same as in model tests, water depth is kept constant to be 0.6 metre during each simulation.

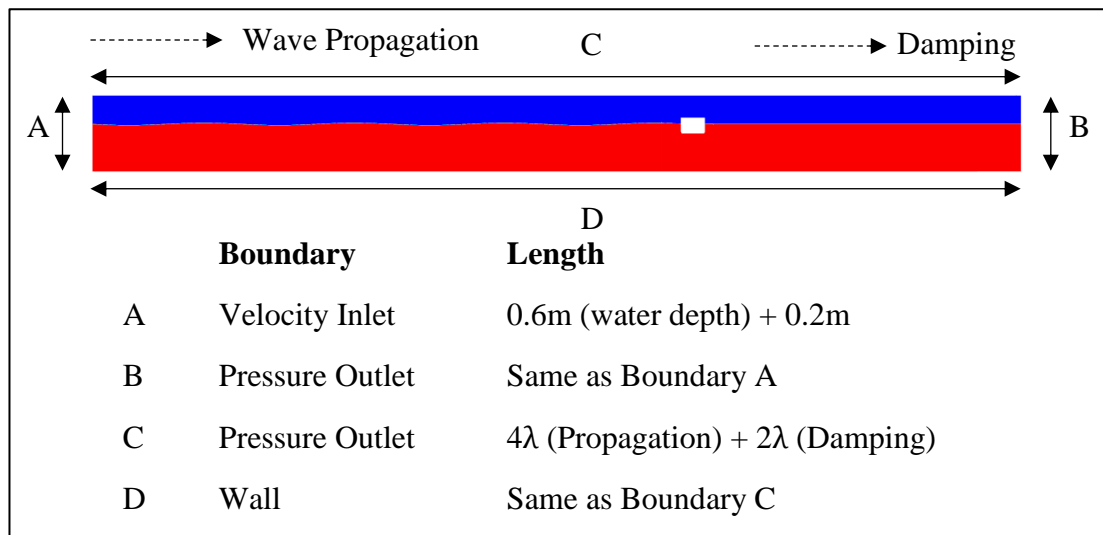


Figure 4.22. Sketch of fluid domain for structure in beam waves

#### 4.4.2 Wave setup

Properties of regular beam waves are listed in Table 4.6. Period of waves varies from 0.75s to 2s but wave height of all generated waves is constantly to be 0.03 metre, and depth of the tank is fixed equally to 0.6m.

Table 4.6. Regular beam waves setup

Wave Height	Wave Period	Wave Frequency	Wave Length
0.03 m	0.75 s	8.378 rad/s	0.877 m
	1 s	6.283 rad/s	1.544 m
	1.05 s	5.984 rad/s	1.682 m
	1.125 s	5.585 rad/s	1.904 m
	1.15 s	5.347 rad/s	2.056 m
	1.25 s	5.027 rad/s	2.273 m
	1.5 s	4.189 rad/s	2.991 m
	1.75 s	3.590 rad/s	3.690 m
	2 s	3.142 rad/s	4.366 m

#### 4.4.3 Mesh dependence study

An overlapping meshing method known as an overset mesh, also known as Chimera mesh is applied so that the entire calculation domain contains two parts. An overset mesh includes the structure, which is superimposed on the background mesh. Grids



between background and overset region are taken as an interface that can be calculated by interpolation. Figure 4.23 gives an example of two zones of grid that overlapping each other. One of the most obvious advantages by overlapping grids is to avoid deformation of grid in case of existence of negative cell. Furthermore, it is easy to set up and simulate complicated motions of structures in waves. Taking consideration of grid dependence and time-step dependence as well as aspect ratio of the cell, mesh scheme is listed in Table 4.7.

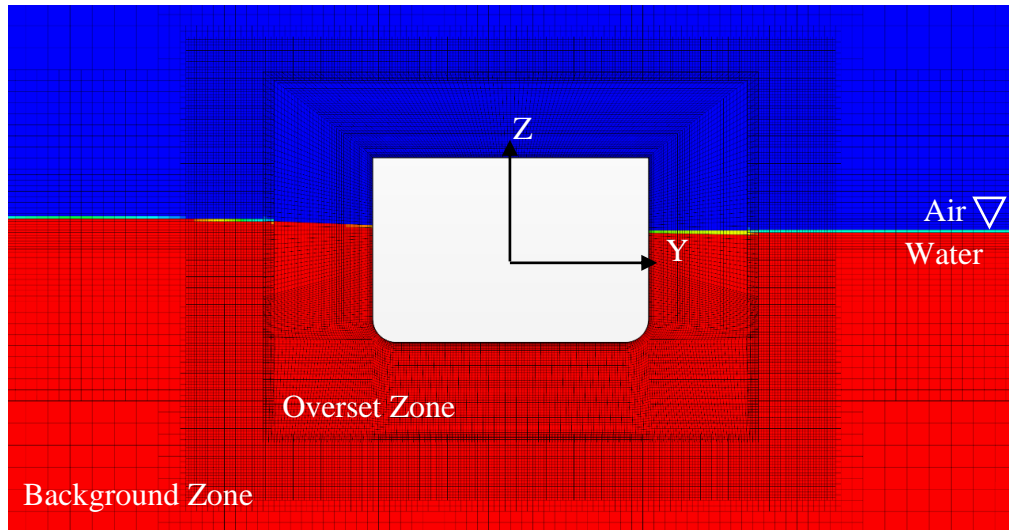


Figure 4.23. Mesh distribution for overset and background region

Table 4.7. Mesh and time-step sensitivity setup

Scheme	Cell Size	$\Delta y: \Delta z$	Total No.	Time Step	RAO	Error
S1	17mm×4mm	4	68307	T/800	21.85	5.2%
S2	12mm×3mm	4	114028	T/800	21.54	3.7%
S3	8mm×2mm	4	211454	T/800	21.53	3.7%
S4	12mm×3mm	4	114028	T/400	22.03	6.1%
S5	12mm×3mm	4	114028	T/1600	21.01	1.2%
S6	6mm×3mm	2	142579	T/800	21.32	2.7%
S7	24mm×3mm	8	91586	T/800	22.17	6.8%

Coarse (S1), medium (S2) and fine (S3) meshes shown in Figure 4.24 are generated for investigation of grid dependence with refinement ratio  $\sqrt{2}$  and results have been

plotted in Figure 4.25. Scientifically, time-step independent verification (S2, S4 and S5) and aspect ratio of the grid (S2, S6 and S7) are investigated as well.

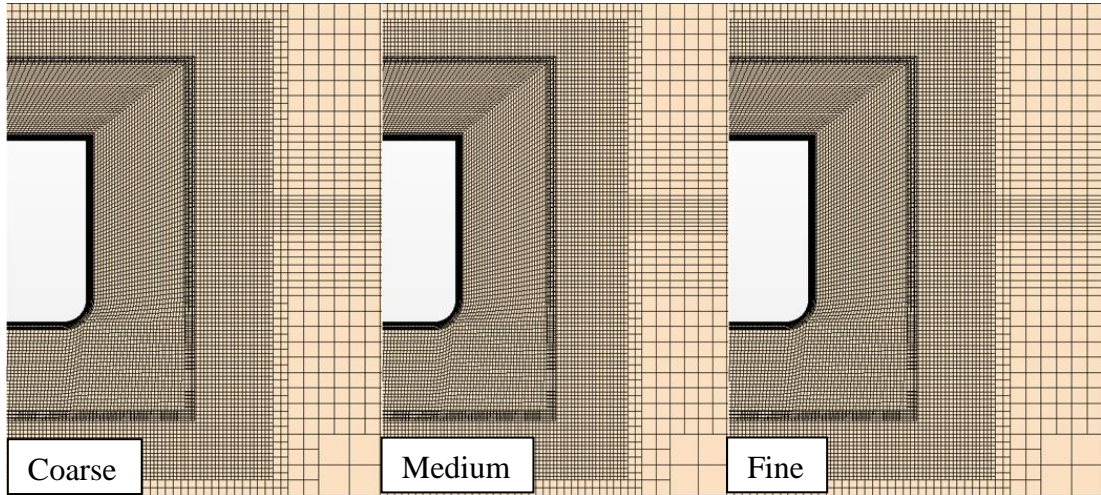


Figure 4.24. Mesh distribution for mesh dependence study

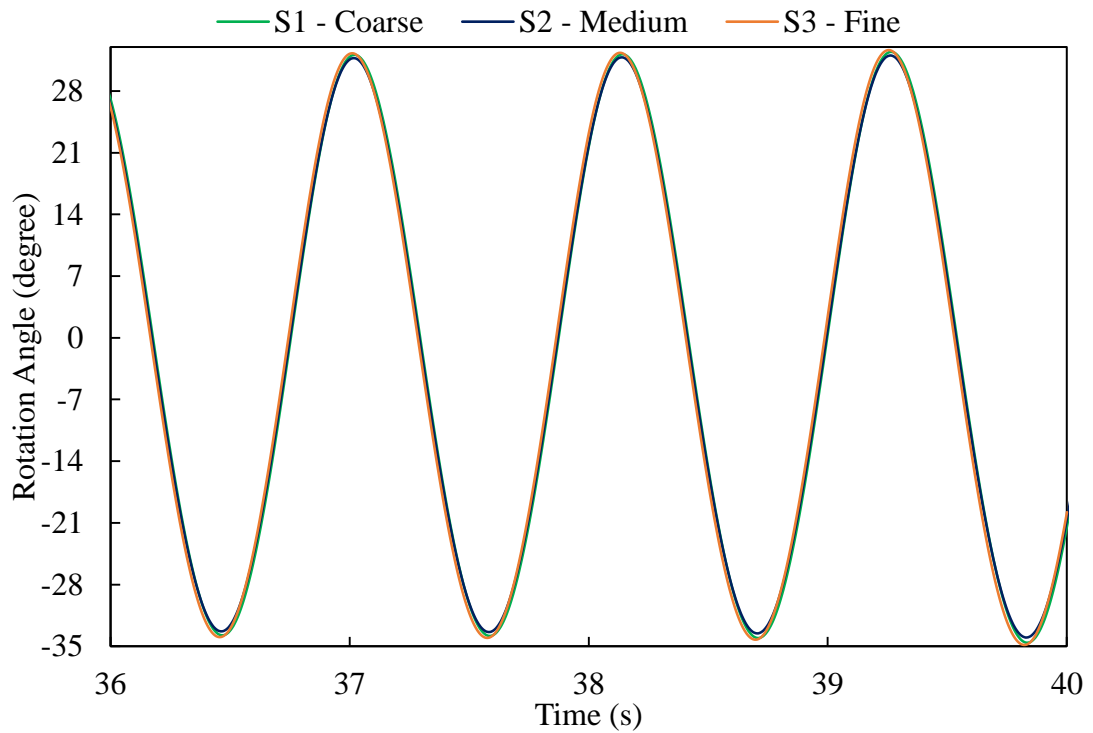


Figure 4.25. Comparison of results for mesh dependence

#### 4.4.4 Results

Figure 4.26 presents the results obtained by RANS solver compared with the results of model tests and numerical method published by Irkal et al. (2014). Response

Amplitude Operator is non-dimensionized by being divided by wave height (rotational angle / wave height) as recommended by authors.

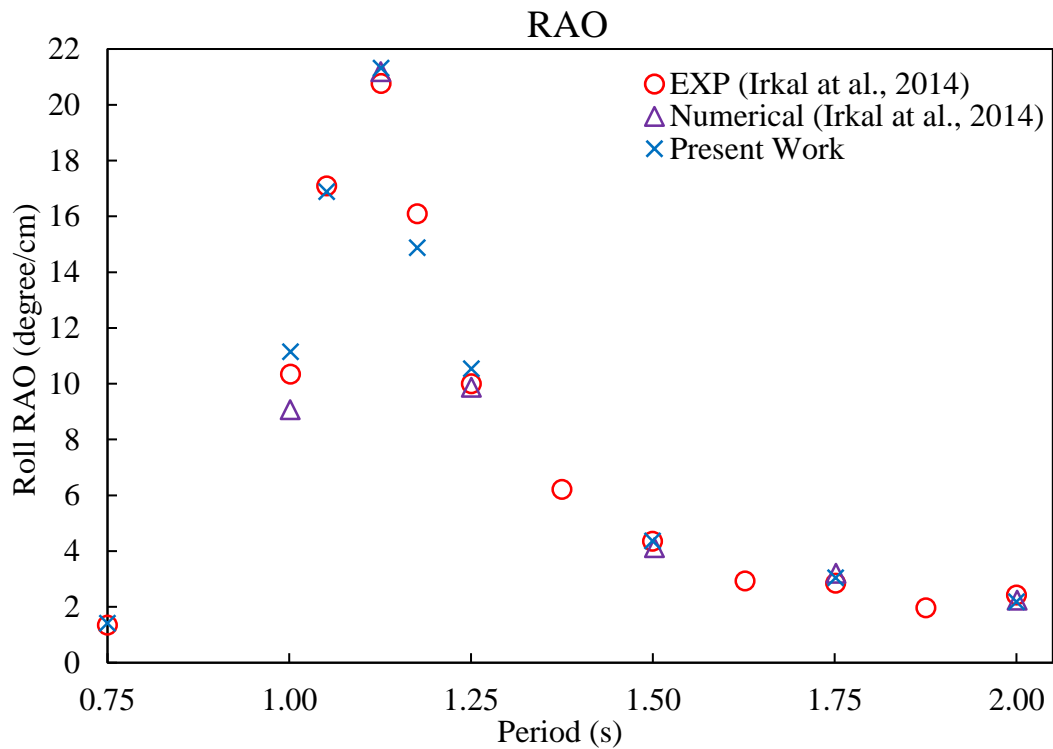
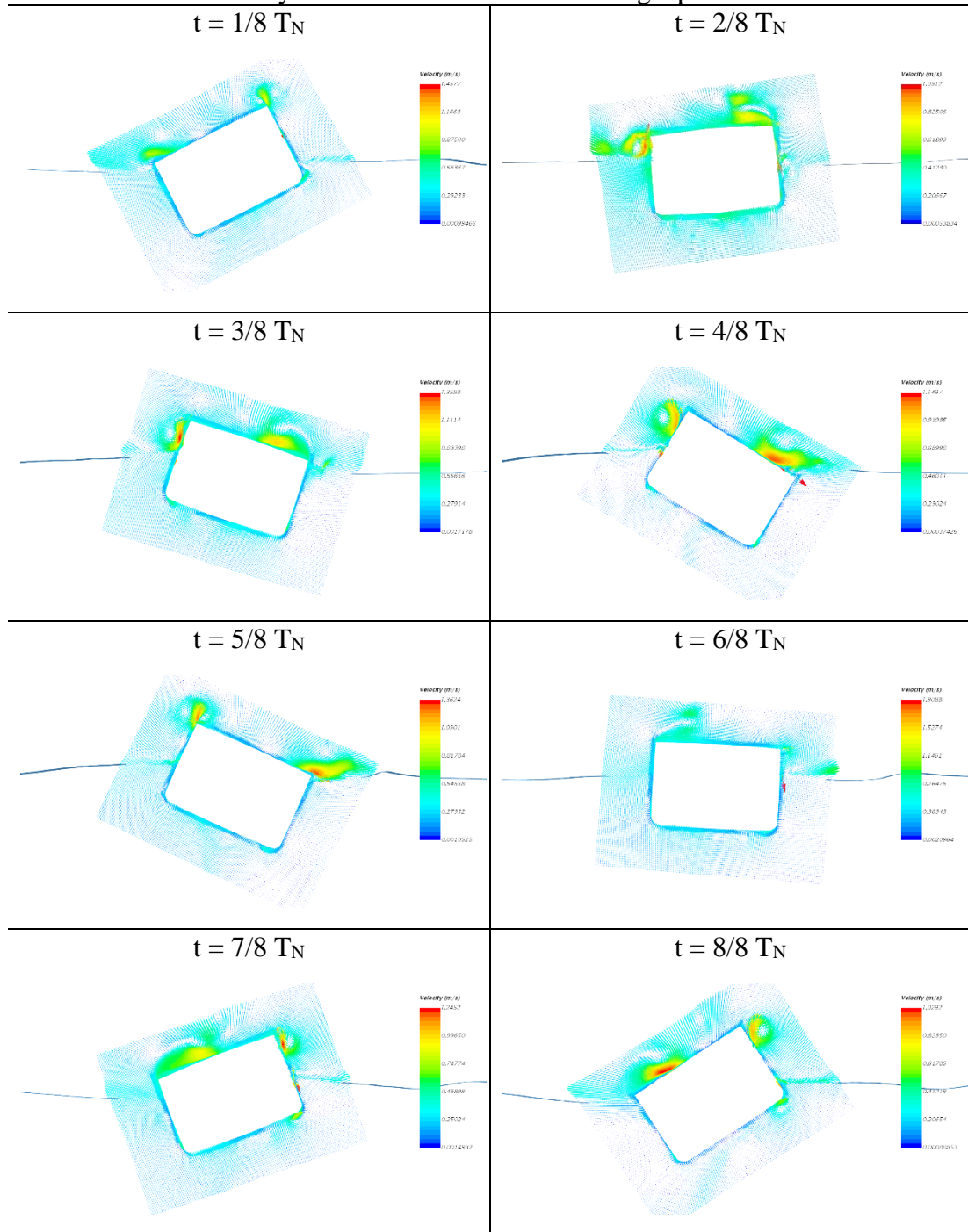


Figure 4.26. Roll motion RAO comparison between numerical methods and experiment

Through the comparison, it can be seen that results obtained by RANS-based method have a generally good agreement. However, as stated in Section 4.3.2.2, it will be much better for model tests to be presented with uncertainty analysis, which unfortunately is unknown. Table 4.8 illustrates a group of plots to present vortex expressed by velocity vector around structure in a period while encountering wave. Even though weakened by the round bilge that installed on the structure, the generated vortex can be clearly observed either in water or in air.

Table 4.8. Velocity vectors around structure during a period of oscillation



## 4.5 2-Dimensional liquid tank sloshing

After the ship loses her structural integrity a large amount of sea water may flood into the compartment adjacent to the damaged opening. With various amount of flooded water in and out of the flooded compartment, the damaged ship has to react to the waves and internal sloshing effect in the compartment. Thus, behaviour and

performance of the damaged ship can be affected by not only hydrodynamic excitation from sea waves, but also internal loads and sloshing influence from the free surface effect of floodwater in the flooded compartment. Meanwhile, interaction between wave excitation and internal floodwater dynamics can be dominant that they have an impact on each other. Despite several disadvantages such as high cost and inevitable error, physical experimental method is a good way to measure the dynamics of floodwater in the flooded compartment, but it cannot be able to obtain all the information about floodwater dynamics including dynamic loading on the hull. In this section, RANS solver is applied for water tank sloshing problem to investigate the free surface dynamics in the compartment. As a compartment is flooded after damage, water may flood into the tank and will be influenced by the excited waves and ship behaviours. Water elevation is captured by probes installed and positioned in the tank during sloshing.

#### **4.5.1 One-DOF motion sloshing**

Firstly, a simplified model of a rectangular structure is half filled. A single lateral excitation is imposed on the structure controlled by a sinusoidal function.

##### **4.5.1.1 Calculation domain**

To specifically investigate free surface effect in the flooded compartment as well as the influence of ship motions on the floodwater, a water sloshing physical test is carried out by Liu and Lin (2008) with a rectangular water tank. A closed water tank with 0.57-metre length, 0.31-metre width and 0.3-metre height is filled with 0.15-metre depth of water (50% volume). A 2D sketch of the water tank is shown in Figure 4.27.

The water tank is installed on a shaker that controlled by amplitude and frequency of movement. During the tests, a sinusoidal function  $y = -a \sin \omega t$  leads the motion of the shaker where the amplitude  $a$  is equal to 0.005 metre and the natural frequency  $\omega_0$  of the water in the tank is equal to 6.0578 Hz. Low frequency and the natural frequency,  $0.583 \omega_0$  and  $\omega_0$  are tested for sloshing problem respectively. Three probes (P1, P2 and P3) for water height are installed in the tank, where P1 and P3 are located at the 20 mm off the sides of the tank, and P2 is positioned at the centre of the tank.

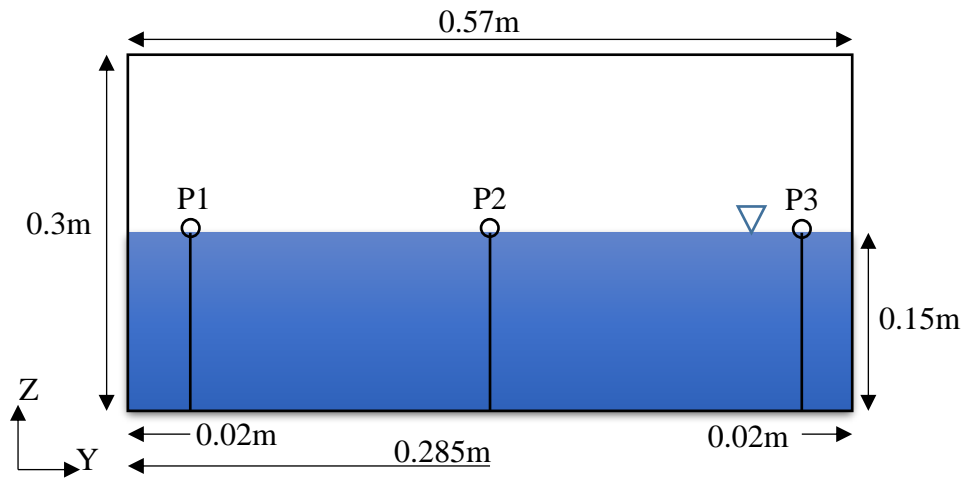


Figure 4.27. 2D sketch of water tank sloshing

To simulate the water sloshing problem in the tank, a 2-dimensional fluid domain is established containing 570mm length in Y-direction and 300mm height in Z-direction, while 310mm width in X-direction is replaced by one-layer cell so that it can be taken as a 2-dimensional simulation. A sample of mesh scheme for low frequency motion is shown in Figure 4.28.

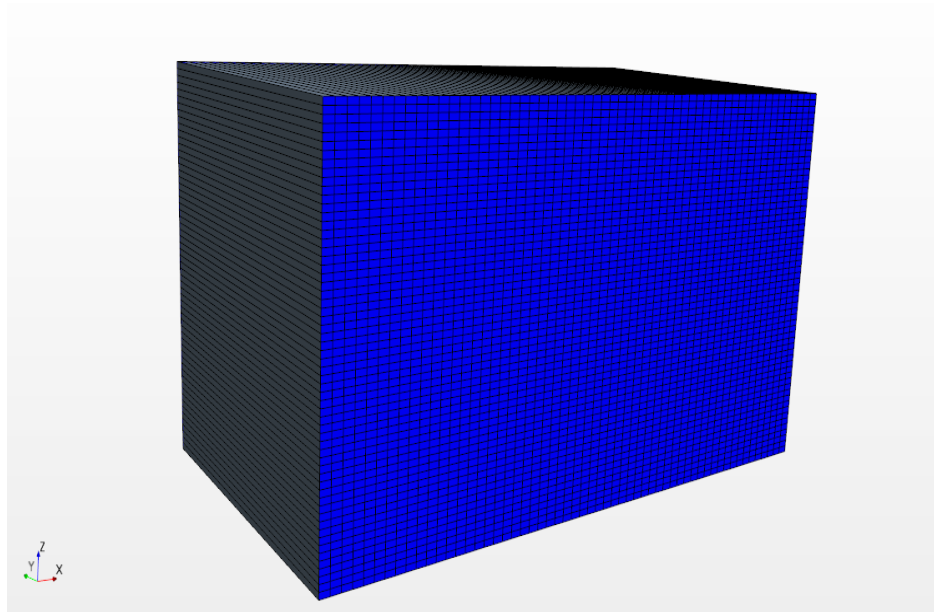


Figure 4.28. Mesh generated for 2-dimensional simulation

#### 4.5.1.2 Non-resonance sloshing

Mesh schemes are employed for non-resonance sloshing. Three mesh schemes are applied by a mesh refinement ratio  $\sqrt{2}$  and a constant aspect ratio 10 from 30 cells in

Z-direction to capture the free surface (S1, S2 and S3), as recommended by Gao et al. (2010). To further investigate the influence of aspect ratio of the cell used to capture the interface between water and air, three more cases with aspect ratio of 8, 4 and 2 are applied (S4, S5 and S6), and they are conclusively listed in Table 4.9.

Table 4.9. Mesh dependence for non-resonance sloshing

<b>Scheme</b>	$\Delta y \times \Delta z$	<b>Aspect ratio</b>	<b>No. of cells</b>	<b>Cells for interface</b>
S1	5mm×0.5mm	10	10260	40
S2	7mm×0.7mm	10	5670	30
S3	10mm×1mm	10	2850	20
S4	4mm×0.5mm	8	12870	40
S5	2mm×0.5mm	4	25650	40
S6	1mm×0.5mm	2	51300	40

Results for grid dependence are shown in Figure 4.29 to Figure 4.31 for non-resonance sloshing cases (S1, S2 and S3) by three wave elevation probes (P1, P2 and P3). As  $\omega=0.583\omega_0$ , water motion in the tank is not dramatic and elevation of water surface appears not to vary rapidly due to the low frequency vibration. It can be clearly seen that water surface that captured by probes P1 and P3 is well agreed with experiments. Elevation measurement at probe P2 fluctuates with small amplitude (0.6mm approximately), and numerical calculation poorly captures the slight perturbation.

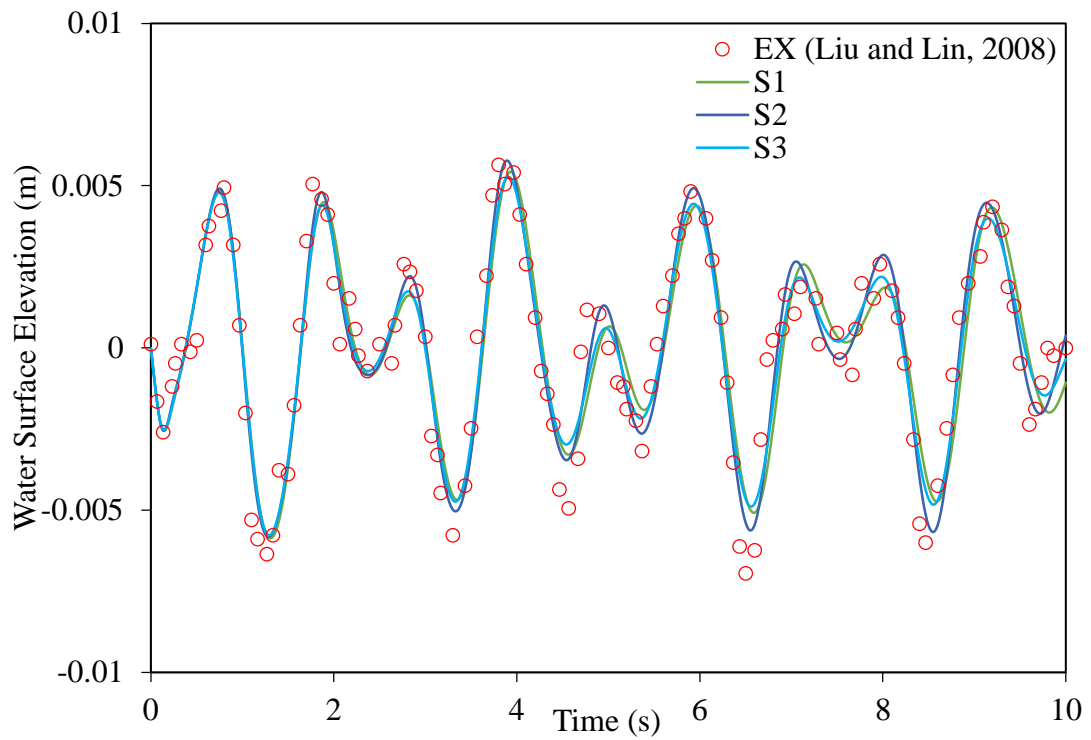


Figure 4.29. Elevation measured by probe P1

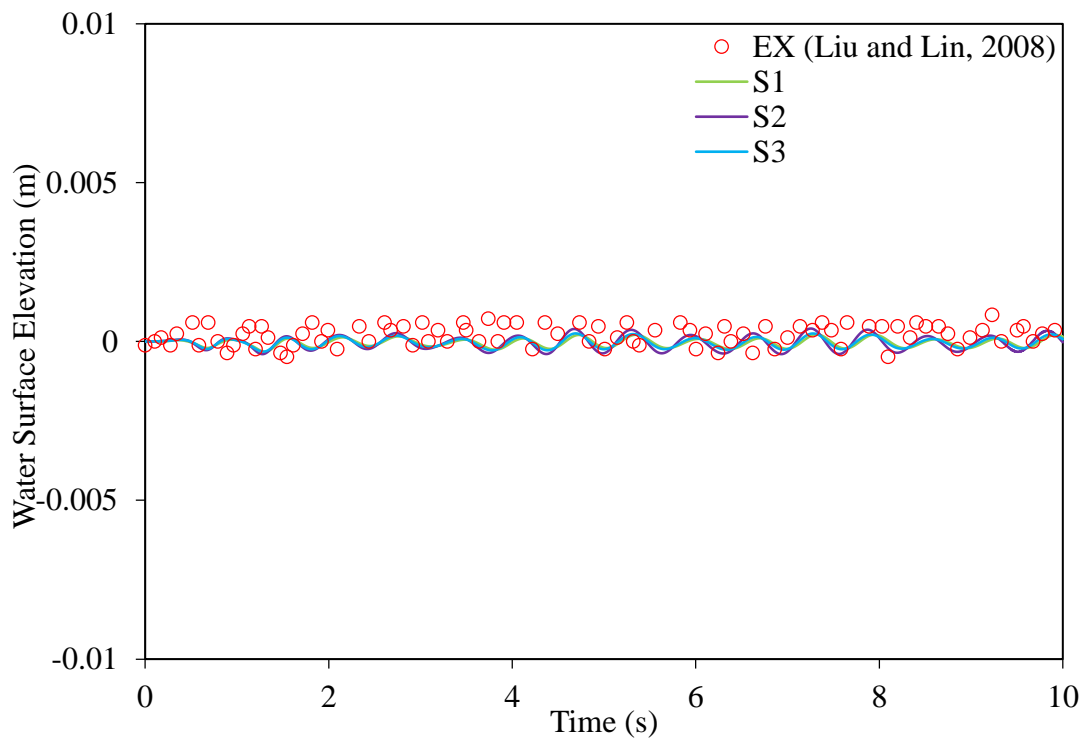


Figure 4.30. Elevation measured by probe P2



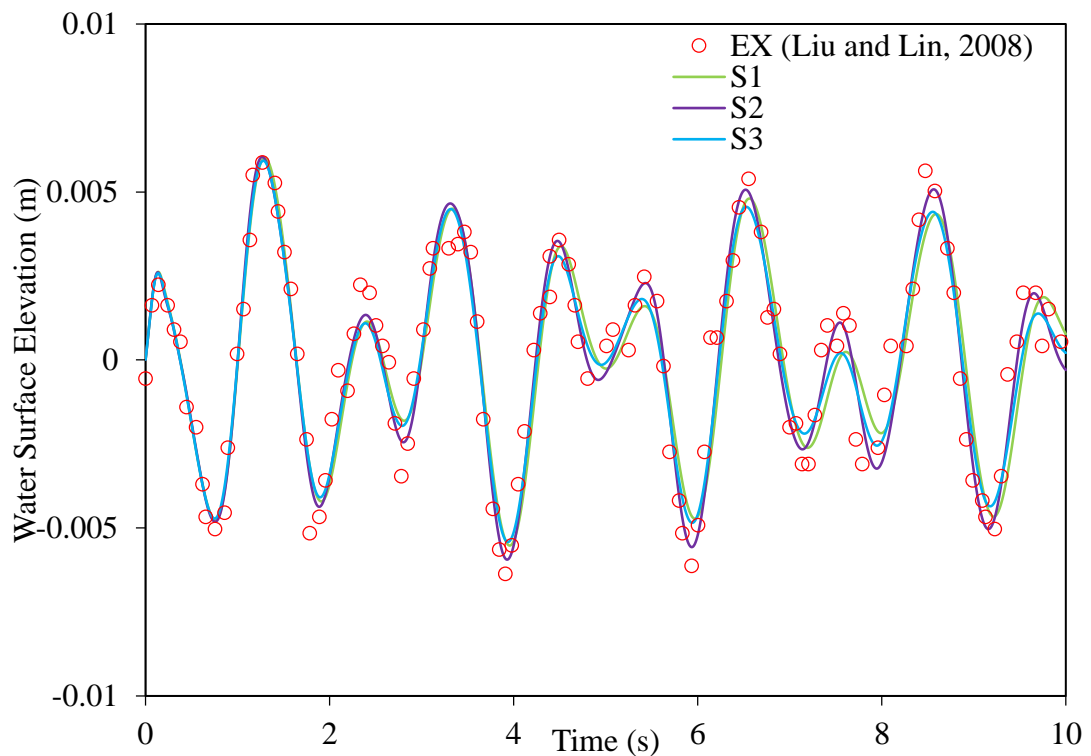


Figure 4.31. Elevation measured by probe P3

With S4, S5 and S6, suitable aspect ratio for cells to capture the free surface seems to be essential to give a better agreement with experimental results. Especially for several peak and bottom values, with a suitable aspect ratio cells can be applied to capture the characteristics of the free surface well. Results can be demonstrated in Figure 4.32 – Figure 4.34.

However, under the non-resonance case, amplitude of elevation of water surface will not be so dramatic and obvious as that under the resonance condition. Therefore, another case study for resonance case, which excitation frequency is equal to  $\omega_0$ , is investigated for water tank sloshing problem.

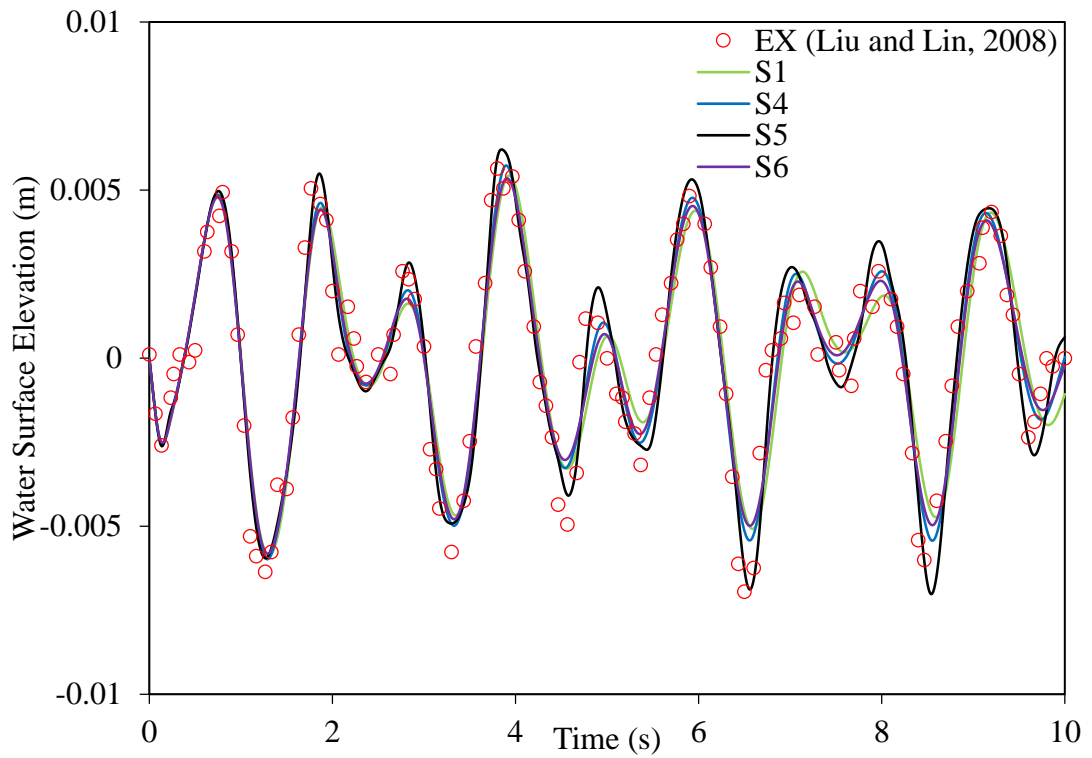


Figure 4.32. Water surface elevation measured at Probe P1

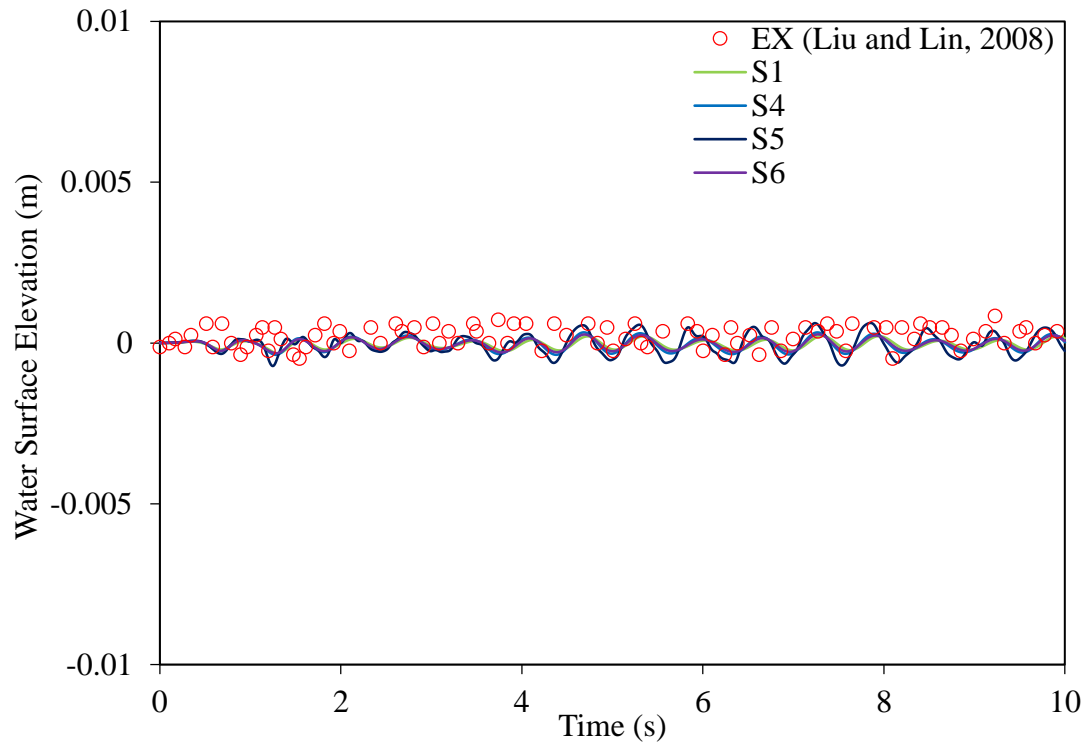


Figure 4.33. Water surface elevation measured at Probe P2

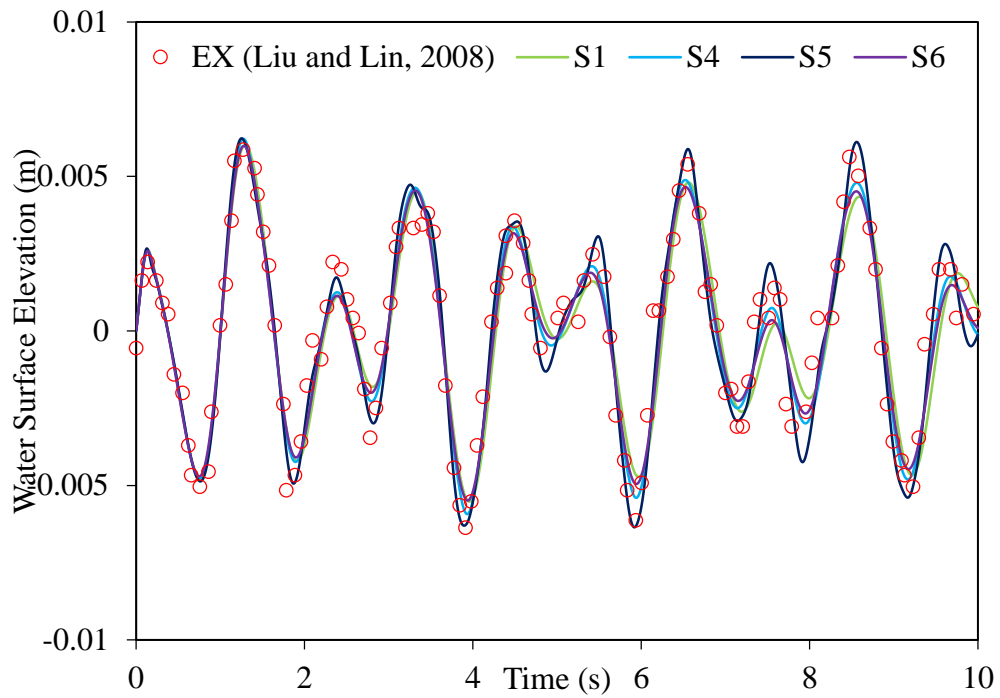


Figure 4.34. Water surface elevation measured at Probe P3

#### 4.5.1.3 Resonance sloshing

As excitation frequency is equal to the natural frequency of the water tank, i.e.  $\omega = \omega_0$ , water dynamics in the tank is going to be violent, which is extremely dangerous in reality. To predict the water surface dynamics accurately, RANS solver is applied for resonance sloshing again for the same tank as stated in previous section.

For resonance sloshing, the mesh scheme for grid dependence is shown in Table 4.10. Again, fine, medium and coarse grids (S1, S2 and S3) are applied to capture the free surface. However, different from the non-resonance case, the mesh is uniform along the length and height of the tank as the free surface is violent and unpredictable under the resonance excitation. Results are shown in Figure 4.35 to Figure 4.37 for resonance sloshing computation compared with experimental measurement at three wave elevation probes.

Table 4.10. Mesh dependence setup for resonance sloshing

Scheme	$\Delta y \times \Delta z$	No. of cells
S1	5mm $\times$ 2mm	17100
S2	7mm $\times$ 3mm	8100
S3	10mm $\times$ 5mm	3420

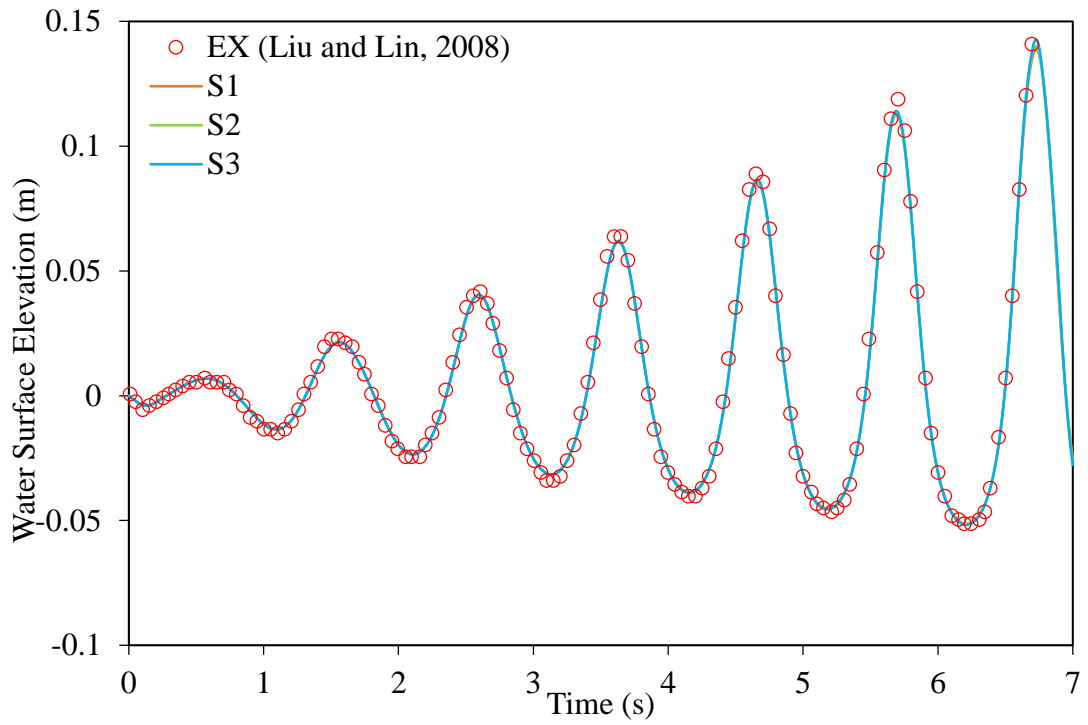


Figure 4.35. Water surface elevation measured by Probe P1

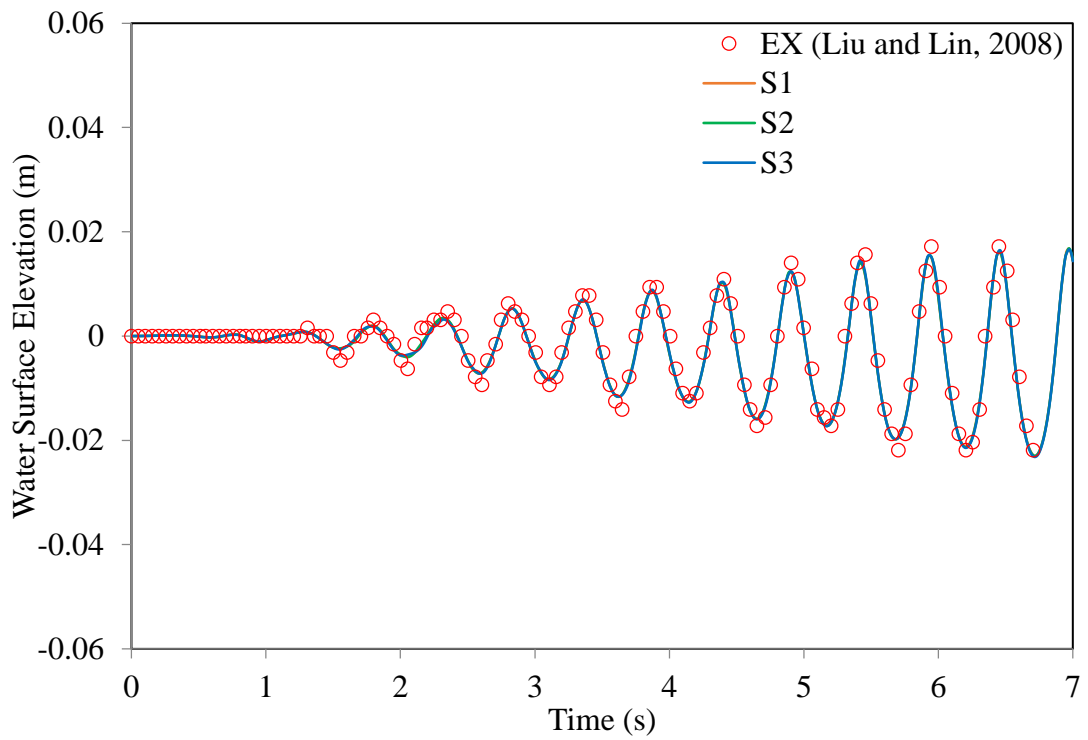


Figure 4.36. Water surface elevation measured by Probe P2

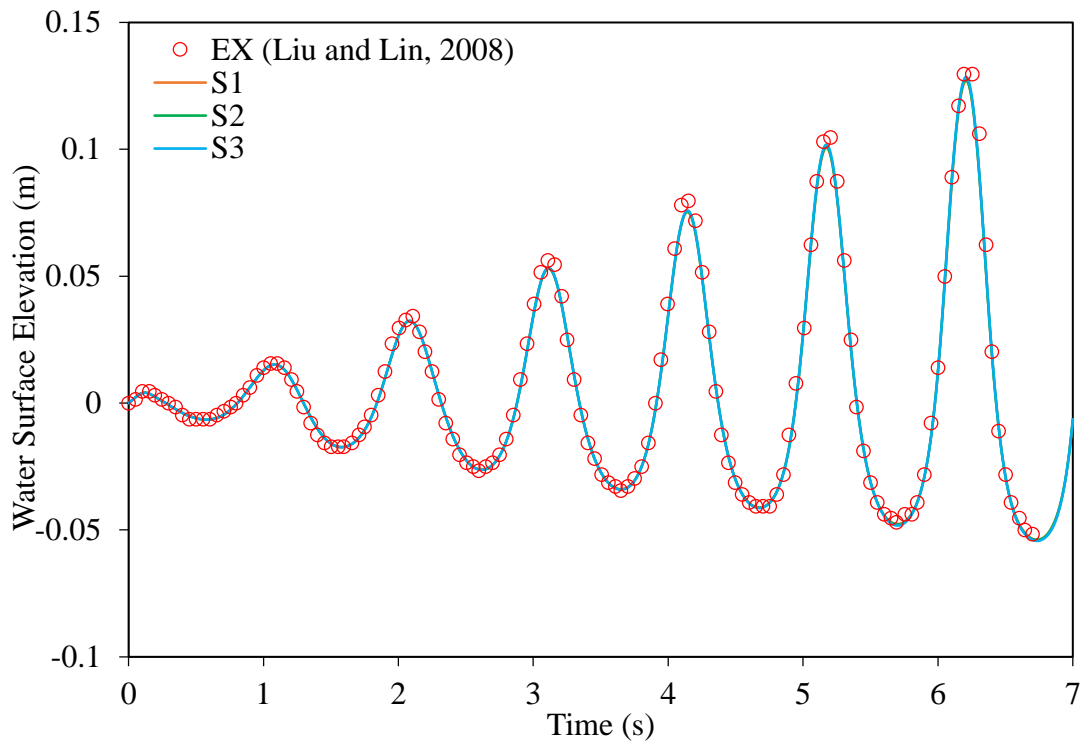


Figure 4.37. Water surface elevation measured by Probe P3

It is apparent that compared with experimental data, numerical solutions show a pretty good agreement with RANS solver. Furthermore, what is more important is that complicated water behaviours with strong nonlinearities in sloshing dynamics can be well calculated.

#### 4.5.2 3-DOF sloshing problem

To study more actual phenomenon related to water tank sloshing problem in two dimensions, another rectangular structure with partially crude oil filled is used to investigate the free surface effect while sloshing in the tank. Three-DOF motions controlled by three different functions are applied on the structure to define heave, sway and rotational motion.

##### 4.5.2.1 Calculation domain

Investigation on the free surface effect by a numerical method is studied by Soo Kim et al. (2003). A two-dimensional rectangular tank filled partially with crude oil to specifically simulate free surface effect as sloshing in the oil tanker. A 2-D tank with 44.5-metre width and 27.5-metre height is filled with 9-metre depth of crude oil with

890 kg/m<sup>3</sup> of density and 0.008 Pa·s of viscosity. The centre of gravity is located at the geometric centre of the structure and sketch can be shown in Figure 4.38.

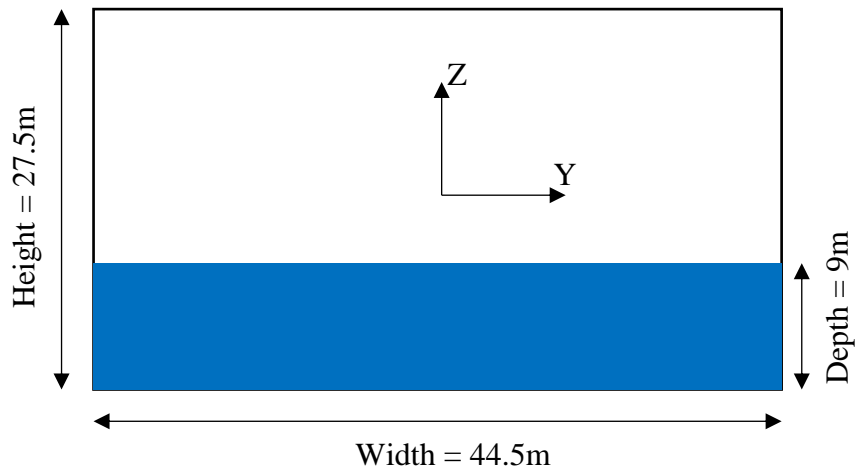


Figure 4.38. Sketch of structure for 3DOF sloshing

#### 4.5.2.2 Forced excitation

Three functions are used to define the motions of structure including heave, sway and rotation, given as

$$Y(t) = A_y \sin(\omega_y t)$$

$$Z(t) = A_z \sin(\omega_z t)$$

$$\theta(t) = \theta_x \sin(\omega_x t)$$

Where

$Y(t)$  presents displacement of sway motion

$Z(t)$  presents displacement of heave motion

$\theta(t)$  presents displacement of roll motion

$A_y$  is amplitude of sway motion

$A_z$  is amplitude of heave motion

$\theta_x$  is amplitude of rotation

$\omega$  is the frequency of each coordinate directions

The parameters that specify the motion functions are listed in Table 4.11.

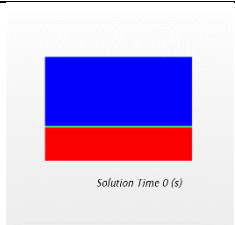
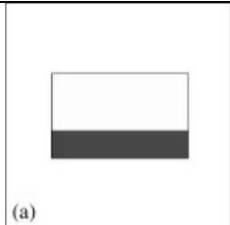
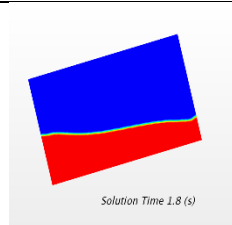
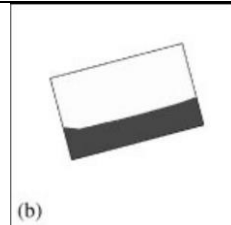
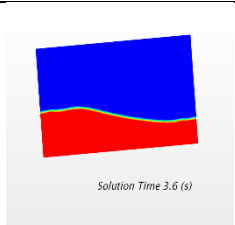
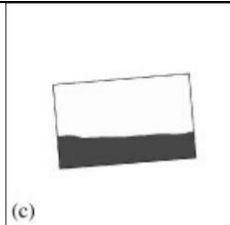
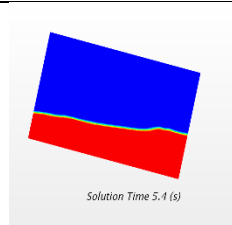
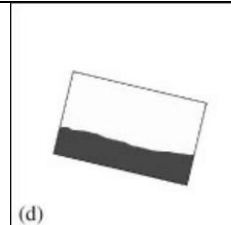
Table 4.11. Coefficients that define motion functions

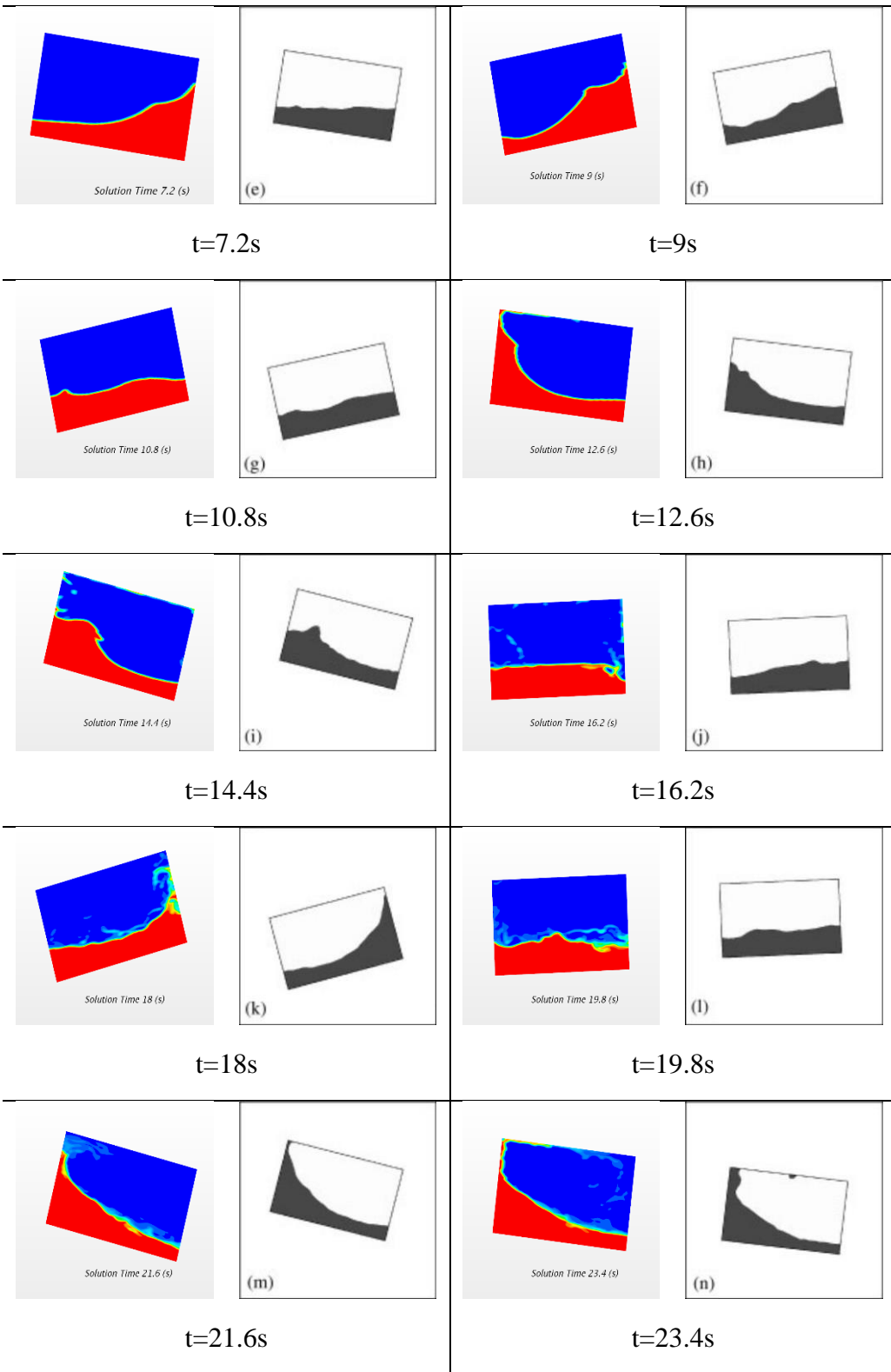
Parameter	Value
$A_y$ (metre)	2
$A_z$ (metre)	5
$\theta_x$ (degree)	15
$\omega_y$ (rad/s)	0.5236
$\omega_z$ (rad/s)	0.9817
$\omega_x$ (rad/s)	0.7854

#### 4.5.2.3 Sloshing in the oil tank

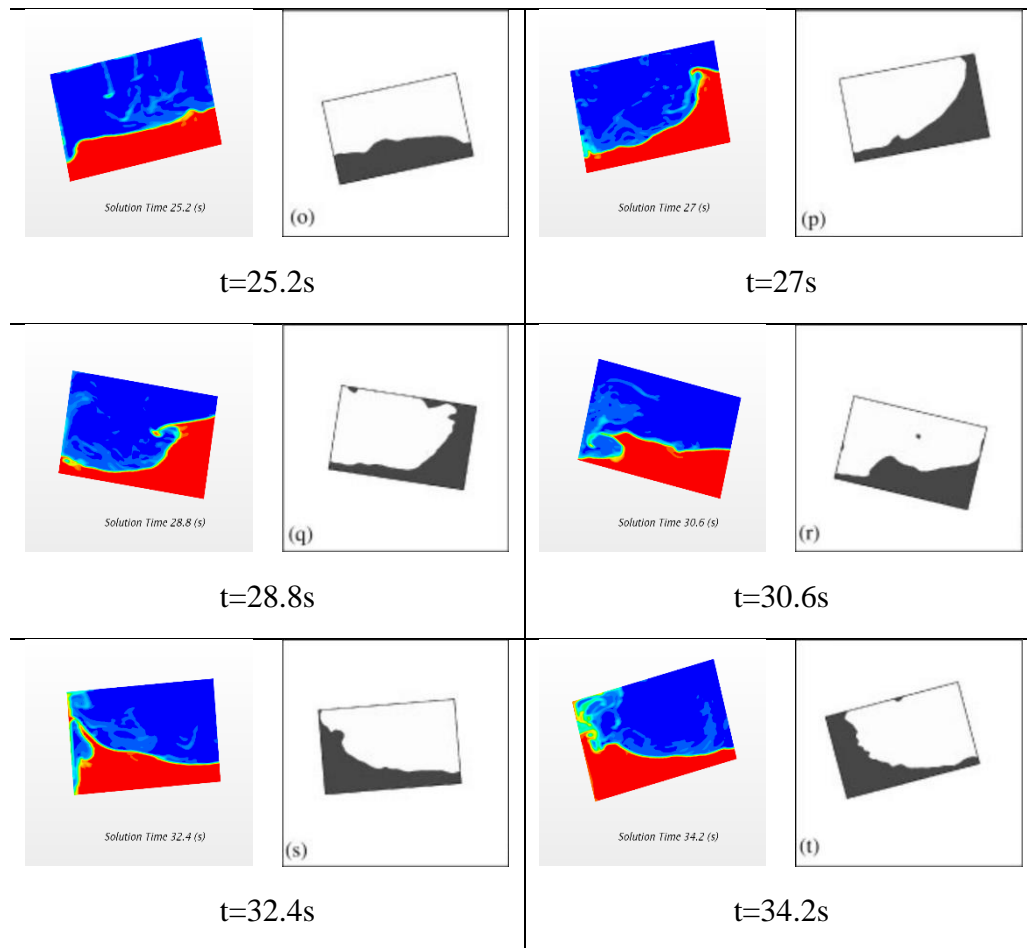
Table 4.12 below compares the results obtained by present work and Soo Kim et al. (2003). It seems that RANS-based solver is able to simulate the free surface effect for sloshing problem in the tank well even though, unfortunately, there is no more detailed data from the published work.

Table 4.12. Free surface evolution comparison

Present work	Kim et al., 2003	Present work	Kim et al., 2003
 <p>Solution Time 0 (s)</p>	 <p>(a)</p>	 <p>Solution Time 1.8 (s)</p>	 <p>(b)</p>
t=0s		t=1.8s	
 <p>Solution Time 3.6 (s)</p>	 <p>(c)</p>	 <p>Solution Time 5.4 (s)</p>	 <p>(d)</p>
t=3.6s		t=5.4s	







## 4.6 Chapter remarks

Water flooding into a damaged ship in the beam seas is a complicated phenomenon composed of regular beam wave generation, free rolling decay, motion excited by waves, floodwater ingress and egress through damaged opening and floodwater dynamics inside the compartment (i.e. water sloshing in tank), etc. As a first step towards modelling the full problem, it can be simplified by decomposing the complexity into several individual 2-dimensional problems based on the basic hydrodynamic characteristics. Thus, in this chapter, to scientifically demonstrate the numerical method for these 2-dimensional problems, simulations for the 2D floating body in calm water and beam waves are generated and all validated with available experimental data. Specifically, regular beam waves generation, free floating body's rotational decrement, floating body motion excited by regular beam waves, and liquid tank sloshing problem have been studied by CFD-based RANS solver respectively.

Prior to calculate the floating body's behaviour in water, a regular beam wave is required to be accurately generated by CFD method. The waves generated by the CFD method can be regarded as acceptable as long as the wave height and wave frequency achieve the target value. It is also useful to gain experience and reasonable to define an appropriate calculation domain for simulating a ship in waves in 3D. A suitable location for the ship away can be determined far enough from the inlet of generated waves to avoid influence on the generation and propagation of waves but not so far as to lead to unnecessary calculation cost.

As a first approximation of a ship excited by waves a two-dimensional section of a ship hull can be treated as a floating body. Using experimental results offered by other researchers, free roll motion decay simulation is carried out with a 2-D rectangular body. Results show that damping in the physical model tests and the numerical result does not present a good agreement. Therefore, another second physical model test with a round-bilge ship body is validated. A good agreement is found between numerical results and experimental data, furthermore, with the rounded bilge considered, fluid field around the body can be more realistic, which is helpful for study on flow field around a ship especially in beam seas.

Floodwater dynamics inside the damaged compartment is a key issue in a damaged ship. It is essential to simulate floodwater behaviour accurately since it can have a significant impact on the behaviour of the damaged ship, which, in turn, affects floodwater dynamics. By defining motions of the water tank, the sloshing problem can be studied through estimating the elevation of floodwater surface at a specific location inside the tank. In 2-dimensional sloshing simulation, one DOF and three DOFs respectively define the movement of water tank, and comparison between 2D numerical simulation and physical tests present an excellent agreement. It should be mentioned that water dynamics inside the 3D compartment may not only suffer three DOFs and sloshing may become even worse if all of the ship's 6 DOF motions are taken into account, especially near the natural frequency (such as an LNG ship carrying with liquified gas). But 3 DOFs (one rotation and two translations) are the most complicated situation that can be defined onto the tank in 2-dimensional simulation.

Studies with 2-dimensional structure in the numerical tank lay a solid foundation for the investigation on the performance of intact and damaged ship in the regular beam seas further. Comparisons between physical model tests and numerical solutions illustrate a fairly good agreement. It suggests a good ability to predict ship motions and free surface dynamic effect within a 2-dimensional simulation. This provides a valuable experience for prediction of the ship motions in the regular waves as well as the non-linear effect of the floodwater free surface in the flooded compartment due to interaction between these two., Accurate calculation of water sloshing problem for further estimation on the floodwater behaviour in the flooded compartment is of importance. According to Jia and Moan (2012), floodwater sloshing in the damaged compartment could have a significant influence on both vertical and horizontal bending moment, especially when ship suffered damaged in beam waves.

However, wave excitation simulation and water tank sloshing are both studied with an “intact” 2D floating body. The body is enclosed and there is no ingress or egress of floodwater through the damaged opening. Thus, specific investigation on the effect of water ingress and egress from a damaged opening is neglected.

In the following chapter, the studies are extended to model the realistic cases of a 3D ship with floodwater flowing in and out of the damaged compartment.

# 5. RANS investigation on an intact and damaged naval combatant vessel

Although a large amount of information can be collected from physical model tests, experiments have limitations such as system stiffness, range of application of measurement devices and uncertainty of post-processing. A CFD-based RANS solver, on the other hand, can be an alternative tool that is able to investigate the intact and damaged ship in calm water and in beam seas. In this chapter the CFD method is applied to investigate the performance of intact and damaged ships in beam waves including ship motions and wave-induced loads acting on the ship hull girder compared with physical experiments. Free roll motion decrement simulations for intact and damaged ship are included to verify modelling consistency of all the details. Due to the unknown tension of moorings used in physical tests, only two DOF motions, namely roll and heave motions are investigated while the rest of motions are restrained. It should be highlighted that this work focuses on estimation of the performance of the ship in the intact and damaged condition by CFD method, and in particular the influence of damage on the ship motions and hull-girder loads acting on the ship that much more traditional seakeeping analysis cannot present, rather than detailed examination of examination of local flows and vorticity, etc.

Star-CCM+, as a CFD solver package, is applied in this three-dimensional study. Due to the very large number of cells employed in these CFD studies, a high-performance computing technology is adopted and provided by High Performance Computers from Archie-West. Dual Inter Xeon X5650 CPUs, which processing capacity is 2.66 GHz, contain 276 calculating nodes totally 3312 cores, where 48 GB RAM can be held per core.

## 5.1 Ship geometry

A 51-scale destroyer model DTMB 5415 is utilized in this study, whose main dimensions are listed in Table 5.1. Three orthographic views of the intact model with geometric dimensions are illustrated in Figure 5.1. The damaged ship hull is shown in Figure 5.2. It should be noted that to eliminate the effect of trapped air compression in

flooded compartments, two pipes are constructed through main deck in each compartment for ventilation, which have been highlighted in Figure 5.2.

Table 5.1. Main properties of DTMB 5415

Particular		Value	Unit
Overall length	$L_{OA}$	3	m
Length of waterline	$L_{WL}$	2.784	m
Overall beam	$B_{OA}$	0.403	m
Beam of waterline	$B_{WL}$	0.374	m
Depth	$D$	0.376	m
Draft (design)	$T$	0.12	m
Block coefficient	$C_B$	0.498	
Mass	$m$	63.5	kg
Vertical centre of gravity	$KG$	0.148	m
Longitudinal centre of gravity from aft perpendicular	$LCG$	1.375	m
Mass moment of inertia of roll	$I_{xx}$	0.897	kgm <sup>2</sup>
Mass moment of inertia of pitch and yaw	$I_{yy}, I_{zz}$	0.25L	kgm <sup>2</sup>

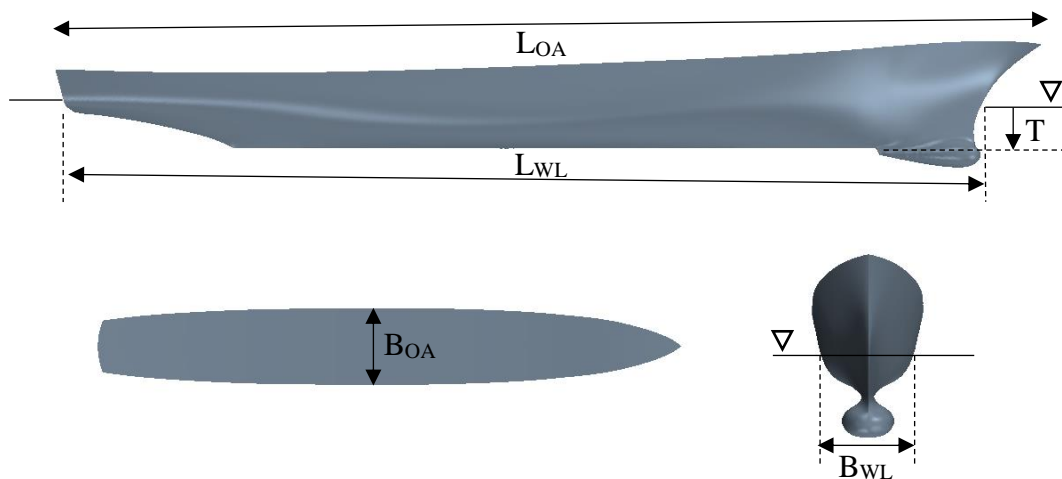


Figure 5.1. Three orthographic views of the geometry with dimensions

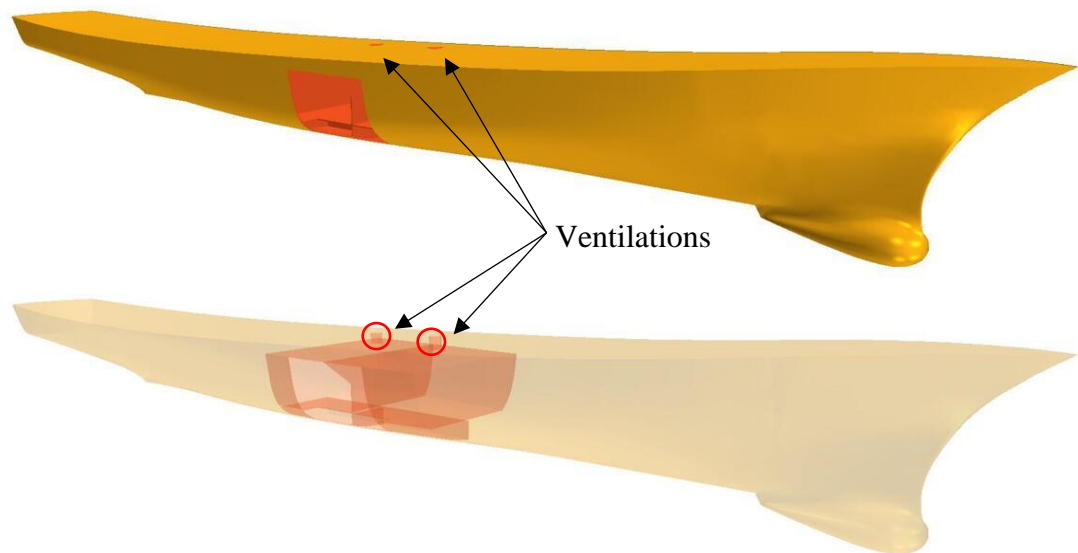


Figure 5.2. Damaged ship geometry with flooded compartments



Figure 5.3. Inner layout of damaged compartments used in CFD and experiment

In order to present a good validation with physical model tests, 3D-CAD geometry, especially flooded compartments in the damaged ship, is generated carefully and approached closely the physical model. Figure 5.3 presents the geometry of flooded compartments generated and used in CFD simulations compared to the damaged

compartments in physical model. It can be clearly seen that the complexity of damaged compartments, i.e. the transverse bulkhead and double bottom in the flooded compartment are generated and it must be highlighted that due to the separation by a longitudinal keel, the double bottom part, as matter of fact, is flooded within only half of the volume (which can be also seen from Figure 5.2).

## 5.2 Free roll motion decay simulation

Free decay simulation is investigated by the CFD method with the intact and the damaged ship hull respectively. To validate the present method, model used in CFD simulation is the same (as much as possible) as the physical model tested in experiment that stated in Chapter 3. As a matter of fact, inevitably the numerical model is almost impossible to exactly be the same as the physical model, especially for the damaged ship model due to the complexity of flooded compartments. It is clear that it is pretty difficult to guarantee a sufficient geometrical similarity between physical model used in experiments and numerical CAD geometry in CFD, so that the uncertainty and error for geometry are unknown.

### 5.2.1 Calculation domain

In order to simulate free decrement motion of the intact and the damaged ship, an initial heel angle is forced onto the ship hull, so that ship is statically positioned in the calm water with a certain heel. To validate with physical model tests, water depth and width in the fluid domain are kept the same as the physical hydrodynamic tank during each numerical simulation. Geometric dimensions and boundary conditions that defined the fluid domain are shown in Figure 5.4.

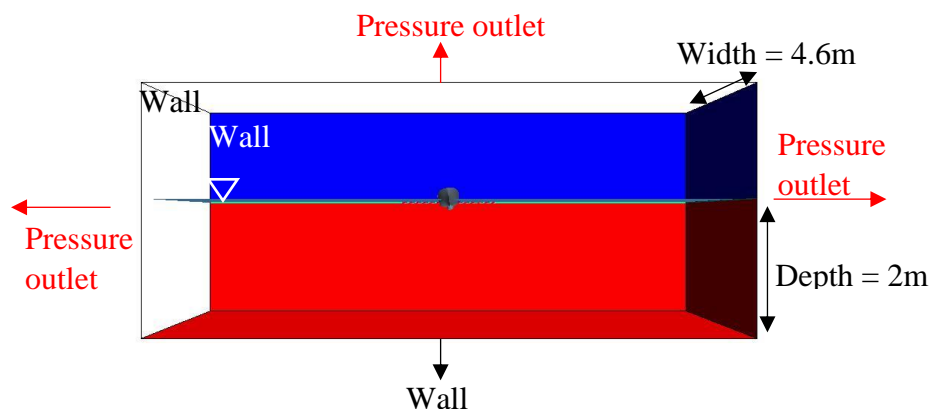


Figure 5.4. Boundary conditions of fluid domain

### 5.2.2 Mesh distribution

Mesh generation is performed by overlapping mesher within STAR-CCM+. Two regions are meshed separately, and mesh refinement is carried out for the water surface, overlapping interface between two regions and sonar dome, and free surface in flooded compartment when damaged. As plotted below, Figure 5.5 illustrates mesh distributed along intact and damaged ship hull, while Figure 5.6 specifically shows the mesh distribution for the flooded compartments. In Figure 5.7 and Figure 5.8 the refined mesh established for interface between regions and water surface can be observed for intact and damaged cases, respectively.

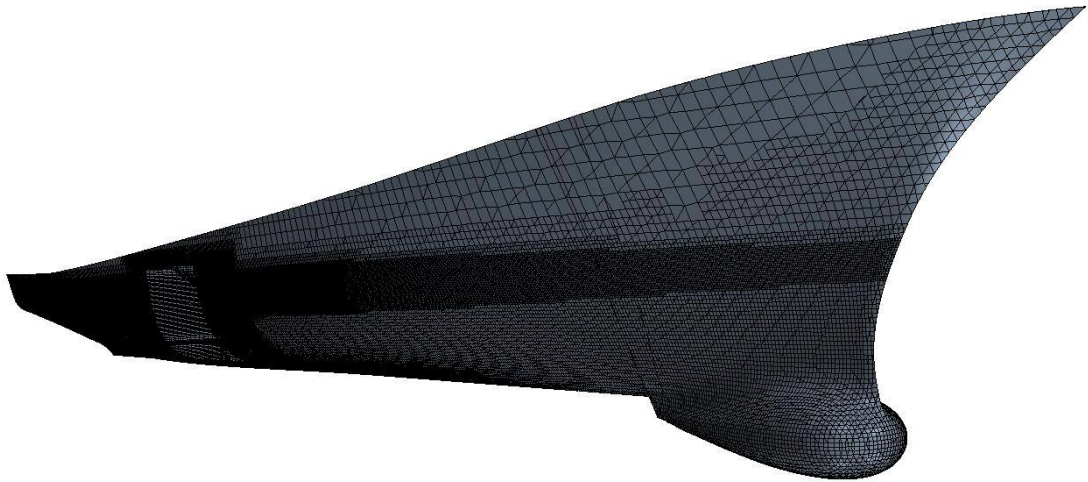


Figure 5.5. Mesh distribution along the damaged ship hull

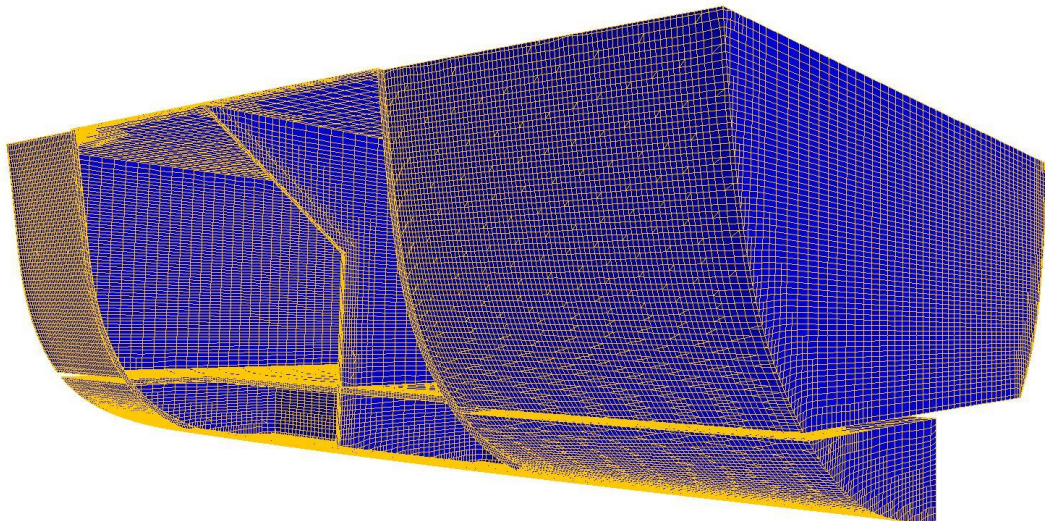


Figure 5.6. Mesh inside the flooded tank



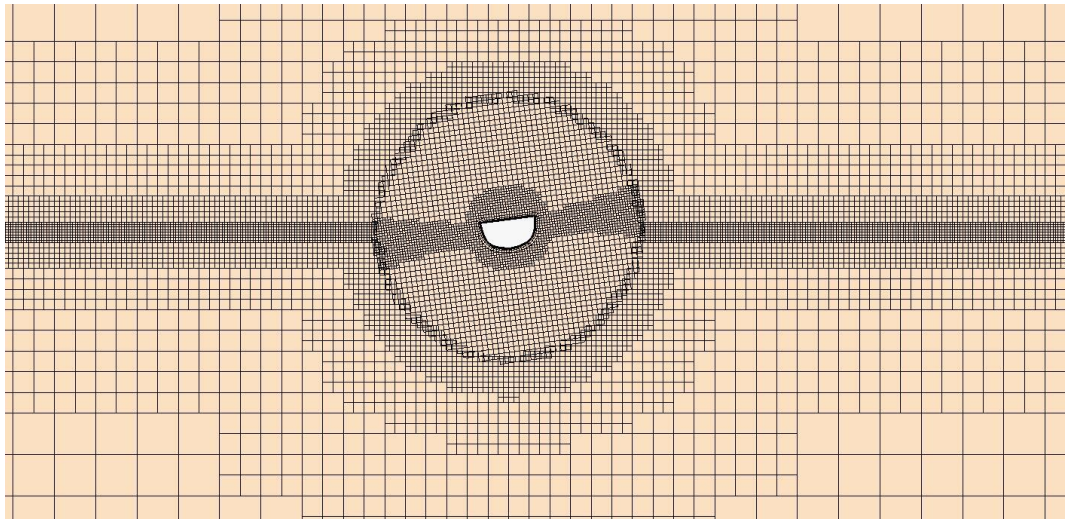


Figure 5.7. Mesh distribution on XOZ plane for intact free decay

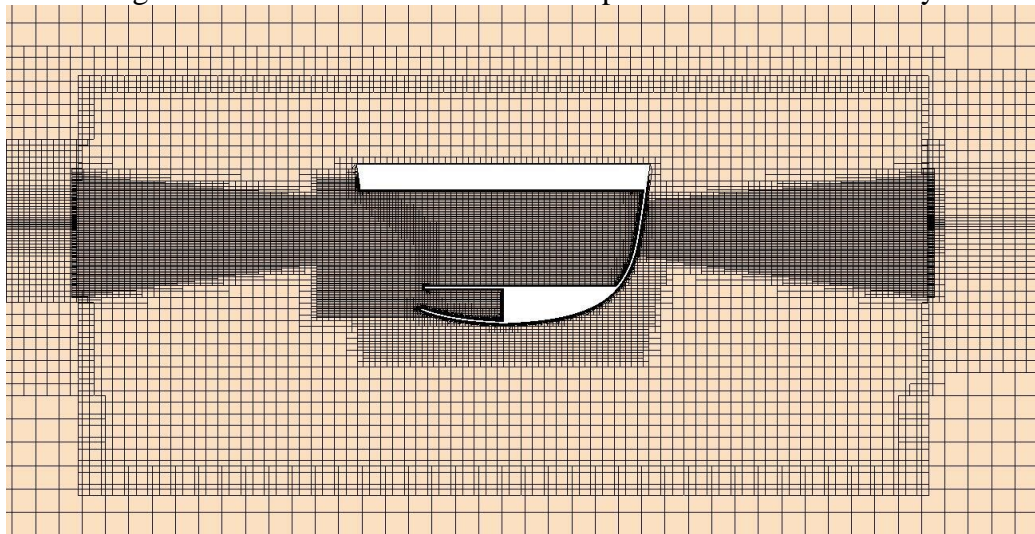


Figure 5.8. Mesh distribution for damaged free decay simulation

### 5.2.3 Results presentation

Figure 5.9 and Figure 5.10 present decay curves of the intact and the damaged ship compared with experimental data, respectively. Although damping obtained by the CFD method is slightly larger than the experimental result, a good agreement has been achieved. It is interesting to observe that for damaged ship decrement, damping effect between Point A and Point B is unforeseen, and obviously larger than the damping effect between Point B and Point C, where point A, B, C are the first three positive peaks during per swing as labelled in Figure 5.10. This is because double bottom is divided by the keel, and only half of the bottom is flooded. The initial angle is brought to bear on the undamaged side, and restoring moment is not symmetric, being bigger at undamaged side than the damage side.

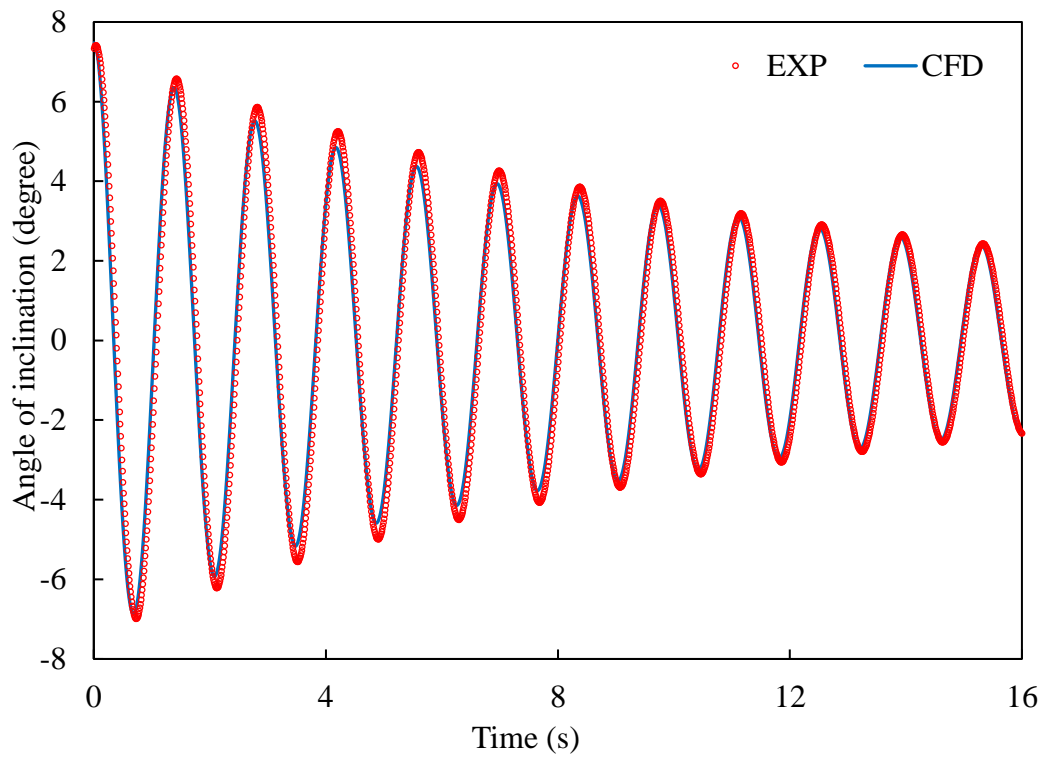


Figure 5.9. Intact free decay result obtained by CFD compared with experiment

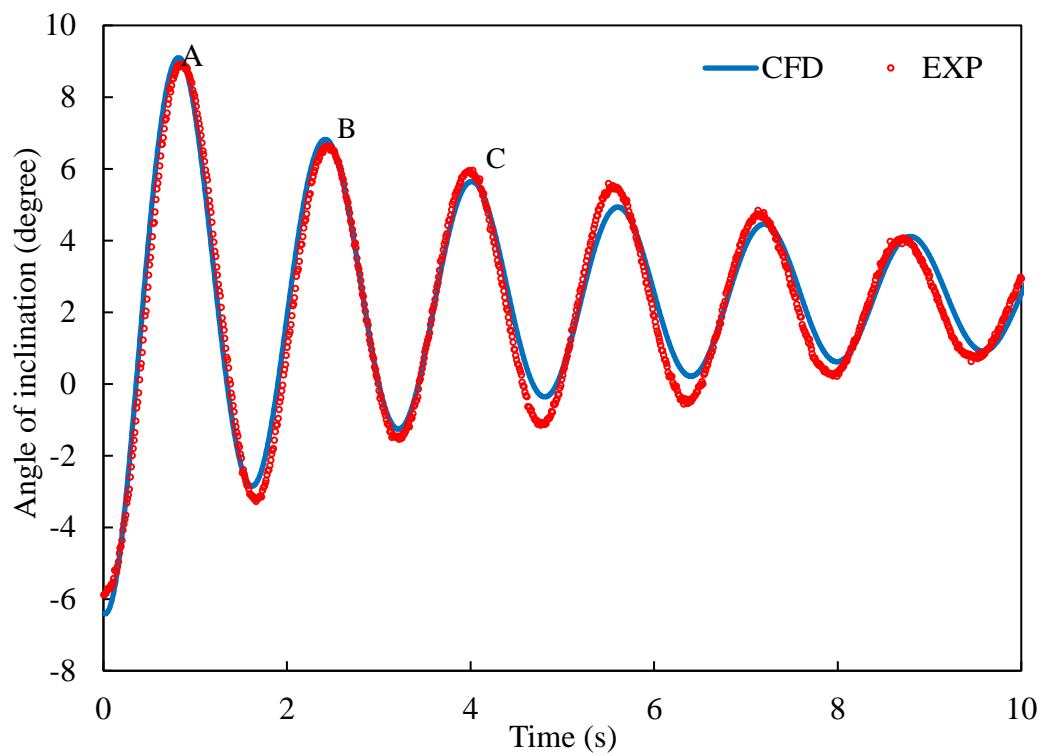


Figure 5.10. Damaged free decay curve comparison between CFD and physical tests

## 5.3 Wave induced loads acting on ship hull in beam seas

### 5.3.1 Coordinate systems

Inertial coordinate system is attached at the centre of gravity of the ship, and a non-inertial coordinate system is established at the centre of gravity of the aft portion so that acceleration conducted according to Appendix A3.1.1 can be applied based on the Newton's Second Law to calculate shear forces due to wave excitation acting on the cross section that separates ship into two portions. Coordinate systems can be demonstrated in Figure 5.11. To simplify the calculation, each axis in the non-inertial coordinate system is respectively parallel to the corresponding axis in the inertial coordinate system.

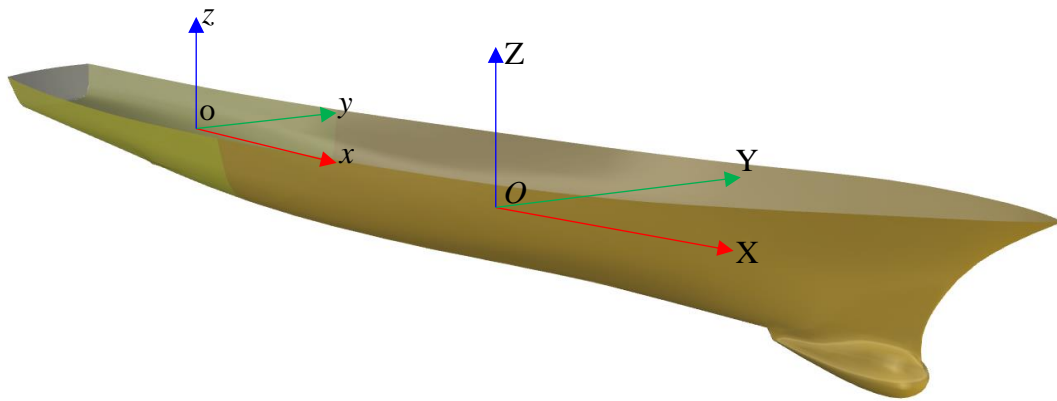


Figure 5.11. Inertial ( $O-XYZ$ ) and non-inertial ( $o-xyz$ ) coordinate systems established

### 5.3.2 Shear forces

Vertical and horizontal shear forces are measured at the cross section where the load cell is installed. As shear force appears in pairs, and magnitudes are equal, but directions are opposite, one portion of two sections can be analysed. For example, forces acting on the aft portion of ship hull can be shown in Figure 5.12.

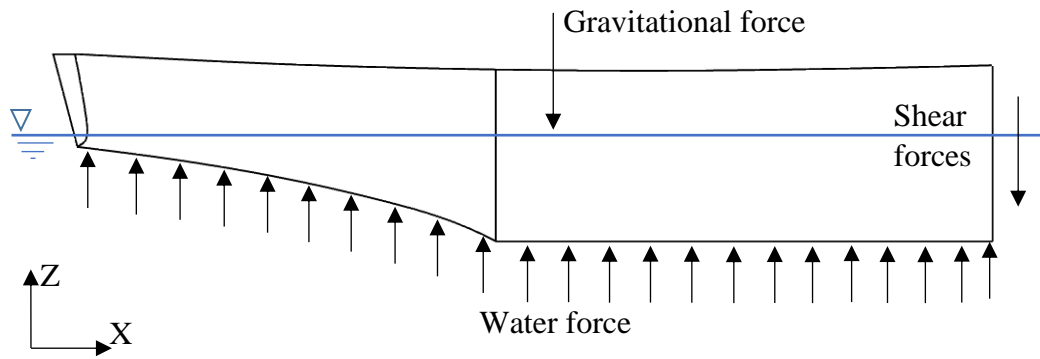


Figure 5.12. Total force components acting on one part of the ship

Equilibrium equation of forces acting on the aft portion based on the Newton's Second Law can be expressed in three directions by vectors as

$$\mathbf{F}_W + \mathbf{G} + \mathbf{SF} = m\mathbf{a}_{load\ cell} \quad \text{Equ. 5.1}$$

Where

$\mathbf{F}_W$  is the force due to the water pressure, which is equal to the pressure integral along the hull surface, i.e.

$$\mathbf{F}_W = \int P\mathbf{n}dS \quad \text{Equ. 5.2}$$

$\mathbf{n}$  is the normal vector to the surface of ship hull

$\mathbf{G}$  is the gravitational force acting at the centre of gravity of aft portion

$\mathbf{SF}$  is the shear force acting at the cross section where the load cell is located.

$\mathbf{a}_{load\ cell}$  is the acceleration of the load cell

$m$  is the mass of the aft portion

As it is known that applying Newton's Second Law for forces must be under the inertial coordinate system and forces acting on the specific portion will be added with another three force components. Since we concentrate on the forces acting at the location of load cell, it means that there is no relative movement between the origin of the non-inertial coordinate system that is established at the centre of gravity of aft portion and the inertial coordinate system that is attached at the centre of gravity of the whole ship. The basic transformation of reference frames and application of Newton's

Second law are given in Appendix 3 . Thus, forces acting on the aft portion of ship hull can be expressed in equilibrium as

$$\mathbf{F}_W + \mathbf{G} + \mathbf{SF} = m\mathbf{a}_{ship} + 2m\boldsymbol{\omega} \times \mathbf{v} + m\boldsymbol{\alpha} \times \mathbf{r} + m\boldsymbol{\omega} \times (\boldsymbol{\omega} \times \mathbf{r}) \quad \text{Equ. 5.3}$$

In which,

$\mathbf{a}_{ship}$  is the acceleration of the ship

$\mathbf{r}$  is the relative vector of the position of load cell relative to the origin of non-inertial coordinate system

$\mathbf{v}$  is the velocity of the load cell relative to the origin of non-inertial coordinate system

$\boldsymbol{\omega}$  is the angular velocity of the ship

$\boldsymbol{\alpha}$  is the angular acceleration of the ship

Since the position of the load cell is fixed at the cross section and moving with the ship hull, the relative vector  $\mathbf{r}$  is immovable and known. Therefore, the relative velocity  $\mathbf{v}$  between load cell and origin of non-inertial coordinate system is zero. Besides, gravitational force  $\mathbf{G}$  is known invariable. The equation is therefore rewritten as,

$$\mathbf{SF} = m\mathbf{a}_{ship} + m\boldsymbol{\alpha} \times \mathbf{r} + m\boldsymbol{\omega} \times (\boldsymbol{\omega} \times \mathbf{r}) - \mathbf{F}_W - \mathbf{G} \quad \text{Equ. 5.4}$$

Now it becomes more easily manageable to calculate shear forces acting at the location of load cell during CFD simulation. Force due to water pressure integration, translational acceleration, angular velocity and angular acceleration of the ship are the components that needs to be concerned and monitored during CFD-based calculations.

### 5.3.3 Moments

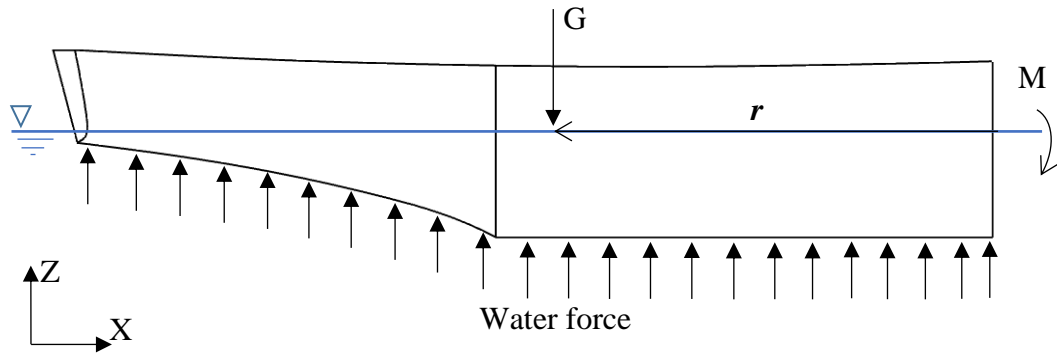


Figure 5.13. Moment components acting on the aft portion

Vertical and horizontal bending moment as well as torsional moment are calculated when the location of load cell is concerned. There are three moments that constitutes total moment acting on the aft portion of ship hull, namely moment due to the gravitational force acting at the centre of gravity of aft part, moment due to the water pressure along surface and bending moment acting at the cross section shown in Figure 5.13. Therefore, moments acting on the aft ship part can be equilibrated as

$$\int \mathbf{r}_i \times P \mathbf{n} dS + \mathbf{r} \times \mathbf{G} + \mathbf{M} = I \boldsymbol{\alpha} + \boldsymbol{\omega} \times (I \boldsymbol{\omega}) \quad \text{Equ. 5.5}$$

Where

$\mathbf{r}_i$  is the position vector of each cell attach along the ship hull to the load cell

$\mathbf{r}$  is the relative vector of the position of load cell relative to the origin of non-inertial coordinate system (as known as the location of centre of gravity of aft part)

$\mathbf{M}$  is the bending moment acting at the cross section

$\mathbf{G}$  is the gravitational force acting at the centre of gravity of aft part

$\boldsymbol{\alpha}$  is angular acceleration of ship

$\boldsymbol{\omega}$  is angular velocity of ship

$I$  is the mass moment of inertia tensor

$\mathbf{n}$  is the normal unit vector

With relative vector  $\mathbf{r}$ , gravitational force  $\mathbf{G}$  and tensor of mass moment of inertia  $I$  known, equation to calculate the moment  $\mathbf{M}$  can be reconstructed under the inertial coordinate system as

$$\mathbf{M} = I\boldsymbol{\alpha} + \boldsymbol{\omega} \times (I\boldsymbol{\omega}) - \int \mathbf{r}_i \times P\mathbf{n}dS - \mathbf{r} \times \mathbf{G} \quad \text{Equ. 5.6}$$

Thus, during the CFD calculation, angular velocity and angular acceleration of ship, sum of the moment acting at each cell surface along ship hull must be carefully monitored.

## 5.4 CFD simulations for intact and damaged ship in regular beam waves

### 5.4.1 Pre-declared specification

With a CFD-based RANS solver, the investigation on the wave-induced loads acting on intact and damaged ship needs to be carried out under a few assumptions in this work.

- Two DOF motions (CFD method) vs. six DOF motions (experiment)

With soft-elastic moorings tied on the ship model, six degree-of-freedom motions can be observed during a physical model test. Different degree-of-freedoms of motion in roll decay tests were investigated by Mancini et al. (2018) with CFD solver. One DOF, three DOF and six DOF motions were considered and it was found that more DOF motions concluded worse agreement would be obtained. When 3 DOF and 6 DOF motions were taken into account sway and yaw motions diverged and roll motion presented poor outcomes compared with one DOF, apart from the reason of incorrect mass moment of inertia about roll motion. It was concluded by authors that one-DOF model could present a better agreement for large amplitude of roll motion.

Besides, due to the unknown stiffness of the soft moorings, two DOF motions – heave and roll motions are the main focus of the present CFD studies.

- Same particulars between intact and damaged ship

The damaged opening is represented by a piece of cover on the hull shown in Figure 5.14. It should be noted that mass of the cover for damaged opening is equal to 0.318 kg (0.5% of the whole ship). As tested in damaged cases, the cover is no

longer attached with the ship hull so that floodwater can flow into and out of the flooded compartments through damaged opening. It means the actual mass of the damaged ship is not equal to the mass of intact ship, and consequently the mass moment of inertia and the centre of gravity of the damaged ship have a slight difference. However, in the present study the change in the solid mass moment of inertia of the damaged ship model is treated as small compared to the mass of the water already inside the compartment when testing the damaged ship in wave conditions. Therefore, the influence due to these differences is neglected during physical tests, and also not taken into account in CFD simulations; it could be taken into consideration in the further tests. In another word, mass, COG location and mass moment of inertia of the ship model are kept constant between intact and damaged cases in CFD studies.



Figure 5.14. Damaged opening in physical model (Cover is unattached)

- Rigid body simulation in CFD

The physical ship model can experience a slight deformation due to wave excited force in beam seas and it is believed that ship model is rigid enough that there is no obvious deformation can be observed during tests. Besides, the five infra-red marks are positioned close to each other so that it can be considered that little deformation has an influence on the movement of the ship. The ship model used in CFD method



is considered as a rigid body and wave-induced loads caused by deformation can be neglected.

#### 5.4.2 Calculation domain

To investigate ship performance in regular beam waves by RANS solver, the ship is placed in a location four wavelengths from the inlet of generated regular beam waves. To eliminate the difference of the size of domain in CFD simulations compared to physical tests, the breadth and water depth of calculation domain is brought into correspondence with those of physical towing tank applied in experiments (4.6-metre width). Two-times-wavelength damping zone is set at outlet boundary, and it can be noted that water depth in all simulations will be kept 2 metres constantly as in the experiments. The whole calculation domain with boundary conditions is present in Figure 5.15.

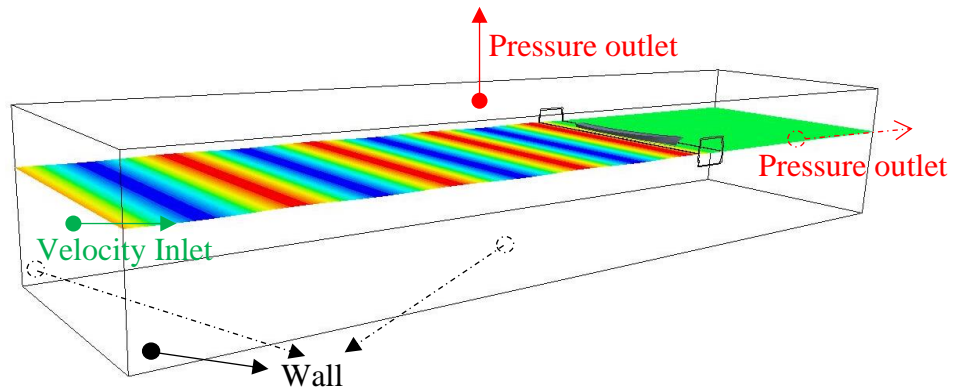


Figure 5.15. Calculation domain with boundaries for ship in beam waves

#### 5.4.3 Wave conditions

To investigate the methodology that is proposed to calculate wave-induced loads acting on intact and damaged ship by the CFD method, regular beam waves are generated respectively with two frequencies, which are the resonance frequencies under the intact and damaged conditions. Again, in order to validate the numerical solutions obtained by the CFD method compared to experimental measurements, properties of two wave conditions are chosen to be the same as those used in physical tests and listed in Table 5.2.

Table 5.2. Regular beam wave settings

Property	Intact	Damaged
Wave length (m)	2.911	3.806
Period (s)	1.365	1.565
Wave frequency (rad/s)	4.6143	4.012
Wave height (m)	0.02	0.02
Water depth(m)	2	2

#### 5.4.4 Mesh distribution

Figure 5.16 presents the overall mesh distribution in the whole calculation domain. Meshes to capture the water surface are specifically refined in the background region, which is partially shown in Figure 5.17(a). In order to capture the ship motions accurately, refined meshes are generated around the ship hull as presented in Figure 5.17(b). Taking shear force into account, boundary layers are generated along the ship hull and partially shown in Figure 5.17(c). Especially for the place where the structure is complicated, such as the sonar dome, refined meshes should be generated as shown in Figure 5.17(d).

For the damaged case, specific mesh refinement needs to be placed at damaged opening to capture floodwater ingress and egress accurately. In the meantime, to take floodwater sloshing/dynamic effect into consideration, a mesh to capture floodwater surface is also refined in flooded compartments as shown in Figure 5.18.

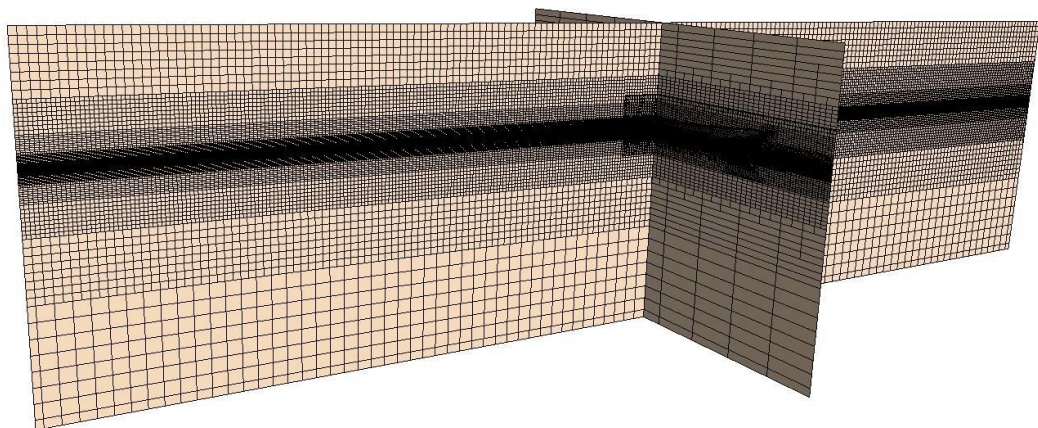


Figure 5.16. Overall mesh distribution

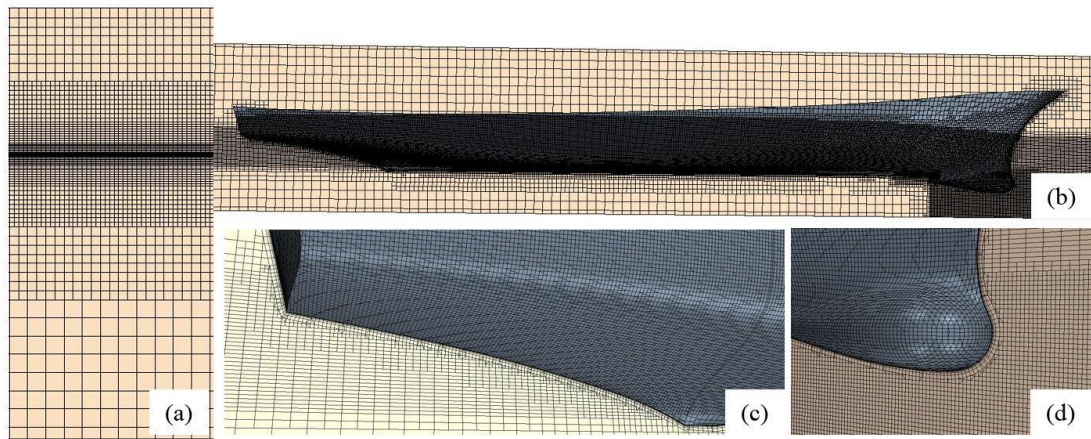


Figure 5.17. (a) Mesh layers to capture waves; (b) Refined mesh along ship hull; (c) Boundary layers partially distributed at stern; (d) Mesh refinement around sonar dome

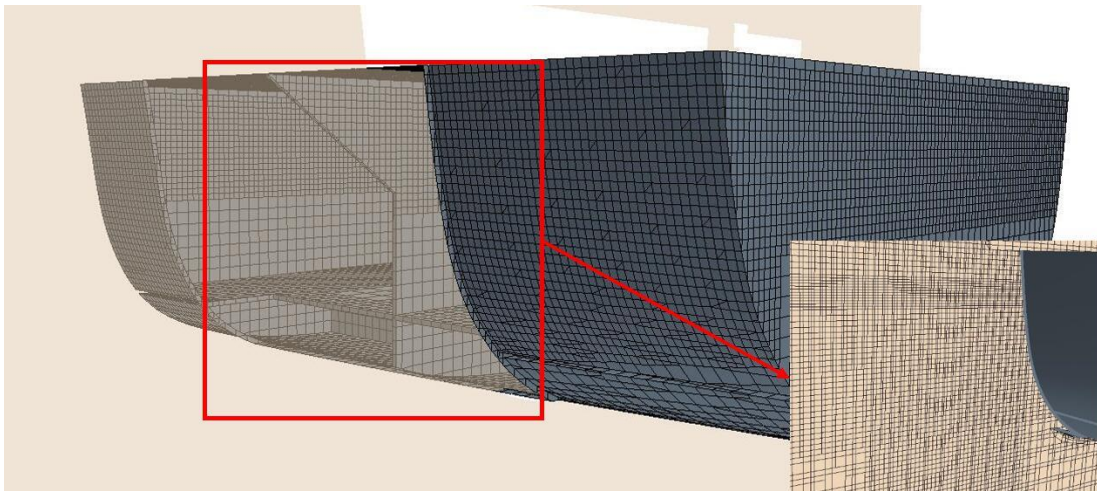


Figure 5.18. Mesh refinement for floodwater

## 5.5 Results

Results obtained by RANS solver, including roll motion, heave motion and wave-induced loads, namely horizontal and vertical shear forces, horizontal and vertical bending moment and torsional moment, will be presented and discussed in this section. Firstly, a grid dependence study is carried out to make sure that the uncertainty introduced by grids is acceptable, and then uncertainty is analysed according to the guided procedure. To end this section, comparison and discussion between results obtained by CFD method and experimental measurements are made to a qualitative validation for applying the present methodology.

### 5.5.1 Mesh sensitivity study

Before applying the CFD method to investigate on the wave-induced loads acting on intact and damaged ship in beam waves, a grid dependence study is performed and a refinement factor, 2, is used among generated fine, medium and coarse meshes. Table 5.3 gives information about meshes employed including size of element, total number of cells and total CPU hours.

Table 5.3. Meshes applied for grid dependency study

Grid	Dimensions $\Delta x \times \Delta y \times \Delta z$ (mm)		Total number	CPU hours
	Overset Region	Background Region		
Fine	4×4×2	4×4×2	10.07 Million	54132
Medium	8×8×4	4×4×2	7.64 Million	22117
Coarse	16×16×8	4×4×2	4.67 Million	8866

To investigate mesh sensitivity, time step and iteration number per time step are kept constant based on one-factor-at-a-time method. The aim of the grid dependency study is to investigate the influence of mesh applied for ship's roll and heave motions in beam waves. Figure 5.19 and Figure 5.20 present roll motion and heave motion calculated based on three sets of meshes, respectively. It can be obviously observed that the difference of roll motion between coarse and medium mesh is much bigger than that between medium and fine mesh. What the fine mesh is employed little improvement can be obtained, but total CPU time for fine meshes takes approximately 40% more than medium ones. However, the heave motion does not present a clear difference among three schemes of grids, so that it has to be stated that heave motion is not so sensitive to the mesh dependency.

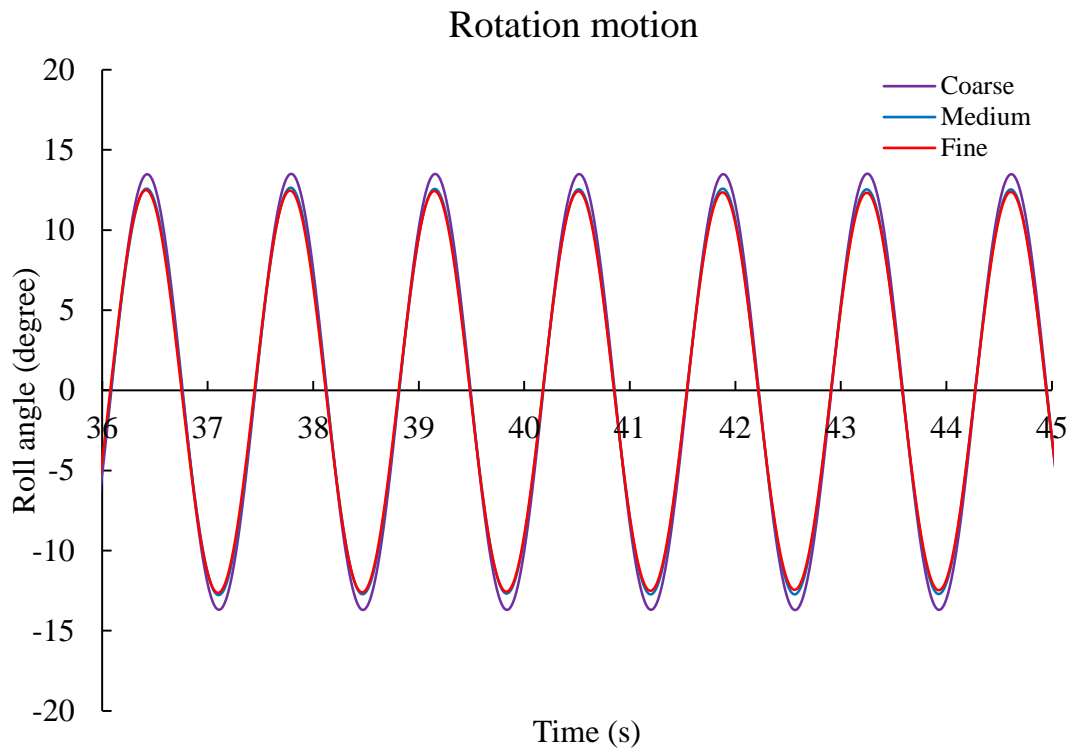


Figure 5.19. Grid dependency results for roll motion

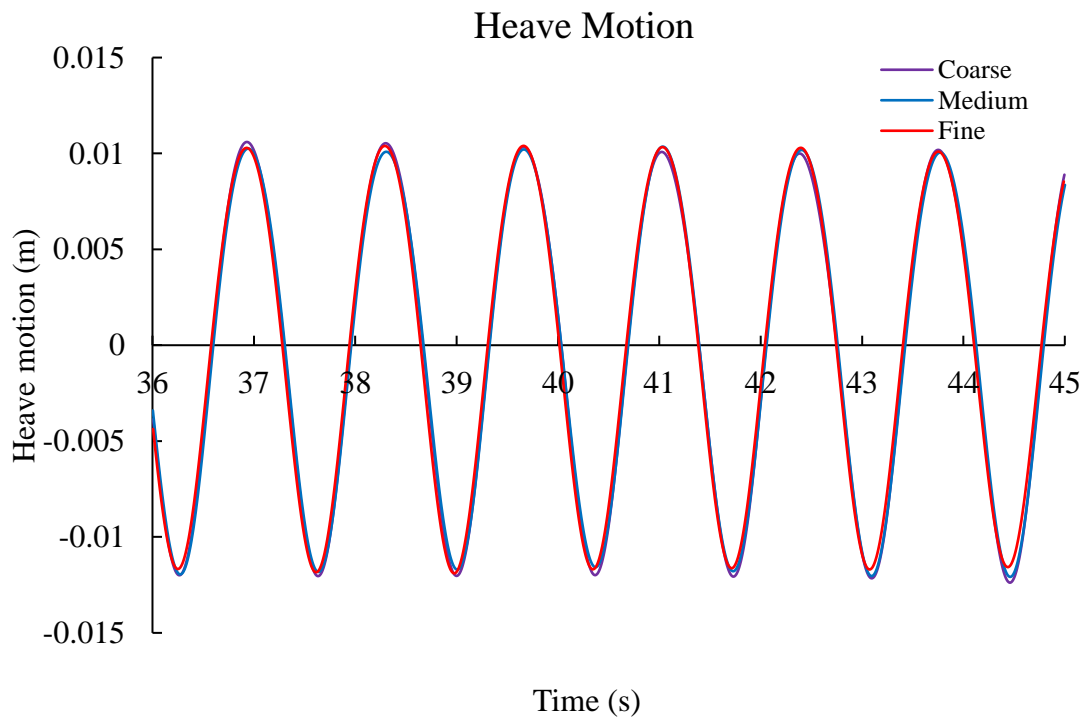


Figure 5.20. Grid dependency results for heave motion

### 5.5.2 Uncertainty

Solutions calculated by a RANS solver will involve uncertainties. Some of the uncertainties introduced by numerical modelling also can come from physical experiments. In this study, uncertainties can be categorized including aforementioned assumptions that applied in CFD study.

- Modelling:
  - Geometric difference between physical model and geometry used in RANS solver
  - Estimation of mass moment of inertia
  - Etc...
- Measurement:
  - Geometric dimensions of physical ship model
  - Round-off error
  - Etc...
- Numerical:
  - Discretization and solution errors
  - 2 Degree-of-Freedom motions vs. 6 Degree-of-Freedom motions
  - Etc...

Although such uncertainties that listed above can have a significant influence on solutions, to generally obtain uncertainties of the current results, the procedure provided by ITTC (2014) is employed. This is based on studying one case with different mesh densities. Assuming the uncertainty for other frequency and other situation can be comparable, results are listed in Table 5.4.

Table 5.4. Summary of uncertainties for grid dependency study

Parameter	$R_G$	$P_G$	$C_G$	$U_G$	
Roll motion	0.56	0.83	0.15	0.67	5.51%
Heave motion	5.68	2.51	1.56	0.41	4.18%

Where,

$R_G$  is parameter refinement ratio

$P_G$  is order of accuracy

$C_G$  is correction factor

$U_G$  is uncertainty

### 5.5.3 Result comparison and discussion

#### 5.5.3.1 Intact ship in regular beam waves

Roll and heave motions are presented in Figure 5.21 and Figure 5.23, respectively, compared with experimental measurement in time history. To give a better comparison between numerical results and experimental data, the FFT (Fast Fourier Transform) algorithm is applied to analyse frequency and amplitude of the result while it reaches steady oscillation after several periods, shown in Figure 5.22 and Figure 5.24. It can be obviously seen that calculated motions have a generally good agreement with experimental measurement. What can be highlighted is the characteristics of motions are captured well. Especially for heave motion, first-order and second-order motions can be captured accurately. However, the amplitude of calculated motions by CFD method is slightly larger than ship motions measured in physical tests. The reason is that, apart from the numerical calculation errors, the wave elevations that generated by RANS solver and generated by wave maker in physical tests are not constantly equally at 10mm. Figure 5.25 illustrates roll and heave motions that ship experienced due to excitation by generated regular beam sea. Detailed vortex behaviour around the sonar dome is demonstrated via velocity vectors shown on a section plane, as presented in Figure 5.26. Due to the fact that vortex generated by ship motions can, in turn, have an influence on ship motions, a refined mesh needs to be placed at sonar dome and ship bow to accurately capture generated vortices, and consequently ship motions.

Wave-induced loads acting on intact ship model calculated by RANS solver include vertical and horizontal shear forces, vertical and horizontal bending moment and torsional moment. Calculated vertical and horizontal shear forces are shown in Figure 5.27 and Figure 5.29 compared with experimental results. And frequencies with amplitudes of steady oscillation for shear forces are analysed and plotted in Figure 5.28 and Figure 5.30. It is observed that the present method can overestimate the second-order part of vertical shear force but underestimate the first-order part. However, comparison of horizontal shear force between RANS solution and experimental data shows a generally good agreement, even though second-order and

third-order amplitudes of calculated horizontal shear force appear to be much too obvious, while they cannot be observed in experimental results.

Vertical and horizontal bending moments, as well as torsional moment obtained by CFD approach are shown in Figure 5.31 to Figure 5.36, compared with moments that measured by load cell. It can be generally concluded that a good qualitative agreement can be reached between CFD solutions and experimental measurements, while magnitude of three moments that calculated by RANS solver are somewhat larger than experimental data. Specifically, the distinct feature for vertical bending moment can be well captured by current method. But as mentioned before, due to generated waves between calculated and measured vertical shear force, magnitude comparison of vertical bending moment shows a reasonable disparity between CFD method and experiment.

Although the time histories of the horizontal wave-induced loads (horizontal shear force and horizontal bending moment) appear to be generally linear, with sinusoidal response resulting from the sinusoidal excitation, an apparent asymmetry can be observed in the vertical loads acting on the ship as shown in Figure 5.27 and Figure 5.31. In particular, it can be seen that the amplitude of sagging and hogging moment is clearly asymmetric. In order to investigate the higher order effects, a Fast Fourier Transform is applied to the vertical loads as demonstrated in Figure 5.28 and Figure 5.32. Results show that there is a clear nonlinear effect. While by comparison between numerical results and experimental measurement, horizontal loads can be predicted by numerical method with a general good agreement.

Several factors are believed to result in the nonlinear vertical loads.

Nonlinear ship hull geometry is one of the main causes of nonlinearity of vertical wave loads. Considerable flare, especially near the bow with a large flare angle at ship sides due to the nature of a destroyer as a combatant naval vessel is associated with nonlinearity of vertical wave loads (Fonseca and Soares, 2004). Kim et al. (2017) stated ships with large flare on the bow and stern experience large wave loads, particularly for the second order vertical bending moment. The vertical bending moment is also sensitive to the ship sides when the ship is moving with forward speed. Furthermore, Fonseca and Guedes Soares, 2004 and Zhu and Moan, 2013 comment



that nonlinear vertical bending moment is significant for ships with small block coefficient such as the DTMB-5415 modelled in this study.

Nonlinear hydrodynamic forces also contribute to the asymmetry of wave induced vertical loads acting on the ship. Nonlinear Froude-Krylov force was taken into account to indicate the strong nonlinearity of vertical loads by Juncher and Terndrup (1979) and Fonseca and Soares (2005). Besides, due to the nonlinearity of the incident waves discussed in wave making (Section 4.2.4), vertical wave loads may present an asymmetric behaviour, even though vertical ship motions behaves with a linear response.

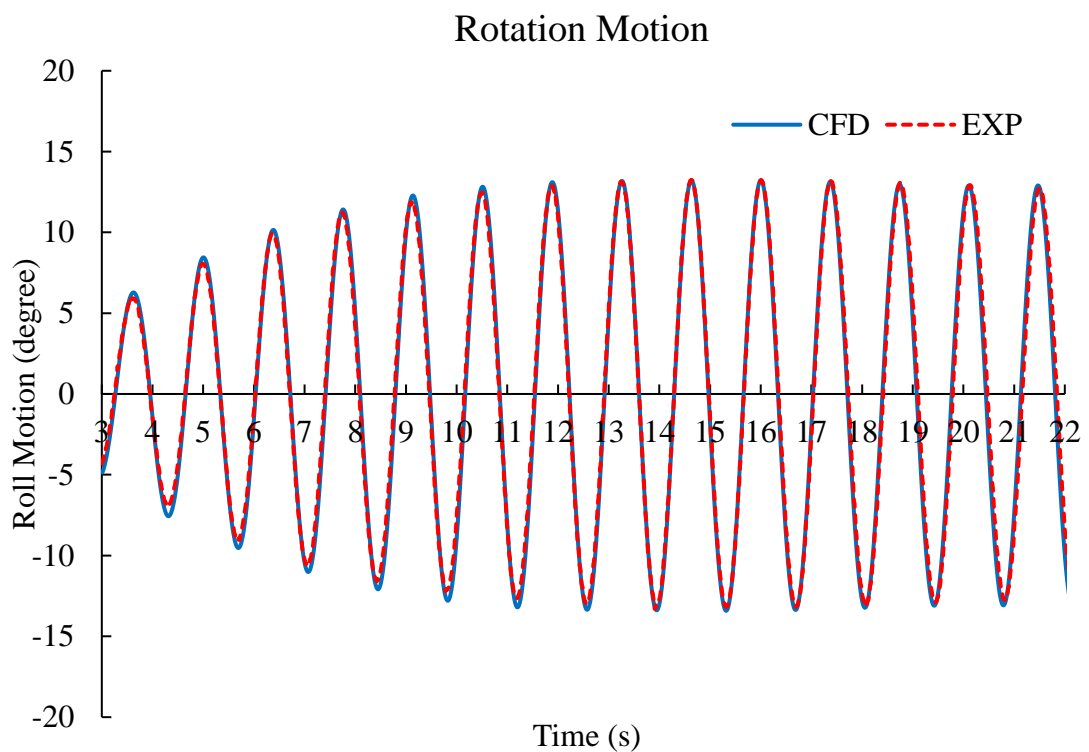


Figure 5.21. Comparison of roll motion in time between CFD method and physical test for intact ship

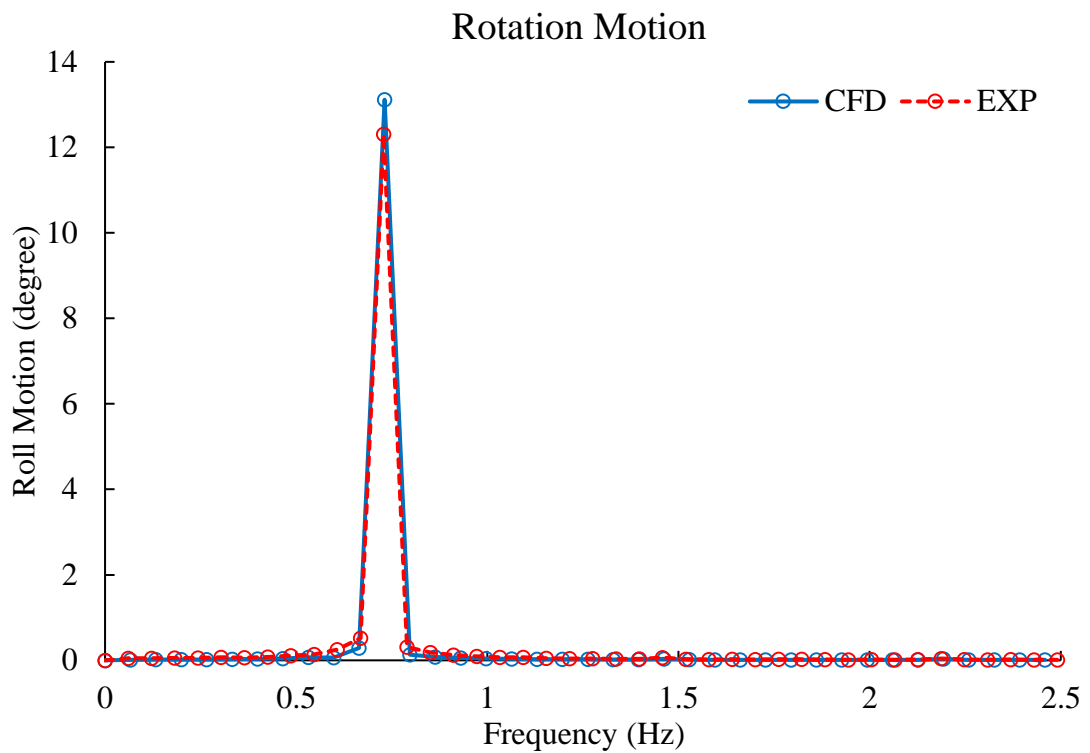


Figure 5.22. Comparison of roll motion by FFT

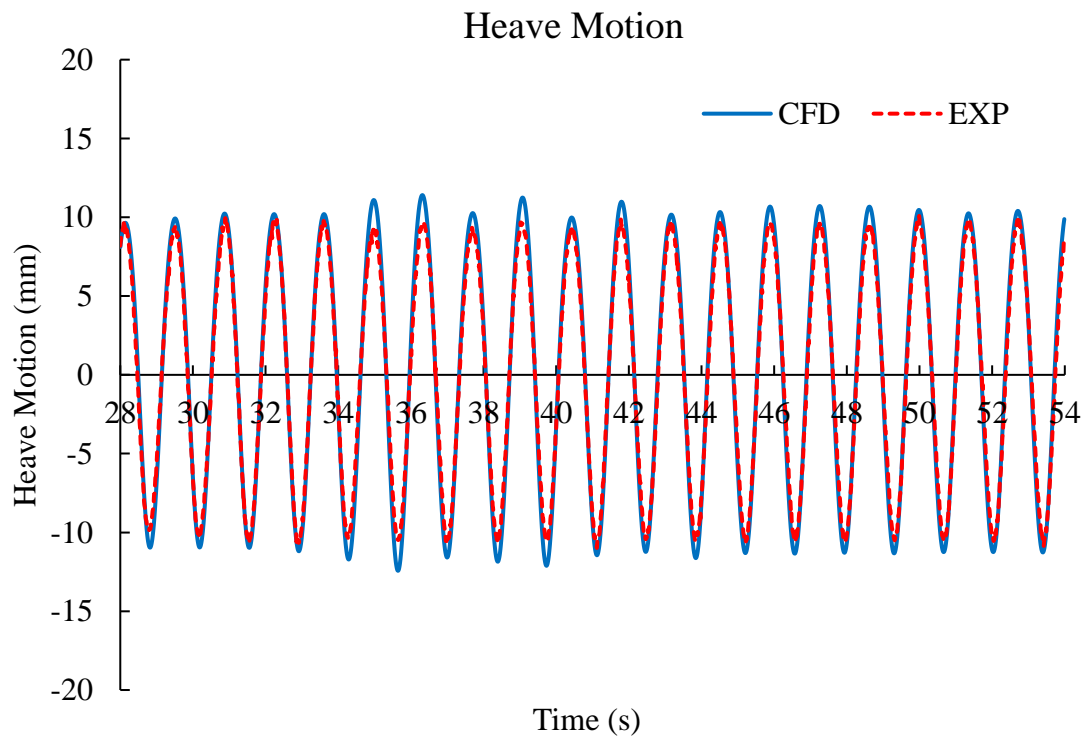


Figure 5.23. Comparison of heave motion in time between CFD method and physical test for intact ship

## Heave Motion

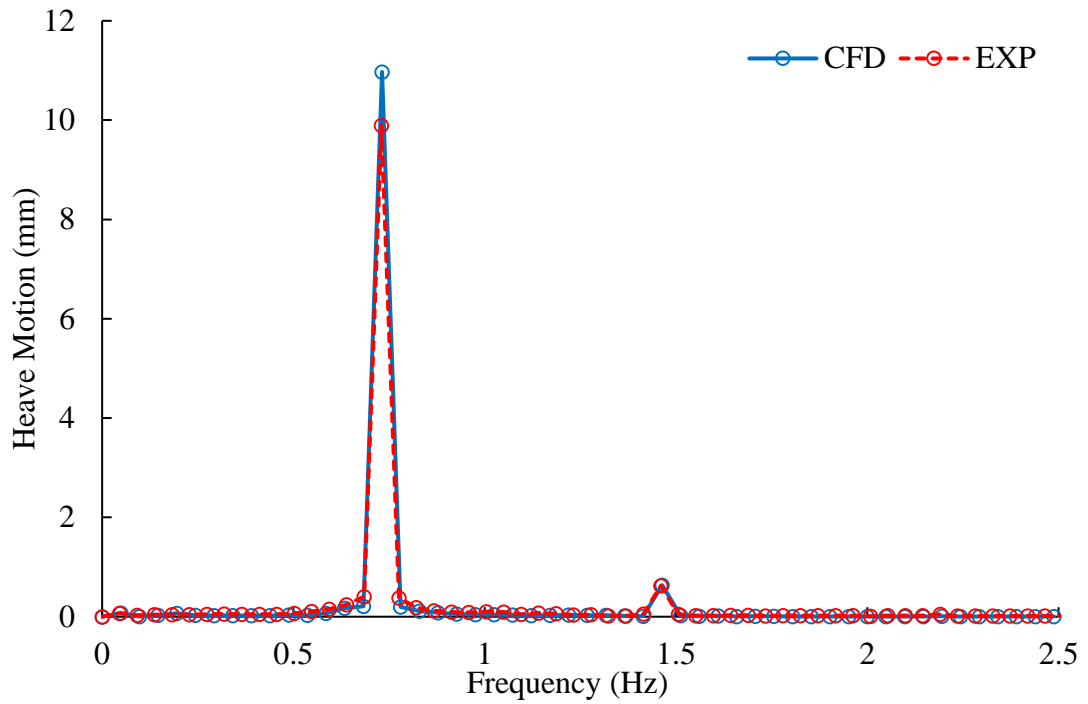
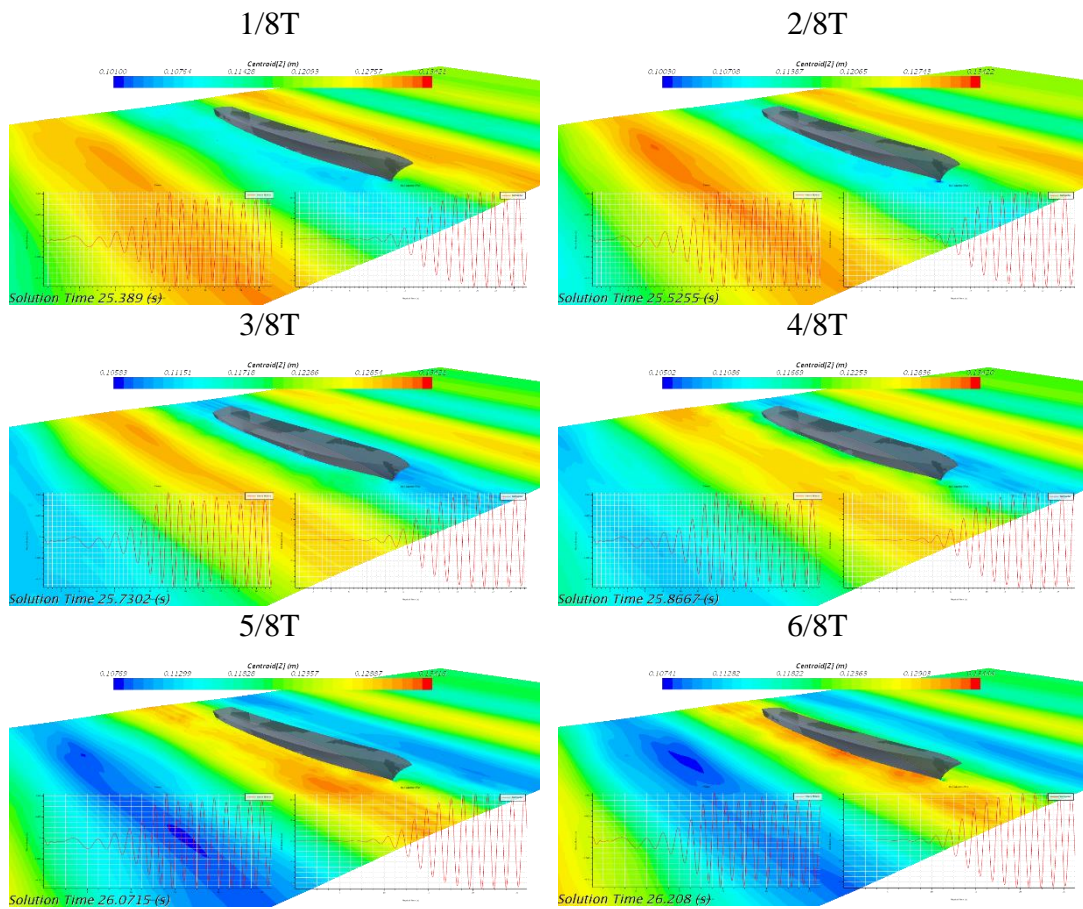


Figure 5.24. Comparison of heave motion by FFT



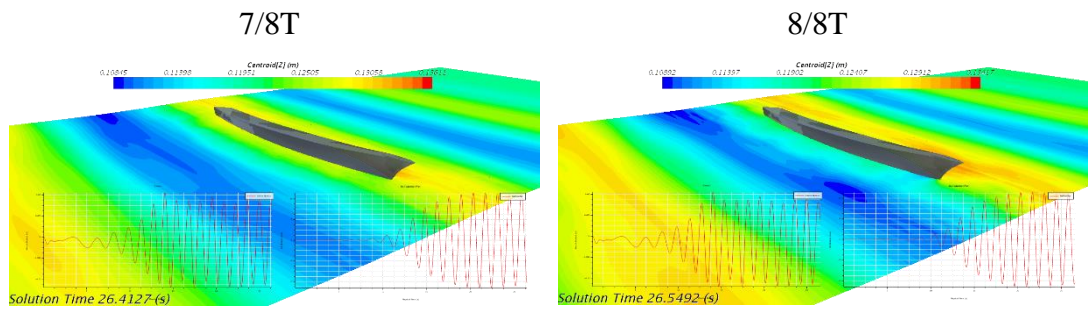


Figure 5.25. Ship motions in one period

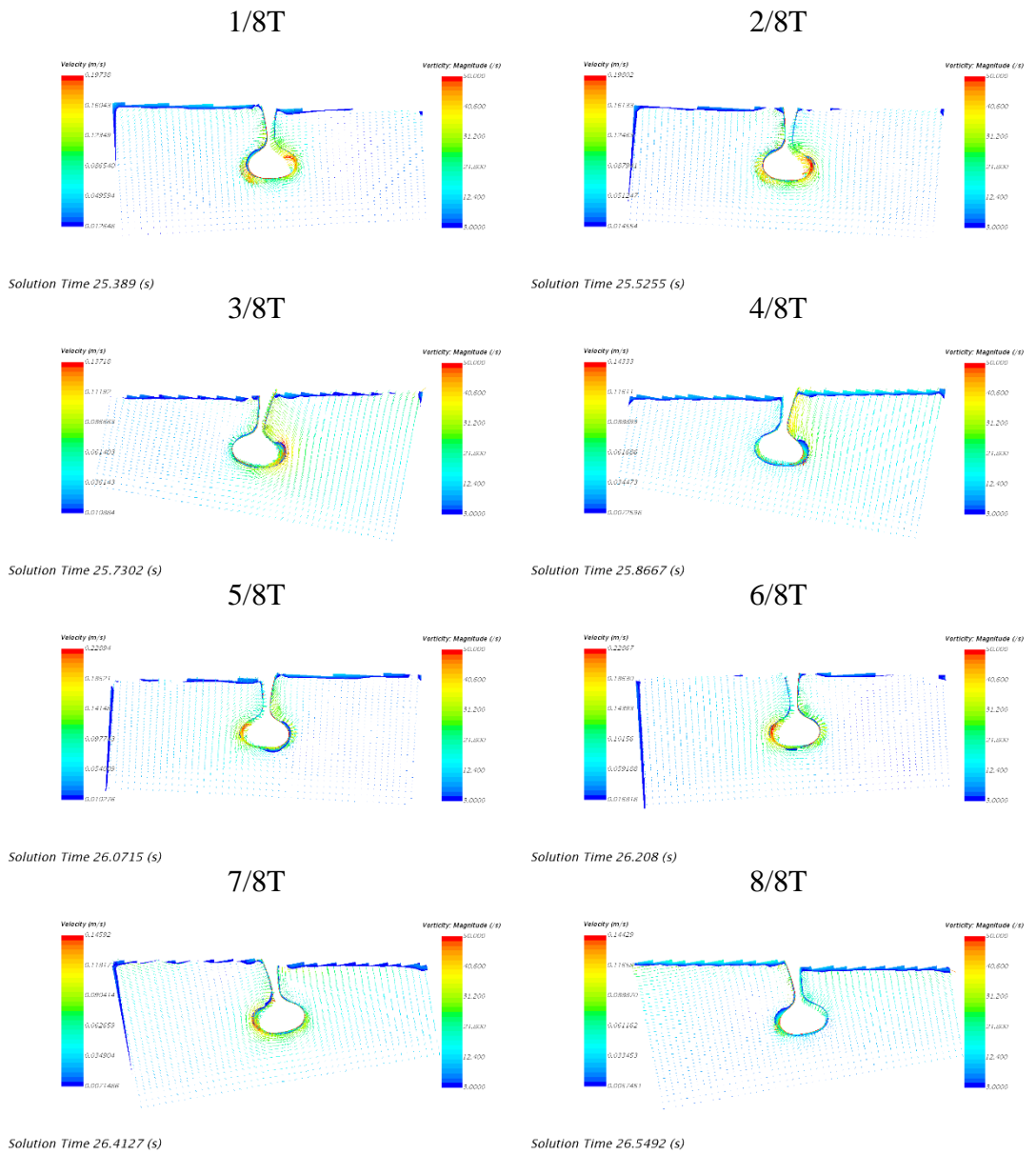


Figure 5.26. Snapshots for vortex at sonar dome

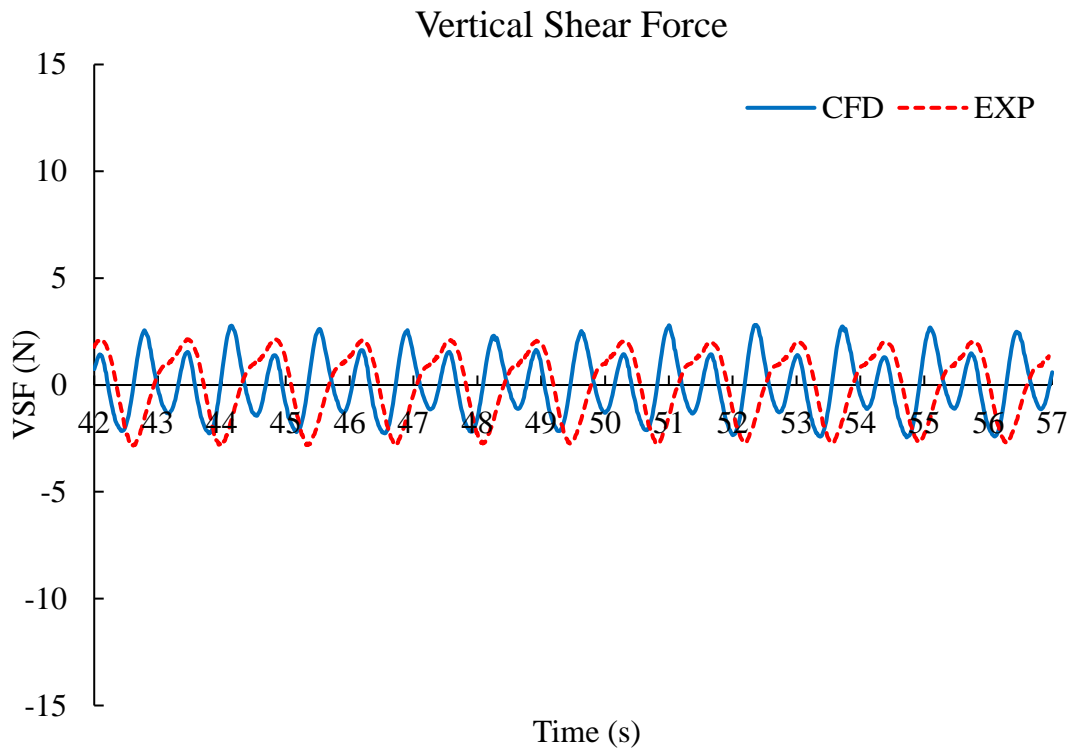


Figure 5.27. Vertical shear force comparison in time history for intact ship

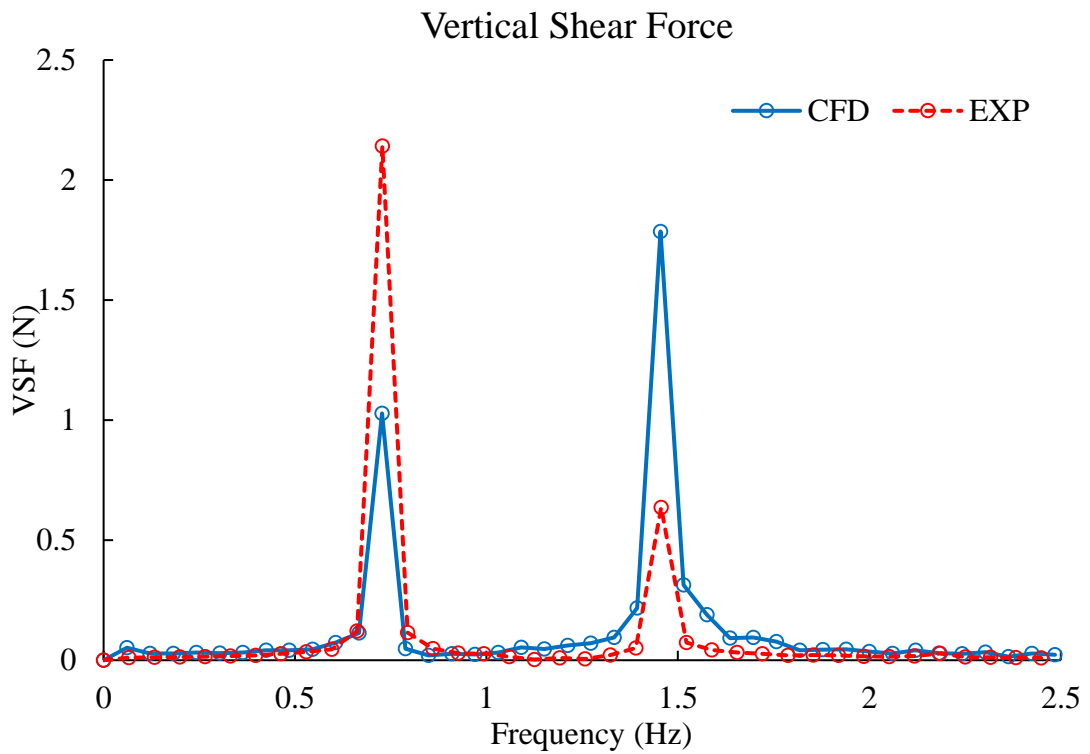


Figure 5.28. Vertical shear force comparison in frequency by FFT

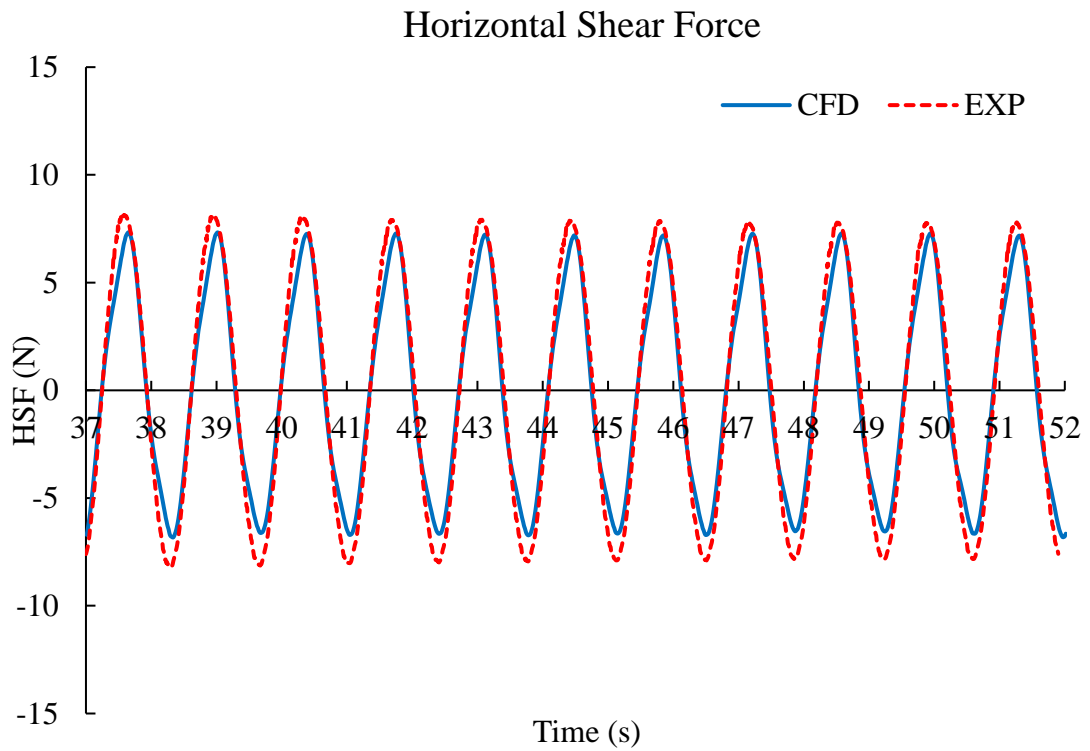


Figure 5.29. Horizontal shear force comparison in time history for intact ship

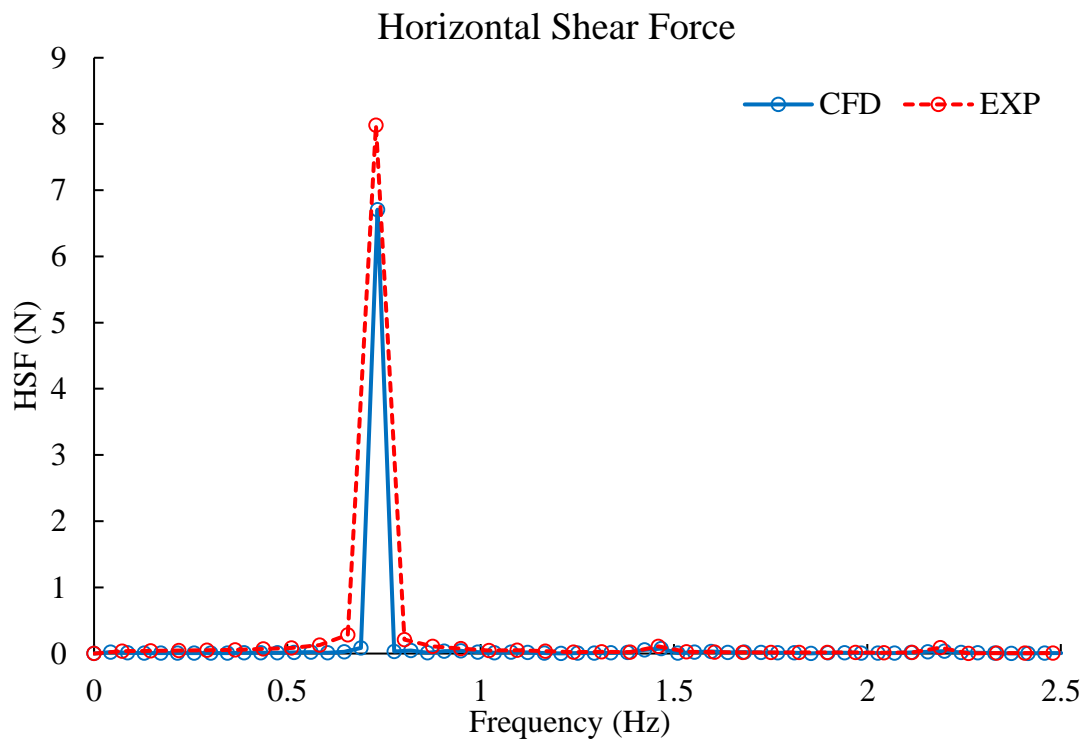


Figure 5.30. Horizontal shear force comparison in frequency by FFT

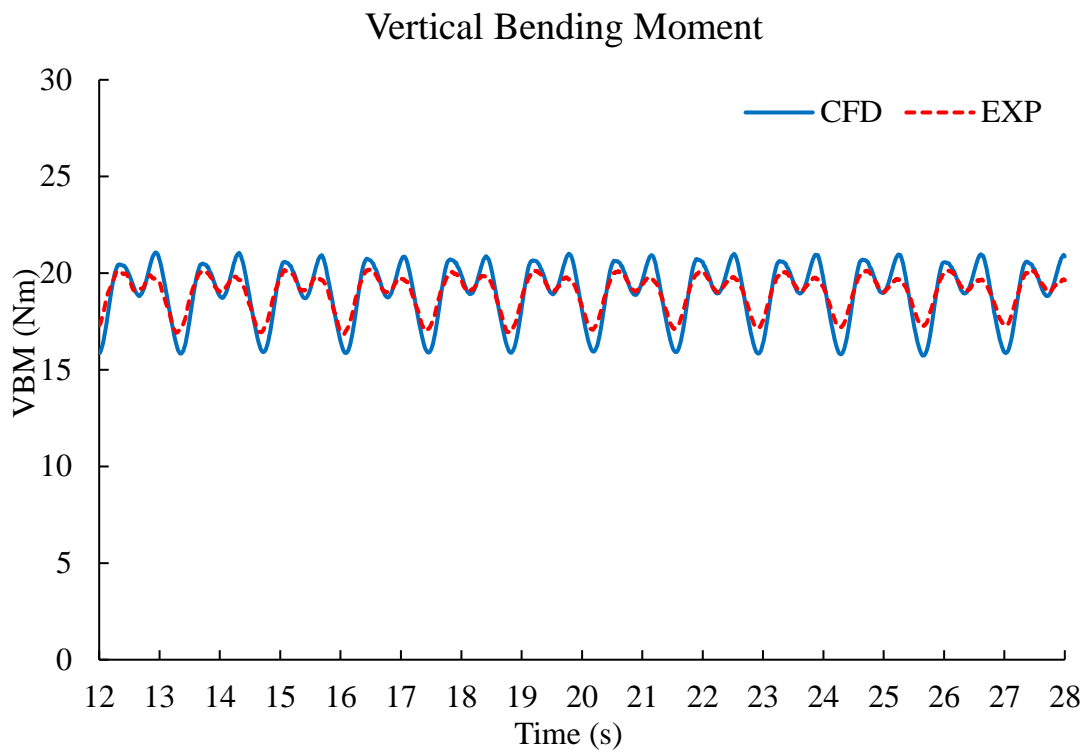


Figure 5.31. Vertical bending moment comparison in time for intact ship

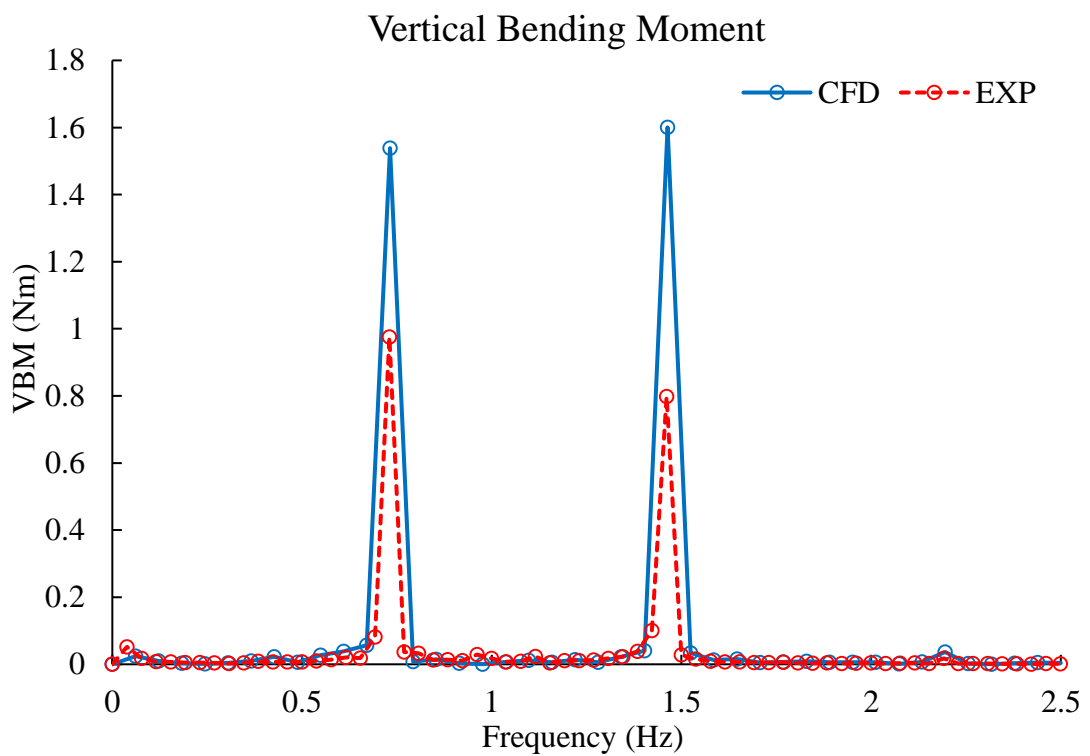


Figure 5.32. Vertical bending moment comparison by FFT

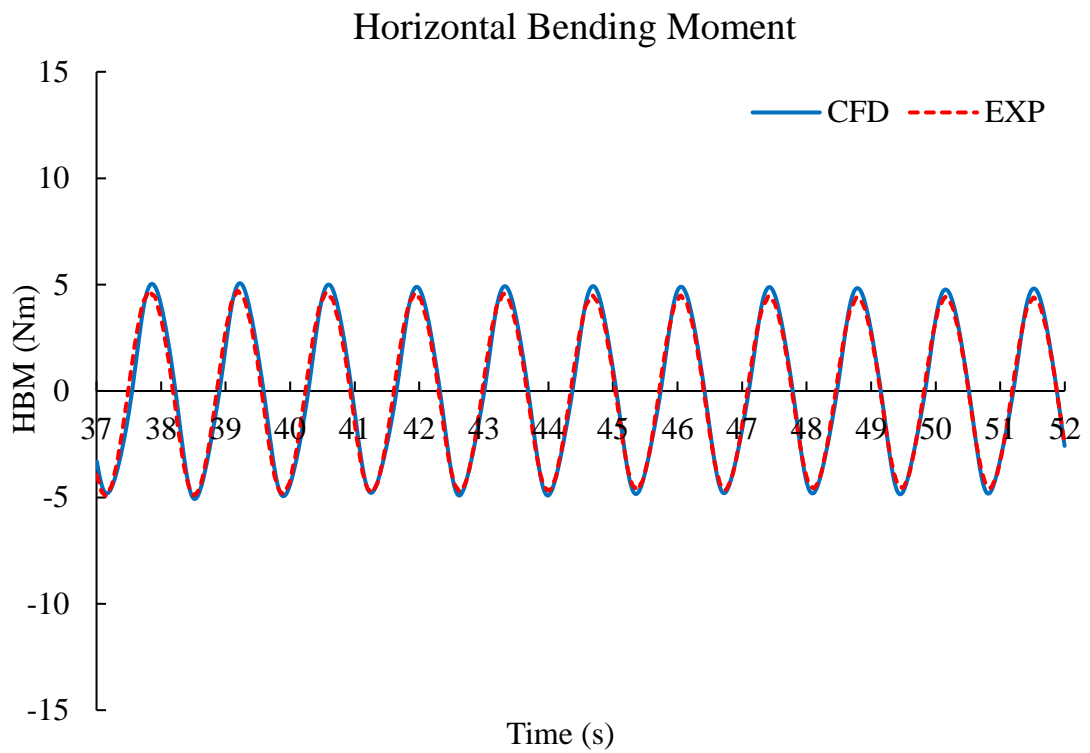


Figure 5.33. Horizontal bending moment comparison in time for intact ship

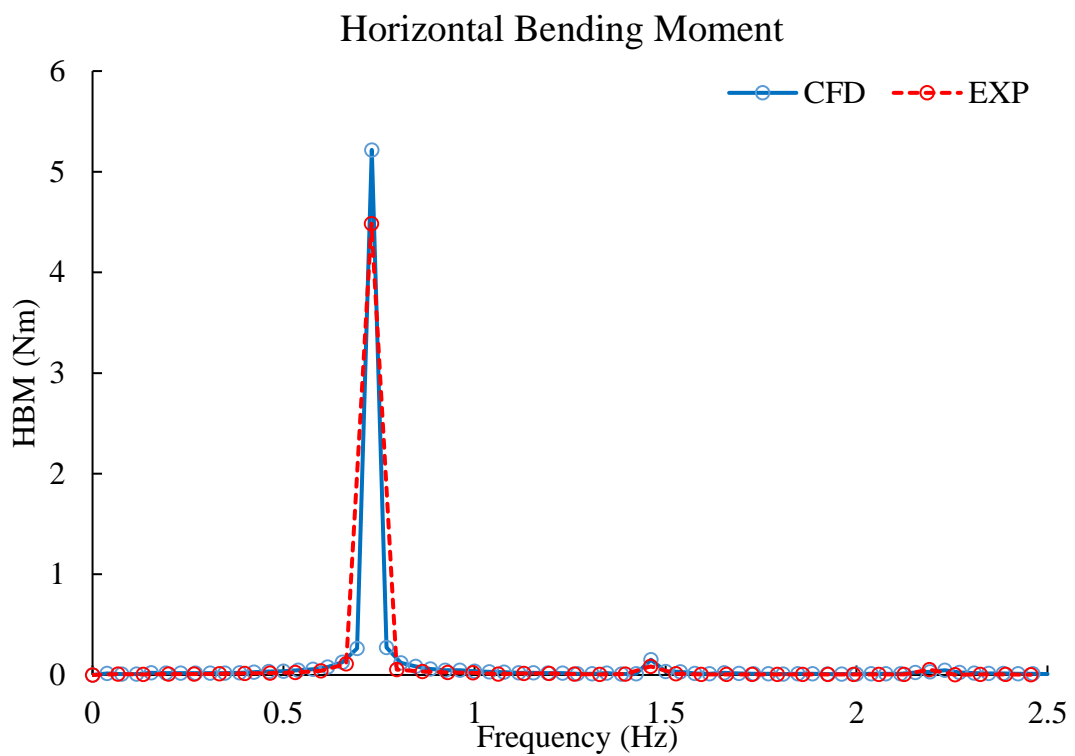


Figure 5.34. Horizontal bending moment comparison by FFT



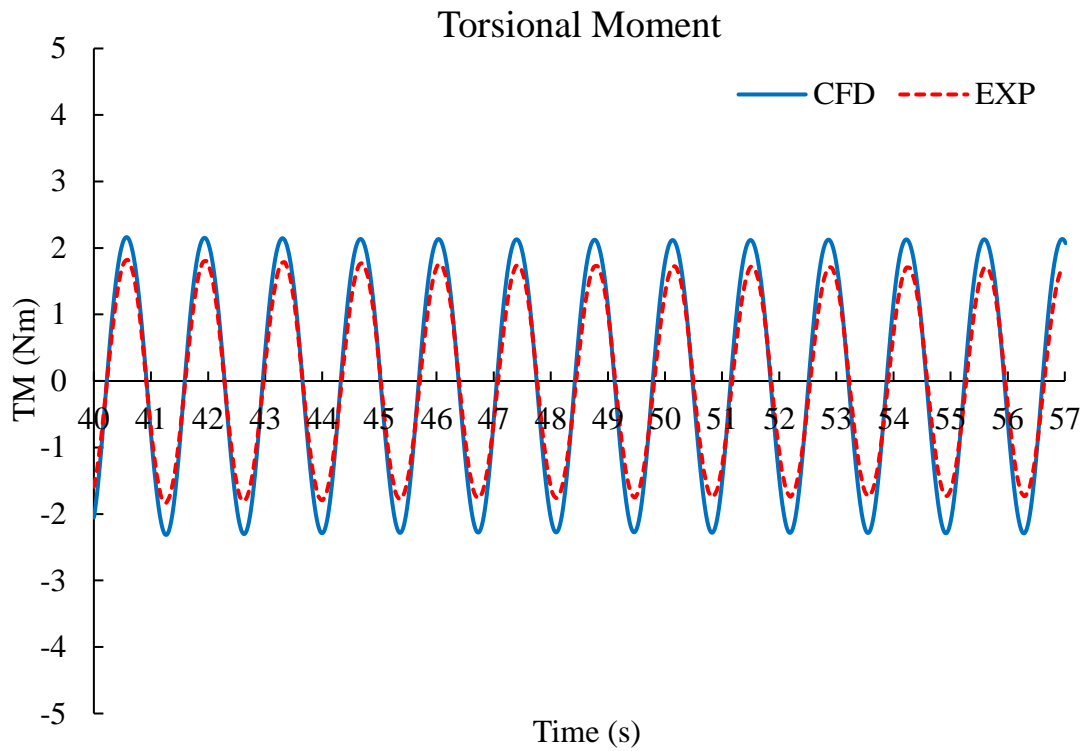


Figure 5.35. Torsional moment comparison in time for intact ship

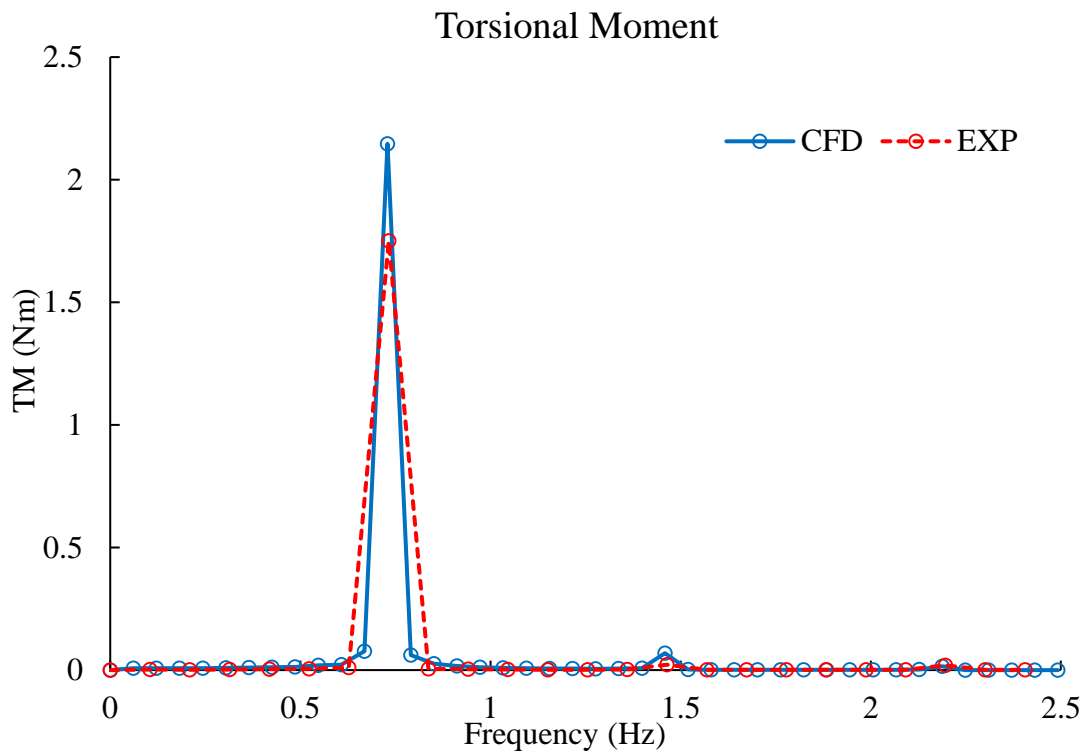


Figure 5.36. Torsional moment comparison by FFT

### 5.5.3.2 Damaged ship in regular beam waves

To scientifically demonstrate the validity, the present methodology is employed also for the damaged situation, which is going to be stated in this section. As elaborated in the last section, two-DOF motions and wave-induced loads that damaged ship suffered are to be shown in the same way and procedure.

Figure 5.37 to Figure 5.40 illustrate roll and heave motions that the damaged ship experienced in time and frequency. It can be seen that ship motions that calculated based by RANS solver have a good agreement with measured ship motions experimentally, even though calculated heave motion is slightly smaller than measurement. The same reason, previously stated in intact case, can be used to explain this, which is related to the difference between calculated and measured wave heights. Figure 5.41 presents ship motions that the damaged ship suffered during a period of waves, and snapshots to emphasize the inflow and outflow from damaged opening shown in Figure 5.42 reveal the phenomenon that captured about ingress and egress of floodwater through damaged opening (to give a better insight at floodwater behaviour in damaged compartments, ship hull, except flooded compartments, is left out).

Wave-induced loads acting on the damaged ship are shown in Figure 5.43 to Figure 5.52 with analysed frequencies by FFT algorithm. It can be observed from presented results that generally calculated wave-induced loads acting on damaged ship hull shows a qualitative agreement with measured loads by physical tests. Elaborately, horizontal shear force and torsional moment achieve a good agreement, but horizontal bending moment is overestimated compared to measured horizontal components. While vertical shear force that calculated is smaller than measured but vertical bending moment comparison shows opposite. The reason for this may originate from the DOF-motion difference between CFD method and physical experiment. In CFD simulations, only two-DOF motions, namely roll and heave motions, are taken into account and the rest four motions are constrained. However, actually in physical tests the ship model can have movement along all six degrees of freedom, even though the physical ship model is moored. So that wave-induced loads introduced by the other four motions are unknown. Besides, the influence of elastic moorings to the wave-induced loads is not clear. This can be described in another manner. In present study, the mass moment of inertia of ship ( $I$ ) is regarded as a scalar (due to the only roll motion), which  $I_{xx}=0.897$

kgm<sup>2</sup>. Then in that case, angular velocity vector,  $\boldsymbol{\omega}$ , is parallel to the product  $(I\boldsymbol{\omega})$ , and therefore, product  $\boldsymbol{\omega} \times (I\boldsymbol{\omega})$  is equal to zero. However, if all the six DOFs need to be taken into consideration, the mass moment of inertia,  $I$ , becomes a tensor rather than scalar, including the moment of inertia about each axis, and combination product of each two inertias (if the interaction between any two DOFs is considered), shown as

$$I_{ij} = \begin{bmatrix} I_{xx} & I_{xy} & I_{xz} \\ I_{yx} & I_{yy} & I_{yz} \\ I_{zx} & I_{zy} & I_{zz} \end{bmatrix}$$

which means, as matter of fact,  $\boldsymbol{\omega}$  is not parallel to  $(I\boldsymbol{\omega})$  in “ $\boldsymbol{\omega} \times (I\boldsymbol{\omega})$ ” component presented in Section 5.3.3.

Due to the presence of complicated internal structural layout of the damaged compartment, sonar dome and sharp bow, which are abrupt structures for the fluid flow, especially when ship is moving in the beam seas, fluid field can be caused to a drastic change when rolling. As shown in Figure 5.53, it can be clearly seen that the vorticity is undisguisably shown around entrance of the damaged compartment, rear of the sonar dome and front of the bow. It should be mentioned that the entrance of the compartment and the bow of the ship are not fully submerged under the water surface so that turbulence/wave generated with ship’s movement can be spread through water surface, while turbulence at the sonar dome is localized. This leads to variation in hydrodynamic pressure calculated around the ship hull, and therefore, causes an obvious change in the estimated loads acting on the ship.

On the other hand, internal free surface and sloshing of flooded water inside the compartment will bring non-linear effect on the hydrodynamics, and further can influence on the accuracy of estimated loads acting on the ship. So much complex flow in and out of the damaged opening and within the damaged compartment, which are all flows that expected to be governed by nonlinear and viscous effects, cannot be modelled by panel method or potential theory.

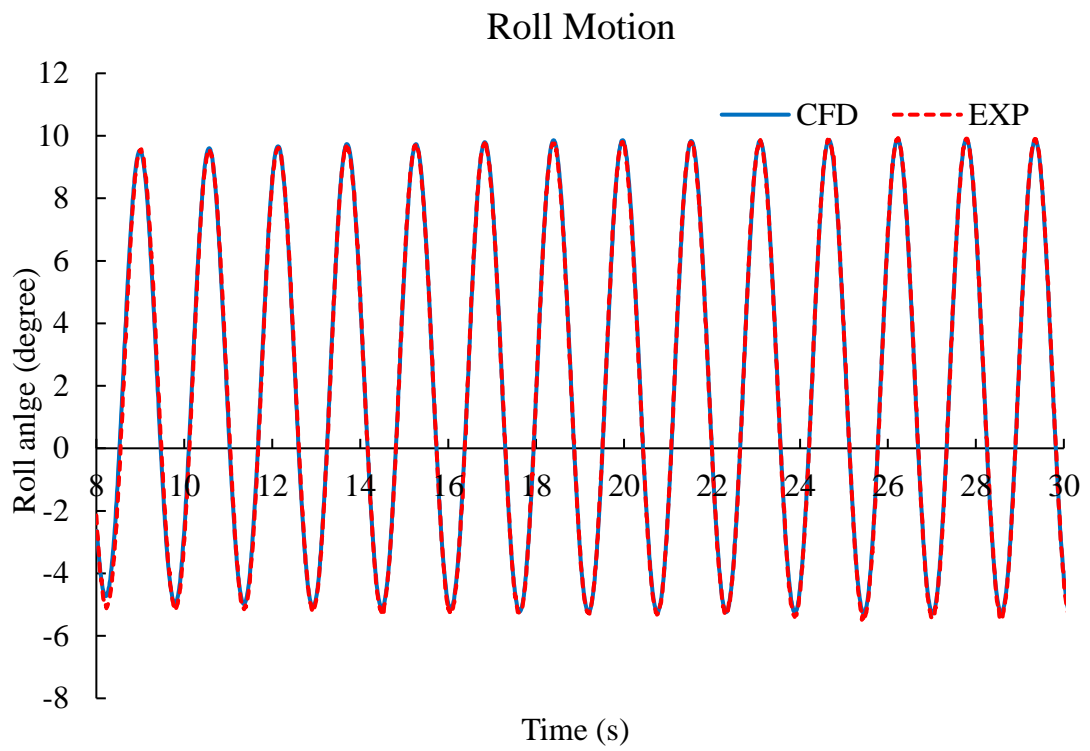


Figure 5.37. Roll motion comparison for damaged ship

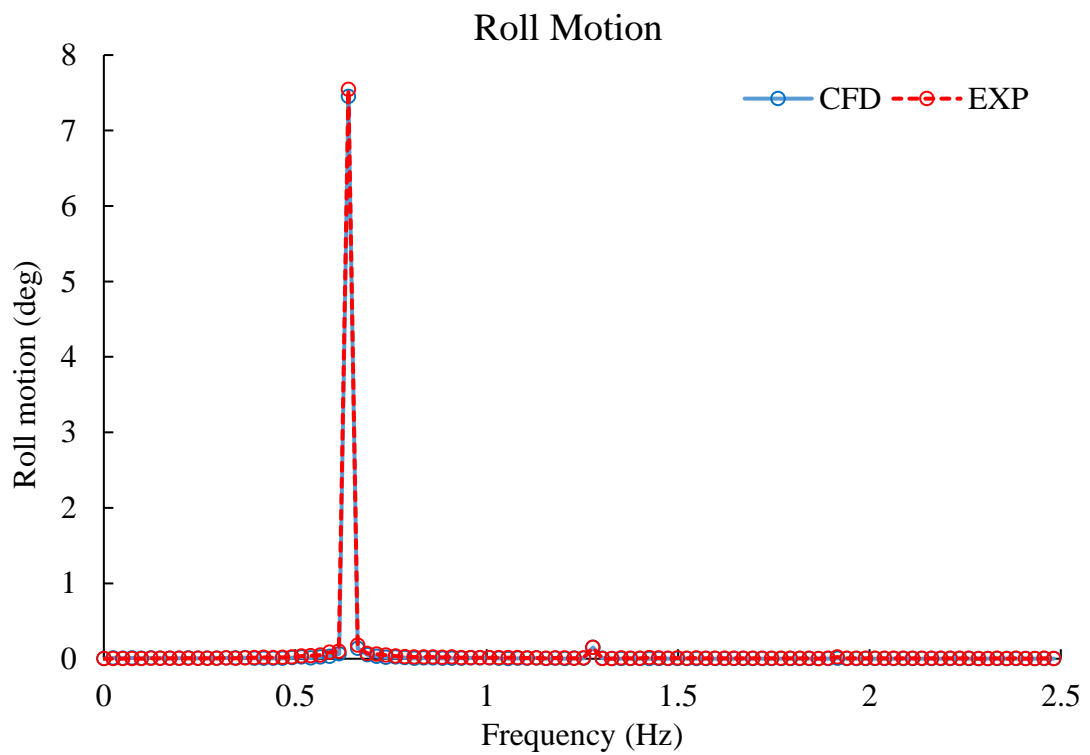


Figure 5.38. Roll motion frequency analysis by FFT

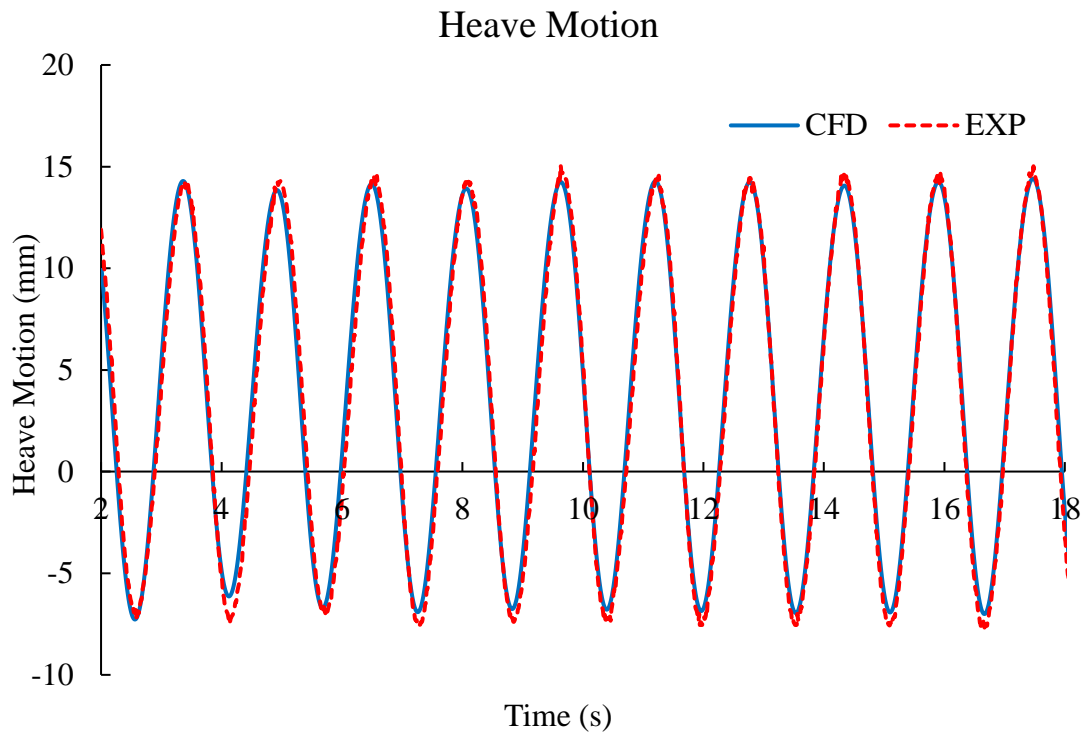


Figure 5.39. Heave motion comparison for damaged ship

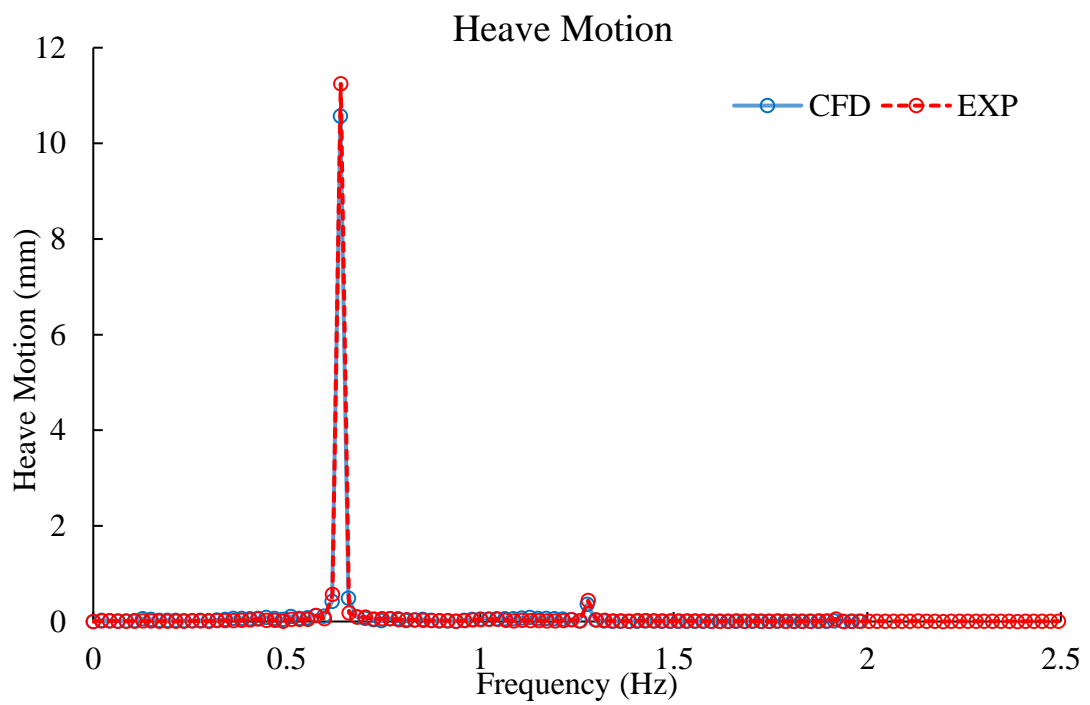


Figure 5.40. Heave motion frequency analysis by FFT

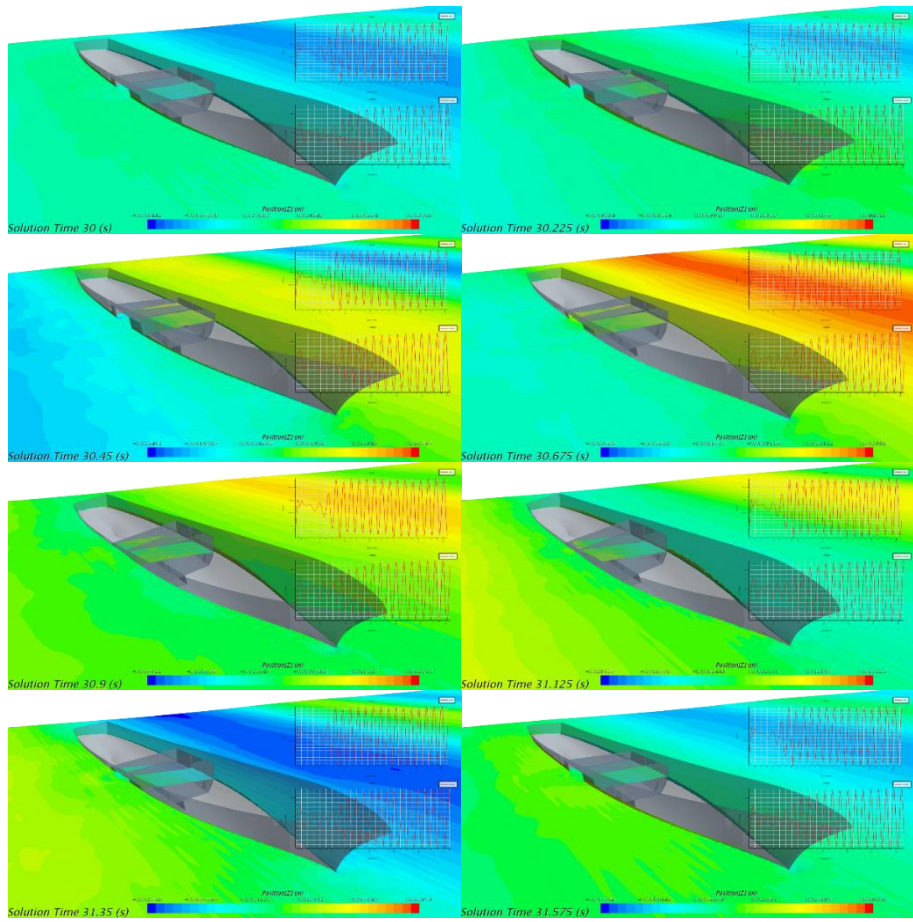
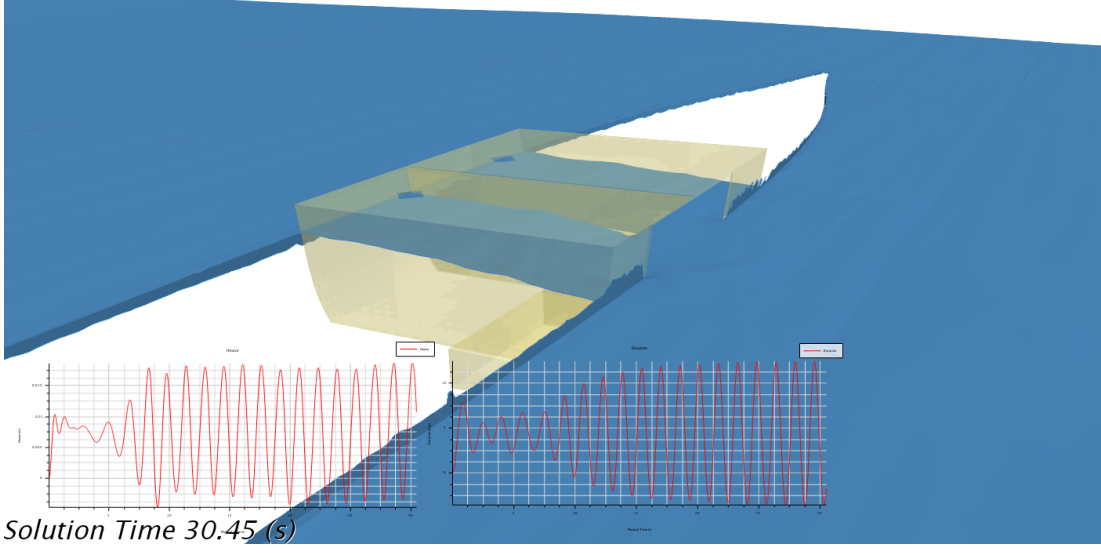
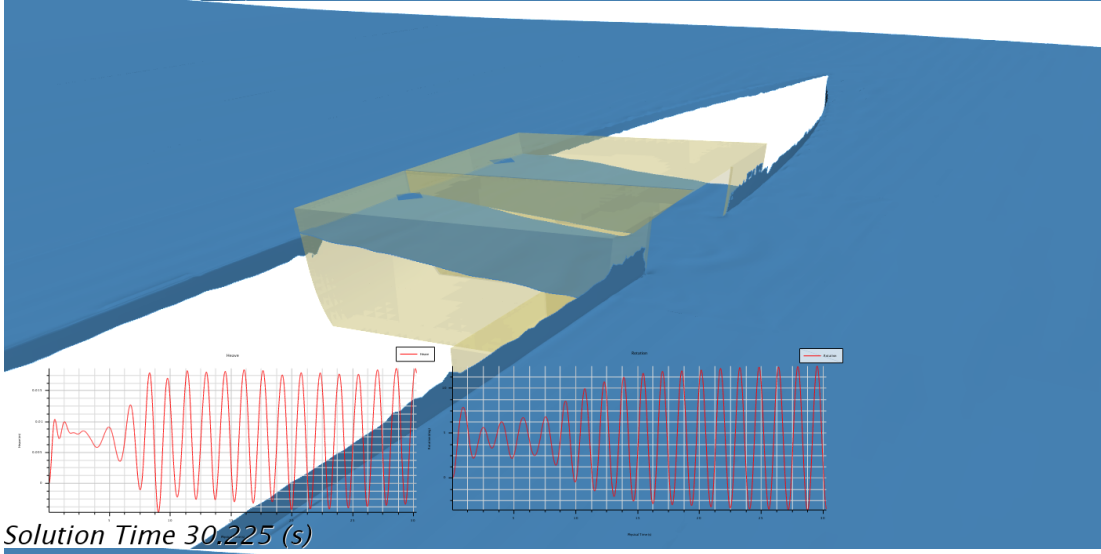
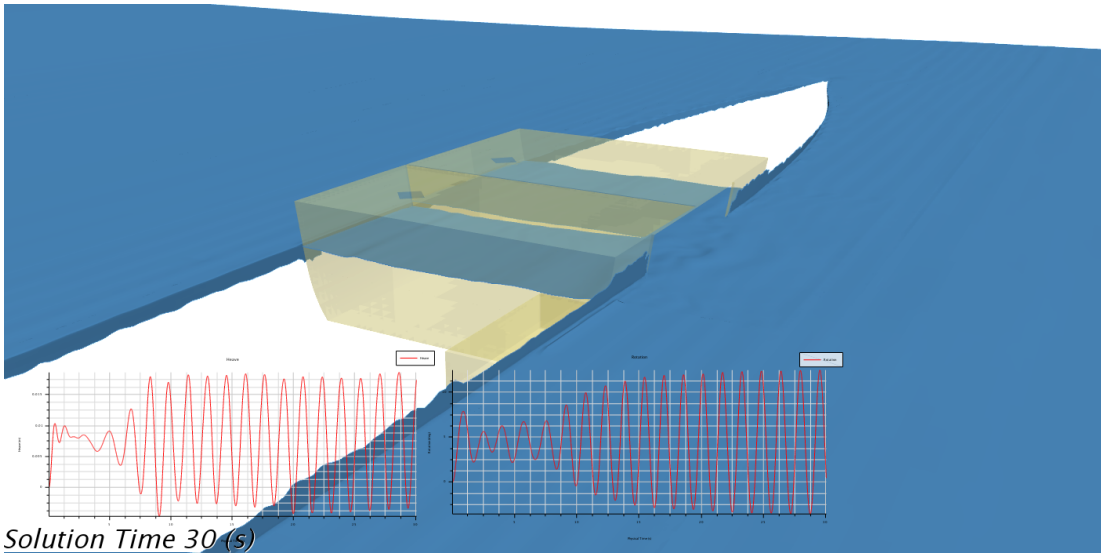
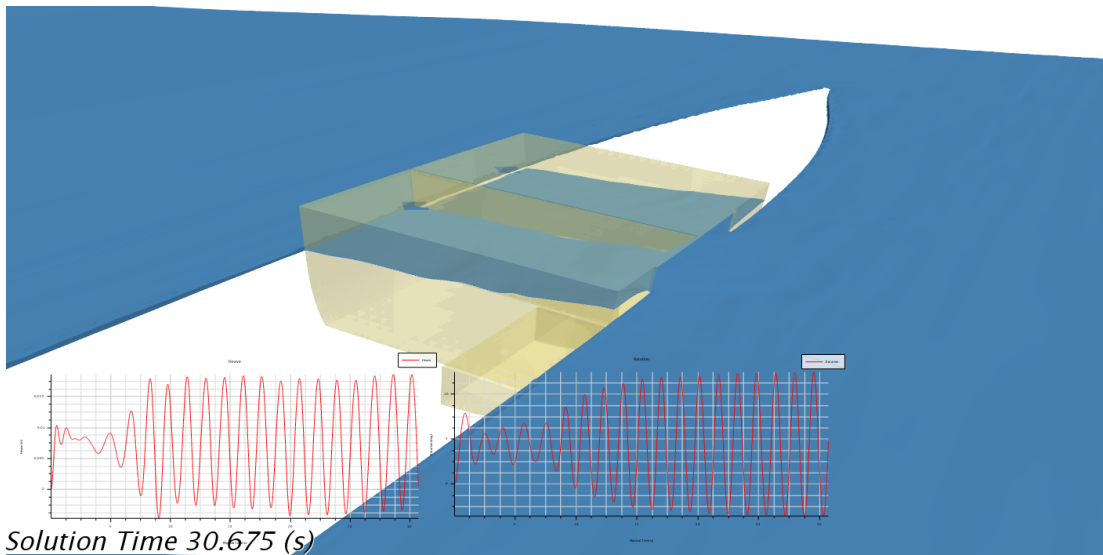
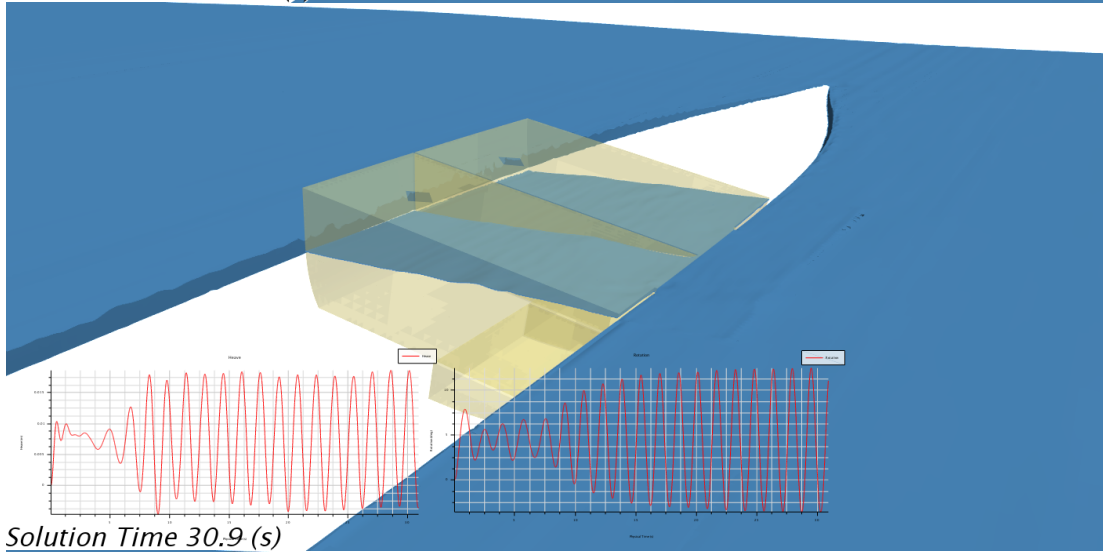


Figure 5.41. Damaged ship motions excited by waves

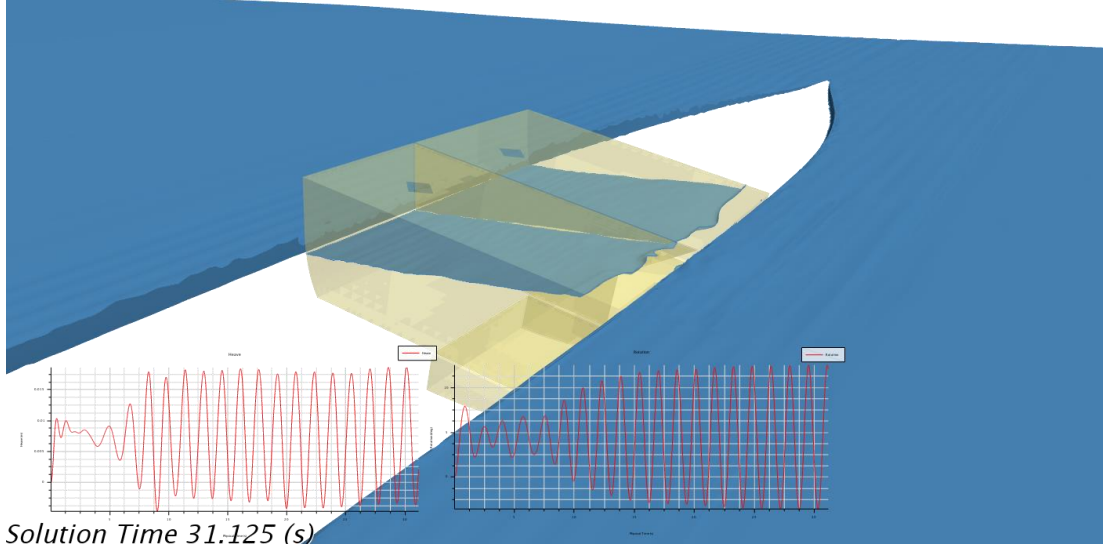




*Solution Time 30.675 (s)*



*Solution Time 30.9 (s)*



*Solution Time 31.125 (s)*



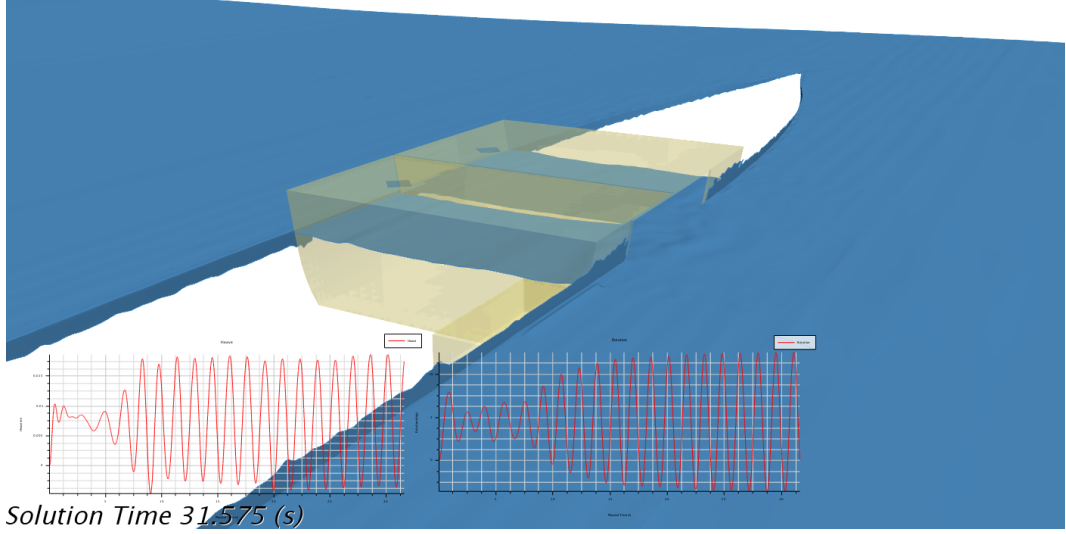
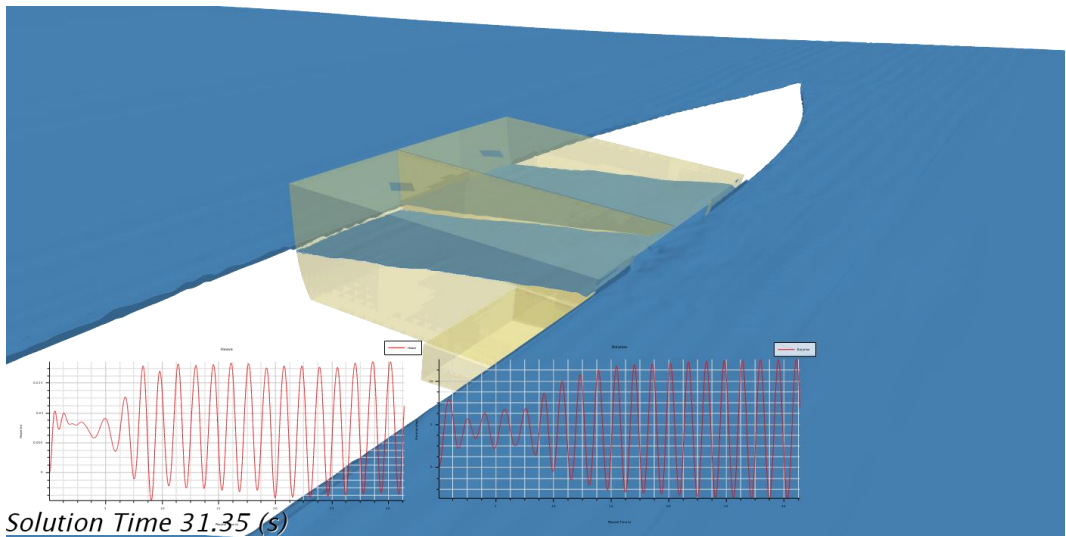


Figure 5.42. Ingress and egress of floodwater through damaged opening  
Horizontal Shear Force

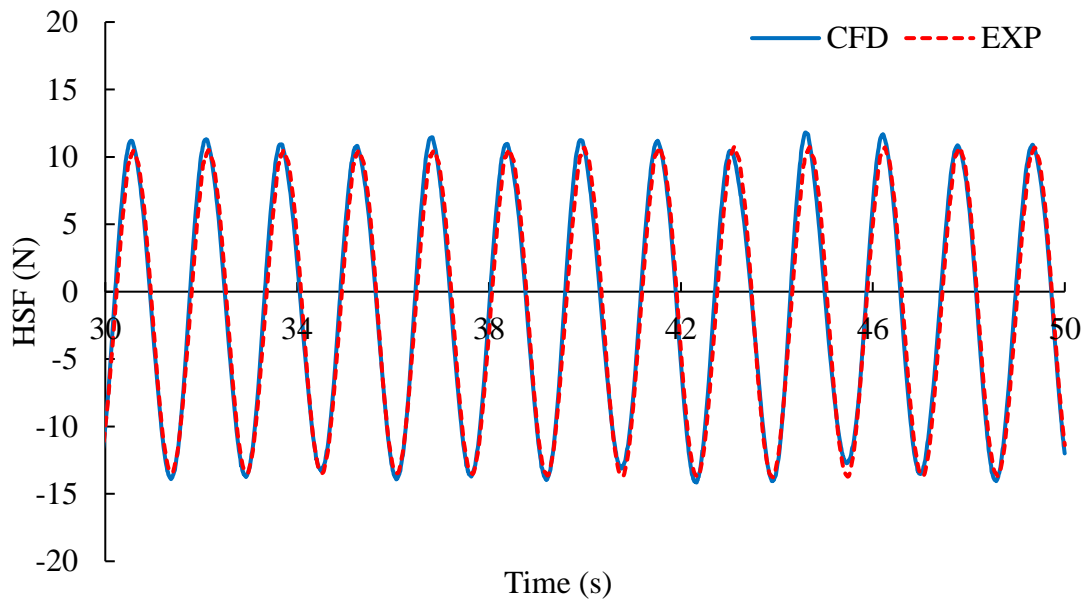


Figure 5.43. Horizontal shear force in time history for damaged ship

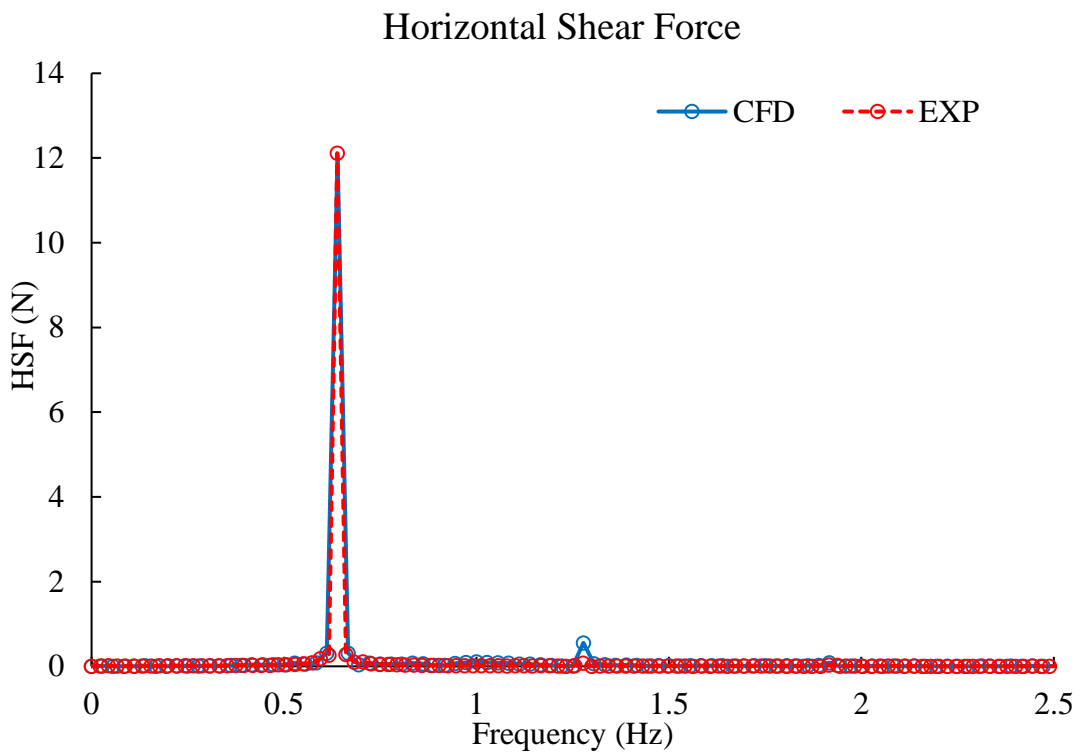


Figure 5.44. Frequency of horizontal shear forces by FFT for damaged ship

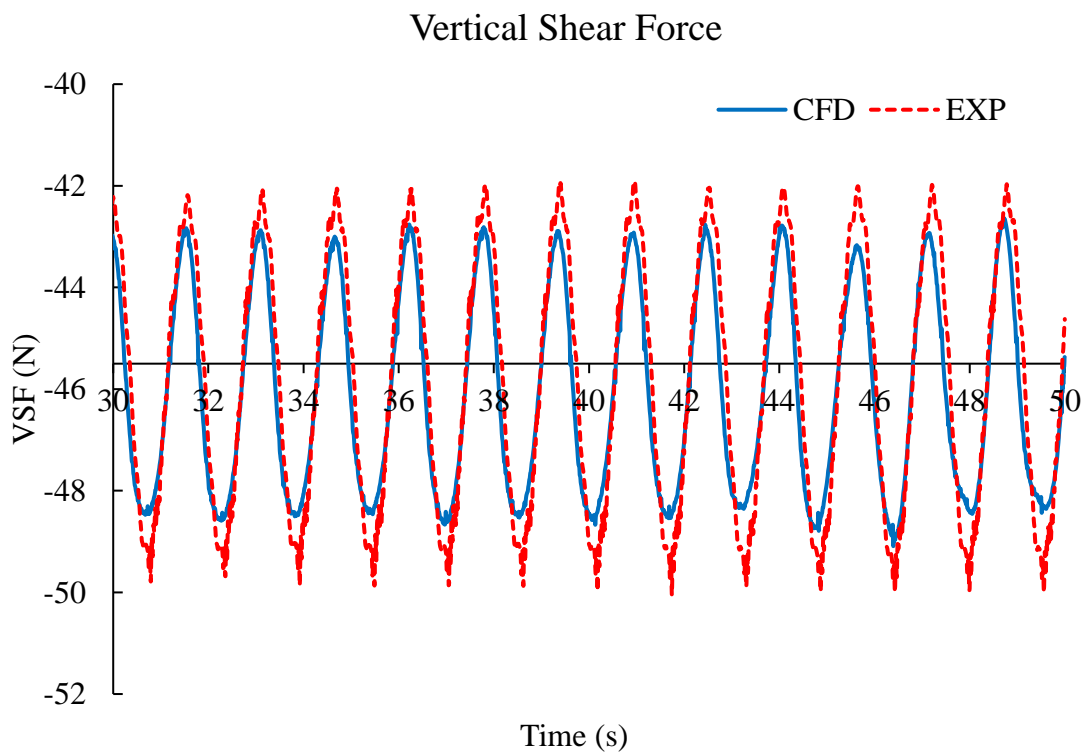


Figure 5.45 Vertical shear force in time history for damaged ship

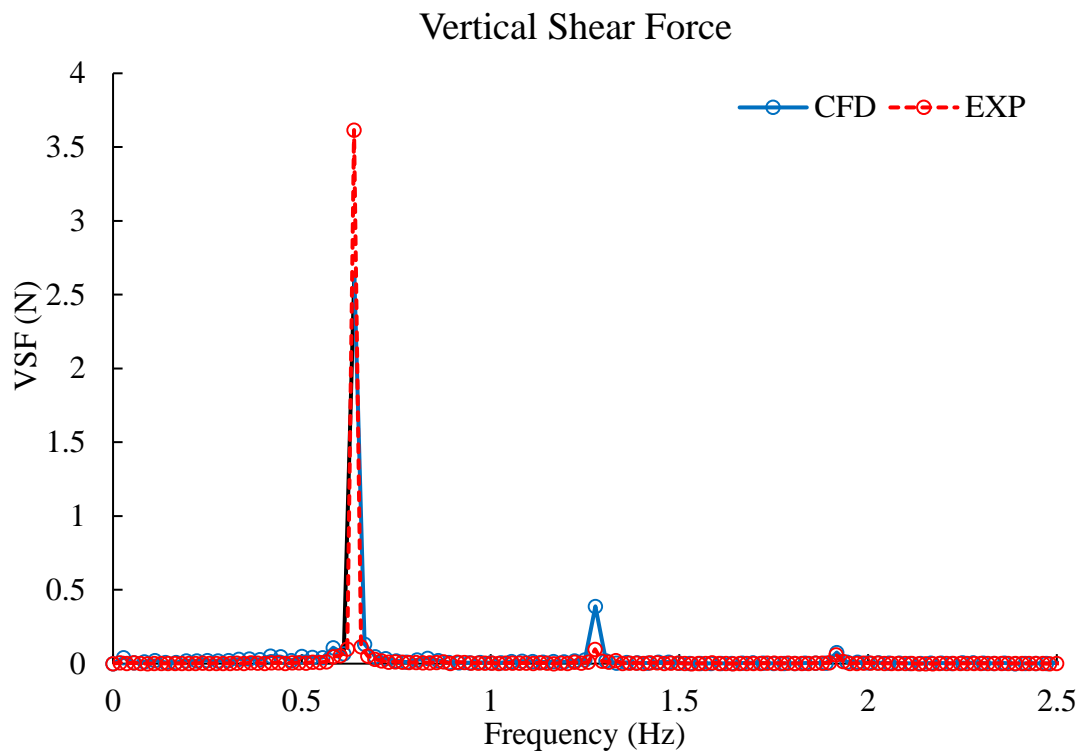


Figure 5.46. Frequency of vertical shear forces by FFT for damaged ship

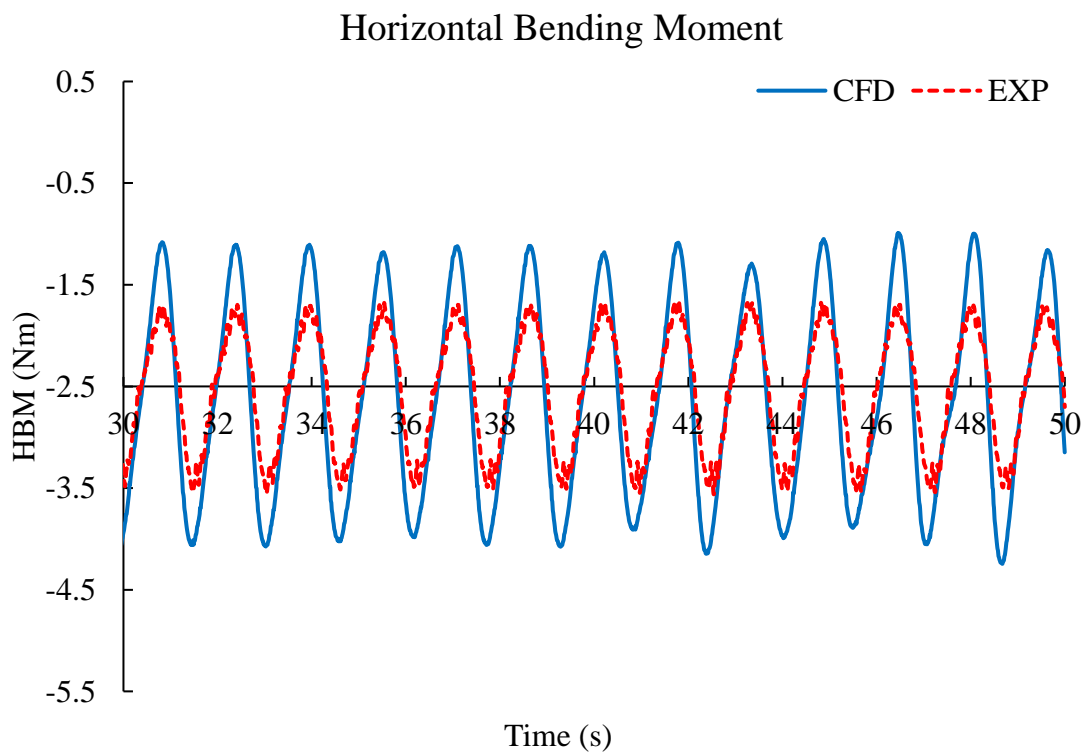


Figure 5.47. Horizontal bending moment in time history for damaged ship

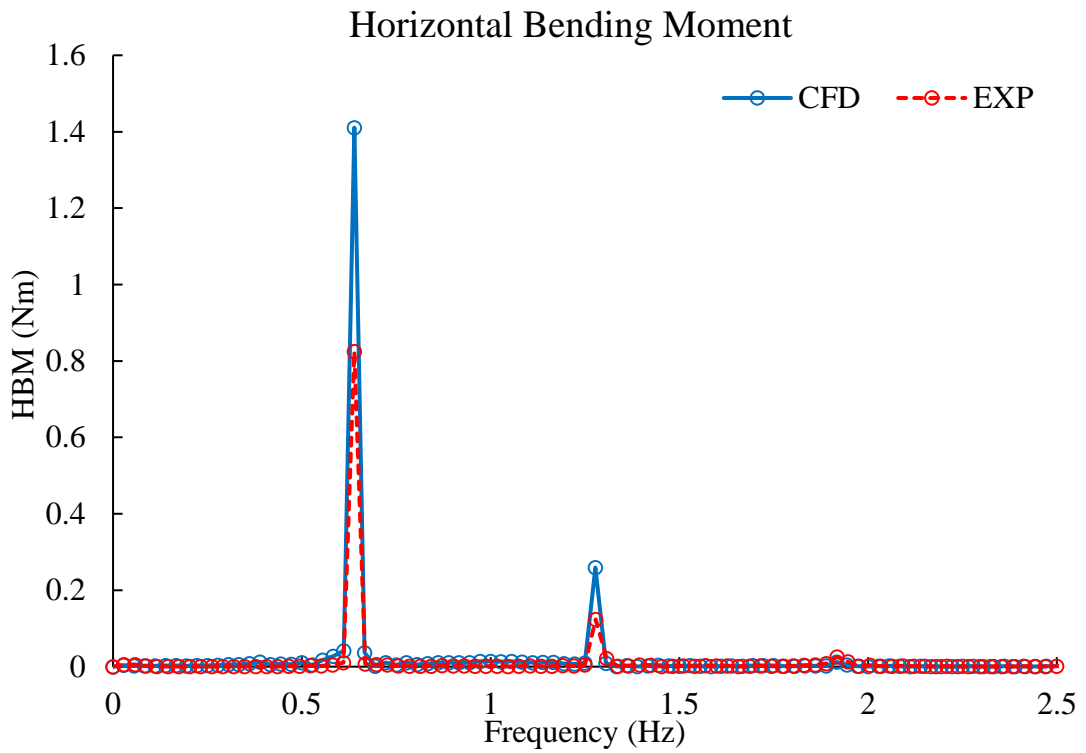


Figure 5.48. Frequency of horizontal bending moment by FFT for damaged ship

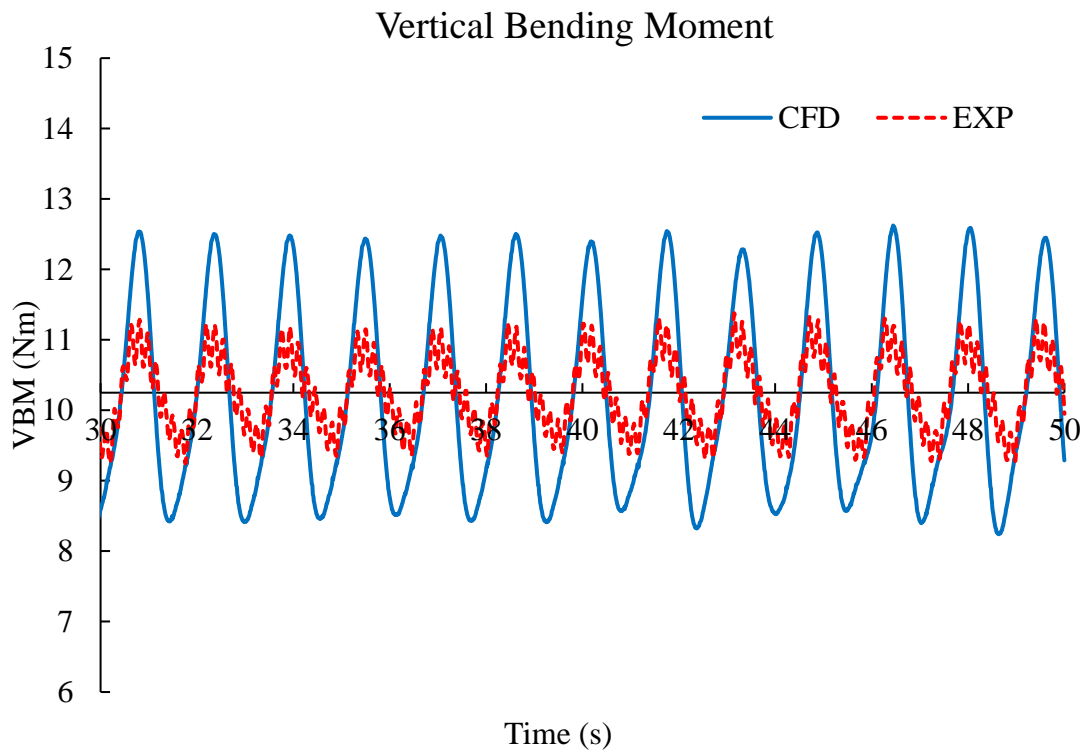


Figure 5.49. Vertical bending moment in time history for damaged ship

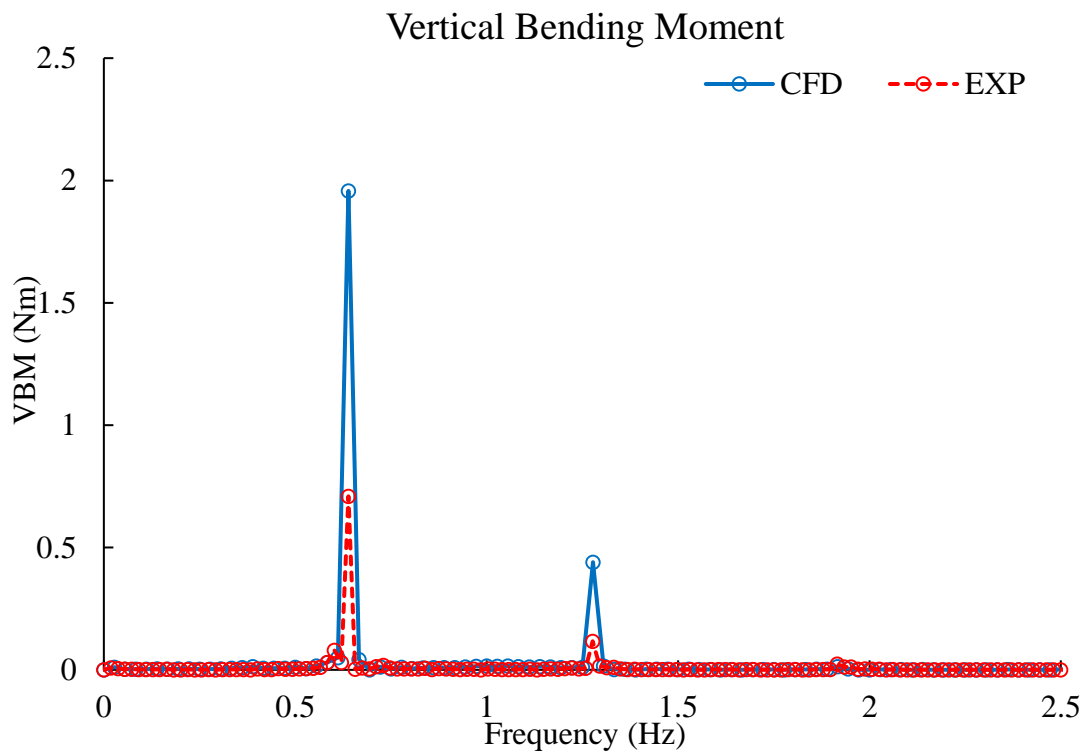


Figure 5.50. Frequency of vertical bending moment by FFT for damaged ship

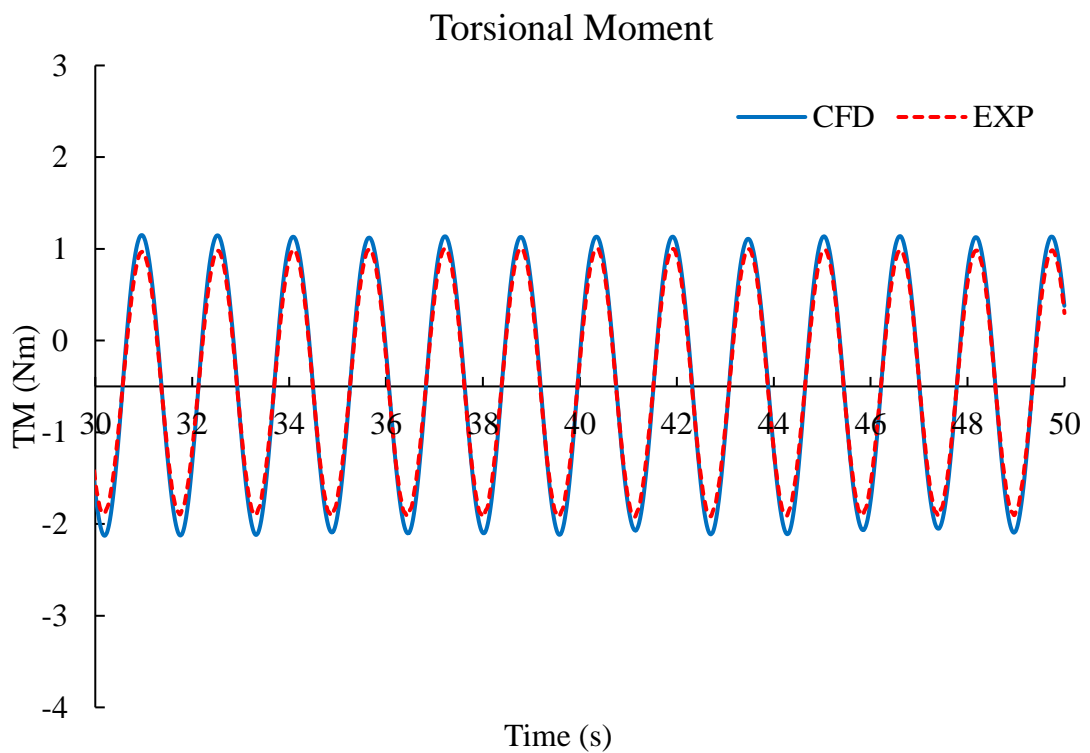


Figure 5.51. Torsional moment in time history for damaged ship

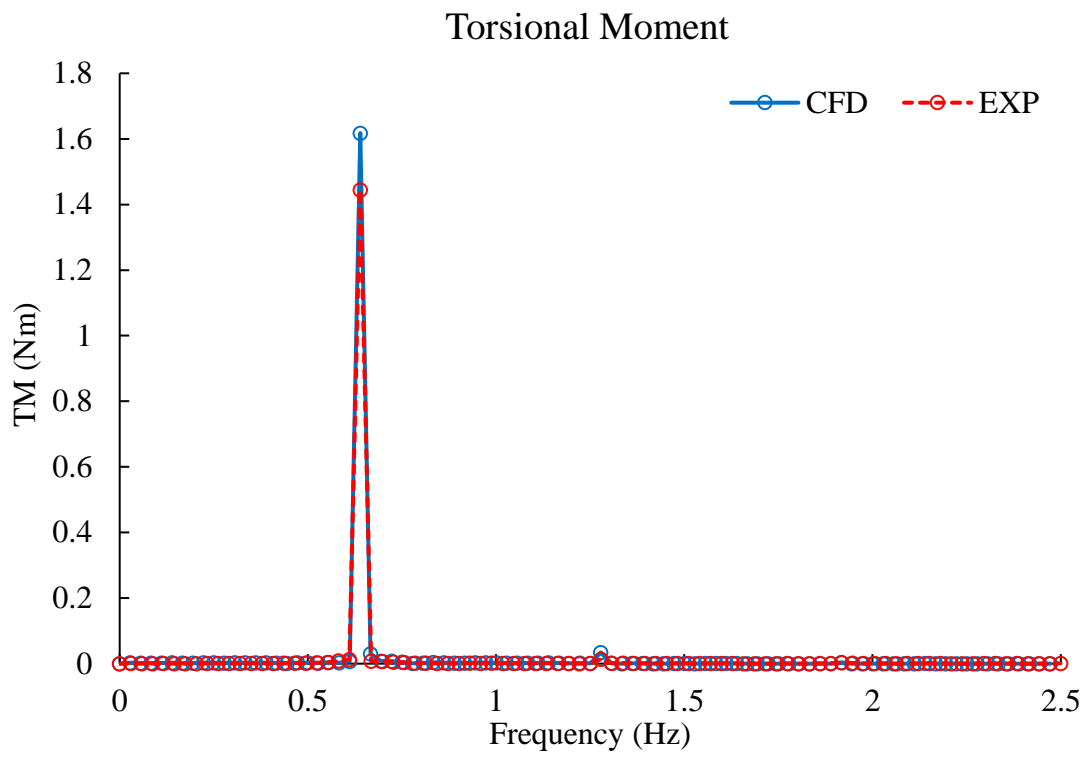
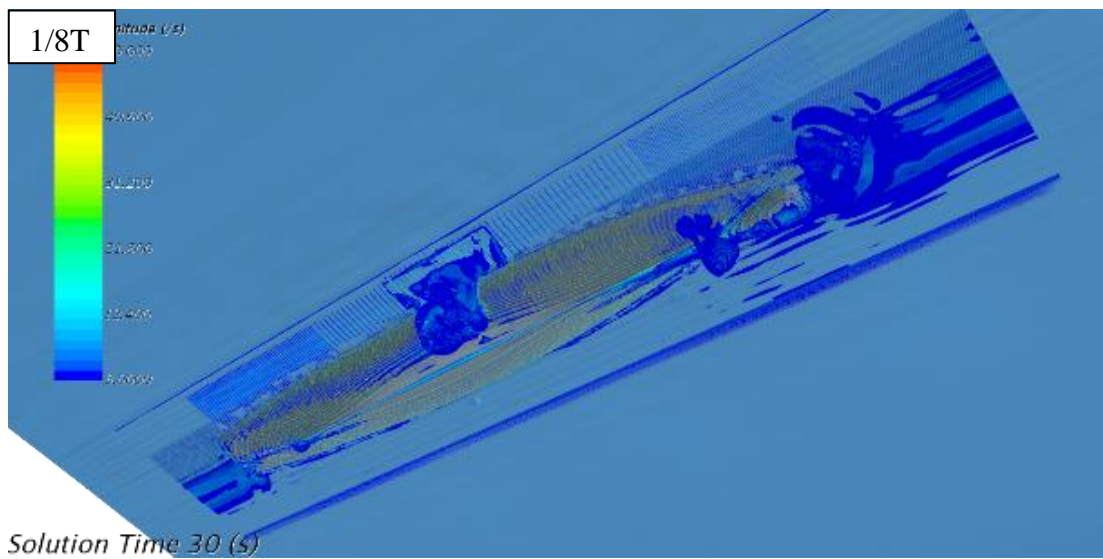
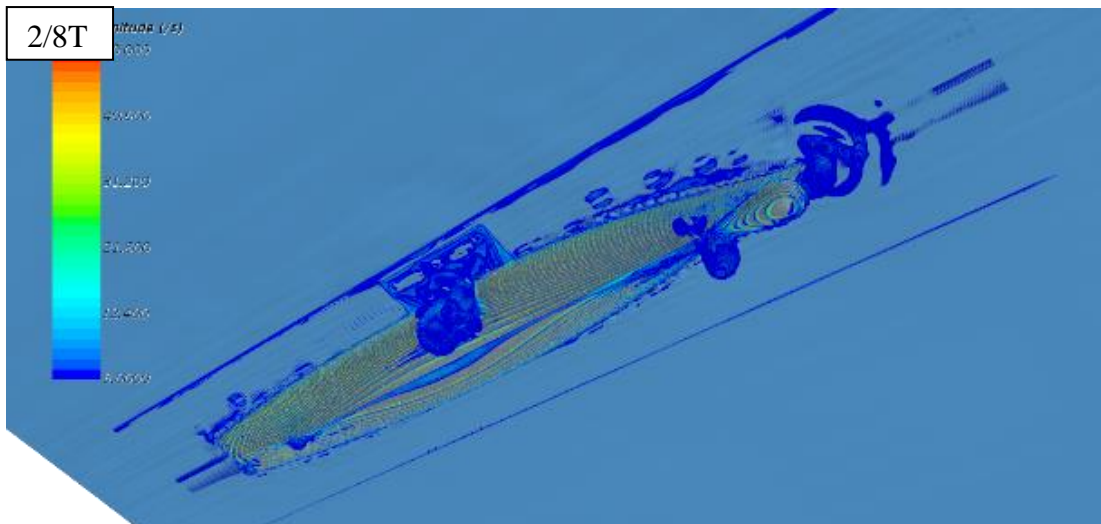
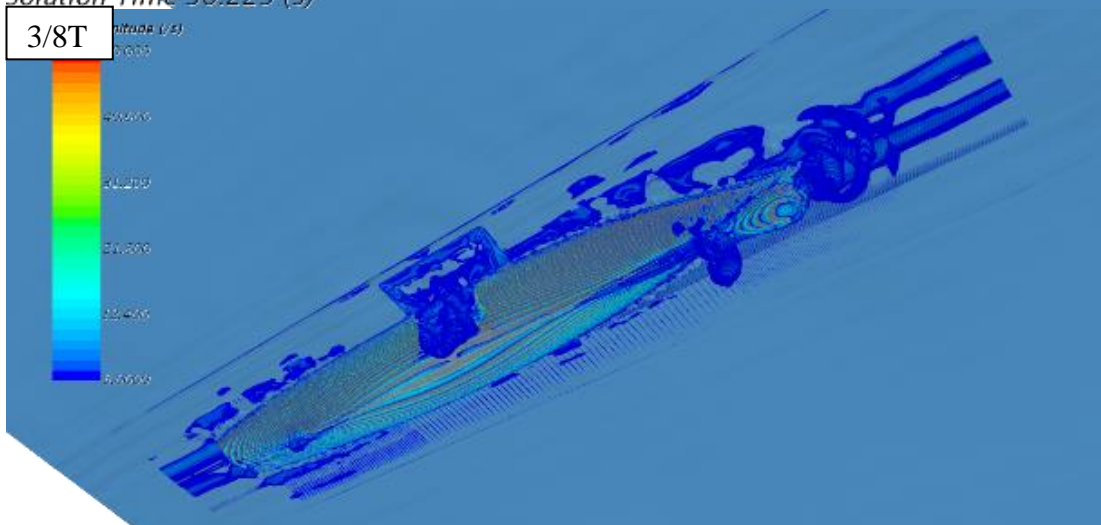


Figure 5.52. Frequency of torsional moment by FFT for damaged ship

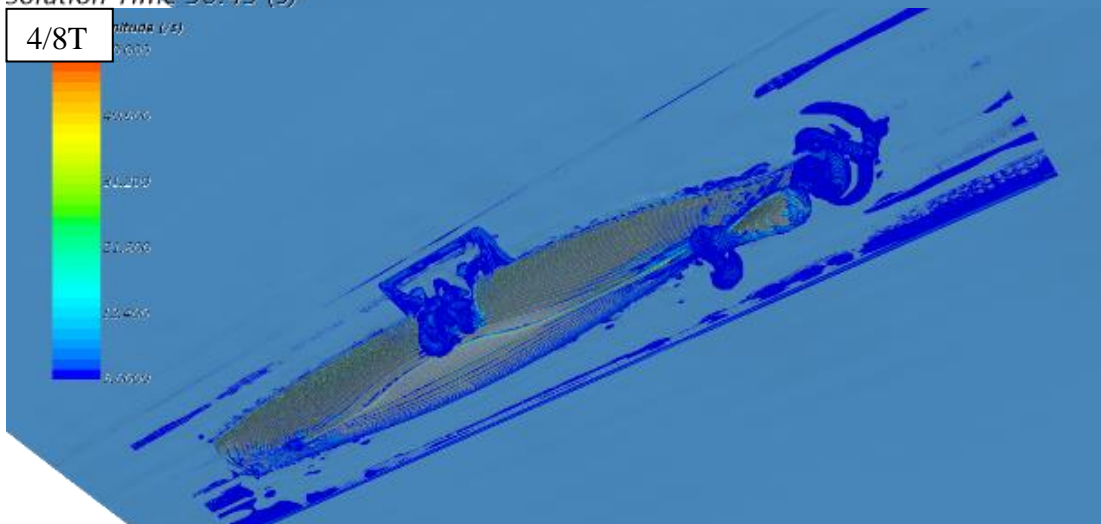




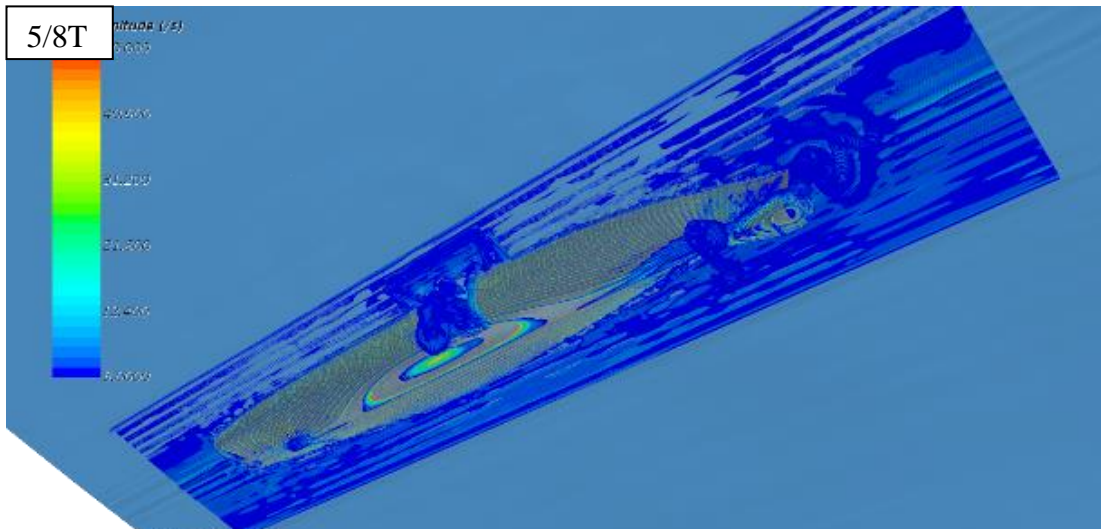
Solution Time 30.225 (s)



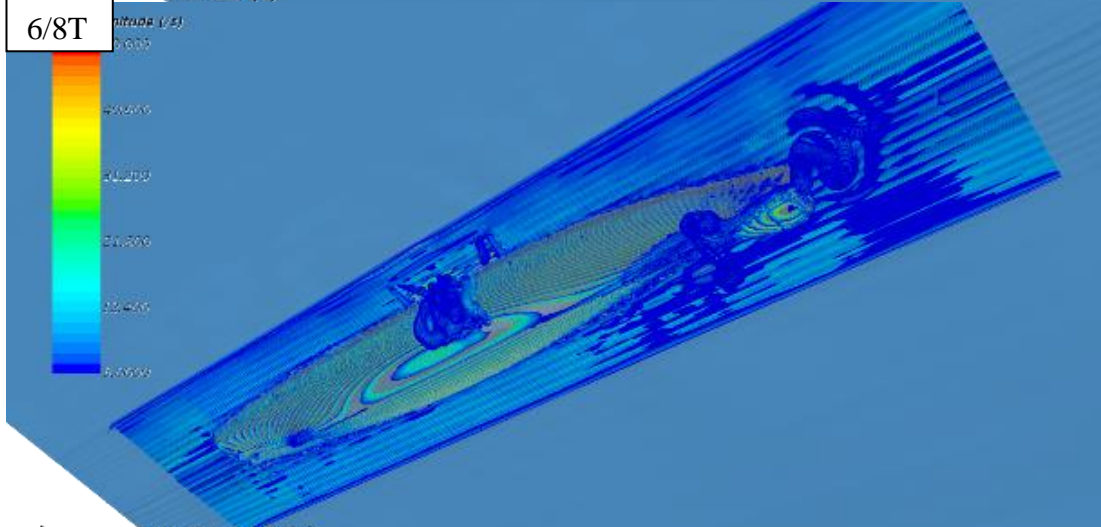
Solution Time 30.45 (s)



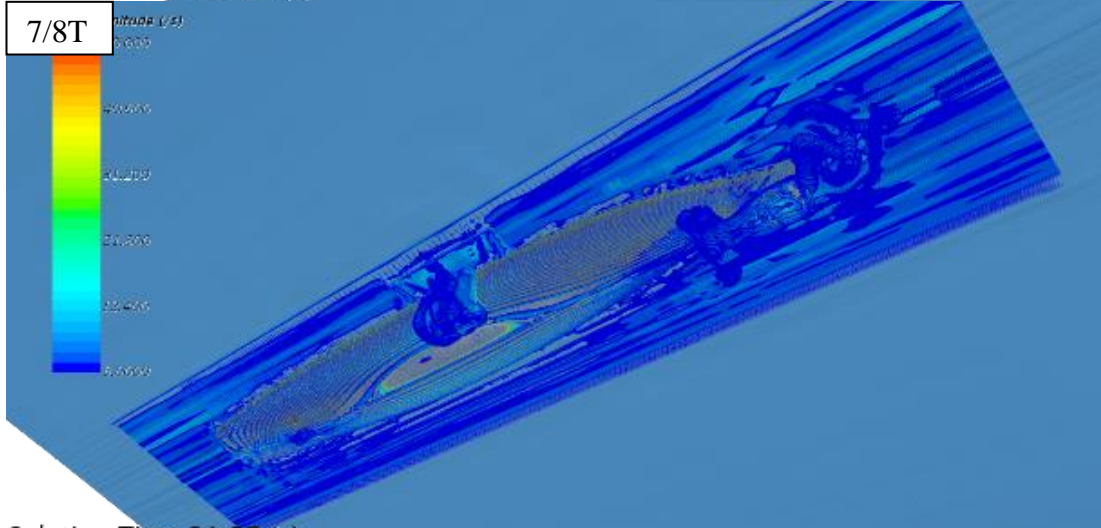
Solution Time 30.675 (s)



*Solution Time 30.9 (s)*



*Solution Time 31.125 (s)*



*Solution Time 31.35 (s)*



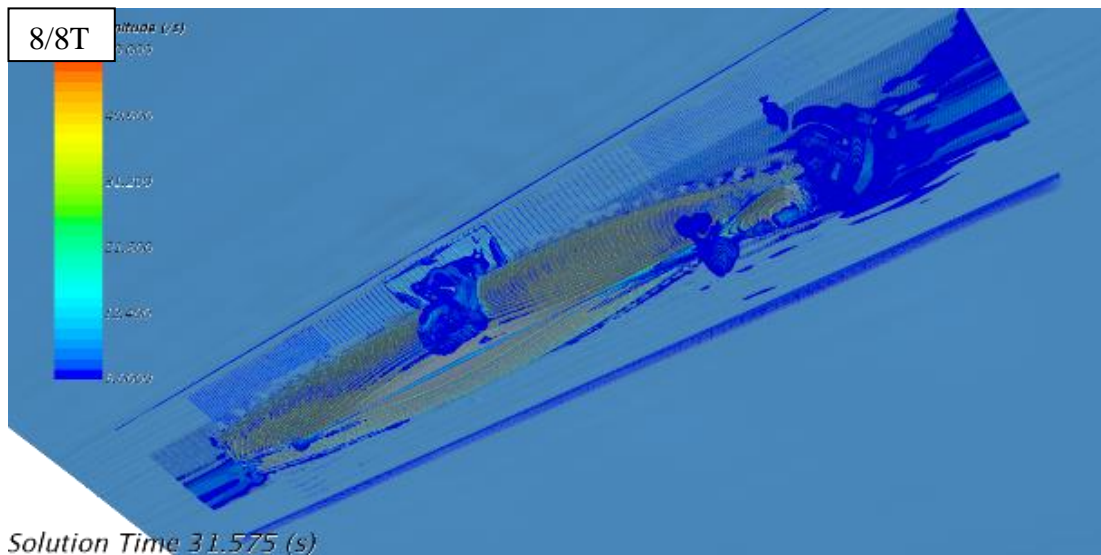


Figure 5.53. Vorticity around the damaged hull under the water surface

## 5.6 Chapter remarks

In this chapter, CFD-based RANS solver is deployed to investigate ship motion and wave-induced loads acting on an intact and damaged ship in regular beam seas. For validation, a naval combatant vessel, 51-scaled DTMB 5415, which is almost identical to the model used in physical tests described in chapter 3, is studied under the same wave conditions. A methodology is proposed to assess wave-induced loads by CFD method, and the flow field around intact and damaged ship hull is also investigated. Considering the influence of floodwater dynamics under the damaged situation, flooded compartments are carefully modelled to represent the physical ones accurately, including a ventilation pipe in each compartment to eliminate trapped air compression.

Although the main particulars are intended to be the same as the physical model, some assumptions are required to simplify the problem. Firstly and importantly, the mass moment of inertia of the ship is determined by approaching free rolling decay curve. Although this method is reasonable and yields acceptable agreement with measured results, the real value of mass moment of inertia is still not directly measured, and the estimated value may cause some difference which is difficult to quantify.

The wave-induced loads measured by the load cell in physical model tests are based on a local coordinate system established in the load cell itself, but the method to assess

wave-induced loads is based on Newton's Second Law, which should be valid under the inertial coordinate system. A connection is established between inertial coordinate system and non-inertial coordinate system by considering a rigid body motion. Results show that ship motion in the beam waves under both intact and damaged scenarios are well predicted by the RANS solver. Horizontal shear force and bending moment and torsional moment calculated by RANS solver generally achieve a good qualitative agreement, whereas the vertical wave-induced loads do not reveal the desired agreement with experimental measurements.

An explain for the agreed ship motions but partly unmatched loads can be due to the different ways to process the CFD calculation. The motion of the ship is obtained from local forces by integration of hydrodynamic pressure over the entire ship, and during this process, rapid local variation in hydrodynamic pressure and consequent force may be effectively smoothed out. However, to calculate the wave-induced loads acting on the intact and damaged ship, forces and moments are calculated and summed depending upon the hydrodynamic pressure distributed along each of the cut section where the integral area is drastically narrowed down. In other words, the calculated loads on each section of the ship are determined by the distribution of local force over a smaller area, and smoothing out of variations will be less. The wave-induced loads at the cut are related to differences between the loads on each side of the cut section, and therefore, the relative error can be much larger in percentage terms for the calculated loads compared to the ship motions.

## 6. Conclusions and recommendations

This work has investigated the behaviour of an intact and damaged ship in regular beam seas experimentally and numerically. Roll and heave motions are addressed as well as five wave-induced loads acting on the ship hull, namely horizontal and vertical shear forces, horizontal and vertical bending moments, and torsional moment. A three-metre naval combatant vessel model, DTMB 5415 is investigated both in physical model test and CFD simulation. The physical experiment, was carried out at Kelvin Hydrodynamic Laboratory in University of Strathclyde, while CFD calculation was executed using a CFD solver package – STAR-CCM+ with a CFD-based RANS solver.

In physical tests, a three-metre naval combatant ship model was moored and tested, without forward speed in calm water and in regular beam waves. A damaged opening was located at the starboard midship facing the direction of incoming waves, allowing two compartments to be flooded. Half of the double bottom was flooded when the ship is damaged, and to avoid the air compression effect on floodwater, ventilation was installed in each flooded compartment. The motions of the intact and damaged ship were recorded by optical capture system, meanwhile wave-induced loads were measured by a force transducer installed at a cross section near midship. Wave-induced loads acting on the intact and damaged naval ship model are mainly investigated.

❖ The ship model was ballasted and tested in calm water with main particulars determined. However, due to the limitation of measurement device, the mass moment of inertia could not be obtained physically.

❖ Free decay tests for intact and damaged ship on roll and sway motions are carried out. A 4<sup>th</sup> order Runge-Kutta method is proposed to assess hydrodynamic components according to time history of angle of inclination. Results illustrate that the method can predict hydrodynamic components well even if the rotational angle is very small. Free decay test results show that, the damping effect of floodwater can drive the damaged ship to arrive at the stable equilibrium faster compared to intact ship. Meanwhile, the natural frequency of the damaged ship appears to be substantially smaller than that of the intact ship. The five-component force transducer used was shown to suffer from substantial cross-coupling. This was analysed in detail following

careful calibration. Results show that shear forces measured by the transducer in two directions can have a relatively large impact on each other, while bending moments may not be obviously affected by forces and moments.

❖ Although both the intact and the damaged ship hull were restrained by soft moorings, rotational and translational movements can be still observed on 6 DOFs in the regular beam waves generated by the wave maker. It can be concluded that floodwater dynamics plays a significant role in the ship motions. Floodwater can be regarded as a damper since it provides an additional damping effect to the ship motion. On the other hand, due to existence of free surface in damaged compartment and interaction between free surface and ship motions, wave-induced loads acting on the damaged ship becomes more complicated; this effect is more noticeable on vertical load components.

A CFD-based RANS solver is utilized to estimate the wave-induced loads acting on the intact and damaged ship model. Prior to the simulations with a complete ship hull, several hydrodynamic problems are investigated in 2-dimension, including float body's free decrement and behaviour in waves.

❖ 2-Dimensional case studies are carried out to decompose and simplify the investigation on water flooding of a damaged ship in the beam waves. Regular beam waves generation, free decay simulation in calm water, excitation by regular beam waves and water sloshing in a tank are respectively investigated. All the 2-dimensional simulation results have the validation with experimental results, and comparisons present good quantitative agreement.

❖ Although for the first stage of the scientific investigation the complicated 3D problem has been decomposed into 2D components, which were individually investigated by CFD method, fluid flow through damaged opening, however, was not included in floating body's behaviour under the beam wave excitation and water tank sloshing investigations. In addition, water sloshing inside the tank is excited by defined motions of the water tank rather than physical wave excitation.

To scientifically validate the numerical method for the full 3D problem, the ship model parameters and wave conditions are set as close as possible to those used in physical tests.

❖ 3D simulation is applied to the intact and damaged ship in calm water and regular beam waves. Excited by the regular beam waves under the natural frequency, roll motion and heave motion are not restrained and wave-induced loads acting on the intact and damaged ship are calculated based on the proposed method. Results show that time histories compared with the data from physical tests indicate that ship motions and horizontal and torsional loads can be quantitatively well estimated for both intact and damaged ship, but vertical load predictions require to be improved.

❖ Water flow around intact and damaged ship in beam waves is also investigated to obtain fluid flow information and hydrodynamic feature about damaged flooding of a ship. Air compression effect is not taken into consideration due to ventilation.

❖ It is suggested that one cause of the discrepancies in vertical load prediction relate to the reduced DOFs in the numerical results. Without attempting to model the properties of the soft moorings as used in physical model tests, a more detailed numerical investigation cannot easily be carried out.

For future work, several aspects can be recommended.

❖ In the physical model tests, an improved method is required to measure the mass moment of inertia in roll of a structure with relatively large dimensions.

❖ Damage creation is the main factor that can influence the further behaviour of a damaged ship. To model the damaged creation, an air-cylinder system can be installed on the cover that replaces the damaged opening to control the beginning of flooding. Under this circumstance, investigation on behaviour of the damaged ship can be more realistic and scientific taking both transient flooding and progressive flooding into account. But in the meantime, this can bring a new challenge for numerical investigation especially for modelling the damage creation.

❖ Since the flow field plays a dominant role for the behaviour of intact and damaged ship excited by waves, fluid field around intact and damaged ship hull and inside the flooded compartment is recommended to be measured. Results present a relatively violent fluid motion inside the compartment and it may be a lack of accuracy in estimation on the hydrodynamic pressured when flooded water sloshing inside. It can be improved in order to match the results obtained by CFD calculation with physical model tests for accuracy, however, at the expense of massive calculation cost. This can be improved to insight into the fluid flow measurement and calculation inside

the damaged compartment, which requires more concentration on the local flow study with parametric variation of damage geometry, and it may be investigated further in the future work.

❖ Given that, only two frequencies, which are respectively resonant frequency of the intact and the damaged ship's roll motion, are considered in current work to investigate the most violent motions under the intact and the damaged conditions, ship behaviour and wave-induced loads acting on the intact and damaged ship would be further studied at other frequencies. However, the qualitatively good agreement of results obtained in the most non-linear conditions (i.e. at the resonant frequencies), allied to the results from the free-decay test, confirm the promise of the CFD-based approach, and it is to be expected that similar or better agreement would result at other frequencies where the responses may be less severe.

❖ In current CFD simulations the ship model is regarded as an entire rigid body. However, considering the measurement method in physical tests, the entire rigid body can be replaced by two floating bodies connected by one or more flexures, to account for hydro-elastic effects, so that wave-induced loads acting on the ship model can be estimated as the loads acting on the flexure. However, this will make numerical solution considerably more complicated due to two- or multi-body motion.

# Reference

Acanfora, M. and Cirillo, A. 2017. A simulation model for ship response in flooding scenario. *Proceedings of the Institution of Mechanical Engineers, Part M: Journal of Engineering for the Maritime Environment*, 231(1), 153-164.

Akyildiz, H. and Ünal, E., 2005. Experimental investigation of pressure distribution on a rectangular tank due to the liquid sloshing. *Ocean Engineering*, 32(11-12), pp.1503-1516.

Akyıldız, H. and Ünal, N.E., 2006. Sloshing in a three-dimensional rectangular tank: numerical simulation and experimental validation. *Ocean Engineering*, 33(16), pp.2135-2149.

Akyildiz, H., 2012. A numerical study of the effects of the vertical baffle on liquid sloshing in two-dimensional rectangular tank. *Journal of Sound and Vibration*, 331(1), pp.41-52.

Armenio, V. and La Rocca, M., 1996. On the analysis of sloshing of water in rectangular containers: numerical study and experimental validation. *Ocean Engineering*, 23(8), pp.705-739.

Armenio, V., Francescutto, A. and La Rocca, M. 1996a. On the roll motion of a ship with partially filled unbaffled and baffled tanks-Part 1: Mathematical model and experimental setup. *International Journal of offshore and polar engineering*, 6, pp. 278-282.

Armenio, V., Francescutto, A. and La Rocca, M. 1996b. On the roll motion of a ship with partially filled unbaffled and baffled tanks-Part 2: Numerical and experimental analysis. *International Journal of offshore and polar engineering*, 6, pp. 283-290.

Arndt, B. 1983. MF EUROPEAN GATEWAY Damage Investigations. Technical report. SCHIFFKO GmbH.

Bass, R.L., Bowles, E.B., Trudell, R.W., Navickas, J., Peck, J.C., Yoshimura, N., Endo, S. and Pots, B.F.M., 1985. Modeling criteria for scaled LNG sloshing experiments. *Journal of Fluids Engineering*, 107(2), pp.272-280.

Begovic, E., Day, A. and Incecik, A. 2017. An experimental study of hull girder loads on an intact and damaged naval ship. *Ocean Engineering*, 133, pp. 47-65.

Bennett, S. and Phillips, A. 2017. Experimental investigation of the influence of floodwater due to ship grounding on motions and global loads. *Ocean Engineering*, 130, 49-63.

- Bennett, S., Hudson, D. and Temarel, P. 2013. The influence of forward speed on ship motions in abnormal waves: experimental measurements and numerical predictions. *Journal of Fluids and Structures*, 39, 154-172.
- Bennett, S., Hudson, D. and Temarel, P. 2014. Global wave-induced loads in abnormal waves: Comparison between experimental results and classification society rules. *Journal of Fluids and Structures*, 49, 498-515.
- Bhattacharyya, R., 1978. Dynamics of marine vehicles. John Wiley and Sons Inc.
- Biswal, K.C., Bhattacharyya, S.K. and Sinha, P.K., 2006. Non-linear sloshing in partially liquid filled containers with baffles. *International Journal for Numerical Methods in Engineering*, 68(3), pp.317-337.
- Bole, M. 2007. Introducing damage structural assessment to onboard decision support tools. *Proceedings of COMPIT 2007*, Cortona, IT.
- Brown, A. J. 2004. AOE 5315 Naval ship vulnerability and underwater explosion - Introduction to survivability online lecture 1. *Virginia Tech Department of Aerospace and Ocean Engineering*.
- Brown, J. and Clarke, J. 1993. Recent progress on wave induced loading measurements in warships. *Marine structures*, 6, 399-419.
- Brown, J., Clarke, J., Dow, R., Jones, G. and Smith, C. 1991. Measurement of wave-induced loads in ships at sea. *Phil Trans Royal Society Lond. A*, 334, 293-306.
- Chan, H., Atlar, M. and Incecik, A. 2003. Global wave loads on intact and damaged Ro-Ro ships in regular oblique waves. *Marine structures*, 16, 323-344.
- Chan, H.-S., Atlar, M. and Incecik, A. 2002. Large-amplitude motion responses of a Ro-Ro ship to regular oblique waves in intact and damaged conditions. *Journal of marine science and technology*, 7, 91-99.
- Chang, B. C. and Blume, P. 1998. Survivability of damaged ro-ro passenger vessels. *Ship Technology Research*, 45, pp. 105-117.
- Chen, B.F. and Chiang, H.W., 2000. Complete two-dimensional analysis of sea-wave-induced fully non-linear sloshing fluid in a rigid floating tank. *Ocean Engineering*, 27(9), pp.953-977.
- Chen, Q., Zang, J., Dimakopoulos, A. S., Kelly, D. M. and Williams, C. J. 2016. A Cartesian cut cell based two-way strong fluid-solid coupling algorithm for 2D floating bodies. *Journal of Fluids and Structures*, 62, pp. 252-271.
- Chen, Z., Zong, Z., Li, H.T. and Li, J., 2013. An investigation into the pressure on solid walls in 2D sloshing using SPH method. *Ocean Engineering*, 59, pp.129-141.



Cho, S., Sung, H., Hong, S., Nam, B. and Kim, Y. 2010. Study on the motions and flooding process of a damaged ship in waves. *Proceedings of the 11th international ship stability workshop*.

Clarke, J. 1986. Wave loading in warships. In: C.S. SMITH, J. D. C. (ed.) *Advances in Marine Structures*. London, New York: Elsevier Science Publishers. pp. 1-25.

Colagrossi, A., Lugni, C., Greco, M. and Faltinsen, O.M., 2004. Experimental and numerical investigation of 2D sloshing with slamming. *In 19th International Workshop on Water Waves and Floating Bodies*, Cartona, Italy, Mar (pp. 28-31).

Cotton, B. and Spyrou, K. 2001. An experimental study of nonlinear behaviour in roll and capsize. *International shipbuilding progress*, 48, 5-18.

Dai, S. 2016. Assessing the performance of an oscillating water column type wave energy device. [PhD thesis], University of Strathclyde.

Dalzell, J. F. 1964. An investigation of midship bending moments experienced in extreme regular waves by models of a tanker and a destroyer. Second Progress Report of Project SR-157 "Model in Extreme Waves". Ship Structure Committee.

Dand, I. 1994. Factors Affecting the Capsize of Damaged RO-RO Vessels in Waves. *Proceedings of the Symposium on Ro-Ro Ships Survivability*. November 1994. London.

Dand, I. W. 1989. Hydrodynamic aspects of the sinking of the ferry Herald of Free Enterprise. *Transactions Royal Institution of Naval Architects*, Vol. 131, pp. 145-165.

De Kat, J. and Van't Veer, R. 2001. Mechanisms and Physics Leading to the Capsize of Damaged Ships. *Proceedings of the Fifth International Workshop on Ship Stability*, Trieste, Italy, Sep.

De Kat, J. O. and Paulling, J. R. 1989. The simulation of ship motions and capsizing in severe seas. *Society of Naval Architects and Marine Engineers-Transactions*, 97, pp. 139-168.

De Kat, J. O. and Peters, A. J. 2002. Model experiments and simulations of a damaged frigate. *IMAM 2002 congress*, Crete.

De Kat, J. O. 2000. Dynamics of a ship with partially flooded compartment. In: Vassalos, D., Hamamoto, M., Papanikolaou, A., Molyneux, D. (ed.) *Contemporary ideas on ship stability*. Oxford: Elsevier Science.

De Kat, J., Kanerva, M., Van't Veer, R. and Mikkonen, I. 2000. Damage survivability of a new Ro-Ro ferry. *Proceedings of the Seventh International Conference on Stability for Ships and Ocean Vehicles (STAB 2000)*, Launceston, Australia, Feb.

Delorme, L., Colagrossi, A., Souto-Iglesias, A., Zamora-Rodriguez, R. and Botia-Vera, E., 2009. A set of canonical problems in sloshing, Part I: Pressure field in forced roll-

comparison between experimental results and SPH. *Ocean Engineering*, 36(2), pp.168-178.

Department of The Navy USA. 2017. Report on the Collision between USS FITZGERALD (DDG 62) and Motor Vessel and Report on the Collision between USS JOHN S MCCAIN (DDG 56) and Motor Vessel ALNIC MC ACX CRYSTAL.

Available: [http://www.navy.mil/submit/display.asp?story\\_id=103130](http://www.navy.mil/submit/display.asp?story_id=103130).

Department of Transport 1987. MV Herald of Free Enterprise: Report of Court n° 8074. Formal investigation. Merchant shipping act 1894. Marine accident. In: LONDON, D. O. T. (ed.). London.

Domeh, V., Sobey, A. and Hudson, D. 2015. A preliminary experimental investigation into the influence of compartment permeability on damaged ship response in waves. *Applied Ocean Research*, 52, 27-36.

Eswaran, M., Saha, U.K. and Maity, D., 2009. Effect of baffles on a partially filled cubic tank: Numerical simulation and experimental validation. *Computers and Structures*, 87(3-4), pp.198-205.

Faulkner, D. 1998. An independent assessment of the sinking of the MV DERBYSHIRE. *The Transactions of the Society of Naval Architects and Marine Engineers*, 106, 59-103.

Fonseca, N. and Soares, C. G. 2002. Comparison of numerical and experimental results of nonlinear wave-induced vertical ship motions and loads. *Journal of Marine Science and Technology*, 6, pp. 193-204.

Fonseca, N. and Soares, C.G., 2004. Experimental investigation of the nonlinear effects on the vertical motions and loads of a containership in regular waves. *Journal of Ship Research*, 48(2), pp.118-147.

Fonseca, N. and Soares, C.G., 2005. Comparison between experimental and numerical results of the nonlinear vertical ship motions and loads on a containership in regular waves. *International Shipbuilding Progress*, 52(1), pp.57-89.

Francescutto, A. and Contento, G., 1994, January. An experimental study of the coupling between roll motion and sloshing in a compartment. In *The Fourth International Offshore and Polar Engineering Conference*. International Society of Offshore and Polar Engineers.

Fujino, M., Yoon, B.S., 1985. A study on wave loads acting on a ship in large amplitude waves (second report). *Journal of the Japan Society of Naval Architects and Ocean Engineers*. In Japanese. 157, 155-167.

Fujiwara, T. and Haraguchi, T. 2002. On estimation of ship rolling motion with flooded water on vehicle deck. *The Twelfth International Offshore and Polar*

*Engineering Conference*. May 26-31. Japan: International Society of Offshore and Polar Engineers.

Gao, Q. and Vassalos, D. 2011. Numerical study of the roll decay of intact and damaged ships. *12th International Ship Stability Workshop*.

Gao, Z., Gao, Q. and Vassalos, D. 2011. Numerical simulation of flooding of a damaged ship. *Ocean Engineering*, 38, 1649-1662.

Gao, Z., Gao, Q. and Vassalos, D. 2013. Numerical study of damaged ship flooding in beam seas. *Ocean Engineering*, 61, 77-87.

Gao, Z., Vassalos, D. and Gao, Q. 2010. Numerical simulation of water flooding into a damaged vessel's compartment by the volume of fluid method. *Ocean Engineering*, 37, pp. 1428-1442.

Ghasemi, A., Anbarsooz, M., Malvandi, A., Ghasemi, A. and Hedayati, F. 2017. A nonlinear computational modeling of wave energy converters: A tethered point absorber and a bottom-hinged flap device. *Renewable energy*, 103, pp. 774-785.

Ghasemi, A., Pathak, A. and Raessi, M. 2014. Computational simulation of the interactions between moving rigid bodies and incompressible two-fluid flows. *Computers and Fluids*, 94, pp. 1-13.

Godderidge, B., Tan, M., Turnock, S.R. and Earl, C., 2006. A verification and validation study of the application of computational fluid dynamics to the modelling of lateral sloshing.

Godderidge, B., Turnock, S., Earl, C. and Tan, M., 2009a. The effect of fluid compressibility on the simulation of sloshing impacts. *Ocean Engineering*, 36(8), pp.578-587.

Godderidge, B., Turnock, S., Tan, M. and Earl, C., 2009b. An investigation of multiphase CFD modelling of a lateral sloshing tank. *Computers and Fluids*, 38(2), pp.183-193.

González, V., Talens, M., Riola, J. M., Valle, J., Quesada, T. and Espín, M. 2003. Numerical prediction of the dynamic behavior of a ro-ro ship after a hull side damage. *Proceedings of the 8th International Conference on the Stability of Ships and Ocean Vehicles*. Madrid. pp. 215-227.

Guo, L.C., Zhang, S., Morita, K. and Fukuda, K., 2012. Fundamental validation of the finite volume particle method for 3D sloshing dynamics. *International Journal for Numerical Methods in Fluids*, 68(1), pp.1-17.

Hashimoto, H., Kawamura, K. and Sueyoshi, M. 2017. A numerical simulation method for transient behavior of damaged ships associated with flooding. *Ocean Engineering*, 143, 282-294.

- Hawass, A., Mostafa, H. E. and Elbeih, A. 2015. Review on underwater explosion. *46th International Annual Conference of the Fraunhofer ICT*. Karlsruhe, Germany.
- Hearn, G. E., Lafforgue, D., Perdriset, E., and Saydan, D. 2008. The hydrodynamic and dynamic motion analysis of a damaged ship. *Transactions of the Royal Institution of Naval Architects Part A International Journal of Maritime Engineering*, 150(2), 1-24.
- Heffernan, J. E. and Tawn, J. A. 2001. Extreme value analysis of a large designed experiment: a case study in bulk carrier safety. *Extremes*, 4(4), 359-378.
- Heffernan, J. E. and Tawn, J. A. 2003. An extreme value analysis for the investigation into the sinking of the MV Derbyshire. *Journal of the Royal Statistical Society: Series C (Applied Statistics)*, 52(3), 337-354.
- Hirdaris, S., Bai, W., Dessi, D., Ergin, A. E., Gu, X., Hermundstad, O., Huijsmans, R., Iijima, K., Nielsen, U. D. and Parunov, J. 2014. Loads for use in the design of ships and offshore structures. *Ocean engineering*, 78, 131-174.
- Hirt, C. W. and Nichols, B. D. 1981. Volume of Fluid (VOF) method for the dynamics of free boundaries. *Journal of computational physics*, 39, 201-225.
- Iglesias, A.S., Delorme, L., Pérez-Rojas, L. and Abril-Pérez, S., 2006. Liquid moment amplitude assessment in sloshing type problems with smooth particle hydrodynamics. *Ocean Engineering*, 33(11-12), pp.1462-1484.
- Iglesias, A.S., Rojas, L.P. and Rodríguez, R.Z., 2004. Simulation of anti-roll tanks and sloshing type problems with smoothed particle hydrodynamics. *Ocean Engineering*, 31(8-9), pp.1169-1192.
- Ikeda, Y. and Kamo, T. 2001. Effects of transient motion in intermediate stages of flooding on the final condition of a damaged PCC. *Proceedings of the 5th International Ship Stability Workshop*. Trieste, Italy.
- Ikeda, Y. and Ma, Y. 2000. An experimental study on large roll motion in intermediate stage of flooding due to sudden ingress of water. *Proceedings of the Seventh International Conference on the Stability of Ships and Ocean Vehicles (STAB 2000)*, Launceston, Australia. pp. 270-285.
- Ikeda, Y., Shimoda, S. and Takeuchi, Y. 2003. Experimental studies on transient motion and time to sink of a damaged large passenger ship. *Proceedings of the Eight International Conference on the Stability of Ships and Ocean Vehicles (STAB 2003)*, Madrid, Spain. pp. 243-252.
- IMO, 2003. Large passenger ship safety: Time-to-flood simulations for a large passenger ship-Initial study. *International Maritime Organization*.

Irkal Mohsin, A., Nallayarasu, S. and Bhattacharyya, S. 2014. Experimental and CFD simulation of roll motion of ship with bilge keel. In: P. Krishnankutty, R. S., V. Anantha Subramanian And S. K. Bhattacharyya. (ed.) *Advances in Computational and Experimental Marine Hydrodynamics*. Vol. 2. *Conference Proceedings of International Conference on Computational and Experimental Marine Hydrodynamics (MARHY 2014)*. Chennai, India.

Irkal, M. A., Nallayarasu, S. and Bhattacharyya, S. 2016. CFD approach to roll damping of ship with bilge keel with experimental validation. *Applied Ocean Research*, 55, pp. 1-17.

Ishida, S., Murashige, S. 1997. Stability of a ro-ro passenger ship with a damage opening in beam seas. *Proceedings of the Sixth International Conference on the Stability of Ships and Ocean Vehicles (STAB 1997)*. Varna, Bulgaria. vol. 2. pp. 99-109.

ITTC, 2014a. Uncertainty analysis, instrument calibration. ITTC-Recommended Procedures and Guidelines.: International Towing Tank Conference.

ITTC, 2014b. Uncertainty analysis in CFD verification and validation methodology and procedures. ITTC-Recommended Procedures and Guidelines.: International Towing Tank Conference.

Jaeger, U. 2008. Verhangnisvolle Wende. *Der Spiegel*. 2:132-133.

Jasionowski, A. and Vassalos, D. 2011. New insights on the sinking of MV Estonia. *Contemporary Ideas on Ship Stability and Capsizing in Waves*. Springer.

Ji, Y.M., Shin, Y.S., Park, J.S. and Hyun, J.M., 2012. Experiments on non-resonant sloshing in a rectangular tank with large amplitude lateral oscillation. *Ocean Engineering*, 50, pp.10-22.

Jia, H. and Moan, T. 2012. The effect of sloshing in tanks on the hull girder bending moments and structural reliability of damaged vessels. *Journal of Ship Research*, 56, 48-62.

Journée, J., Vermeer, H. and Vredeveldt, A. 1997. Systematic model experiments on flooding of two Ro-Ro vessels. *6th International Conference on Stability of Ships and Ocean Vehicles*, 22-27 September 1997. Varna, Bulgaria.

Juncher, J.J. and Terndrup, P.P., 1979. Wave induced bending moments in ships--a quadratic theory. *Trans RINA* 121:151-165.

Jung, J.H., Yoon, H.S., Lee, C.Y. and Shin, S.C., 2012. Effect of the vertical baffle height on the liquid sloshing in a three-dimensional rectangular tank. *Ocean Engineering*, 44, pp.79-89.

Jung, K. H., Chang, K.-A. and Jo, H. J. 2006. Viscous effect on the roll motion of a rectangular structure. *Journal of engineering mechanics*, 132, pp. 190-200.

Kang, D.H. and Lee, Y.B., 2005. Summary report of sloshing model test for rectangular model. Daewoo Shipbuilding and Marine Engineering Co., Ltd. South Korea, (001).

Kehren, F.I. 2009. The Sinking Sequence of MV Estonia. [PhD thesis], Technische University at Hamburg-Harburg.

Khaddaj-Mallat, C., Alessandrini, B., Rousset, J.-M. and Ferrant, P. 2012. An experimental study on the flooding of a damaged passenger ship. *Ships and Offshore Structures*, 7, 55-71.

Khaddaj-Mallat, C., Rousset, J.-M. and Ferrant, P. 2009. On factors affecting the transient and progressive flooding stages of damaged Ro-Ro vessels. *Proceedings of the Tenth International Conference on Stability of Ships and Ocean Vehicles*, 2009 Jun 22-26. St. Petersburg, Russia.

Khaddaj-Mallat, C., Rousset, J.-M. and Ferrant, P. 2011. The transient and progressive flooding stages of damaged ro-ro vessels: A systematic review of entailed factors. *Journal of Offshore Mechanics and Arctic Engineering*, Vol. 133, 031105.

Khan, I. and Das, P. 2008. Reliability analysis of intact and damaged ships considering combined vertical and horizontal bending moments. *Ships and Offshore Structures*, 3, 371-384.

Kim, J.K.W., Shin, Y., Sim, I.H., Kim, Y.S. and Bai, K.J., 2003, January. Three-Dimensional Finite-Element Computation for the Sloshing Impact Pressure in LNG Tank. *In The Thirteenth International Offshore and Polar Engineering Conference*. International Society of Offshore and Polar Engineers.

Kim, J.-S., Roh, M.-I. and Ham, S.-H. 2017. A method for intermediate flooding and sinking simulation of a damaged floater in time domain. *Journal of Computational Design and Engineering*, Vol. 4, pp. 1-13.

Kim, S., Ryue, J. and Park, I.K., 2018. Prediction of the wave induced second order vertical bending moment due to the variation of the ship side angle by using the quadratic strip theory. *International Journal of Naval Architecture and Ocean Engineering*, 10(3), pp.259-269.

Kim, Y., Nam, B.W., Kim, D.W. and Kim, Y.S., 2007. Study on coupling effects of ship motion and sloshing. *Ocean Engineering*, 34(16), pp.2176-2187.

Kukkanen, T. 2010. Wave load predictions for marine structures. *Journal of Structural Mechanics*, 43, 150-166.

- Landrini, M., Colagrossi, A. and Faltinsen, O.M., 2003, September. Sloshing in 2-D Flows by the SPH Method. *In 8th International Conference on Numerical Ship Hydrodynamics*, Busan, Korea, Sept (pp. 22-25).
- Larsson, L., Stern, F. and Visonneau, M. 2013. CFD in ship hydrodynamics-results of the Gothenburg 2010 workshop. *MARINE 2011, IV International Conference on Computational Methods in Marine Engineering*. Netherlands: Springer.
- Lee, D., Hong, S. and Lee, G.-J. 2007a. Theoretical and experimental study on dynamic behavior of a damaged ship in waves. *Ocean Engineering*, 34, 21-31.
- Lee, D.H., Kim, M.H., Kwon, S.H., Kim, J.W. and Lee, Y.B., 2007b. A parametric sensitivity study on LNG tank sloshing loads by numerical simulations. *Ocean Engineering*, 34(1), pp.3-9.
- Lee, D.Y. and Choi, H.S., 1999. Study on sloshing in cargo tanks including hydroelastic effects. *Journal of marine science and technology*, 4(1), pp.27-34.
- Lee, S., You, J.-M., Lee, H.-H., Lim, T., Park, S. T., Seo, J., Rhee, S. H. and Rhee, K.-P. 2016. Experimental study on the six degree-of-freedom motions of a damaged ship floating in regular waves. *IEEE Journal of Oceanic Engineering*, Vol. 41, pp. 40-49.
- Lee, S., You, J.-M., Lee, H.-H., Lim, T., Rhee, S. H. and Rhee, K.-P. 2012a. Preliminary tests of a damaged ship for CFD validation. *International Journal of Naval Architecture and Ocean Engineering*, Vol. 4, pp. 172-181.
- Lee, S.J. and Kim, M.H., 2010. The effects of inner-liquid motion on LNG vessel responses. *Journal of Offshore Mechanics and Arctic Engineering*, 132(2), p.021101.
- Lee, S.J., Kim, M.H., Lee, D.H., Kim, J.W. and Kim, Y.H., 2007c. The effects of LNG-tank sloshing on the global motions of LNG carriers. *Ocean Engineering*, 34(1), pp.10-20.
- Lee, Y., Chan, H.-S., Pu, Y., Incecik, A. and Dow, R. S. 2012b. Global wave loads on a damaged ship. *Ships and Offshore Structures*, 7, 237-268.
- Letizia, L. 1996. Damage survivability of passenger ships in a seaway. [Ph.D. Thesis], University of Strathclyde.
- Li, H.T., Li, J., Zong, Z. and Chen, Z., 2014. Numerical studies on sloshing in rectangular tanks using a tree-based adaptive solver and experimental validation. *Ocean Engineering*, 82, pp.20-31.
- Liu, D. and Lin, P. 2008. A numerical study of three-dimensional liquid sloshing in tanks. *Journal of Computational physics*, 227, pp. 3921-3939.
- Liu, D. and Lin, P., 2009. Three-dimensional liquid sloshing in a tank with baffles. *Ocean engineering*, 36(2), pp.202-212

- Loots, E., Pastoor, W., Buchner, B. and Tveitnes, T., 2004, January. The numerical simulation of LNG sloshing with an improved volume of fluid method. *In ASME 2004 23rd International Conference on Offshore Mechanics and Arctic Engineering* (pp. 113-121). American Society of Mechanical Engineers.
- Lutzi, P. C. 1957. Ship model bending moments in waves. [Doctoral dissertation], Massachusetts Institute of Technology, 1957.
- Macfarlane, G., Renilson, M. and Turner, T. 2010. The transient effects of flood water on a Warship in calm water immediately following damage. *Transactions of the Royal Institution of Naval Architects Part A: International Journal of Maritime Engineering*, 152, A209-A224.
- Malenica, S., 2003. Dynamic coupling of seakeeping and sloshing. *In Proceedings of the 13th international offshore and polar engineering conference*, Hawaii, USA, 2003 (Vol. 3, pp. 484-490).
- Mancini, S., Begovic, E., Incecik, A. and Day, S. 2018. Verification and validation of numerical modelling of DTMB 5415 roll decay. *Ocean Engineering*. 162. pp. 209-223.
- Manderbacka, T. and Ruponen, P. 2016. The impact of the inflow momentum on the transient roll response of a damaged ship. *Ocean Engineering*, 120, 346-352.
- Manderbacka, T. L., Mikkola, T. K. and Matusiak, J. E. 2015a. Study of damping effect of the floodwater on a damaged ship roll motion. *The Twenty-fifth International Ocean and Polar Engineering Conference*. International Society of Offshore and Polar Engineers.
- Manderbacka, T., Ruponen, P., Kulovesi, J. and Matusiak, J. 2015b. Model experiments of the transient response to flooding of the box shaped barge. *Journal of Fluids and Structures*, 57, 127-143.
- Maritime Safety Committee. 2004. Report of The Maritime Safety Committee on its Seventy-Ninth Session. Agenda item 3 and Annex 2.
- Menter, F. R. 1994. Two-equation eddy-viscosity turbulence models for engineering applications. *AIAA journal*, 32, pp. 1598-1605.
- Mikelis, N.E. and Journee, J.M.J., 1984, July. Experimental and numerical simulations of sloshing behaviour in liquid cargo tanks and its effect on ship motions. *In National Conference on Numerical Methods for Transient and Coupled Problems* (pp. 9-13).
- Mikelis, N.E.M., 1984. Sloshing in partially filled liquid tanks and its effect on ship motions: numerical simulations and experimental verification. *In Royal Institution of Naval Architects 1984 spring meeting* (pp. 1-11)



- Miller, N. L. and Shattuck, L. G. 2004. A process model of situated cognition in military command and control. *2004 Command and Control Research and Technology Symposium*.
- Mitra, S., Wang, C.Z., Reddy, J.N. and Khoo, B.C., 2012. A 3D fully coupled analysis of nonlinear sloshing and ship motion. *Ocean Engineering*, 39, pp.1-13.
- Molyneux, D., Rousseau, J., Cumming, D. and Koniecki, M. 1997. Model experiments to determine the survivability limits of damaged ro-ro ferries in waves. *Transactions of the Society of Naval Architects and Marine Engineers*, 105, pp. 297-321.
- Monaghan, J. J. 1994. Simulating free surface flows with SPH. *Journal of computational physics*, 110, 399-406.
- Nam, B.W. and Kim, Y., 2007, April. Effects of Sloshing on the Motion Response of LNG-FPSO in Waves. *In The 22nd Workshop on Water Waves and Floating Bodies*, Plitvice, Croatia.
- Nasar, T., Sannasiraj, S.A. and Sundar, V., 2008. Experimental study of liquid sloshing dynamics in a barge carrying tank. *Fluid Dynamics Research*, 40(6), p.427.
- Nasar, T., Sannasiraj, S.A. and Sundar, V., 2010. Motion responses of barge carrying liquid tank. *Ocean Engineering*, 37(10), pp.935-946
- Nematbakhsh, A., Olinger, D. J. and Tryggvason, G. 2013. A nonlinear computational model of floating wind turbines. *Journal of fluids Engineering*, 135, pp. 121103.
- NMI. 1983. Investigation into the Sinking of MV EUROPEAN GATEWAY. Technical report. National Maritime Institute.
- Palazzi, L. and De Kat, J. 2004. Model experiments and simulations of a damaged ship with air flow taken into account. *Marine Technology*, 41, 38-44.
- Panigrahy, P.K., Saha, U.K. and Maity, D., 2009. Experimental studies on sloshing behavior due to horizontal movement of liquids in baffled tanks. *Ocean Engineering*, 36(3-4), pp.213-222.
- Papanikolaou, A. and Spanos, D. 2004. 24th ITTC Benchmark study on numerical prediction of damage ship stability in waves - Preliminary analysis of results. *Proc. of 7th Inter. Workshop on Stability and Operational Safety of Ships*, Jiao Tong University, Shanghai, China.
- Papanikolaou, A. 2001. Benchmark study on the capsizing of a damaged ro-ro passenger ship in waves-Final report. *Report of the Second ITTC Damage Stability Benchmark Study*. National Technical University of Athens.

- Papanikolaou, A., Spanos, D., Boulougouris, E., Eliopoulou, E. and Alissafaki, A. 2004. Investigation into the sinking of the ro-ro passenger ferry express samina. *International shipbuilding progress*, 51, pp. 95-120.
- Papanikolaou, A., Zaraphonitis, G., Spanos, D., Boulougouris, E. and Eliopoulou, E. 2000. Investigation into the capsizing of damaged Ro-Ro passenger ships in waves. *Proc. 7th Inter. Conf. On Stability of Ships and Ocean Vehicles (STAB2000)*, Australia, Tasmania.
- Parker, C. 1987. Herald of Free Enterprise. *Seaways*, pp. 2-4.
- Peters, A. J., Galloway, M. and Minnick, P. V. 2003. Cross-flooding design using simulations. *Proceedings of the Eight International Conference on Stability of Ships and Ocean Vehicles (STAB 2003)*, Madrid, Spain, Sep.
- Pletcher, R. H., Tannehill, J. C. and Anderson, D. 2012. Computational fluid mechanics and heat transfer, CRC Press.
- Pope, S. B. 2001. Turbulent flows, IOP Publishing.
- Rafiee, A., Pistani, F. and Thiagarajan, K., 2011. Study of liquid sloshing: numerical and experimental approach. *Computational Mechanics*, 47(1), pp.65-75.
- Research Excellence Framework (REF). 2014. Investigating the sinking of the M.V. Derbyshire and the setting of global design standards for bulk carriers using statistical extreme value research.
- Rhee, S.H., 2005. Unstructured grid based Reynolds-averaged Navier-Stokes method for liquid tank sloshing. *Journal of fluids engineering*, 127(3), pp.572-582.
- Rodrigues, J. and Guedes Soares, C. 2017. Still water vertical loads during transient flooding of a tanker in full load condition with a probabilistic damage distribution. *Ocean Engineering*, 129, 480-494.
- Rognebakke, O.F. and Faltinsen, O.M., 2003. Coupling of sloshing and ship motions. *Journal of Ship Research*, 47(3), pp.208-221.
- Ruponen, P. 2006. Model tests for the progressive flooding of a box-shaped barge. Helsinki University of Technology Helsinki.
- Ruponen, P. 2007. Progressive flooding of a damaged passenger ship. [PhD thesis], Helsinki University of Technology.
- Ruponen, P., Sundell, T. and Larmela, M. 2007. Validation of a simulation method for progressive flooding. *International Shipbuilding Progress*, 54, pp. 305-321.

- Sadat-Hosseini, H., Kim, D.-H., Carrica, P. M., Rhee, S. H. and Stern, F. 2016. URANS simulations for a flooded ship in calm water and regular beam waves. *Ocean Engineering*, 120, 318-330.
- Salvesen, N., Tuck, E. and Faltinsen, O. 1970. Ship motions and sea loads. *Trans. SNAME*, 78, 250-287.
- Santos, T. and Guedes Soares, C. 2000. The influence of obstructions on the transient asymmetric flooding of Ro-Ro ships. *Proceedings of the 7th International Conference on Stability for Ships and Ocean Vehicles (STAB2000)*. Feb 7-12. Launceston, Australia.
- Santos, T. and Guedes Soares, C. 2008a. Global loads due to progressive flooding in passenger ro-ro ships and tankers. *Ships and Offshore Structures*, 3, 289-303.
- Santos, T. A. and Guedes Soares, C. 2008b. Study of damaged ship motions taking into account floodwater dynamics. *Journal of Marine Science and Technology*, 13, 291-307.
- Santos, T. A. and Guedes Soares, C. 2009. Numerical assessment of factors affecting the survivability of damaged Ro-Ro ships in waves. *Ocean Engineering*, 36, 797-809.
- Santos, T., Dupla, P. and Guedes Soares, C. 2009. Numerical simulation of the progressive flooding of a box-shaped barge. *Proceedings of the 10th International Conference on Stability of Ships and Ocean Vehicles*. St. Petersburg.
- Saydan, D. 2006. Damage stability as a safety criterion for optimization tools. [PhD Thesis], University of Southampton.
- Santos, T., Winkle, I. and Guedes Soares, C. 2002. Time domain modelling of the transient asymmetric flooding of Ro-Ro ships. *Ocean Engineering*, 29, pp. 667-688.
- Sen, P. and Konstantinidis, C. 1987. A time simulation approach to the assessment of damage survivability of RO/RO cargo ships. *Society of Naval Architects and Marine Engineers-Transactions*, 95, pp. 337-355.
- Serani, A., Fasano, G., Liuzzi, G., Lucidi, S., Iemma, U., Campana, E. F., Stern, F. and Diez, M. 2016. Ship hydrodynamic optimization by local hybridization of deterministic derivative-free global algorithms. *Applied Ocean Research*, 59, pp. 115-128.
- Shao, J.R., Li, H.Q., Liu, G.R. and Liu, M.B., 2012a. An improved SPH method for modeling liquid sloshing dynamics. *Computers and Structures*, 100, pp.18-26.
- Shao, J.R., Liu, M.B., Yang, X.F. and Cheng, L., 2012b. Improved smoothed particle hydrodynamics with rans for free-surface flow problems. *International journal of computational methods*, 9(01), p.1240001

Skaar, D., Vassalos, D. and Jasionowski, A. 2006. The use of a meshless CFD method in modelling progressive flooding and damaged stability of ships. *Proceedings of the 9th International Conference on the Stability of Ships and Ocean Vehicles*. Rio de Janeiro. pp. 625-632.

Soo Kim, M., Sun Park, J. and Lee, W. I. 2003. A new VOF-based numerical scheme for the simulation of fluid flow with free surface. Part II: application to the cavity filling and sloshing problems. *International Journal for Numerical Methods in Fluids*, 42, pp. 791-812.

Spanos, D. and Papanikolaou, A. 2001a. Numerical study of the damage stability of ships in intermediate stages of flooding. *Proceedings of the Fifth International Workshop on Ship Stability*, Trieste, Italy, Sep.

Spanos, D. and Papanikolaou, A. 2001b. On the stability of fishing vessels with trapped water on deck. *Ship Technology Research*, 48, 124-133.

Spanos, D., Maron, A. and Papanikolaou, A. 2002a. On the motions of a flooded ro-ro ferry in beam seas. *Proceedings 10th International Conference, IMAM'02*. Crete, Greece. May, 2002.

Spanos, D., Papanikolaou, A. and Tzabiras, G. 2002b. On the effect of water on deck on ship motions and capsizing. *Proceeding of 21st International Conference on Offshore Mechanics and Arctic Engineering, OMAE'02*. Oslo, Norway. June 23-28, 2002.

Spouge, J. 1985. The technical investigation of the sinking of the Ro-Ro ferry EUROPEAN GATEWAY. *Transactions of Royal Institution of Naval Architects*, 127, pp. 49-72.

SSPA Consortium. 2008. Final Report-Research Study on the Sinking Sequence of MV Estonia. No. 134. SSPA Research Report.

STAR-CCM+. 2017. STAR-CCM+ User Guide. Version 12.06 ed.: SIEMENS.

Strasser, C., Jasionowski, A. and Vassalos, D. 2009. Calculation of the time-to-flood of a box-shaped barge by using CFD. *Proceedings of 10th International Conference on Stability of Ships and Ocean Vehicles*. St. Petersburg, Russia.

Stubbs, J. and Molyneux, D. 1996. Flooding protection of ro-ro ferries. *Transactions of the Royal Institution of Naval Architects*, 138, pp. 103-116.

Tang, Alan Shung-tse. 1991. Large amplitude forced roll motion in two dimensions: experiments and theory. [PhD Thesis]. University of Southampton.

Temarel, P., Bai, W., Bruns, A., Derbanne, Q., Dessi, D., Dhavalikar, S., Fonseca, N., Fukasawa, T., Gu, X. and Nestegård, A. 2016. Prediction of wave-induced loads on ships: Progress and challenges. *Ocean Engineering*, 119, 274-308.

- Valanto, P. 2009. Research for the Parameters of the Damage Stability Rules including the Calculation of Water on Deck of Ro-Ro Passenger Vessels, for the amendment of the Directives 2003/25/EC and 98/18/EC. HSVA Report.
- Vandeveldt, K. 2006. Herald of free enterprise. Handbook on drowning. Heidelberg: Springer.
- Van't Veer, R., Peters, W., Rimpela, A.-L. and De Kat, J. 2011. Exploring the influence of different arrangements of semi-watertight spaces on survivability of a damaged large passenger ship. *Contemporary Ideas on Ship Stability and Capsizing in Waves*. Springer.
- Vassalos, D. and Turan, O. 1994. A realistic approach to assessing the damage survivability of passenger ships. *Transactions of the Society of Naval Architects and Marine Engineers*, Vol. 102, pp. 367-394.
- Vassalos, D. 2000. The water on deck problem of damage Ro-Ro ferries. *Contemporary ideas on ship stability*. Oxford: Elsevier Science.
- Vassalos, D., Ikeda, Y., Jasionowski, A. and Kuroda, T. 2004. Transient flooding on large passenger ships. *Proceedings of the Seventh International Ship Stability Workshop*. Shanghai, China.
- Vermeer, H., Vredeveldt, A. and Journée, J. 1994. Mathematical modelling of motions and damaged stability of ro-ro ships in the intermediate stages of flooding. *Fifth International Conference on Stability of Ships and Ocean Structures*. Melbourne, Florida, USA.
- Versteeg, H. K. and Malalasekera, W. 2007. An introduction to computational fluid dynamics: the finite volume method, Pearson Education.
- Vredeveldt, A. and Journée, J. 1991. Roll motions of ships due to sudden water ingress, calculations and experiments. *International Conference on Ro-Ro Safety and Vulnerability-The Way Ahead*. London. Apr. 17-19, 1991.
- Wang, X. and Arai, M., 2011. A study on coupling effect between seakeeping and sloshing for membrane-type LNG carrier. *International Journal of Offshore and Polar Engineering*, 21(04).
- Wood, C., Hudson, D. A. and Tan, M. 2010. CFD simulation of orifice flow for the flooding of damaged ships. *Proceedings of the 3th Numerical Towing Tank Symposium*. Duisburg, Germany.
- Woodburn, P. 2000. Fundamentals of damaged ship survivability. W.S. Atkins Consultants Ltd. Report, AM3896-R4.

- Wu, M. and Hermundstad, O. A. 2002. Time-domain simulation of wave-induced nonlinear motions and loads and its applications in ship design. *Marine Structures*, 15, 561-597.
- Xia, J., Jensen, J. J. and Pedersen, P. T. 1999. A Dynamic Model for Roll Motion of Ships due to Flooding. *Ship Technology Research*, 46, 208-216.
- Xue, M.A., Zheng, J. and Lin, P., 2012. Numerical simulation of sloshing phenomena in cubic tank with multiple baffles. *Journal of Applied Mathematics*, 2012.
- Yeung, R., Roddier, D., Alessandrini, B., Gentaz, L. and Liao, S. 2001. On roll hydrodynamics of cylinders fitted with bilge keels. *Twenty-Third Symposium on Naval Hydrodynamics Office of Naval Research*. Bassin d'Essais des Carenes National Research Council.
- Younes, M.F., Younes, Y.K., El-Madah, M., Ibrahim, I.M. and El-Dannanh, E.H., 2007. An experimental investigation of hydrodynamic damping due to vertical baffle arrangements in a rectangular tank. *Proceedings of the Institution of Mechanical Engineers, Part M: Journal of Engineering for the Maritime Environment*, 221(3), pp.115-123.
- Yunus, A.C. and Cimbala, J.M. 2006. Fluid mechanics fundamentals and applications. International Edition, McGraw Hill Publication.
- Zhang, A.-M., Cao, X.-Y., Ming, F.-R. and Zhang, Z.-F. 2013. Investigation on a damaged ship model sinking into water based on three dimensional SPH method. *Applied Ocean Research*, 42, 24-31.
- Zhang, H. and Sun, B., 2014. Numerical simulation of sloshing in 2D rectangular tanks based on the prediction of free surface. *Mathematical Problems in Engineering*, 2014.
- Zhang, Y.X., Wan, D.C. and Hino, T., 2014. Comparative study of MPS method and level-set method for sloshing flows. *Journal of hydrodynamics*, 26(4), pp.577-585.
- Zhao, W., Yang, J., Hu, Z. and Tao, L., 2014a. Coupled analysis of nonlinear sloshing and ship motions. *Applied Ocean Research*, 47, pp.85-97.
- Zhao, W., Yang, J., Tao, L. and White, D., 2014b, June. Research on the coupling effects between ship motions and sloshing. In *ASME 2014 33rd International Conference on Ocean, Offshore and Arctic Engineering* (pp. V08BT06A005-V08BT06A005). American Society of Mechanical Engineers.
- Zhu, S. and Moan, T., 2013. New insight into the wave-induced nonlinear vertical load effects of ultra-large container ships based on experiments. *Journal of marine science and technology*, 18(1), pp.87-114.

Zhuang, Y., Yin, C.H., Wan, D.C., 2016, August. Numerical study on ship motion coupled with LNG tank sloshing using dynamic overset grid approach. *The 7th International Conference on Computational Methods (ICCM-2016)*, Berkeley, USA.

URL 1 :

<https://www.strath.ac.uk/engineering/navalarchitectureoceanmarineengineering/ourfacilities/kelvinhydrodynamiclaboratory/>

# Appendix

## Appendix 1

In Appendix 1, plots are supplemented for coupling effect of load cell (Section 3.5.2).

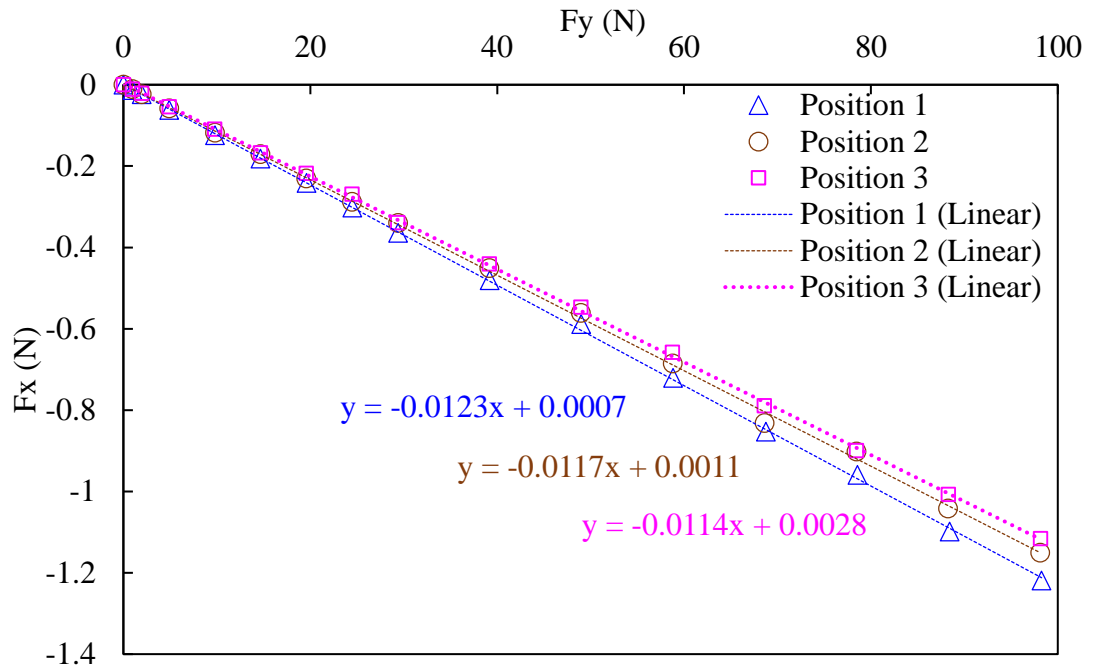


Figure A1.1.  $F_x$  caused by  $F_y$

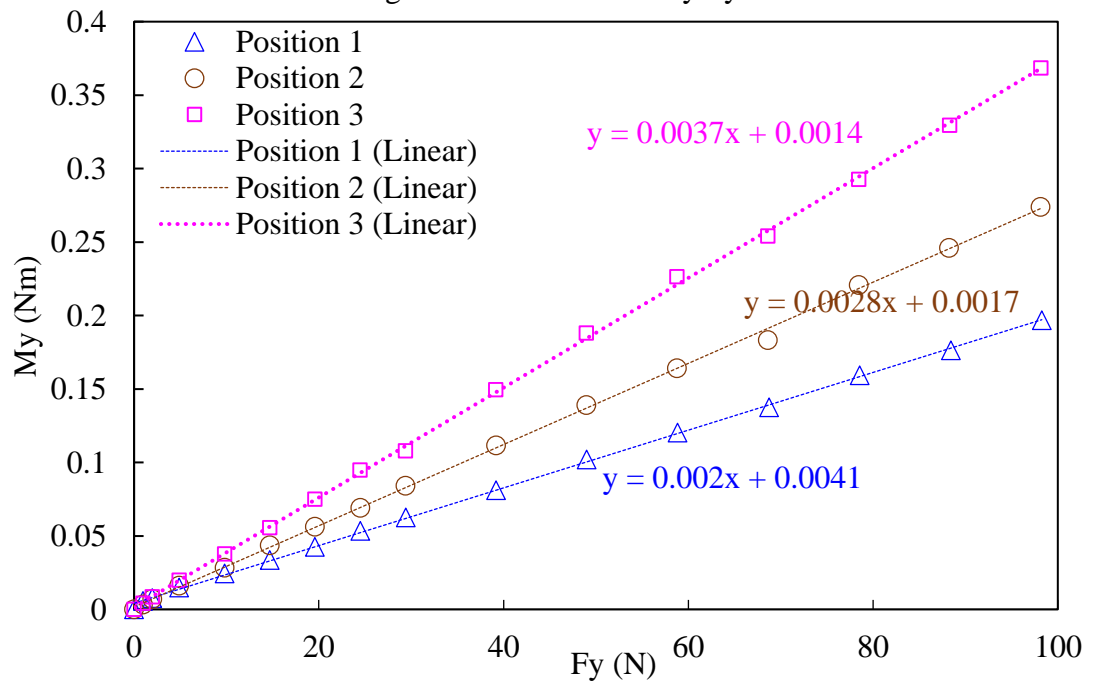


Figure A1.2.  $M_y$  caused by  $F_y$



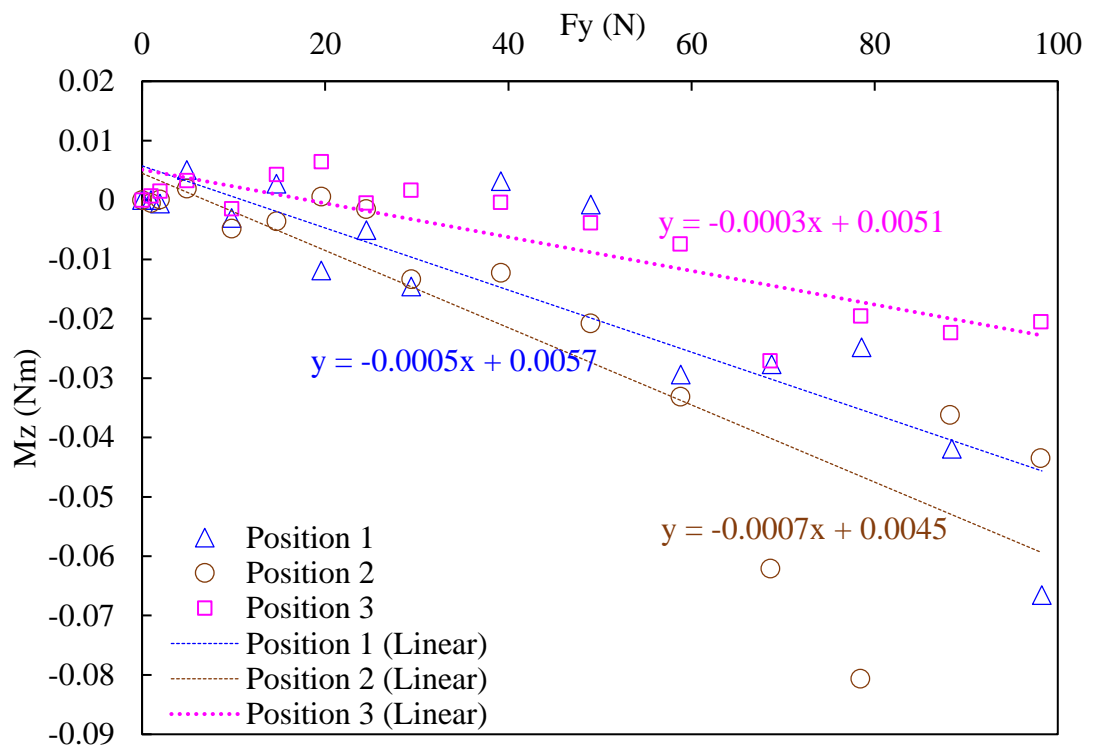


Figure A1.3.  $M_z$  caused by  $F_y$

## Appendix 2 Runge-Kutta method and $I_{xx}$ approximation by CFD

### A2.1 Methodology

This section introduces an alternative way to estimate the mass moment of inertia of roll motion. Runge-Kutta method can be applied to obtain the coefficients in roll motion equation. Since there is zero wave excitation moment in free roll decrement, total mass moment of inertia, damping and restoring items then can be solved due to Runge-Kutta method. Considering linear equation of free roll decay motion, which is shown as Equation (A2.1):

$$(I_{xx} + A_{xx})\ddot{\theta} + b\dot{\theta} + k\theta = 0 \quad (\text{A2.1})$$

where

$I_{xx}$  is the mass moment of inertia of roll motion

$A_{xx}$  is the added mass moment of inertia of roll motion

$b$  is the linear damping

$k$  is the linear restoring

$\theta$  is angle of roll motion

The root-mean-square errors (RMSE) between measured data from the experiments and solutions are minimized by the Generalized Reduced Gradient (GRG) method. Total mass moment of inertia ( $I_{xx}+A_{xx}$ ) of roll motion can be obtained until the RMSE reaches a minimum value. The root-mean-square errors (RMSE) is expressed by

$$RMSE = \sqrt{\frac{\sum_{i=1}^N (\theta_{s,i} - \theta_{t,i})^2}{N}}$$

Where

$\theta_{s,i}$  is the generated value by Runge-Kutta method

$\theta_{t,i}$  is the measured data from physical model tests.

Since  $I_{xx}+A_{xx}$  has been obtained, the mass of moment of inertia of the ship model ( $I_{xx}$ ) now has scope to below  $I_{xx}+A_{xx}$  and it can be estimated by trial and error with CFD

simulations. To simulate free roll decay test by CFD method, mass moment of inertia is taken as the only changeable variable, so different mass moments of inertia are trial to be input into CFD simulations, but other particulars including draft, mass, initial angle are remained. Besides, it is assumed that added mass moment of inertia of roll motion ( $A_{xx}$ ) is not changed no matter how much the specified mass moment of inertia is imported. Meanwhile, to eliminate the effectiveness of RANS solver, mesh scheme, boundary conditions and solver's setting are kept constant. With decay curves obtained by CFD simulation due to input values of mass moment of inertia of ship's roll motion, Runge-Kutta method is applied to obtain total mass moment of inertia considering linear equation of roll decay motion. Then the total mass moment of inertia obtained from CFD simulations are compared with that obtained by physical tests so that an error between them means the difference between the input mass moment of inertia about ship's roll motion into CFD simulation and true value. Through trial and error, a reasonable mass moment of inertia about ship's roll motion can be eventually approximated.

## **A2.2 2-Dimensional validation**

To validate the feasibility of this methodology, a 2-dimensional simulation that stated in Section 4.3.2 is applied. Let us suppose that the mass moment of inertia about the structure's roll motion is unknown so that an initial guess is given to the mass moment of inertia ( $I_{xx}$ ). It is assumed that added mass moment of inertia ( $A_{xx}$ ) is maintained to be the same when the input of mass moment of inertia varies. Considering linear mass and restoring in motion equation shown as below, total mass moment of inertia ( $I_{xx}+A_{xx}$ ), linear damping ( $b$ ) and linear restoring ( $k$ ) can be obtained by Runge-Kutta method.

$$(I_{xx} + A_{xx})\ddot{\theta} + b\dot{\theta} + k\theta = 0$$

where  $I_{xx}$  is the mass moment of inertia of roll motion, which can be expressed by mass of the body  $m$  and radius of gyration  $k_{xx}$ , as

$$I_{xx} = mk_{xx}^2$$

Firstly, free decay curve obtained by physical model test is approximated by Runge-Kutta method applied to roll motion equation, and solution is presented in Figure A2.1 and Table A2.1.

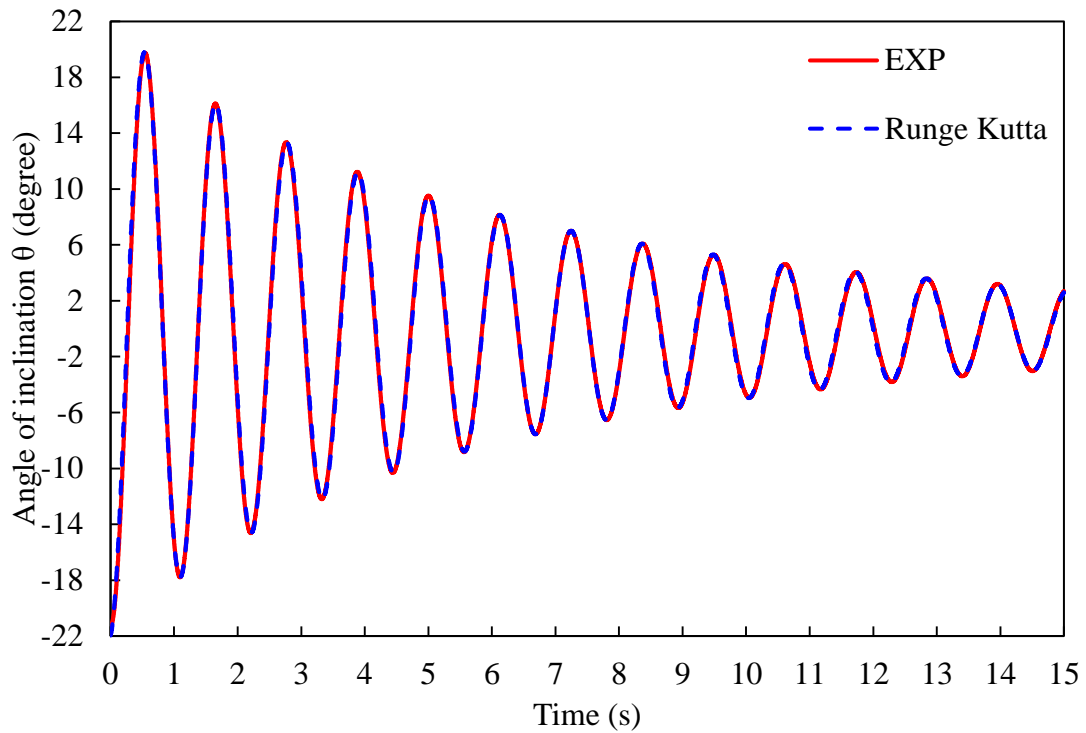


Figure A2.1. Solution by Runge-Kutta method

Table A2.1 Solutions by Runge-Kutta method

	$I_{xx}+A_{xx}$	$b$	$k$	$RMSE$
EXP	0.0138	0.0026	0.4353	0.3148

A reasonably initial (guessed) value for the radius of gyration of rolling can be  $k_{xx}=0.31B$  based on the approximation range recommended by Bhattacharyya (1978). By  $I_l=0.009 \text{ kgm}^2$  ( $k_l=0.31B$ ), approximations as well as solutions that solved by Runge-Kutta method are shown in Figure A2.2 and Table A2.2.

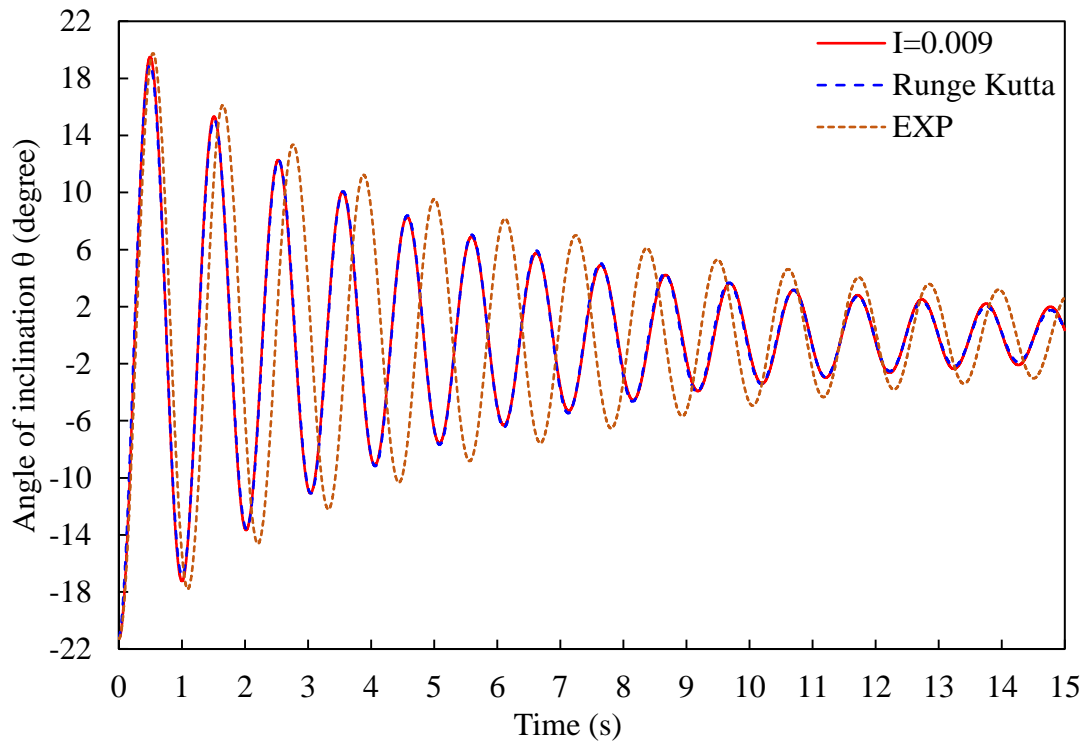


Figure A2.2. Free decay solution solved by Runge-Kutta with  $I=0.009 \text{ kgm}^2$

Table A2.2. Summary of solutions with Runge-Kutta method

	$I_{xx}+A_{xx}$	$b$	$k$	RMSE
EXP	0.0138	0.0026	0.4353	0.3148
I=0.009	0.0115	0.003	0.4357	0.2463

From Table A2.2, added mass moment of inertia ( $A_{xx}$ ) can be equal to  $0.0025 \text{ kgm}^2$ , which is assumed to be kept constant so that  $I_{xx}$  is the difference between the total mass moment of inertia ( $I_{xx}+A_{xx}=0.0138 \text{ kgm}^2$ ) solved for model test and obtained added mass moment of inertia ( $A_{xx}=0.0025 \text{ kgm}^2$ ), and therefore,  $I_{xx}$  equals to  $0.0113 \text{ kgm}^2$ . Compared to  $I_{xx}=0.01122 \text{ kgm}^2$  provided by Irkal et al. (2016), error is about 0.7%.

To further scientifically validate this method, another two input values for mass moment of inertia,  $I=0.01 \text{ kgm}^2$  and  $I=0.011 \text{ kgm}^2$  are calculated by RANS solver. Solutions are given in Figure A2.3, applied Runge-Kutta method, and the summary can be shown in Table A2.3. It can be seen that error of solved results can be less than 1% to approach the desired value of actual mass moment of inertia, which is validated for this method to be applied for obtaining an approximate value of actual mass

moment of inertia of the physical model (DTMB-5415) in physical experiment, and it will be further described in the next section.

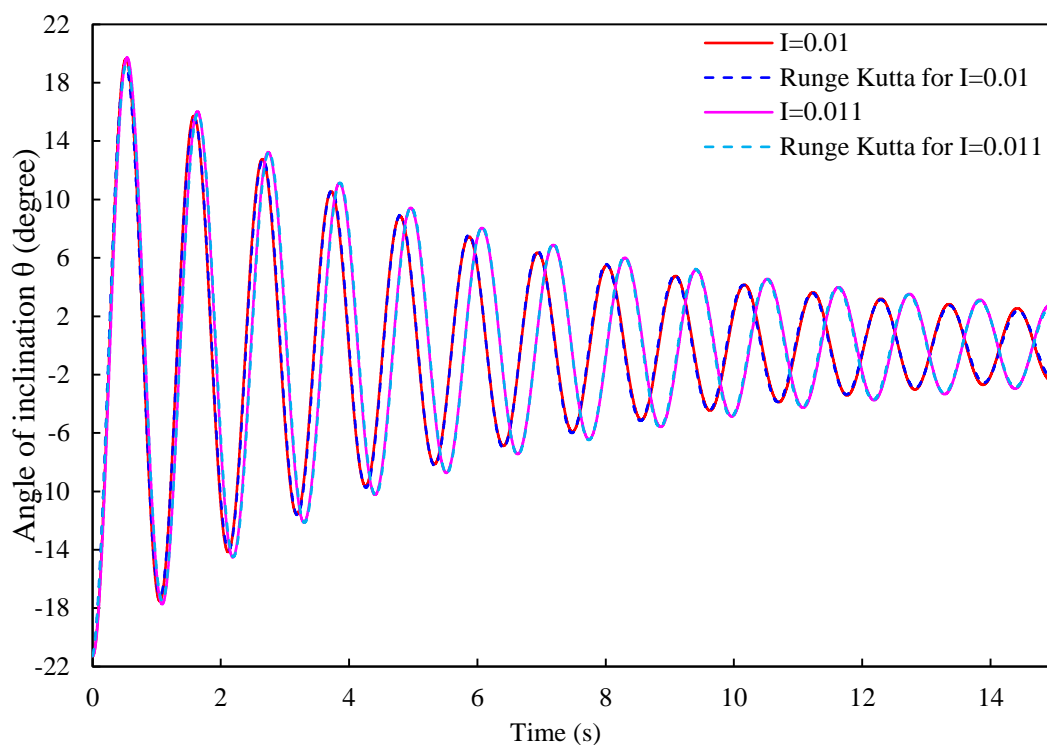


Figure A2.3. Free decay solution solved by Runge-Kutta with  $I=0.01 \text{ kgm}^2$  and  $I=0.011 \text{ kgm}^2$

Table A2.3. Summary of coefficients solved by Runge-Kutta method

	EXP	I=0.009	I=0.010	I=0.011
$I_{xx}$ input	-	0.009	0.010	0.011
$I_{xx} + A_{xx}$	0.01377	0.01148	0.01260	0.01351
$b$	0.0026	0.0030	0.0029	0.0028
$k$	0.4353	0.4357	0.4344	0.4344
RMSE	0.3148	0.2463	0.2915	0.3150
$A_{xx}$	-	0.00248	0.00260	0.00251
$I_{xx}$ calculated	-	0.01129	0.01117	0.01126
Error	-	0.624%	0.446%	0.357%

### A2.3 Estimation on mass moment of inertia about ship's roll motion

Firstly, Runge-Kutta method is applied to solve ship's roll decay motion in physical tests to obtain the total mass moment of inertia about ship's roll motion ( $I_{xx}+A_{xx}$ ).

Figure A2.4 illustrates comparisons for roll decrement tests on intact ship model with moorings between measurement and solution by Runge-Kutta method considering linear mass, damping and restoring items. Solution of damaged ship's roll decay test with moorings is shown in Figure A2.5. It can be seen that a good fit is achieved for the intact and damaged ship's free roll decrements with linear roll motion equation. Summary of results about roll decay tests for intact and damaged scenarios is listed in Table A2.4.

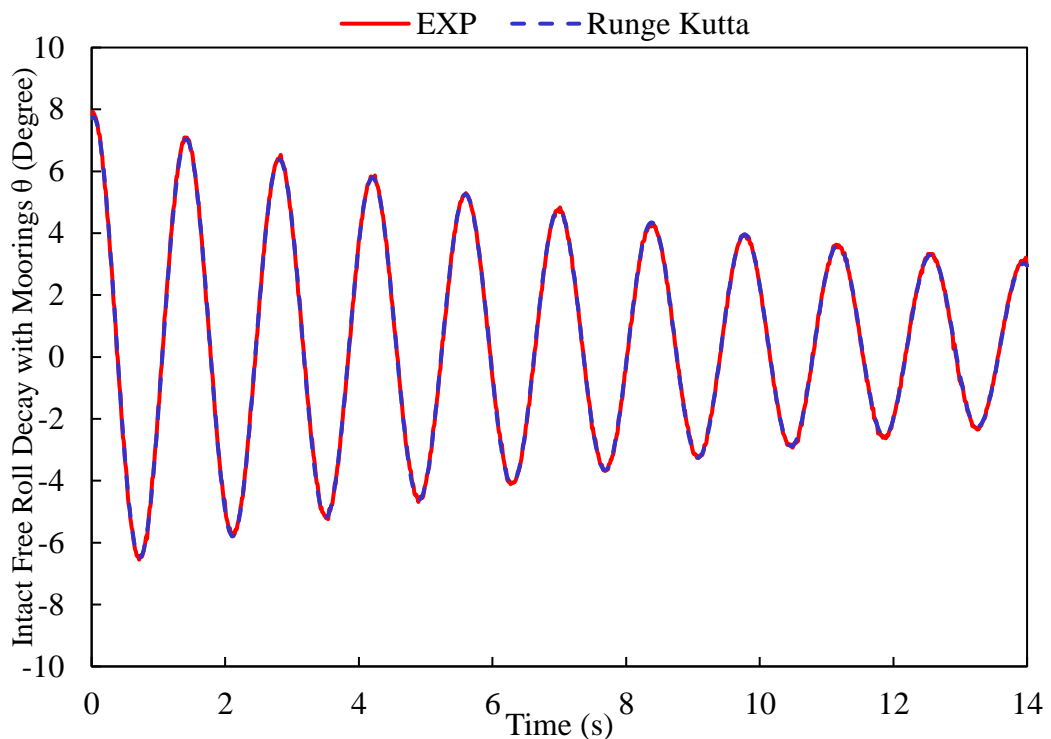


Figure A2.4. Comparison between measurement and solution by Runge-Kutta method with all linear components

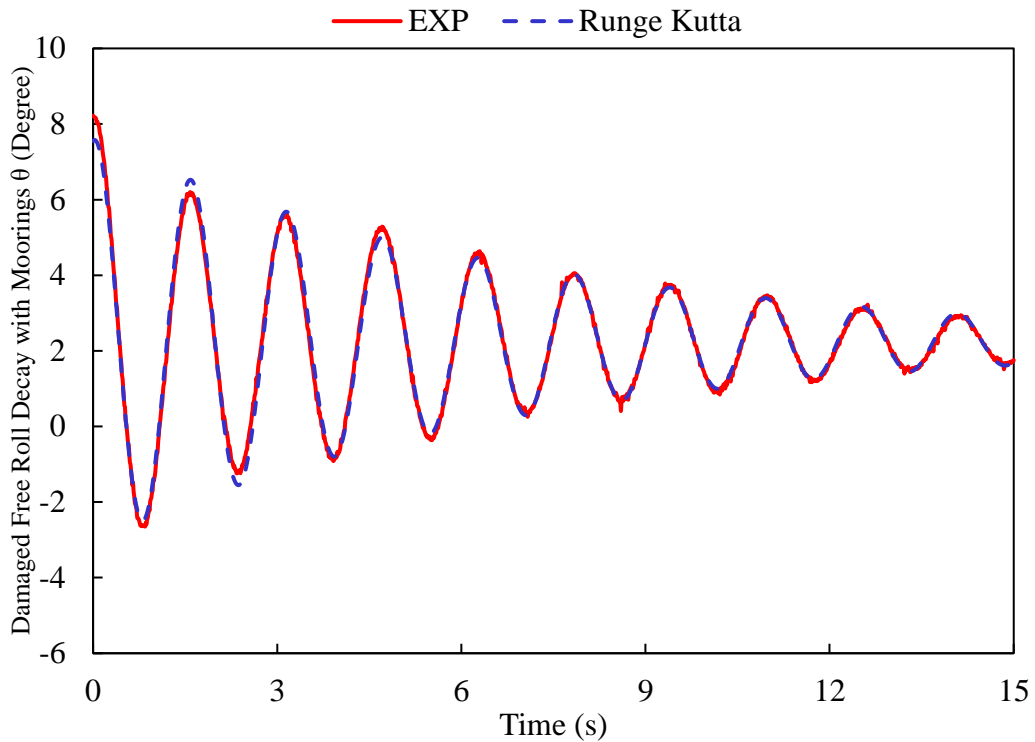


Figure A2.5. Runge-Kutta solution for decay curve of the damaged ship

Table A2.4. Summary of calculation results by Runge-Kutta method

Case	Linear mass	Linear damping	Linear restoring	RMSE
Intact with moorings	1.177	0.177	24.001	0.067
Damaged with moorings	1.481	0.419	24.003	0.114

To estimate mass moment of inertia about ship's roll motion by CFD method, an initial value  $0.928 \text{ kgm}^2$  (radius of gyration  $k_{xx}=0.3B$ ) is assigned to mass moment of inertia of ship's roll motion about its longitudinal axis. Ship model is heeled with 7.5 degree and released to freely rotate. With solution by Runge-Kutta method, results are compared with experimental data which are shown in Figure A2.6. Table A2.5 lists solutions by Runge-Kutta method considering linear mass ( $I_{xx}+A_{xx}$ ), linear damping ( $b$ ) and restoring ( $k$ ) items.



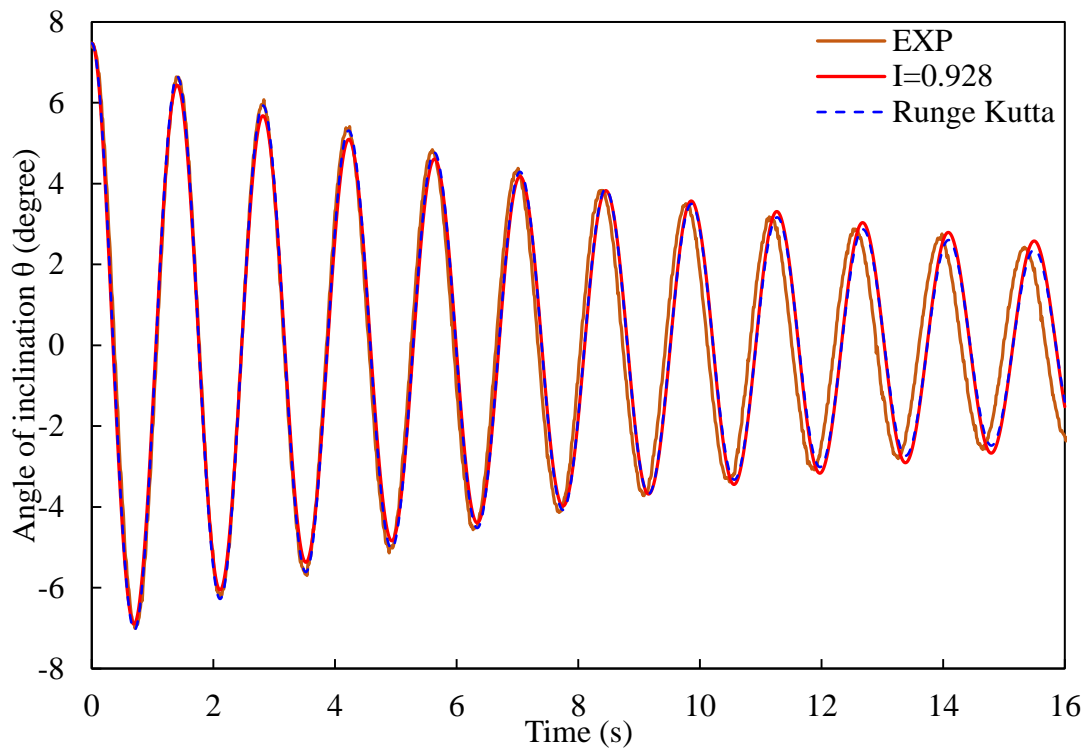


Figure A2.6. Comparisons among experimental data and solutions as  $I=0.928 \text{ kgm}^2$

Table A2.5. Solutions by Runge-Kutta method

	$I_{xx} + A_{xx}$	$b$	$k$	RMSE
EXP	1.177	0.159	24.044	0.095
I=0.928	1.209	0.184	24.043	0.120

As total mass moment of inertia obtained by Runge-Kutta method is equal to  $1.209 \text{ kgm}^2$ , calculated added mass moment of inertia ( $A_{xx}$ ) equals to  $0.281 \text{ kgm}^2$ . Then calculated mass moment of inertia ( $I_{xx}$ ) is  $0.897 \text{ kgm}^2$ . To scientifically validate this calculated  $I_{xx}$ , it is input as mass moment of inertia about the ship's roll motion once more to simulate free rotation decay by CFD method, and decay curve can be shown in Figure A2.7 compared with physical test. Summary of solutions by Runge-Kutta method are listed in Table A2.6, where it is seen that an approximation of mass moment of inertia about ship's roll motion can be well estimated.

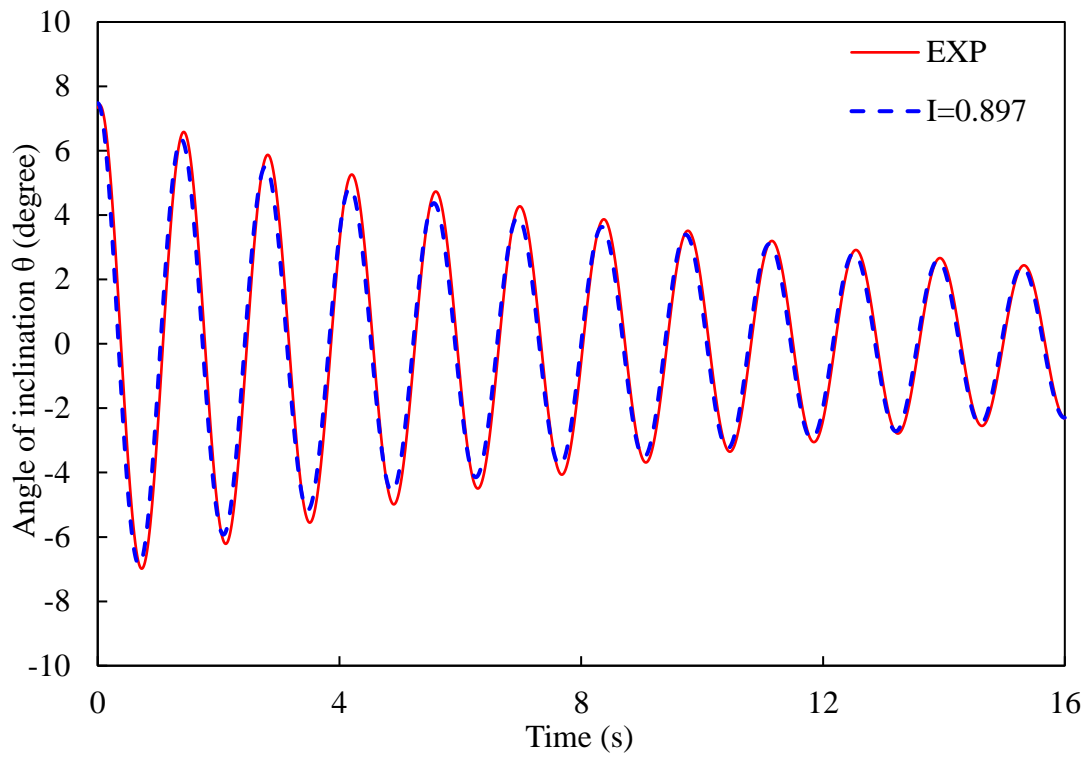


Figure A2.7. Angle of inclination of free decay for  $I=0.897 \text{ kgm}^2$

Table A2.6. Summary of solutions by Runge-Kutta method

	$I_{xx} + A_{xx}$	$A_{xx}$	$b$	$k$	RMSE
EXP	1.177	-	0.159	24.044	0.095
I=0.928	1.209	0.281	0.184	24.043	0.120
I=0.897	1.178	0.281	0.160	24.053	0.115

## Appendix 3 Transformation of reference frames and the application of Newton's law

### A3.1 Methodology

#### A3.1.1 Acceleration

Since all the wave induced loads measured by the load cell are detected based on the coordinate system established at the origin of the load cell, but Newton's Second Law is only valid in an inertial coordinate system, to analyse an acceleration of an arbitrary particle in the ship, a non-inertial coordinate system is established at the centre of gravity of ship.

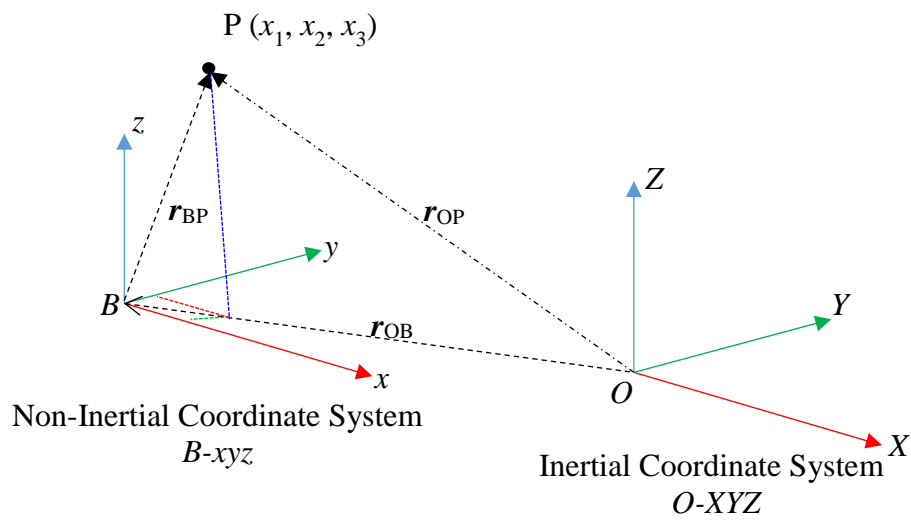


Figure A3. 1. Sketch of inertial and non-inertial coordinate system for rigid body motion

Considering inertial coordinate system ( $O-XYZ$ ) and a body-with non-inertial coordinate system ( $B-xyz$ ) shown in Figure A3. 1. Let  $e$  be the unit vector fixed in the body-with coordinate system, i.e.

$$e = \sum_{i=1}^3 e_i = e_1 \mathbf{i} + e_2 \mathbf{j} + e_3 \mathbf{k}$$

Then, the rate of rotational change of  $e$  from the view of the non-inertial coordinate system  $B$  can be expressed as

$$\frac{de}{dt} = \omega \times e$$

Considering a particle  $P(x_1, x_2, x_3)$ ,  $\mathbf{r}_{OB}$  is the relative vector from the origin of inertial coordinate system  $O$  to that of non-inertial coordinate system  $B$ ;  $\mathbf{r}_{PB}$  is the position vector from the origin of non-inertial coordinate system  $B$  to particle  $P$ ;  $\mathbf{r}_{OP}$  is the position vector of particle  $P$  relative to the origin of inertial coordinate system  $O$ , then

$$\mathbf{r}_{OP} = \mathbf{r}_{OB} + \mathbf{r}_{BP} = \mathbf{r}_{OB} + \sum_{i=1}^3 x_i \mathbf{e}_i$$

As particle  $P$  moves, the rate of positional change is

$$\frac{d\mathbf{r}_{OP}}{dt} = \frac{d\mathbf{r}_{OB}}{dt} + \frac{d\mathbf{r}_{BP}}{dt} = \frac{d\mathbf{r}_{OB}}{dt} + \frac{d(\sum_{i=1}^3 x_i \mathbf{e}_i)}{dt}$$

where,

$$\frac{d(\sum_{i=1}^3 x_i \mathbf{e}_i)}{dt} = \sum_{i=1}^3 \frac{dx_i}{dt} \mathbf{e}_i + \sum_{i=1}^3 x_i \frac{d\mathbf{e}_i}{dt}$$

Thus, the rate of positional change can be rewritten as

$$\frac{d\mathbf{r}_{OP}}{dt} = \frac{d\mathbf{r}_{OB}}{dt} + \sum_{i=1}^3 \frac{dx_i}{dt} \mathbf{e}_i + \sum_{i=1}^3 x_i \frac{d\mathbf{e}_i}{dt}$$

Further,

$$\begin{aligned} \frac{d^2\mathbf{r}_{OP}}{dt^2} &= \frac{d}{dt} \left( \frac{d\mathbf{r}_{OB}}{dt} + \sum_{i=1}^3 \frac{dx_i}{dt} \mathbf{e}_i + \sum_{i=1}^3 x_i \frac{d\mathbf{e}_i}{dt} \right) \\ &= \frac{d^2\mathbf{r}_{OB}}{dt^2} + \frac{d}{dt} \left( \sum_{i=1}^3 \frac{dx_i}{dt} \mathbf{e}_i \right) + \frac{d}{dt} \left( \sum_{i=1}^3 x_i \frac{d\mathbf{e}_i}{dt} \right) \\ &= \frac{d^2\mathbf{r}_{OB}}{dt^2} + \sum_{i=1}^3 \frac{d^2x_i}{dt^2} \mathbf{e}_i + \sum_{i=1}^3 \frac{dx_i}{dt} \frac{d\mathbf{e}_i}{dt} + \sum_{i=1}^3 \frac{dx_i}{dt} \frac{d\mathbf{e}_i}{dt} + \sum_{i=1}^3 x_i \frac{d^2\mathbf{e}_i}{dt^2} \\ &= \frac{d^2\mathbf{r}_{OB}}{dt^2} + \sum_{i=1}^3 \frac{d^2x_i}{dt^2} \mathbf{e}_i + 2 \sum_{i=1}^3 \frac{dx_i}{dt} \frac{d\mathbf{e}_i}{dt} + \sum_{i=1}^3 x_i \frac{d^2\mathbf{e}_i}{dt^2} \end{aligned}$$

The above two equations illustrate the velocity and acceleration of particle  $P$  as it motions in the inertial coordinate system. For each item

$d\mathbf{r}_{OP}/dt$  is the velocity vector of particle  $P$  moving in the inertial coordinate system

$d^2\mathbf{r}_{OP}/dt^2$  is the acceleration vector of particle  $P$  moving in the inertial coordinate system

$d\mathbf{r}_{OB}/dt$  is the relative velocity vector of non-inertial coordinate system relative to the inertial coordinate system

$d^2\mathbf{r}_{OB}/dt^2$  is the relative acceleration vector of non-inertial coordinate system relative to the inertial coordinate system

$\sum dx_i \mathbf{e}_i/dt$  is the velocity vector of particle  $P$  in the non-inertial coordinate system

$\sum d^2x_i \mathbf{e}_i/dt^2$  is the acceleration vector of particle  $P$  in the non-inertial coordinate system

$d\mathbf{e}_i/dt$  and  $d^2\mathbf{e}_i/dt^2$  are the components about the rotational change of non-inertial coordinate system relative to the inertial coordinate system. If non-inertial coordinate system  $B$  does not have rotational motion relative to the inertial coordinate system  $O$ ,  $d\mathbf{e}_i/dt$  and  $d^2\mathbf{e}_i/dt^2$  are equal to zero.

Let  $\boldsymbol{\omega}$  be the rotational velocity vector of non-inertial coordinate system  $B$  relative to the inertial coordinate system  $O$ . Again, it can be reminded that if non-inertial coordinate system  $B$  has a rotational motion relative to inertial coordinate system, the differentiated vector  $d\mathbf{e}/dt$  with respect to time can be conducted as

$$\frac{d\mathbf{e}}{dt} = \boldsymbol{\omega} \times \mathbf{e}$$

therefore,

$$\frac{d^2\mathbf{e}}{dt^2} = \frac{d}{dt}(\boldsymbol{\omega} \times \mathbf{e}) = \frac{d\boldsymbol{\omega}}{dt} \times \mathbf{e} + \boldsymbol{\omega} \times \frac{d\mathbf{e}}{dt} = \frac{d\boldsymbol{\omega}}{dt} \times \mathbf{e} + \boldsymbol{\omega} \times (\boldsymbol{\omega} \times \mathbf{e})$$

So that as it is substituted back to the acceleration of  $\mathbf{r}_{OP}$ , it can be expressed as

$$\frac{d^2\mathbf{r}_{OP}}{dt^2} = \frac{d^2\mathbf{r}_{OB}}{dt^2} + \frac{d^2\mathbf{r}_{BP}}{dt^2} + 2 \sum_{i=1}^3 \frac{dx_i}{dt} (\boldsymbol{\omega} \times \mathbf{e}_i) + \sum_{i=1}^3 x_i \left[ \frac{d\boldsymbol{\omega}}{dt} \times \mathbf{e}_i + \boldsymbol{\omega} \times (\boldsymbol{\omega} \times \mathbf{e}_i) \right]$$

Where,

$$\sum_{i=1}^3 \frac{dx_i}{dt} (\boldsymbol{\omega} \times \mathbf{e}_i) = \boldsymbol{\omega} \times \mathbf{v}_{BP}$$

$$\sum_{i=1}^3 x_i \left[ \frac{d\boldsymbol{\omega}}{dt} \times \mathbf{e}_i + \boldsymbol{\omega} \times (\boldsymbol{\omega} \times \mathbf{e}_i) \right] = \boldsymbol{\alpha} \times \mathbf{r}_{BP} + \boldsymbol{\omega} \times (\boldsymbol{\omega} \times \mathbf{r}_{BP})$$

Finally, it can be written as

$$\mathbf{a}_{OP} = \mathbf{a}_{OB} + \mathbf{a}_{BP} + 2\boldsymbol{\omega} \times \mathbf{v}_{BP} + \boldsymbol{\alpha} \times \mathbf{r}_{BP} + \boldsymbol{\omega} \times (\boldsymbol{\omega} \times \mathbf{r}_{BP})$$

i.e. when a ship moves discretionarily with translation and rotation in inertial (or global) coordinate system ( $O\text{-}XYZ$ ), a non-inertial coordinate system ( $B\text{-}xyz$ ) is attached at its centre of gravity, acceleration of an arbitrary particle  $P$  on the ship can be expressed within separated components as

$\mathbf{a}_{OP}$  is the acceleration of the particle  $P$  relative to the inertial coordinate system

$\mathbf{a}_{OB}$  is the acceleration of the ship relative to the inertial coordinate system

$\mathbf{a}_{BP}$  is the acceleration of the particle  $P$  relative to the non-inertial coordinate system

$\mathbf{r}_{BP}$  is the position vector of the particle  $P$  relative to the origin of the non-inertial coordinate system

$\mathbf{v}_{BP}$  is the translational velocity of the particle  $P$  relative to the non-inertial coordinate system

$\boldsymbol{\omega}$  is the angular velocity of the ship

$\boldsymbol{\alpha}$  is the angular acceleration of the ship

### A3.1.2 Force acting on the particle

As stated earlier Newton's Second Law is only valid on inertial coordinate system. Applying Newton's Second Law on the particle  $P$ , i.e. the total external forces acting on the particle is equal to the mass times acceleration, as seen from the inertial coordinate system, it can be expressed as

$$\mathbf{F}_T = m\mathbf{a}_{OP}$$

Thus, total forces acting on the particle P can be

$$m\mathbf{a}_{OP} = m\mathbf{a}_{OB} + m\mathbf{a}_{BP} + 2m\boldsymbol{\omega} \times \mathbf{v}_{BP} + m\boldsymbol{\alpha} \times \mathbf{r}_{BP} + m\boldsymbol{\omega} \times (\boldsymbol{\omega} \times \mathbf{r}_{BP})$$

Here,

$m\boldsymbol{\omega} \times \mathbf{v}_{BP}$  is called Coriolis Force component

$m\boldsymbol{\alpha} \times \mathbf{r}_{BP}$  is called Euler Force component

$m\boldsymbol{\omega} \times (\boldsymbol{\omega} \times \mathbf{r}_{BP})$  is called Centrifugal Force component

So, it can be described that correct forces acting on the object of arbitrary particle needs to be considered with additional force components, namely Coriolis force, Centrifugal force and Euler force.

### A3.1.3 Moment acting on the particle

Considering roll motion of a rigid body, concept of momentum  $\mathbf{L}$  needs to be introduced

$$\mathbf{L} = I\boldsymbol{\omega}$$

where  $I$  is the tensor of mass moment of inertia about rotational axes of the body.

And moment acting on the rigid body can be obtained by time differential momentum as

$$\boldsymbol{\tau} = \frac{d\mathbf{L}}{dt} = \frac{d(I\boldsymbol{\omega})}{dt}$$

Similar to the Newton's Second Law, total moment acting on the rigid body is equal to the mass moment of inertia times angular acceleration, which is, however only valid at the inertia coordinate system. Considering the rigid body at the non-inertial coordinate system, the total moment can be expressed by

$$\boldsymbol{\tau} = \frac{d\mathbf{L}}{dt} = \frac{d(I\boldsymbol{\omega})}{dt} + \boldsymbol{\omega} \times (I\boldsymbol{\omega}) = I\boldsymbol{\alpha} + \boldsymbol{\omega} \times (I\boldsymbol{\omega})$$

Where

$\boldsymbol{\alpha}$  is the angular acceleration of the rigid body

$\omega$  is the angular velocity of the rigid body



# List of Figures

Figure 1.1 Damaged hole at waterline (Brown, 2004).....	5
Figure 1.2. Damaged hole at waterline (Brown, 2004).....	5
Figure 1.3. Water inflow from damaged opening (Brown, 2004) .....	6
Figure 1.4. Heel after damage (Miller and Shattuck, 2004).....	7
Figure 1.5. Tear damage (Bole, 2007) .....	8
Figure 1.6. Severe damage (Bole, 2007).....	8
Figure 1.7. Flooding into engine room (Bole, 2007) .....	9
Figure 1.8. A large damaged opening causing flooding (Department of the Navy of USA, 2017) .....	10
Figure 2.1. MV Estonia with bow visor opening (Jaeger, 2008).....	19
Figure 2.2. Flooded compartments during progressive flooding (SSPA Consortium, 2008) .....	19
Figure 2.3. Physical Ro-Ro ship model for reconstruction of Estonia (note the visor attached at bow) (SSPA Consortium, 2008) .....	20
Figure 2.4. Main flooding process (Ruponen, 2007) .....	20
Figure 2.5. Experiment setup. (Ruponen, 2006) .....	24
Figure 2.6. Flooding control mechanism (Manderbacka et al., 2015b).....	25
Figure 2.7. Ship model with a sketch of internal flooded compartments (Lee et al., 2016) .....	26
Figure 2.8. Rapid damage opening indication (Lee et al., 2016).....	26
Figure 2.9. Sketch of experimental settings by Fujiwara and Haraguchi (2002).....	28
Figure 2.10. (a) Flooded compartment with opening system; (b) Internal view at flooded compartment (Khaddaj-Mallat et al., 2012).....	29
Figure 2.11. Large flow obstructions in flooded compartment (Veer and De Kat, 2000) .....	29
Figure 2.12. Model tests setup by Ji et al. (2012) .....	31
Figure 2.13. LNG-FPSO model (Nam and Kim, 2007).....	32
Figure 3.1 Kelvin Hydrodynamic Tank at University of Strathclyde (URL.1) .....	42
Figure 3.2. Wave maker .....	42
Figure 3.3. Wave absorbing beach.....	43
Figure 3.4. Hullform of DTMB-5415 .....	44
Figure 3.5. Physical naval combatant ship model.....	44
Figure 3.6. Internal view at flooded compartments .....	45
Figure 3.7. Stationary model in calm water with moorings.....	46
Figure 3.8. Dimensions of the flooded compartments .....	46
Figure 3.9. Infra-red markers and force gauge installed on the ship.....	49
Figure 3.10. Type 206/5C 5-Component force gauge by DHI .....	49
Figure 3.11. Sketch of transducer calibration setup with dimensions (unit: mm) .....	50
Figure 3.12. Illustration of load cell calibration in two directions.....	51
Figure 3.13. Torsional moment ( $M_z$ ) marked on transducer .....	51

Figure 3.14. Sketch of transducer's calibration for $M_z$ .....	51
Figure 3.15. Calibration for forces acting on the load cell.....	52
Figure 3.16. Calibration for moments acting on the axes of the load cell .....	52
Figure 3.17. $F_y$ triggered by $F_x$ .....	54
Figure 3.18. $M_x$ triggered by $F_x$ .....	55
Figure 3.19. $M_z$ triggered by $F_x$ .....	55
Figure 3.20. Wooden support used to hold the ship model.....	57
Figure 3.21. Decrement curves of free decay tests .....	58
Figure 3.22. Natural frequency analysed by FFT .....	59
Figure 3.23. A sample of data acquisition by Spike .....	60
Figure 3.24. Intact ship motion in beam waves .....	62
Figure 3.25. Free surface near the damaged opening under damaged condition.....	63
Figure 3.26. Non-dimensioned roll motion against non-dimensional excitation frequency.....	63
Figure 3.27. Non-dimensioned heave motion against non-dimensional excitation frequency.....	64
Figure 3.28. Definition of wave-induced loads on the ship hull.....	65
Figure 3.29. 5-component wave-induced loads acting on the damaged ship.....	66
Figure 3.30. Non-dimensional vertical shear force against non-dimensional excitation frequency.....	67
Figure 3.31. Non-dimensional horizontal shear force against non-dimensional excitation frequency.....	67
Figure 3.32. Non-dimensional vertical bending moment with non-dimensional frequency.....	69
Figure 3.33. Non-dimensional horizontal bending moment with non-dimensional frequency.....	69
Figure 3.34. Non-dimensional torsional moment with non-dimensional frequency .	70
Figure 3.35. Comparison of the intact ship's roll motion .....	71
Figure 3.36. Comparison of the damaged ship's roll motion.....	71
Figure 3.37. Roll motion of the intact ship at the resonance frequency of roll motion .....	73
Figure 3.38. Roll motion of the damaged ship at the resonance frequency of roll motion .....	74
Figure 3.39. Comparison of the intact ship's vertical shear force .....	76
Figure 3.40. Comparison of the damaged ship's vertical shear force.....	76
Figure 3.41. Vertical shear force acting on the intact ship at the resonance frequency .....	77
Figure 3.42. Vertical shear force acting on the damaged at the resonance frequency	77
Figure 3.43. Comparison of the intact ship's horizontal shear force .....	78
Figure 3.44. Comparison of the damaged ship's horizontal shear force.....	78
Figure 3.45. Horizontal shear force acting on the intact ship at the resonance frequency.....	79
Figure 3.46. Horizontal shear force acting on the damaged ship at the resonance frequency.....	79
Figure 3.47. Comparison of the intact ship's vertical bending moment .....	80

Figure 3.48. Comparison of the damaged ship's vertical bending moment.....	80
Figure 3.49. Vertical bending moment acting on the intact ship at the resonance frequency.....	81
Figure 3.50. Vertical bending moment acting on the damaged ship at the resonance frequency.....	81
Figure 3.51. Comparison of the intact ship's horizontal bending moment.....	82
Figure 3.52. Comparison of the damaged ship's horizontal bending moment .....	82
Figure 3.53. Horizontal bending moment acting on the intact ship at the resonance frequency.....	83
Figure 3.54. Horizontal bending moment acting on the damaged ship at the resonance frequency.....	83
Figure 3.55. Comparison of the intact ship's torsional moment.....	84
Figure 3.56. Comparison of the damaged ship's torsional moment .....	84
Figure 3.57. Torsional moment acting on the intact ship at the resonance frequency.....	85
Figure 3.58. Torsional moment acting on the damaged ship at the resonance frequency.....	85
Figure 4.1. Workflow with STAR-CCM+ .....	90
Figure 4.2. The flow of a fluid over a flat plate (Yunus and Cimbala, 2006).....	93
Figure 4.3. Turbulent boundary layer for a typical incompressible flow over a smooth flat plate (Pletcher et al., 2012) .....	93
Figure 4.4. Boundary conditions of the fluid domain .....	95
Figure 4.5. Free surface (interface) between air and water.....	96
Figure 4.6. Generated mesh for fluid domain .....	97
Figure 4.7. Wave elevation at t=30s .....	98
Figure 4.8. Wave elevation against time history.....	99
Figure 4.9. Mesh dependence verification .....	99
Figure 4.10. Generated wave by CFD compared with the wave in the tank.....	101
Figure 4.11. First and second order frequencies and amplitudes of the generated wave by FFT .....	101
Figure 4.12. A sketch of experiment (Jung et al., 2006).....	102
Figure 4.13. Mesh distribution in fluid domain .....	103
Figure 4.14. Roll decrement results comparison.....	104
Figure 4.15. Physical model (Irkal et al., 2016).....	105
Figure 4.16. A sketch of experimental setup.....	105
Figure 4.17. Geometry and boundary conditions of calculation domain.....	106
Figure 4.18. Decrement curves of mesh sensitivity compared between CFD method and physical test .....	107
Figure 4.19. Results for mesh dependence.....	108
Figure 4.20. Frequency obtained by FFT method.....	108
Figure 4.21. Comparison presented for time-step sensitivity .....	109
Figure 4.22. Sketch of fluid domain for structure in beam waves .....	110
Figure 4.23. Mesh distribution for overset and background region.....	111
Figure 4.24. Mesh distribution for mesh dependence study .....	112
Figure 4.25. Comparison of results for mesh dependence .....	112

Figure 4.26. Roll motion RAO comparison between numerical methods and experiment.....	113
Figure 4.27. 2D sketch of water tank sloshing.....	116
Figure 4.28. Mesh generated for 2-dimensional simulation .....	116
Figure 4.29. Elevation measured by probe P1 .....	118
Figure 4.30. Elevation measured by probe P2 .....	118
Figure 4.31. Elevation measured by probe P3 .....	119
Figure 4.32. Water surface elevation measured at Probe P1.....	120
Figure 4.33. Water surface elevation measured at Probe P2.....	120
Figure 4.34. Water surface elevation measured at Probe P3.....	121
Figure 4.35. Water surface elevation measured by Probe P1 .....	122
Figure 4.36. Water surface elevation measured by Probe P2 .....	122
Figure 4.37. Water surface elevation measured by Probe P3 .....	123
Figure 4.38. Sketch of structure for 3DOF sloshing .....	124
Figure 5.1. Three orthographic views of the geometry with dimensions.....	131
Figure 5.2. Damaged ship geometry with flooded compartments .....	132
Figure 5.3. Inner layout of damaged compartments used in CFD and experiment .	132
Figure 5.4. Boundary conditions of fluid domain .....	133
Figure 5.5. Mesh distribution along the damaged ship hull.....	134
Figure 5.6. Mesh inside the flooded tank.....	134
Figure 5.7. Mesh distribution on XOZ plane for intact free decay .....	135
Figure 5.8. Mesh distribution for damaged free decay simulation .....	135
Figure 5.9. Intact free decay result obtained by CFD compared with experiment ..	136
Figure 5.10. Damaged free decay curve comparison between CFD and physical tests .....	136
Figure 5.11. Inertial ( $O-XYZ$ ) and non-inertial ( $o-xyz$ ) coordinate systems established .....	137
Figure 5.12. Total force components acting on one part of the ship.....	138
Figure 5.13. Moment components acting on the aft portion.....	140
Figure 5.14. Damaged opening in physical model (Cover is unattached) .....	142
Figure 5.15. Calculation domain with boundaries for ship in beam waves.....	143
Figure 5.16. Overall mesh distribution .....	144
Figure 5.17. (a) Mesh layers to capture waves; (b) Refined mesh along ship hull; (c) Boundary layers partially distributed at stern; (d) Mesh refinement around sonar dome.....	145
Figure 5.18. Mesh refinement for floodwater .....	145
Figure 5.19. Grid dependency results for roll motion.....	147
Figure 5.20. Grid dependency results for heave motion .....	147
Figure 5.21. Comparison of roll motion in time between CFD method and physical test for intact ship .....	151
Figure 5.22. Comparison of roll motion by FFT.....	152
Figure 5.23. Comparison of heave motion in time between CFD method and physical test for intact ship.....	152
Figure 5.24. Comparison of heave motion by FFT .....	153
Figure 5.25. Ship motions in one period.....	154

Figure 5.26. Snapshots for vortex at sonar dome.....	154
Figure 5.27. Vertical shear force comparison in time history for intact ship.....	155
Figure 5.28. Vertical shear force comparison in frequency by FFT .....	155
Figure 5.29. Horizontal shear force comparison in time history for intact ship .....	156
Figure 5.30. Horizontal shear force comparison in frequency by FFT .....	156
Figure 5.31. Vertical bending moment comparison in time for intact ship .....	157
Figure 5.32. Vertical bending moment comparison by FFT .....	157
Figure 5.33. Horizontal bending moment comparison in time for intact ship .....	158
Figure 5.34. Horizontal bending moment comparison by FFT.....	158
Figure 5.35. Torsional moment comparison in time for intact ship.....	159
Figure 5.36. Torsional moment comparison by FFT .....	159
Figure 5.37. Roll motion comparison for damaged ship.....	162
Figure 5.38. Roll motion frequency analysis by FFT .....	162
Figure 5.39. Heave motion comparison for damaged ship .....	163
Figure 5.40. Heave motion frequency analysis by FFT .....	163
Figure 5.41. Damaged ship motions excited by waves.....	164
Figure 5.42. Ingress and egress of floodwater through damaged opening.....	167
Figure 5.43. Horizontal shear force in time history for damaged ship .....	167
Figure 5.44. Frequency of horizontal shear forces by FFT for damaged ship .....	168
Figure 5.45 Vertical shear force in time history for damaged ship.....	168
Figure 5.46. Frequency of vertical shear forces by FFT for damaged ship .....	169
Figure 5.47. Horizontal bending moment in time history for damaged ship .....	169
Figure 5.48. Frequency of horizontal bending moment by FFT for damaged ship .	170
Figure 5.49. Vertical bending moment in time history for damaged ship .....	170
Figure 5.50. Frequency of vertical bending moment by FFT for damaged ship .....	171
Figure 5.51. Torsional moment in time history for damaged ship.....	171
Figure 5.52. Frequency of torsional moment by FFT for damaged ship .....	172
Figure 5.53. Vorticity around the damaged hull under the water surface.....	172

## Appendix

Figure A1.1. $F_x$ caused by $F_y$ .....	198
Figure A1.2. $M_y$ caused by $F_y$ .....	198
Figure A1.3. $M_z$ caused by $F_y$ .....	199
Figure A2.1. Solution by Runge-Kutta method .....	202
Figure A2.2. Free decay solution solved by Runge-Kutta with $I=0.009 \text{ kgm}^2$ .....	203
Figure A2.3. Free decay solution solved by Runge-Kutta with $I=0.01 \text{ kgm}^2$ and $I=0.011 \text{ kgm}^2$ .....	204
Figure A2.4. Comparison between measurement and solution by Runge-Kutta method with all linear components .....	205
Figure A2.5. Runge-Kutta solution for decay curve of the damaged ship.....	206
Figure A2.6. Comparisons among experimental data and solutions as $I=0.928 \text{ kgm}^2$ .....	207
Figure A2.7. Angle of inclination of free decay for $I=0.897 \text{ kgm}^2$ .....	208

Figure A3. 1. Sketch of inertial and non-inertial coordinate system for rigid body motion ..... 209

# List of Tables

Table 1.1 Maritime accidents .....	3
Table 1.2. Naval combatant ship accidents .....	4
Table 1.3. Widely known water basin.....	13
Table 3.1. Particulars of the ship model.....	43
Table 3.2. Particulars of the damaged ship .....	46
Table 3.3. Wave settings .....	47
Table 3.4. Uncertainty analysis of the five-component loads.....	53
Table 3.5. Summary of analysed natural frequencies and periods.....	59
Table 3.6. Roll natural period and frequency of two physical model tests.....	70
Table 4.1. Wave properties with mesh dependence .....	97
Table 4.2. Main characteristics of structure .....	102
Table 4.3. Summary of geometry used in physical test and CFD simulation.....	105
Table 4.4. Mesh and time step dependence.....	106
Table 4.5. Summary of results for mesh dependence .....	108
Table 4.6. Regular beam waves setup .....	110
Table 4.7. Mesh and time-step sensitivity setup .....	111
Table 4.8. Velocity vectors around structure during a period of oscillation.....	114
Table 4.9. Mesh dependence for non-resonance sloshing.....	117
Table 4.10. Mesh dependence setup for resonance sloshing .....	121
Table 4.11. Coefficients that define motion functions.....	125
Table 4.12. Free surface evolution comparison .....	125
Table 5.1. Main properties of DTMB 5415 .....	131
Table 5.2. Regular beam wave settings.....	144
Table 5.3. Meshes applied for grid dependency study.....	146
Table 5.4. Summary of uncertainties for grid dependency study .....	148
Appendix 2	
Table A2.1 Solutions by Runge-Kutta method.....	202
Table A2.2. Summary of solutions with Runge-Kutta method.....	203
Table A2.3. Summary of coefficients solved by Runge-Kutta method .....	204
Table A2.4. Summary of calculation results by Runge-Kutta method .....	206
Table A2.5. Solutions by Runge-Kutta method .....	207
Table A2.6. Summary of solutions by Runge-Kutta method.....	208

# Abbreviations

CAD	Computer Aided Design
CFD	Computational Fluid Dynamics
DDG	Hull classification symbol for U.S. Navy guided missile destroyer
DHI	Danish Hydraulic Institute
DOF	Degree-of-Freedom
DTMB	David Taylor Model Basin
FFT	Fast Fourier Transform
MPS	Moving Particle Simulation
ITTC	International Towing Tank Conference
LNG	Liquefied Natural Gas
RAMS	Root-Mean-Square Error
RANS	Reynolds-Averaged Navier–Stokes
RAO	Response Amplitude Operator
SEE	Standard Error of Estimate
SIMPLE	Semi-Implicit Method for Pressure-Linked Equations
SPH	Smoothed Particle Hydrodynamics
SSR	sum of the square of residuals
SST	Shear Stress Transport
VOF	Volume of Fluid



# Nomenclature

Label	Unit	Indication
a	m/s <sup>2</sup>	Acceleration
A	m or mm	Wave amplitude
A <sub>XX</sub>	kgm <sup>2</sup>	Added mass moment of inertia about roll motion
B <sub>OA</sub>	m	Overall beam
B <sub>WL</sub>	m	Beam at waterline
C <sub>B</sub>		Block coefficient
C <sub>M</sub>		Midship section coefficient
C <sub>P</sub>		Prismatic coefficient
C <sub>WP</sub>		Water plane coefficient
C <sub>G</sub>		Correction factor
COG		Centre of gravity
D	m	Depth
<i>e</i>		Unit vector = [ <i>e</i> <sub>1</sub> , <i>e</i> <sub>2</sub> , <i>e</i> <sub>3</sub> ]
f	Hz	Wave frequency
F	N	Force
F <sub>w</sub>	N	Water force
g	m/s <sup>2</sup>	Gravitational acceleration
G	N	Gravitational force
GM	m	Metacentric height
H	m or mm	Wave height
HBM	Nm	Horizontal bending moment
HSF	N	Horizontal shear force
( <i>i, j, k</i> )		Unit vectors in x-, y- and z- axes
I <sub>xx</sub>	kgm <sup>2</sup>	Mass moment of inertia about roll motion
I <sub>yy</sub>	kgm <sup>2</sup>	Mass moment of inertia about pitch motion
I <sub>zz</sub>	kgm <sup>2</sup>	Mass moment of inertia about yaw motion

$k$		Wave number
KG	m	COG above keel
KM	m	Metacentre above keel
$k_{xx}$	m	Radius of gyration in x-axis
$k_{yy}$	m	Radius of gyration in y-axis
$k_{zz}$	m	Radius of gyration in z-axis
$L$	$\text{kgm}^2/\text{s}$	Angular momentum
LCG	m	Longitudinal position of COG
Lpp	m	Length between perpendiculars
LOA	m	Overall length
LWL	m	Length at waterline
$m$	kg	Mass
$M$	Nm	Moment
$\mathbf{n}$		Normal unit vector
$P$	pa	pressure
$P_G$		Order of accuracy
$\mathbf{r}$	m	Relative position vector
$R_G$		Parameter refinement ratio
$S$	$\text{m}^2$	Area
SF	N	Shear Force
$t$	s	Time
$T$	m	Draft
$T_N$	s	Natural period
$T_w$	s	Wave period
TM	Nm	Torsional moment
$\mathbf{u}$	m/s	Velocity vector = $(u, v, w)$
$U_G$		Uncertainty
$v$	m/s	velocity
VBM	Nm	Vertical bending moment

VSF	N	Vertical shear force
$\nabla$	$m^3$	Volume displacement/ differential operator Del
$\nabla^2$		Laplace operator
$\Delta$	kg or ton	Weight displacement
$\alpha$	rad/s <sup>2</sup>	Volume fraction/ angular acceleration
$\omega$	rad/s	Wave frequency/angular velocity/ Specific dissipation rate
$\omega_N$	rad/s	Natural frequency
$\lambda$		Scale factor
$\lambda_w$	m	Wave length
$\mu$	kg/ms	Dynamic viscosity
$\theta$	deg or rad	Roll angle
$\rho$	kg/m <sup>3</sup>	Density
$\kappa$		Turbulence kinetic energy